2016

3D Infrastructure Condition Assessment For Rail Highway Applications

Teng Wang
University of Kentucky, wangtengyilang@gmail.com
Digital Object Identifier: http://dx.doi.org/10.13023/ETD.2016.156

STUDENT AGREEMENT:

I represent that my thesis or dissertation and abstract are my original work. Proper attribution has been given to all outside sources. I understand that I am solely responsible for obtaining any needed copyright permissions. I have obtained needed written permission statement(s) from the owner(s) of each third-party copyrighted matter to be included in my work, allowing electronic distribution (if such use is not permitted by the fair use doctrine) which will be submitted to UKnowledge as Additional File.

I hereby grant to The University of Kentucky and its agents the irrevocable, non-exclusive, and royalty-free license to archive and make accessible my work in whole or in part in all forms of media, now or hereafter known. I agree that the document mentioned above may be made available immediately for worldwide access unless an embargo applies.

I retain all other ownership rights to the copyright of my work. I also retain the right to use in future works (such as articles or books) all or part of my work. I understand that I am free to register the copyright to my work.

REVIEW, APPROVAL AND ACCEPTANCE

The document mentioned above has been reviewed and accepted by the student's advisor, on behalf of the advisory committee, and by the Director of Graduate Studies (DGS), on behalf of the program; we verify that this is the final, approved version of the student's thesis including all changes required by the advisory committee. The undersigned agree to abide by the statements above.

Teng Wang, Student

Dr. Reginald R. Souleyrette, Major Professor

Dr. Yi-Tin Wang, Director of Graduate Studies

3D INFRASTRUCTURE CONDITION ASSESSMENT FOR RAIL HIGHWAY APPLICATIONS

DISSERTATION

A dissertation submitted in partial fulfillment of the
requirements for the degree of Doctor of Philosophy in the
College of Engineering at the University of Kentucky

By

Teng Wang
Lanzhou, China

Director: Dr. Reginald R. Souleyrette
Commonwealth Chair Professor of Civil Engineering
Lexington, Kentucky
2016

ABSTRACT OF DISSERTATION

3D INFRASTRUCTURE CONDITION ASSESSMENT FOR
RAIL HIGHWAY APPLICATIONS

Highway roughness is a concern for both the motoring public and highway authorities. Roughness may even increase the risk of crashes. Rail-highway grade crossings are particularly problematic. Roughness may be due to deterioration or simply due to the way the crossing was built to accommodate grade change, local utilities, or rail elevation. With over 216,000 crossings in the US, maintenance is a vast undertaking. While methods are available to quantify highway roughness, no method exists to quantitatively assess the condition of rail crossings. Conventional inspection relies on a labor-intensive process of qualitative judgment. A quantifiable, objective and extensible procedure for rating and prioritizing improvement of crossings is thus desired.

In this dissertation, a 3D infrastructure condition assessment model is developed for evaluating the condition and performance of rail highway grade crossings. Various scanning techniques and devices are developed or used to obtain the 3D “point cloud” or surface as a first step towards quantifying crossing roughness. Next, a technique for repeatable field measurement of acceleration is presented and tested to provide a condition index. Acceleration-based metrics are developed, and these can be used to rate and compare crossings for improvement programs to mitigate potential vehicle damage and provide passenger comfort. A vehicle dynamic model is next customized to use surface models to estimate vertical accelerations eliminating the need for field data collection. Following, crossing roughness and rideability is estimated directly from 3D point clouds. This allows isolation of acceleration components derived from surface condition and original design profile. Finally, a practice ready application of the 3D point cloud is developed and presented to address hump crossing safety.

In conclusion, the dissertation presents several methods to assess the condition and performance of rail crossings. It provides quantitative metrics that can be used to evaluate designs and construction methods, and efficiently implement cost effective improvement programs. The metrics provide a technique to measure and monitor system assets over time, and can be extended to other infrastructure components such as pavements and bridges.

KEYWORDS: 3D Infrastructure Condition Assessment,
Simulation, Vehicle Dynamics, Roughness,
Rail-Highway Grade Crossing

Teng Wang

Student's Signature

April 26, 2016

Date

3D INFRASTRUCTURE CONDITION ASSESSMENT FOR RAIL HIGHWAY APPLICATIONS

By

Teng Wang

Dr. Reginald R. Souleyrette
Director of Dissertation

Dr. Yi-Tin Wang
Director of Graduate Studies

April 26, 2016
Date

To my parents, families and friends in China,

My parents, families and friends in the US,

And to all the people who walked with me through this journey,

I dedicate this work.

ACKNOWLEDGEMENTS

First, I would like to thank my all committee members, Dr. Reginald Souleyrette, Dr. Jerry Rose, Dr. Daniel Lau and Dr. William Maloney for the time they spent with me on this research. Without their support, guidance, expertise, and recommendations this dissertation would have never come together. Second, I would like to thank Professor Ahmed Shabana and Dr. Ahmed Boubakr from University of Illinois at Chicago Department of Mechanical and Industrial Engineering for their help developing the vehicle dynamic model.

A special thanks go to my parents Yunfeng Teng and Yuping Wang in China for giving me life and everything in the past twenty seven years. At the end I would like express appreciation to my family here, Rosemary Souleyrette, Reginald Souleyrette and David Souleyrette for their hospitality and giving me warmth of the family.

Finally, I would like to thank the National University Rail (NURail) Center, a US DOT-OST Tier 1 University Transportation Center for sponsoring this research. I would like to thank the following individuals for their contributions: Mr. Sam Carter from CSX railroad, Dr. Peng Xu from Beijing Jiaotong University, Mr. Qingjie Liu from East China Jiaotong University, Mr. Brad Rister of the Kentucky Transportation Center, Ms. Sheila Williams, Ms. Suzanna Wampler and Mr. William Staats from University of Kentucky Department of Civil Engineering. All opinions and recommendations are those of the author only.

Table of Contents

LIST OF TABLES

LIST OF FIGURES

CHAPTER 1. INTRODUCTION

1.1 Problem and Background

The railroad-highway crossing represents a unique and problematic junction of two of the most ubiquitous transportation modes. Quality of surface is an important aspect affecting both the safety and the performance of at-grade crossings. Poor rideability (bumpiness) for highway vehicles may increase the risk of collisions with trains, fixed objects or other highway traffic. Steep grades and short vertical transitions in crossing profiles increase the likelihood of low-profile vehicles becoming stuck, and possibly struck by oncoming trains (Operation Lifesaver, 2015). Further, the US DOT Railroad-Highway Grade Crossing Handbook (US Department of Transportation, 2007) suggests that rough surfaces could distract a driver's attention from oncoming trains and that the unevenness of the crossing could result in a driver losing control of their vehicle resulting in a crash.

Crossing safety has been a concern for many years, as an early planning report of the city of Lexington, Kentucky demonstrates (Segoe, 1931). Crossing safety and delay are well-illustrated by a hand-drawn figure from that report (see Figure 1.1). A more recently study from the University of Massachusetts, Amherst (Horan, 2013) evaluated at-grade crossing safety and grade separation.

While crashes at rail-highway crossings have diminished over recent decades, the problem continues. For example, there were 2,291 rail-highway crossing incidents in the US in 2014 and over 2,000 incidents in 2015 (Federal Railroad Administration, 2016). The problem is also ubiquitous as there are over 216,000 rail-highway grade crossings in the United States, with over 4,500 in the state of Kentucky alone (Federal Railroad Administration Office of Safety Analysis, 2016).

With so many crossings, managing maintenance is a large undertaking. Even keeping a simple and up-to-date inventory requires significant time and effort. As with other highway assets, crossings deteriorate if not maintained, and life cycle costs increase without preventive maintenance. Prioritizing limited maintenance dollars is, well, a priority.

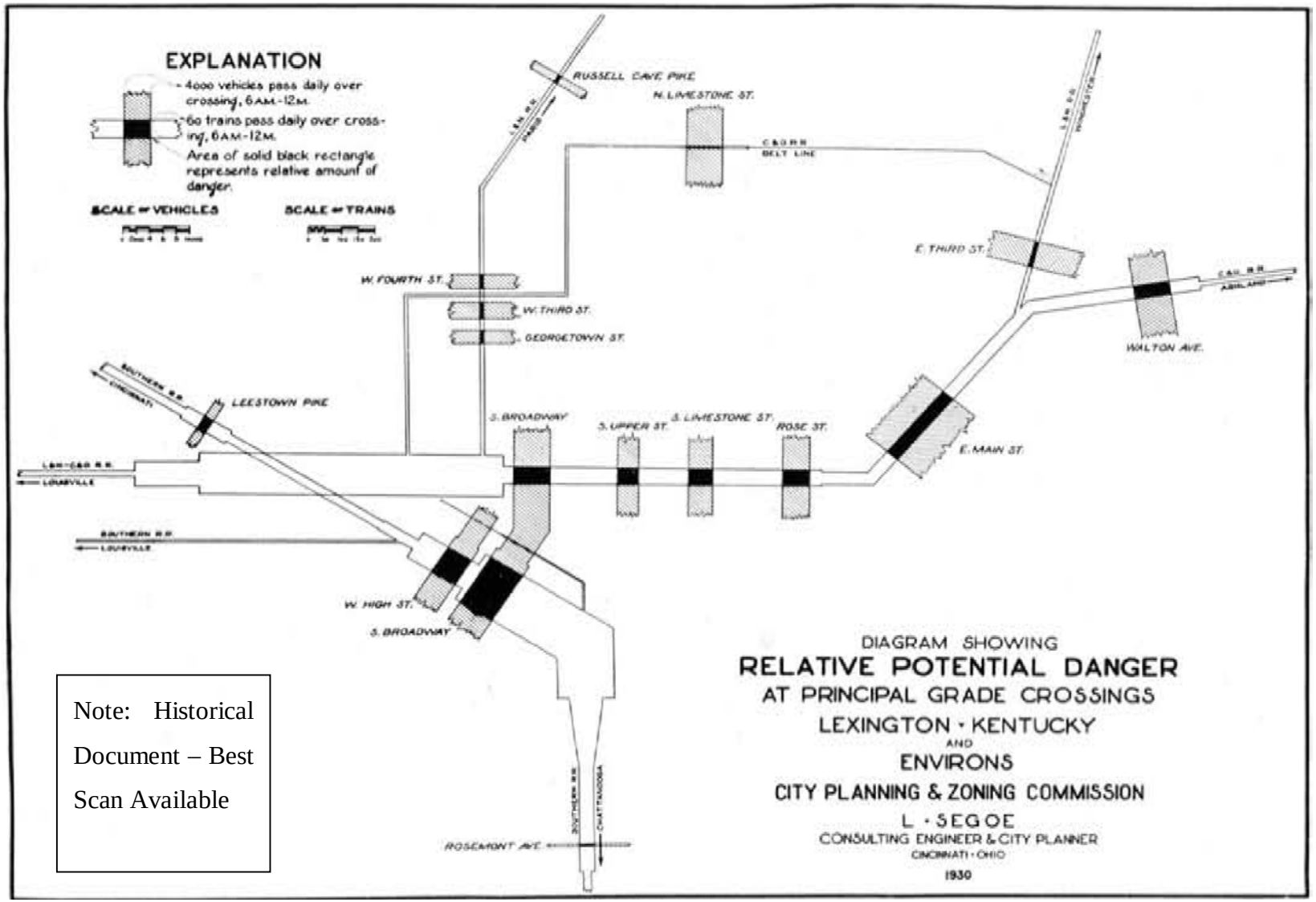

Note: Historical Document – Best Scan Available

Figure 1.1 Lexington crossing safety analysis in 1931.

Today, no quantitative method exists to quickly and economically evaluate the rideability of rail crossings and provide objective input to renewal programs. Conventional approaches assess the quality of crossings based on expert judgment. Typically, crossing surfaces are classified as poor, fair or good by inspectors upon examination or driving over the crossing. Crossings rated as poor may not always be the most cost-effective locations for preventive maintenance to lower overall life-cycle costs, and two crossings rated as fair may have vastly different current performance as well as useful remaining life. Variations in ratings may also be induced by the use of different inspection vehicles, crossing material and training and experience levels of inspectors. A quantifiable, reliable and repeatable, procedure is desired.

With rapid advances in computer science, 3D sensing and imaging technologies, as well as the availability of low cost computers and sensors, the time is right for the development of cost-effective, quantitative methods, tools and procedures. These technologies hold promise for quantitative rating of rail crossings rideability (overall experience) and its principal components: crossing surface condition, design profile and vehicle response characteristics.

To advance safety and facilitate the prioritization of crossings for renewal, this dissertation investigates and advances sensor capabilities and introduces several methodologies for quantifying rideability, roughness and condition of at-grade crossings. The research presented herein provides important first steps towards automating the crossing inspection process. These steps may also be applicable to other transportation infrastructure including, but not limited to highway and airfield pavements, as well as to other functions of road management such as asset management and safety assessment.

1.2 Research Objectives

The goals of this research are facilitated by several objectives:

1) As 3D surface models are a key data input for crossing evaluation, a low cost 3D sensor and data collection protocol is developed and tested.

2) As the key perceived and real determinants of rideability are passenger comfort and vehicle damage, and both of these depend on induced accelerations, a technique to measure accelerations experienced by drivers and vehicles at crossings was developed and assessed.

3) To facilitate quantitative rating, and because accelerations experienced by vehicles at crossings are highly erratic, an acceleration-based metric for comparing crossings is developed.

4) To attempt to provide an office-based assessment capability whereby inspectors may not need to visit every crossing site, a vehicle dynamic simulation model is developed to estimate acceleration for a design vehicle.

5) To provide a systematic means for quickly assessing and ranking crossings, a railroad crossing "roughness index" is developed based on standard roughness measures and surface models (3D point clouds).

6) To take into account the effects of geometric profile on relative vehicle accelerations, a railroad crossing "rideability index" is developed based on first principles of physics and surface model (3D point cloud)

7) To separate the effects of condition and design on rideability, the "design" component of acceleration (that which would be experienced by a vehicle if the crossing were in original condition, as designed and constructed) is estimated.

8) Finally, to provide a more reliable way to assess the potential of vehicles becoming high-centered and stuck at a crossing, a method to systematically identify and assess hump crossings from surface models (3D point clouds) is developed.

1.3 Approach

In this section, the basic research approach is described.

1.3.1 3D MEASUREMENTS: DESIGN AND BUILD STRUCTURED LIGHT SCANNER

Several technologies are available to accurately and relatively quickly measure 3D surfaces to obtain surface models (LiDAR, InSAR, and photogrammetry). However, a lower cost, less expensive technology is desired due to the vast number of rail-highway

crossings. The first part of this dissertation describes the development and testing of such a low-cost device and method. The design, construction and testing of a 3D Structured Light Scanner (SL Scanner) is reported. Both lab tests and field tests are reported. Analysis and measurements of the crossing surface data is also presented.

1.3.2 RIDEABILITY MEASUREMENT USING ACCELEROMETERS

As mentioned, determinants of rideability are passenger comfort and vehicle damage, and both of these depend on the presence or lack of externally induced accelerations. In this dissertation, a test and practical application of in-vehicle accelerometers, GPS and data collection computers/applications is presented. Accelerometers and GPS data have been used previously in vehicle road response studies for road simulation and rideability purposes (Cong, Shang, Ren, & Guo, 2012). In this study, vehicle accelerations at crossings were collected from test vehicles over several crossings at various speeds. Test repeatability, sensor reliability and data accuracy were examined. Multiple tests were conducted to identify an accurate and repeatable metric for quantifying the rideability of crossings.

1.3.3 DYNAMIC SIMULATION

Accelerations were estimated without field measurement, by a modified vehicle dynamic simulation model. 3D surface point clouds were used to provide wheel path profiles for use in the model. Speed and vehicle attributes (weight, tire size, tire width, suspension characteristics) were also input to estimate vehicle accelerations (Hou, Shan, & Ma, 2007). Field measured acceleration data were used as a reference to calibrate and validate the vehicle dynamic model.

1.3.4 DIRECT ROUGHNESS MEASUREMENT USING 3D POINT CLOUD

Later in this work, a crossing roughness index is developed from standard roughness metrics and the 3D point cloud. A crossing rideability index is also calculated which is based on the second derivative of a smoothed crossing profile. The methods were then compared and validated to measures derived from the same field measured accelerations. Next, rideability is separated into its principle components, effect of surface condition and effect of basic profile.

1.3.5 HUMP CROSSING ASSESSMENT

Lastly, this dissertation directly addresses a serious safety and operational concern—the hump crossing. Safety is obvious as having a low profile vehicle high-centered and stuck at a crossing is never a good thing. At a minimum, there will be delays experienced by the stuck vehicle or trains forced to stop to avoid a collision (if adequate notice is received). Further, trucks may avoid such crossings causing detours and related costs of wasted fuel and time. A simulation methodology is presented to identify and quantify rail-highway hump crossings using 3D surface models and vehicle characteristics. Vehicles with different dimensions and clearances were evaluated at different crossings. Results identify precisely the contact spots on vehicle frame as well as crossing surface. The method further assesses the likelihood of a vehicle getting stuck by providing relative height conflicts as well as potential conflict areas.

1.4 Outline/Structure of the Dissertation

Following this introduction, Chapter 2 of this dissertation presents a review of literature related to previous rail and highway condition assessment methods, advanced measurement technologies, and safety studies of the rail-highway crossing. In Chapter 3, various scanning techniques and devices were explored that may be used to obtain a 3D "point cloud" or surface as a first step towards quantifying crossing roughness. In that chapter, a low-cost 3D scanner based on structured light technology is proposed, developed, and tested. In chapter 4, a technique for repeatable field measurement of acceleration is presented and tested. Two summary metrics were proposed for rideability. In chapter 5, a vehicle dynamic model is modified, calibrated and validated to estimate vertical accelerations for various highway vehicles at crossings. The model employs the 3D surface, vehicle characteristics, and operating speed. Results were compared with accelerometer-derived performance data. In chapter 6, a crossing "roughness index" is developed which relies only on the 3D point cloud. A crossing rideability index is then calculated based on the second derivative of crossing profile. These indices were compared to field acceleration measurements. Finally, two components of rideability (condition effect and profile effect) were separated, evaluated and checked for reasonableness. In chapter 7, a practice ready 3D application is developed and presented to address hump

crossing safety. A flow chart depicting the relationships and synergies in the steps from each chapter is shown in Figure 1.2.

Concepts and methods introduced in this dissertation are principally intended to address cost and performance issues of rail-highway crossings. Safety should also benefit as smooth crossings may allow vehicles to proceed more safely as attention is not diverted from the driver's key task: yield to the train. Community livability may also be enhanced through reduced noise and delay for vehicles at the crossings. Vehicle maintenance costs may also be reduced by implementation of more effective crossing renewal programs. Where crossing rehabilitation is jointly (or entirely) funded by the railroad, economic benefits may accrue to the railroad as well. The proposed method and technology allows crossings to be better and more objectively managed as assets, more effective preventative maintenance should reduce overall life cycle costs. It is also possible that the methods and techniques developed in this research and applied to precise 3D datasets could benefit those analyzing long term performance of innovative rail track designs and materials, such as asphalt underlayment or tie cushioning. Finally, this research may have the potential for application to other transportation infrastructure that can be better represented and analyzed using 3D technology.

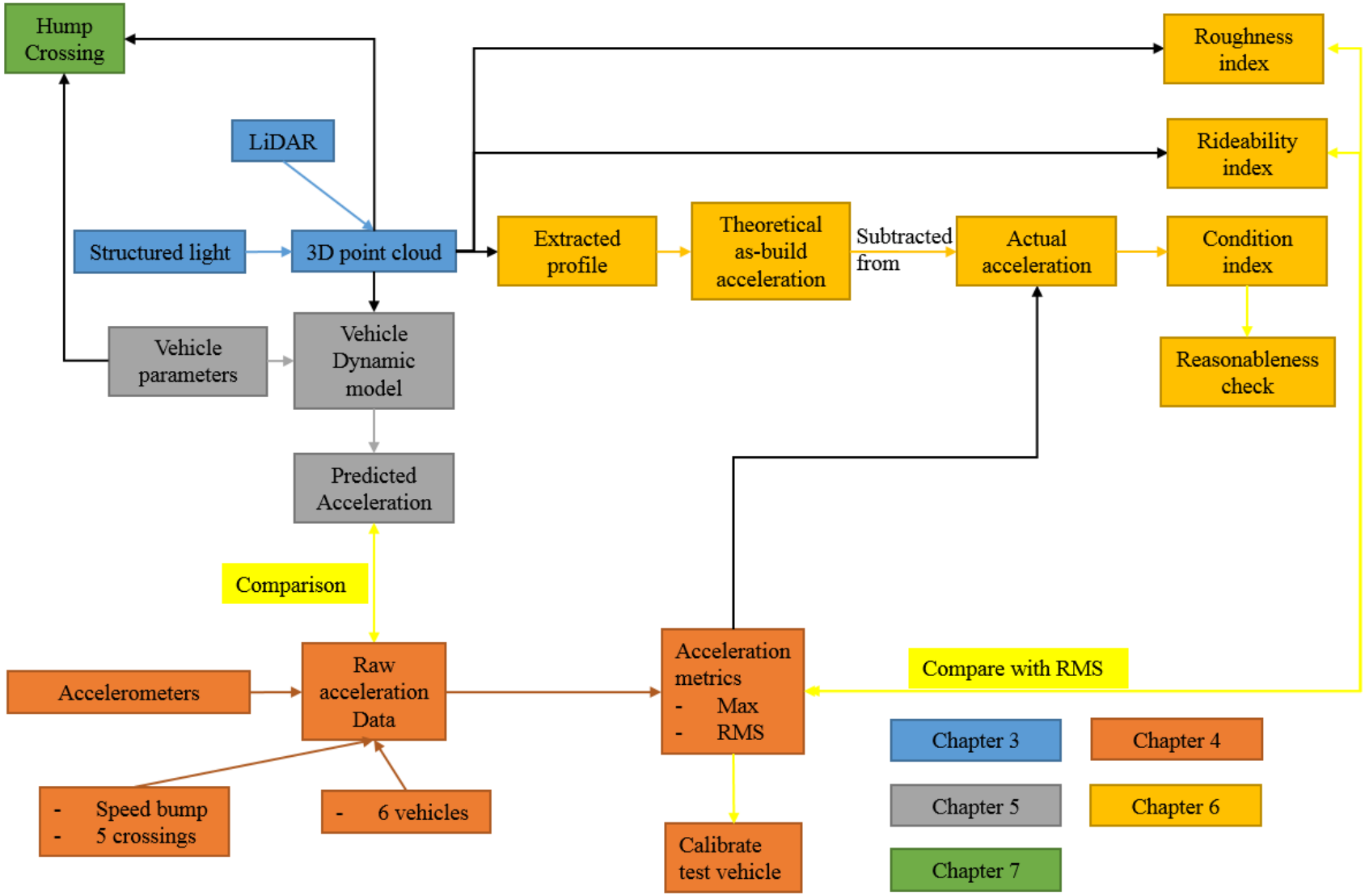

Figure 1.2 Methodological summary.

CHAPTER 2. LITERATURE REVIEW

2.1 Introduction

This chapter presents the principal literature utilized in the development of the tools and methods comprising this dissertation. It is organized along the same lines as the remaining chapters of this document. This review provides a convenient collection of resources for readers and researchers who may wish to build upon the foundation set forth by this work, as well as providing a summary of additional relevant literature not specifically referenced in later chapters.

2.2 Design and Test of a Low Cost 3D Scanner

Due to the various geometries that need to be accommodated at a highway rail crossing (grade of rail, elevation of rail, grade of highway, cross section of highway, drainage, …), it is difficult or impossible to field rate a crossing (by driving over it) and establish its performance for many combinations of crossing vehicle types, speeds and lateral placement of highway vehicle. To model its performance, an accurate 3D terrain model is required.

Technology exists to map crossing surfaces at different levels of precision and at various costs. For example, structured light 3D scanning uses projected light patterns and a high resolution digital camera system (Lakatos, 2010; Lanman & Taubin, 2009) to measure the shape, depth and surface information of an object. A known pattern of pixels (light strip) is distorted when projected on a non-flat surface (Casey, 2011). From recording of this information, depth and shape of the object may be calculated (Bevilacqua, Liguori, & Paolillo, 2010; Geng, 2011). A structured light 3D scanner can provide scan data at sub-centimeter accuracy with a relatively low investment of about $5,000 in equipment. A projected structured light system were displayed in Figure 2.1 and Figure 2.2 below.

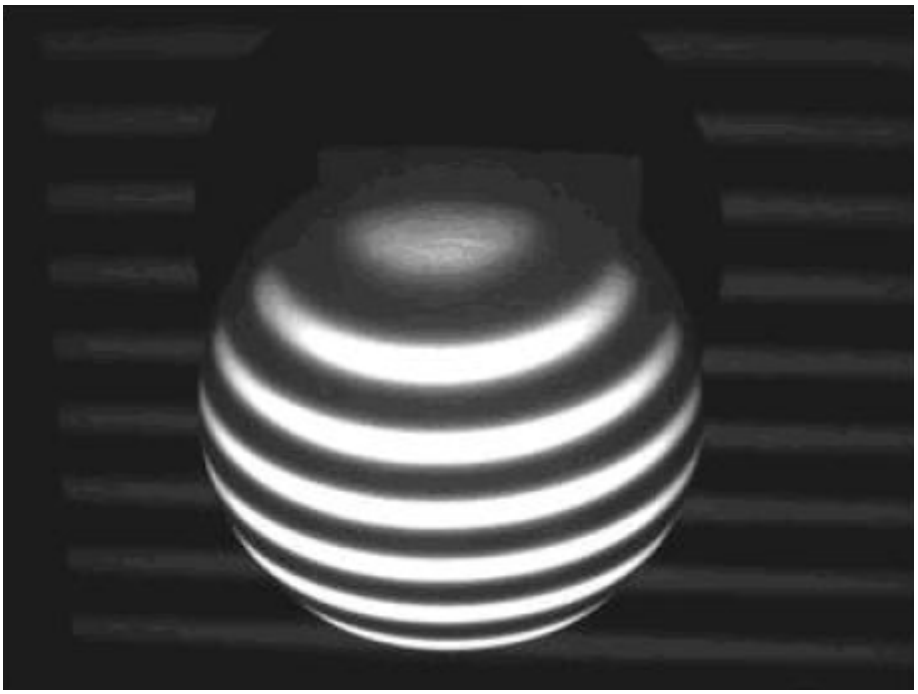

Figure 2.1 Pattern distortion due to subject surface (Casey, 2011).

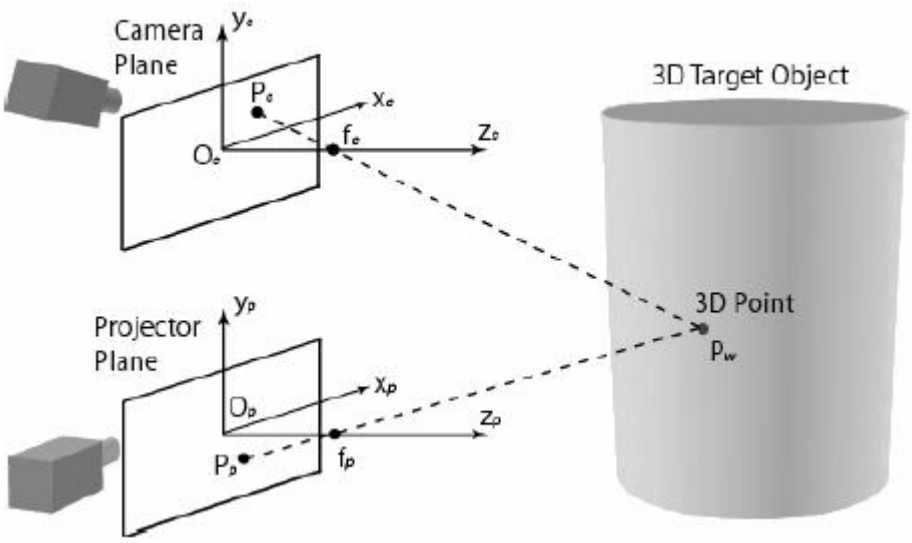

Figure 2.2 Structured light system (Casey, 2011).

Several studies conducted by Carnegie Mellon University (Mertz, 2011), Budapest University of Technology and Economics (Barsi, István-Lovas, Gábor-Takács, & Charles-Tóth, 2005; Kertész, Lovas, & Barsi, 2008) and University of Texas (Li, Yao,

Yao, & Xu, 2009), use projected structured light or a laser strip (a form of structured light technology) to create a 3D map of road surfaces to monitor and measure pavement quality on highway. Algorithms were programmed to automatically detect and record areas with pavement cracks or potholes, but no application of structured light on railroad-highway crossing has been found.

Another 3D imaging technology known as LiDAR (Light Detection Ranging) is a remote sensing technology that measures distance and other properties such as shapes and dimensions by illuminating a target with a laser and analyzing the reflected light (Olsen, 2013). LiDAR and 3D sensing in general find many applications in civil, construction and transportation engineering. For example LiDAR has been used to verify highway bridge clearance (Rister, McIntosh, & Whelan, 2013), collect roadway inventory data such as highway grade, side slope, cross slope, terrain and contours as well as stopping and passing sight distances (Shamayleh & Khattak, 2003; Souleyrette, Hallmark, Pattnaik, O'Brien, & Veneziano, 2003; Veneziano, Hallmark, & Souleyrette, 2002) and identify potential sight-distance problems at intersections to help improve highway safety (Khattak, Hallmark, & Souleyrette, 2003).

Mobile LiDAR data can achieve an average accuracy of +/- 3cm or better, but comes with a high equipment cost (about 1 million USD). See Figure 2.3 for an example LiDAR image where colors depict elevation.

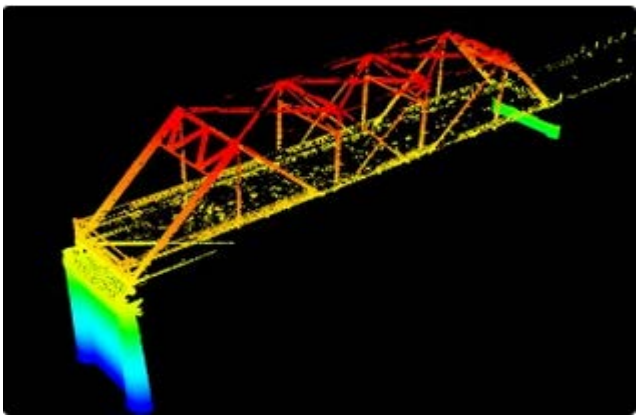

Figure 2.3 LiDAR scan of a bridge (Rister et al., 2013).

Another method, aerial photogrammetry as shown in Figure 2.4, uses high resolution photographic images and digital photogrammetry to determine the geometric location and elevation of terrain (Marzolff & Poesen, 2009). Today, 3D models (image-based modeling) can be created by using Unmanned Aerial Vehicles (UAV) and close-range photogrammetry (Bemis et al., 2014). Precision on the order of a few inches is attainable. However, photogrammetric data collection may be constrained by environmental factors, such as sun angle and cloud condition (Veneziano et al., 2002).

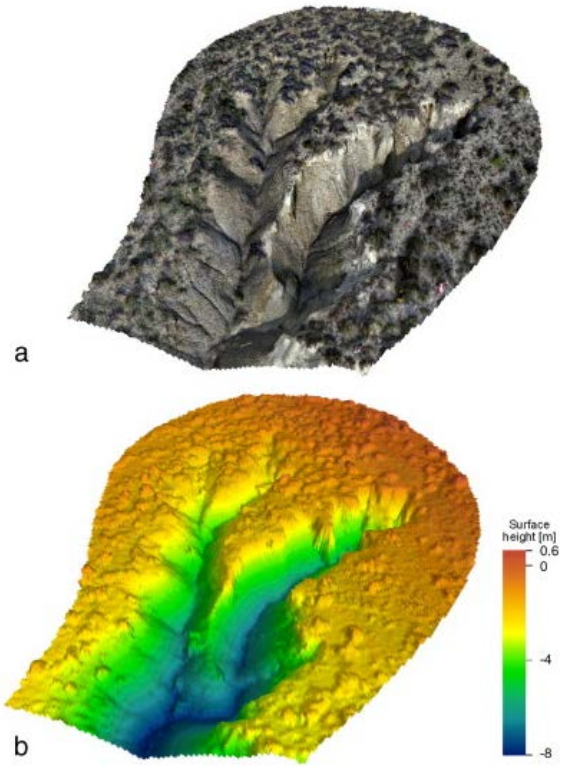

Figure 2.4 3D surface model using aerial photogrammetry (Marzolff & Poesen, 2009).

With the advent of new sensing and imaging technologies, much more capability has become available at very low cost. For example, the Microsoft Kinect sensor (around $150) features an RGB camera, laser depth sensor and multi-array microphone. While originally designed to support video gaming, the sensor platform is beginning to find alternative practical and scientific applications. For example, the Kinect sensor has been applied to road pavement management at the University of Southern California

(Jahanshahi, Jazizadeh, Masri, & Becerik-Gerber, 2012; Jahanshahi, Karimi, Masri, & Becerik-Gerber, 2015)

Figure 2.5 Kinect sensor (Jahanshahi et al., 2012).

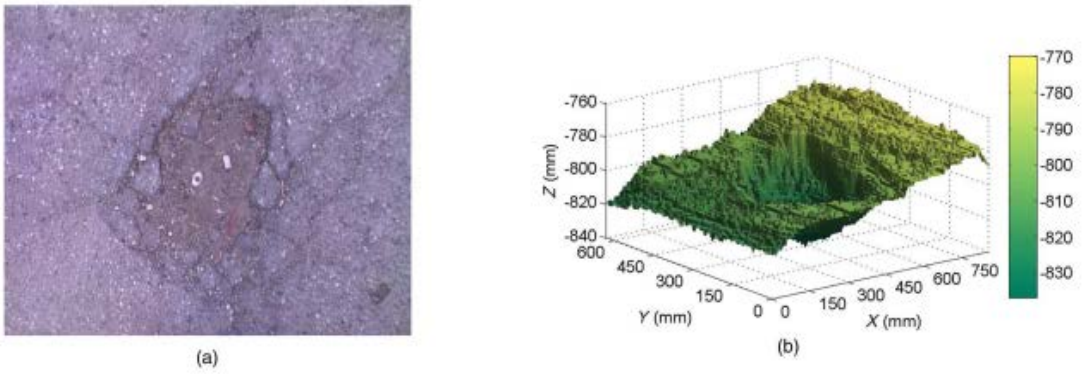

Figure 2.6 Use Kinect sensor to measure a pothole (Jahanshahi et al., 2012).

2.3 Use of Accelerometers to Assess Rideability of Crossing

An early study (Butcher, 1973) noted that drivers will change speed based on the rideability of a crossing. A more recent study (Rudin-Brown, George, & Stuart, 2014) suggested that poor surface conditions tend to divert drivers' attention while driving over crossings. The US DOT Railroad-Highway Grade Crossing Handbook (US Department of Transportation, 2007) also suggests that rough surfaces could distract a driver's attention from oncoming trains and that the unevenness of the crossing could result in a driver losing control of their vehicle, potentially contributing to the cause of a crash.

Many studies have been conducted on the response of the human body and vehicles to accelerations. Safety studies include (Proctor, Grimes, Fournier, Rigol, &

Sunseri, 1995; Quinn & Hildebrand, 1972). Health research includes (Katu, Desavale, & Kanai, 2003; Shanahan, 2004). Comfort related to acceleration has been studied by (Fine, 1963; Hou et al., 2007; Nahvi, Fouladi, & Nor, 2009; Smith, McGehee, & Healey, 1978).

The analysis of acceleration has also played an important role in studies of highway (Long, 2000; Papagiannakis, 1995, 1997) and vehicle design (Faris, BenLahcene, & Hasbullah, 2012; Nickmehr, 2011; Shirahatti, Prasad, Panzade, & Kulkarni, 2008; Ward & Iagnemma, 2009). These studies tend to focus on the relationship between highway rideability and vehicle acceleration. Accordingly, accelerometers and GPS have been used to assess rideability for roadway sections (Cong et al., 2012; Gregg & Foy, 1955; Mertz, 2011; Wiki, 2016). However, no applications to railroad crossings could be identified.

Collectively, these studies suggest that human comfort and highway vehicle rideability can be quantitatively measured by acceleration metrics, such as maximum acceleration or root mean square of accelerations. They also show that, expectantly, vehicle vertical accelerations were highly correlated with road profile as well as vehicle characteristics such as weight, tires, and suspension.

2.4 Vehicle Dynamic Model

Vehicle dynamic models have been used for predicting maximum and typical accelerations of passenger vehicles (Garcia-Pozuelo, Gauchia, Olmeda, & Diaz, 2014; Snare, 2002). In order to simulate train vertical accelerations for various crossing profiles, a vehicle dynamic model known as ATTIF (Analysis of Train/Track Interaction Forces) was developed (Dynamic Simulation Laboratory (DSL), 2013). This model was developed at the University of Illinois at Chicago (UIC). UIC and the University of Kentucky are partner schools in the National University Rail Consortium (NURail). ATTIF includes a detailed wheel/rail contact model based on surface geometry (Shabana, Aboubakr, & Ding, 2012).

ATTIF can be modified to simulate any vehicle using a crossing. Profiles for input to ATTIF can be extracted from 3D models. Vehicle characteristics such as weight, dimensions and suspension can be modified to simulate a highway vehicle driving over a

crossing. Profile is dependent on wheel path when a crossing surface varies in cross section. To determine wheel path, (Fitzsimmons, Souleyrette, & Nambisan, 2013) Z-tubes can be used to determine the position of wheels as a vehicle negotiates a crossing. However, the practical application of Z-tubes is limited to relatively straight approaches.

2.5 Quantitative Crossing Assessment Indices

Over the last 30 or more years, highway pavement roughness has been extensively studied. Various quantitative metrics have been developed, such as the international roughness index (IRI) (Sayers, 1995), and profile index (PI) (Sayers & Karamihas, 1998). Evaluation method using lasers (Freeman & McGhee, 1995; Li et al., 2009) and photogrammetry (Jahanshahi et al., 2015; Kertész et al., 2008) have been widely applied. To date, these technologies have not been expressly applied to evaluation of crossings.

The Railroad-Highway Grade Crossing Handbook (US Department of Transportation, 2007) indicates that rough surfaces may distract a driver's attention taking their eyes off oncoming trains. It also suggests that the unevenness of a crossing could result in a driver losing control, resulting in a crash. The handbook further suggests that improper drainage can result in track settlement which in turn may result in crossing surface deformation.

While track roughness may be evaluated by a railroad geometry car, highway crossings are usually qualitatively evaluated. Previous work by the University of Kentucky (Rose, Witt, Renfro, & Ridgeway, 2009) investigated a laser based inertial profiler and rolling dipstick for applicability in evaluating rail crossing roughness. In that report, three factors contributing to crossing roughness were identified as: roughness of the immediate crossing surface area, roughness of the highway approaches, and the vertical profile of the crossings. The ratings of the crossing roughness given by individuals who participated in the research are shown in Figure 2.7. Results were described as being of limited practicality, and investigation of alternative technology was recommended.

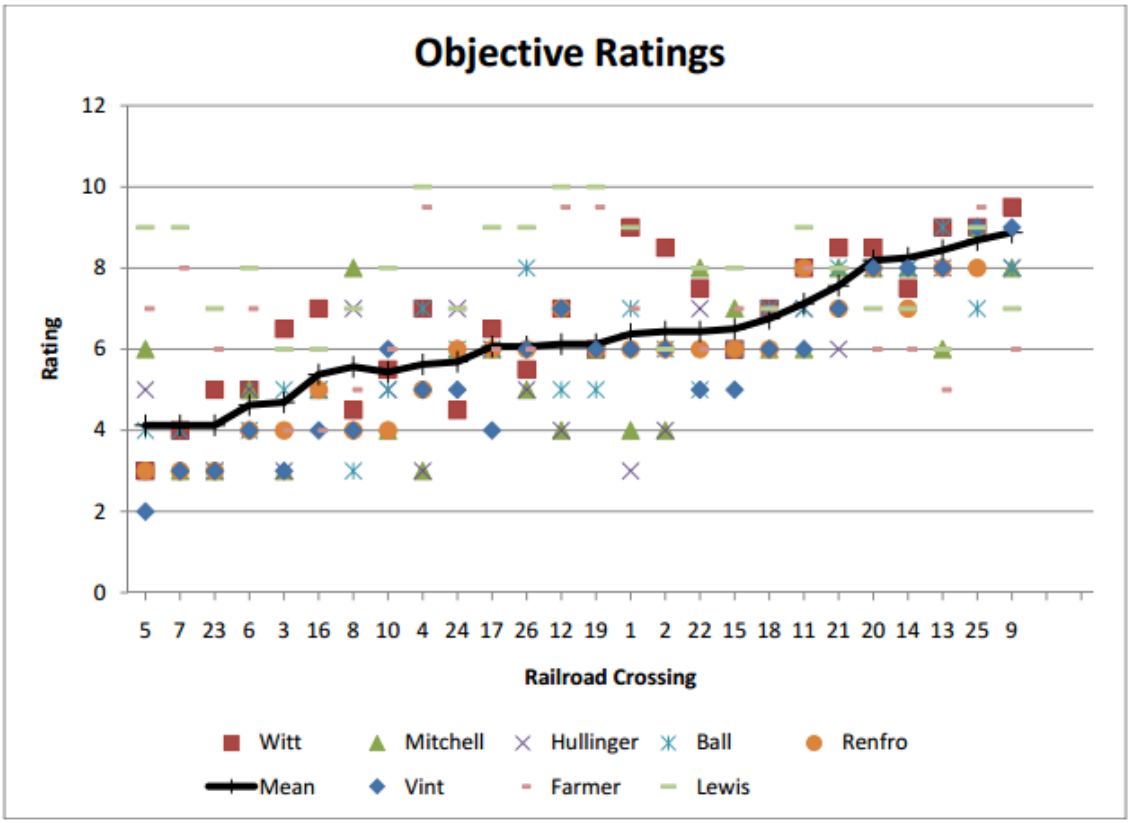

Figure 2.7 Rail crossing roughness objective ratings (Rose et al., 2009).

A study from Purdue University (Williams, 2003) of railroad crossing roughness classification in Indiana and a report from the Illinois DOT (Illinois Department of Transportation, 2001) shows how railroad crossing roughness may be classified as smooth, medium, and rough based on qualitative rideability evaluations (good, fair, poor) at different driving speeds. However, more recent documents (Illinois Department of Transportation, 2014) from Illinois indicate that such ratings are no longer recommended. This may be due to the fact that subjective ratings for crossings are likely to vary across raters and vehicles. Further, the effect of crossing condition cannot be differentiated from effects of original geometric design using such a method. Consequently, condition cannot be assessed by simply driving over a crossing. Moreover, the effect of surface quality cannot be distinguished from that of track subsidence over time (or even dynamic movement of the rails induced by the vehicle itself.)

2.6 Standard Measures of Surface Roughness

Several standard measures of surface roughness are available. These measures are used for applications ranging from industrial manufactured surfaces texture (Lonardo, Trumpold, & De Chiffre, 1996) to characterization of surface deposits from volcanic eruptions (Whelley, Glaze, Calder, & Harding, 2014). Two basic measures are relevant to the current work.

First, areal arithmetic mean height (Sa) (Abouelatta, 2010) may be computed from Equation 1-1 as the average of absolute differences between a surface and a plane:

Equation 2-1

$$S_a = \frac{1}{MN}\sum_{j=1}^{N}\sum_{i=1}^{M}\left|z(x_i, y_j)\right|$$

Where:

M = total number of points along the X axis.

N = total number of points along the Y axis.

z = the elevation of point (xi, yj) at the XY plane.

Figure 1.5 presents a physical interpretation of this measure.

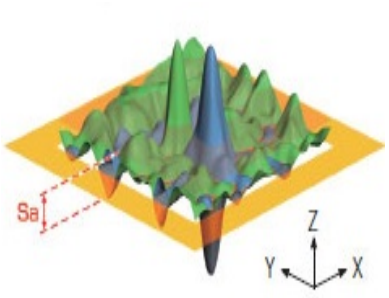

Figure 2.8 Arithmetic mean height (Olympus Corporation, 2016).

Second, areal root mean squared height (Sq) (Abouelatta, 2010) may be computed from Equation 1-2. Figure 2.9 presents a physical interpretation of this second measure.

Equation 2-2

$$S_q = \sqrt{\frac{1}{MN}\sum_{j=1}^{N}\sum_{i=1}^{M} z^2(x_i, y_j)}$$

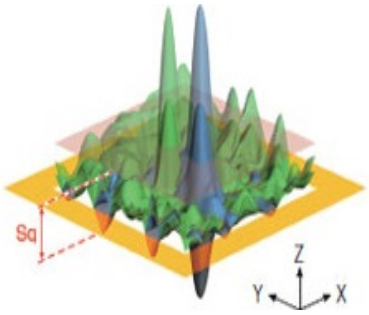

Figure 2.9 Root mean squared height (Olympus Corporation, 2016).

2.7 Identification and Assessment of Hump Crossings

The Rail-highway grade crossing is a complex structure created to facilitate the intersection of two very different transportation modes. Due to the unique characteristics of the crossing itself and varying dynamic performance of the vehicle and train, crossings represents a potentially dangerous situation for both rail and highway users.

A hump crossing, defined as a crossing where a vehicle with low ground clearance may become high-centered or stuck, may increase the risk of crashes for both trains and automobiles (Bauer, 1958). In addition to the safety implications presented by the potential of a high-centered vehicle becoming stuck on the tracks, there are operational costs associated with slowing to negotiate such a crossing, planning a trip to make sure a hump crossing will not be encountered and even more-so, the costs of diversion. Hump crossings are addressed in the design materials of agencies of the various different states (Mutabazi & Russell, 2003; Sobanjo, 2006; Wooldridge, 2000). Due to the types of vehicles that are most likely to become stuck, hump crossing collisions can result in catastrophic events (United States National Transportation Safety Board, 1996). Crashes at hump crossings, besides being devastating, attract public attention, as the vehicles can be vehicles designed to transport large numbers of people. For example, video of a recent limousine-train crash

at a hump crossing in New Paris, Indiana was posted on the Internet (StudioNoeProductions, 2015). Although in this case no one was injured, the video attracted over two million viewers and highlights the hump crossing safety issue. Stuck vehicles also pose a particular hazard to train crews, shipments of hazardous materials, and passenger trains. Figure 2.10 shows the result of a train-truck collision at a hump crossing.

Figure 2.10 Aftermath of a hump crossing collision (Operation Lifesaver, 2015).

Crossing geometric design guidelines are provided in AASHTO's A Policy on Geometric Design of Highways and Streets (the Green book) (American Association of State Highway and Transportation Officials (AASHTO), 2011), US DOT Railroad-Highway Grade Crossing Handbook (US Department of Transportation, 2007) and American Railway Engineering and Maintenance-of-Way Association (AREMA) Manual for Railway Engineering (American Railway Engineering Maintenance-of-Way Association (AREMA), 2015). These guides promote constructing crossings in such a way as to reduce or eliminate the probability of a vehicle becoming high-centered. Designs indicate that the surface of the highway should be neither more than 3 inches higher nor more than 6 inches lower than the top of the nearest rail at a point 30 feet from the rail, measured at a right angle, unless track superelevation dictates otherwise.

Previous efforts have been made to address the hump crossing issue. The "HANG-UP" software (Eck & Kang, 1992; Kang & Eck, 1991), developed in the early 1990s prepared design recommendations for low-clearance vehicles that experience "hang-ups" on vertical curves. Design vehicle dimensions are determined by using crossing profiles and vehicle wheel base, overhang distance and ground clearance. A lot of vehicle dimensions data were collected from the manufactures and direct measurement. Later,

related papers, (Clawson, 2002; French, Clawson, & Eck, 2003), approach the hump crossing problem based on two dimensional geometric design. Although recent research suggests the use of 3D technologies such as LiDAR to collect the crossing surface profile and address the hump crossing problem (Ranganathan & Olson, 2010; Van Arman & Al-Nazer, 2008), only two-dimensional simulation approaches have thus been developed. Two-dimensional approaches include only vehicle length and clearance as well as the crossing profile to identify conflict points, as shown in Figure 2.11. These solutions do not consider that actual field crossings vary in cross section due to highway or rail superelevation, construction abnormalities or conditions such as rutting or potholes. Previous work has examined only a very sparse grid of potential conflict points (e.g., every five feet) and computing power limited the extension of the application into three dimensions.

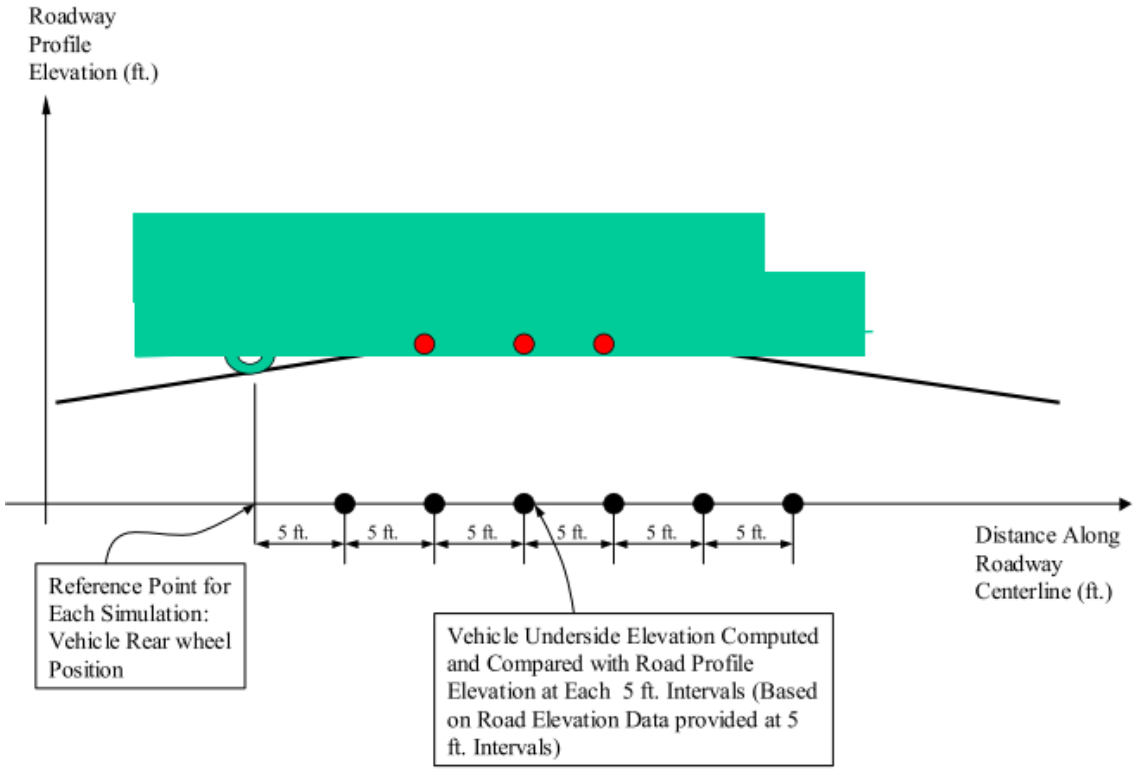

Figure 2.11 Two dimensional hump crossing conflict identification (Sobanjo, 2006).

Another approach to the identification of hump crossings has been to build physical models with frame and wheels and “drive” the model over crossings to as shown

in Figure 2.12. The physical model must be taken to each crossing and traffic control must be provided to conduct systematic evaluation.

Figure 2.12 Measurement with the Kansas Study's Physical Model (Mutabazi & Russell, 2003).

The literature reported and summarized in this chapter provides the point of departure for the research reported in the balance of this dissertation.

CHAPTER 3. DESIGN AND TEST OF LOW COST 3D SCANNER

3.1 Introduction

While track roughness may be evaluated by the railroad geometry car, highway crossings are usually qualitatively evaluated. Previous work by the University of Kentucky (Rose et al., 2009) investigated a laser based inertial profiler and rolling dipstick for applicability in evaluating rail crossing roughness. Results were of limited practicality. Future research with alternative technology was recommended. A study from Purdue University (Williams, 2003) of railroad crossing roughness classification in Indiana and documents from Illinois DOT (Illinois Department of Transportation, 2001) showed how railroad crossing roughness could be classified into different groups such as smooth, medium, and rough based on qualitative rideability evaluations of good, fair and poor at different driving speeds.

Highway pavement roughness has been studied and various quantitative methods such as international roughness index (IRI) (Sayers, 1995), and profile index (PI) (Sayers & Karamihas, 1998) have been developed in the last 30 years. However, none of these technologies are applicable to measuring rail-highway crossing roughness due to the short distance and unique structure of the crossing.

Technology already exists to map crossing surfaces at different levels of precision and at various costs. LiDAR (Light Detection Ranging), for example, is a remote sensing technology that measures distance and other properties such as shapes and dimensions by illuminating a target with a laser and analyzing the reflected light (Olsen, 2013). There are many applications of LiDAR in civil, construction and transportation engineering. One local example (Rister et al., 2013) uses LiDAR to verify bridge clearance heights on a western Kentucky parkway. Mobile LiDAR data can achieve an average accuracy of +/- 3cm or better, but comes with a high equipment cost (about 1 million USD). A lower cost option is desired in this research.

The objective of this chapter is to present the development and testing of a low-cost scanner for measuring rail crossing surfaces and a method for evaluating the crossings to support both safety and maintenance programs. The rest of the chapter is organized as follows. The processes of designing and building the structured-light scanner (SL Scanner)

follows in section 2. The use of the SL Scanner to collect 3D point cloud data is presented in section 3. Data analysis using the crossing surface data is demonstrated in section 4. Finally, conclusions regarding the current research and recommendations for future research are summarized.

3.2 Design and Construction

This section describes the design, construction and testing of a 3D structured light-based scanner to create an accurate point cloud of a crossing surface. The scanner was designed and built to use light patterns from a projector and a high resolution digital camera system to measure distortions of the shape of the image caused by depth and surface deviations to collect 3D position information of an object. Major parts included a frame, computer projector, computer, digital camera and data controller. The scanner provides high accuracy 3D data from a relatively low investment of about $5,000 in equipment.

As a scanner platform, a rail cart was built to include a frame with wheels, a laptop computer with structured light (SL) data capturing software, an 1100 watt AC/DC converter, power cables and power provided by the battery of a test vehicle as shown in Figure 3.1. Two cameras and projectors were used to practically double the scan area.

Figure 3.1 SL Scanner prototype.

A series of lab tests were performed as shown in Figure 3.2 to test the camera, lens, projector and software. During these tests, the SL scanner prototype was incrementally improved. For example, lenses were changed to the wide angle variety in order to capture larger scanning areas. The resulting scanner specifications include a minimum scan area of 3'x5' when the projector's lens is 42" above the surface to be imaged and a maximum scan area of 6'x10' when the projector's lens is 80" above the ground.

As the SL scanner projectors had 1280*800 resolution, pixels are about 0.25 centimeters average in size when the lens is at its highest point above the ground as shown in Figure 3.2. It is possible to scan at a rate of about one scan per 30 seconds in the field.

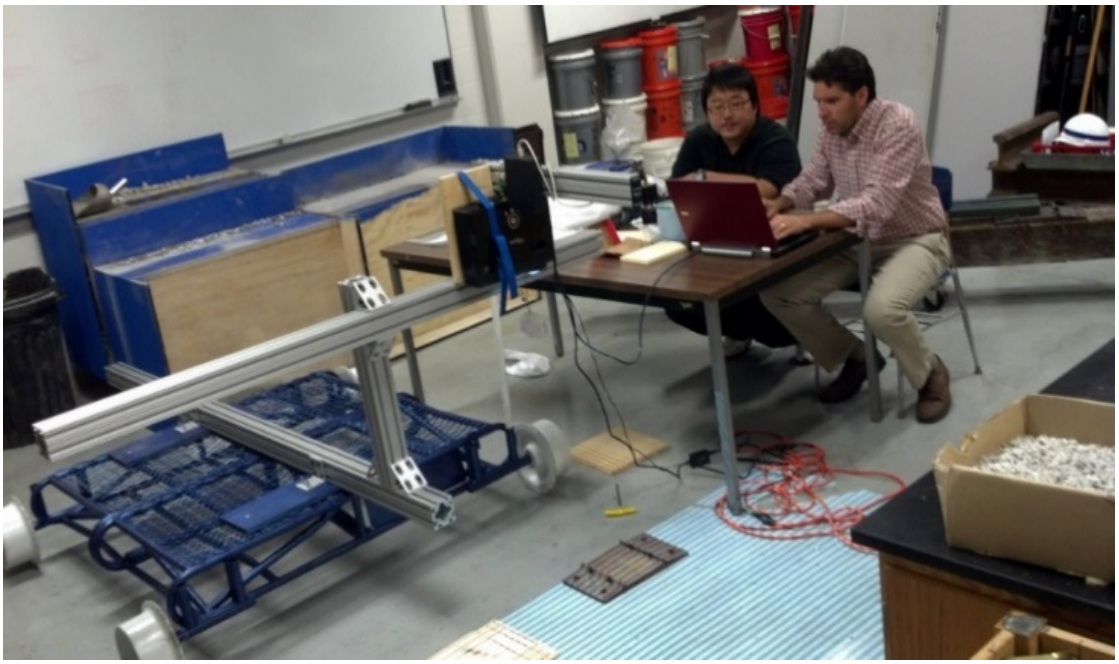

Figure 3.2 Lab test.

3.3 Field Tests

Several field tests were conducted at crossings around Lexington, KY and at the site of the Bluegrass Railroad Museum in Versailles, KY. Figure 3.3 pictures one field test at a crossing (USDOT 719862A) on Beasley Road, Versailles, KY. One scanner was mounted at each end of the beam of the SL scanner. Each scanner took one scan of one side of the crossing alternatively to avoid light patterns crossing. In the end, there were

total 52 scans collected for this crossing. The test took about 2 hours. During the scanning process, each scan was 6'x10' in size and one foot overlapped area in the longitudinal direction with the other scans before and after it. Two scanned 3D points clouds were shown in Figure 3.4 and Figure 3.5.

Figure 3.3 Field Test at crossing (USDOT 719862A) on Beasley Road, Versailles, KY.

Figure 3.4 Sample image of railroad approach to crossing.

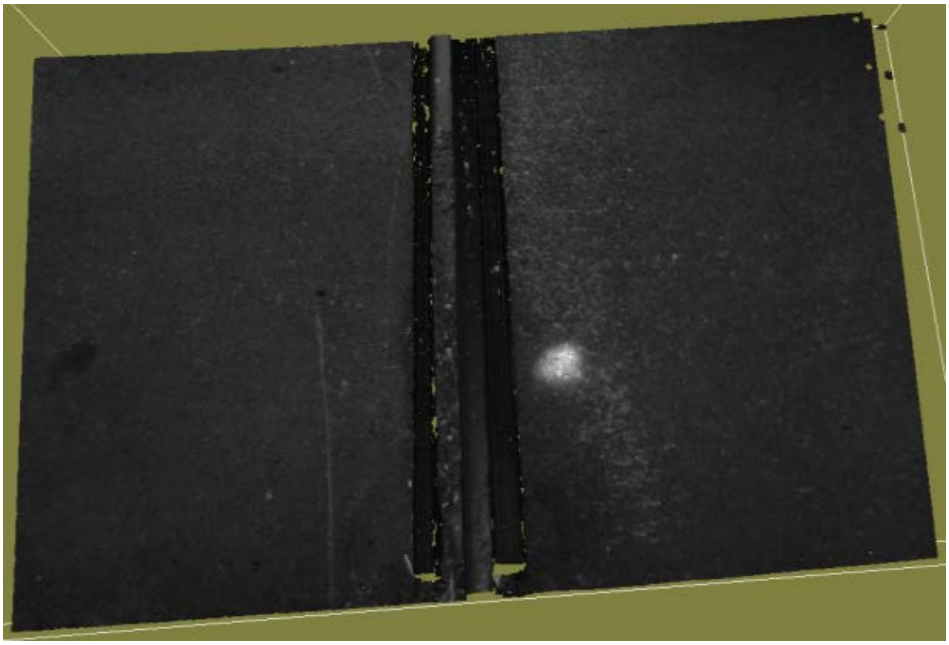

Figure 3.5 Sample image of flangeway.

Field test procedures and time needed for each are listed below.

Equipment loading……..30 minutes.

Equipment unloading and assembling……30 minutes.

Marking on the tie and road (every other tie) ……...5 minutes.

20 scans for one side of the track……15 minutes.

20 scans for another side of the track……..15 minutes.

Both scanners were mounted on the frame for weight balance, but only one scanner was used at a time due to the reasons of light interference at the overlapping area and limited power supply. Some overlapping areas are required for data merging, about 5 feet for lateral direction and 2 feet for longitudinal direction.

Some problems during the field test were encountered, first the scanner was very sensitive to vibration and need to be stabilized after every cart movement; second, although the data collection was performed at night starting at 9pm at a relative low traffic volume

road, the highway traffic still interrupted the data collection and more safety protections were required.

3.4 Data Analysis

Each 3D point cloud for the 10’ x 6’ in area at 1280x800 resolution is approximately 30 Megabytes in size. Adjacent scans can be stitched and merged by using data comparison (using scanning software developed by a research team member). In the field test, there were a total of 52 scanned 3D point clouds collected for the crossing. Using the overlapped area of every two contiguous scans, all scans were stitched and merged into one 3D surface image as shown in Figure 3.6.

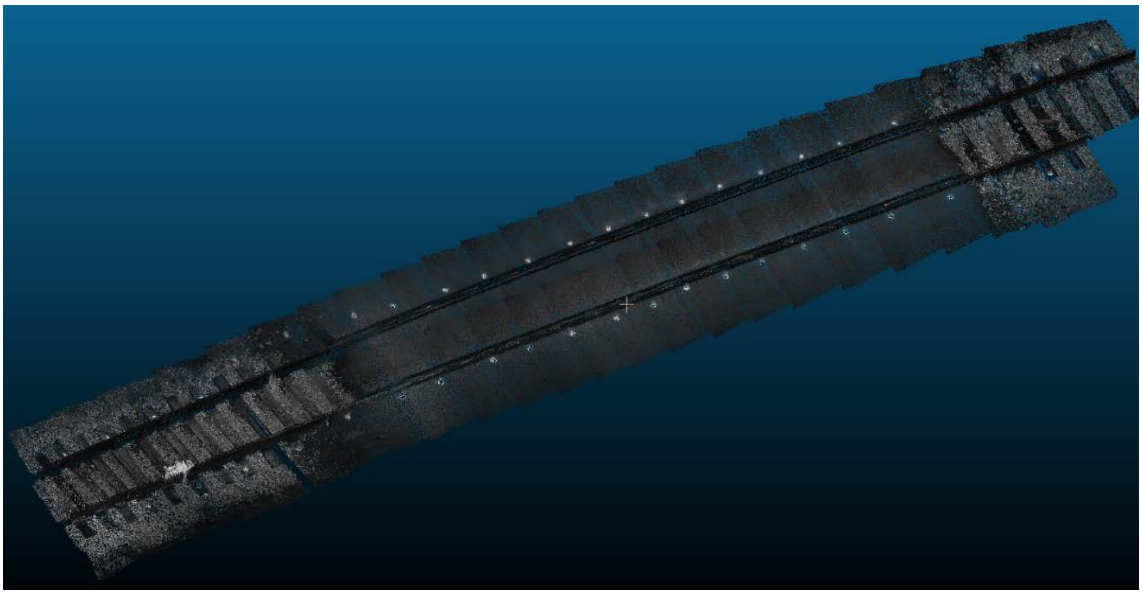

Figure 3.6 A composite rail-highway crossing surface 3D point cloud.

Each pixel’s coordinate is recorded to the nearest millimeter. Z coordinate values are plotted and can be visualized in Figure 3.7. Blue points indicate lower elevation, while red points are higher.

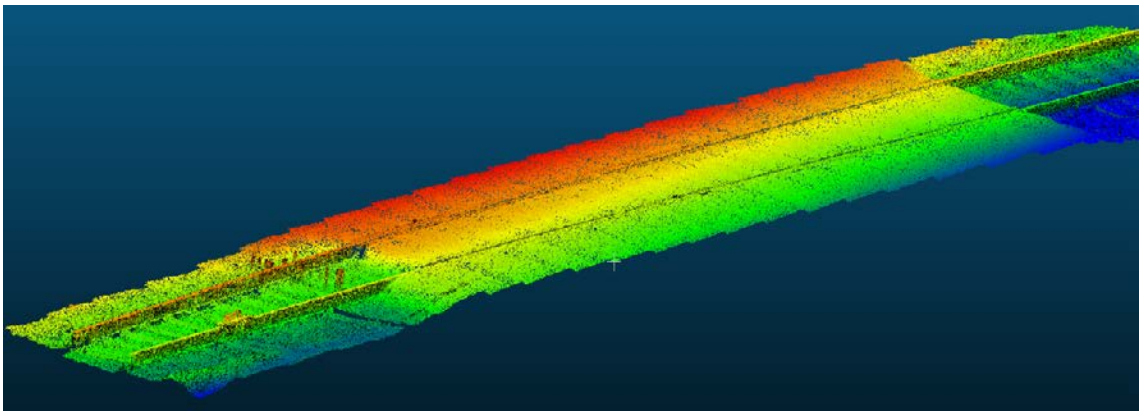

Figure 3.7 Elevation distribution of the crossing.

Figure 3.8 shows how the high resolution imagery can be used to measure depth of cracks, volume of bumps or area of pot-holes at the same crossing. In the figure, the blue area indicates relatively smooth surface while red indicates rougher area areas.

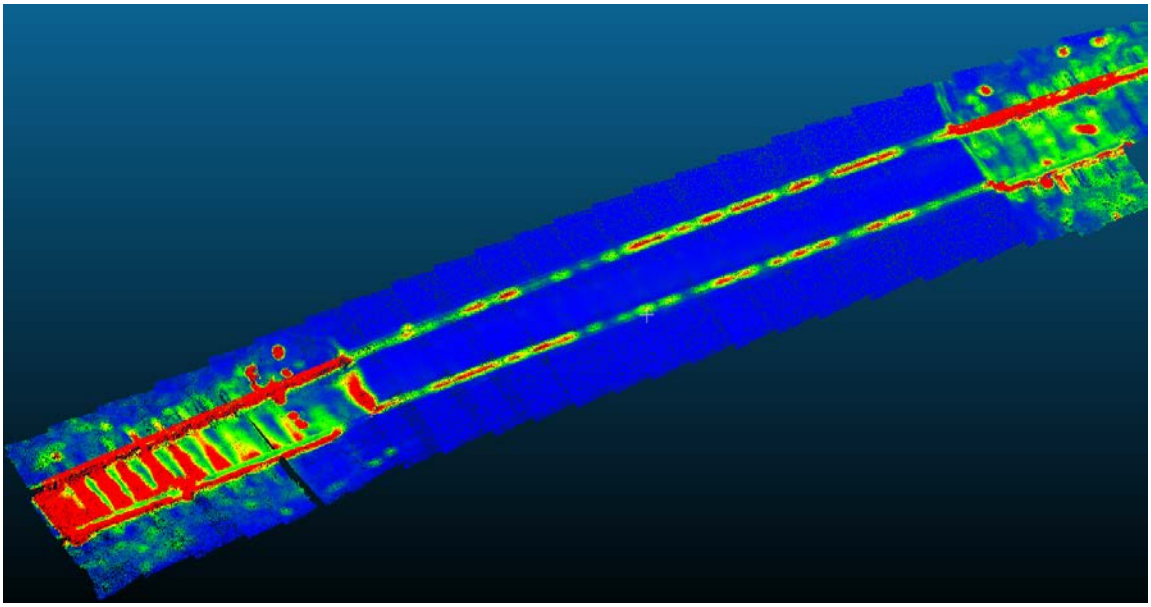

Figure 3.8 Surface condition of the crossing

3.5 Conclusion and Recommendations for Future Research

This chapter presented the development and testing of a prototype low-cost 3D scanner based on structured light technology. By creating a 3D point cloud using the SL scanner, the distance between any two points of the crossing can be measured. This

facilitates applications such as simulation of vehicle accelerations (Chapter 5), crossing roughness measurement (Chapter 6) or hump crossing identification and evaluation (Chapter 7). However, because the SL scanner could not be fully developed and deployed under the scope of this work, LiDAR is used to obtain 3D surface point clouds for the remainder of the work presented in this dissertation. For future application of the methodologies described in this dissertation, a fully developed LS scanner could be much cheaper and therefore accessible to smaller agencies or divisions of larger ones, as LiDAR units are currently capital intensive. Note that the applications of 3D data for roughness and rideability analysis would be the same, no matter the 3D collection method.

CHAPTER 4. USE OF ACCELEROMETERS TO ASSESS RIDEABILITY OF CROSSING

4.1 Introduction

Safety should always be a primary consideration for rail highway grade crossings. Driver inattention and decision making may be especially critical in the vicinity of a crossing. Thus, it has long been speculated that rail highway crossing roughness may be related to highway safety. As far back as 1973, a study by Thomas Butcher (Butcher, 1973) noted that drivers will change speed based on the roughness of the crossing. A more recent study by Christina Brown (Rudin-Brown et al., 2014) suggested that poor surface conditions tend to divert drivers' attention while driving over crossings. The US DOT Railroad Highway Grade Crossing Handbook (US Department of Transportation, 2007) also suggests that rough surfaces could distract a driver's attention from oncoming trains and that the unevenness of the crossing could result in a driver losing control of their vehicle, potentially contributing to the cause of a crash.

To determine if surface plays a role in crossing safety, one must first be able to quantify the rideability of the surface. Conventionally, inspectors rate crossings by driving over the crossing several times to determine what is typically a poor, fair or good rating. In addition to crossing rideability, these subjective ratings may also be influenced by an inspector's experience, test vehicle, or even how the inspector is feeling at the time of the test. Clearly, these may be different from inspector to inspector for actual crossings. A quantifiable method is therefore desired.

In the past, accelerometers have been used to assess rideability for roadway sections (Cong et al., 2012), but not for crossings. The objectives of this chapter are to 1) develop and assess a technique to measure accelerations experienced by drivers at crossings and 2) develop an acceleration-based metric for quantifying rideability.

The objective of this research was to develop a method to quantify rideability as a function of accelerations for various vehicle types. The method is tested for repeatability, sensor reliability, and data accuracy. In addition to providing a way to quantify crossing rideability, acceleration data collected and reported in this chapter are also used to calibrate and validate a vehicle dynamic model presented in Chapter 5 of this dissertation.

4.2 Development and Assessment of Acceleration Data Collection and Testing Protocol

A 2011 Chevrolet Impala sedan was chosen as the vehicle for collecting initial acceleration data and developing the testing protocol. Other equipment and devices used included 1) a real time accelerometer (PASCO® model number PS-2119) which records and stores 3 axis (XYZ) acceleration data at 100 hertz within the range of +/- 10 g, an accuracy +/- 1% and a resolution of 0.010 g, 2) a laptop PC preloaded with PASCO® real time recording software, 3) a smart phone to record and store GPS coordinates and vehicle speeds at 1 hertz (see Figure 4.1), and, 4) a stop watch. Both the accelerometer and smart phone were mounted on the top center of the dashboard of the vehicle during the test.

Figure 4.1 Smart phone GPS user interface.

A field test was conducted at the Norfolk Southern Brannon Road Crossing in Jessamine County, KY, just south of Lexington (USDOT Crossing number 841647U) as shown in figure 4.2. Approximately 5,900 highway vehicles and about 70 trains per day use the crossing. The FRA Web Accident Prediction System (WBAPS) predicted number of crashes per year at this crossing is 0.042 (Federal Railroad Administration (FRA)). Along the proximate three mile section of Brannon Road, there have been 263 highway crashes in the past ten years. Typically, crash contributing factors include narrow lanes, insufficient shoulders, poor visibility due to numerous hills and curves and others.

Highway traffic is projected to grow to 14,000 vehicles per day by 2040 (Essig). To improve the safety of the road, a major highway project is being planned and scheduled by the Kentucky Transportation Cabinet.

The crossing is generally rough as can be seen in elevation changes on the highway approaches as depicted in Figure 4.3.

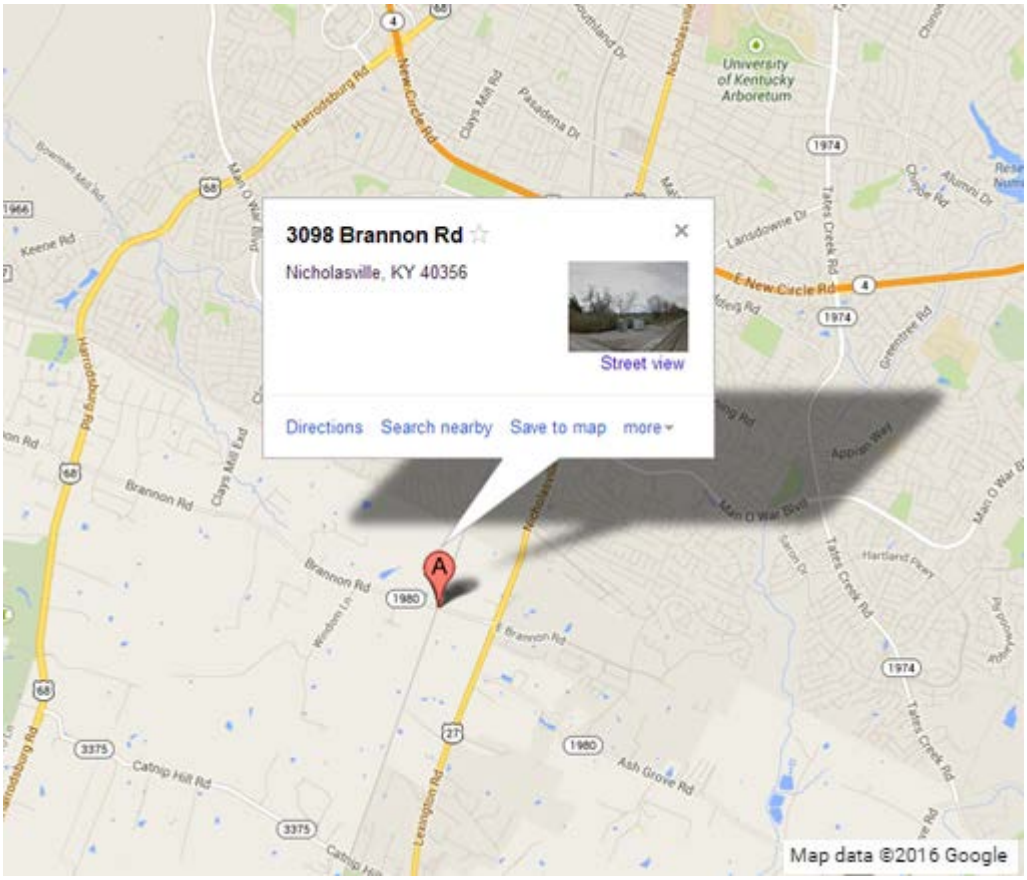

Figure 4.2 Location of the Brannon Road crossing.

Figure 4.3 Brannon Road crossing.

Two students performed data collection: a driver who tried to drive at a constant speed over the crossing, and a passenger recording the time before and after passing the crossing at reference points. The accelerometer and GPS were kept running during the entire test. See Figure 4.4 for a photo of the test vehicle.

Figure 4.4 Field acceleration data collection.

Acceleration data were divided into eastbound and westbound groups for the crossing. The driver tried to maintain the 35 mph posted highway speed or as close to it as possible. Other tests were run at speeds as low as 15 mph (posted for the crossing) and as high as 45 mph. However, accelerations at 15 mph were negligible.

4.3 Repeatability

For each test, the vehicle was driven at a constant speed and as straight as possible through the crossing. Acceleration on the Z axis (vertical direction) was collected for later analysis of crossing roughness. Acceleration was plotted versus time for a period of approximately 10 seconds before and 10 seconds after the vehicle passed the crossing. Average vehicle speed was obtained from the smart phone GPS (using time stamps).

To begin with, 16 tests were performed eastbound and 18 westbound. Aggregated results are shown in Figure 4.5 and 4.6 for each direction, respectively. (Individual test plots can be found in **APPENDIX A**.)

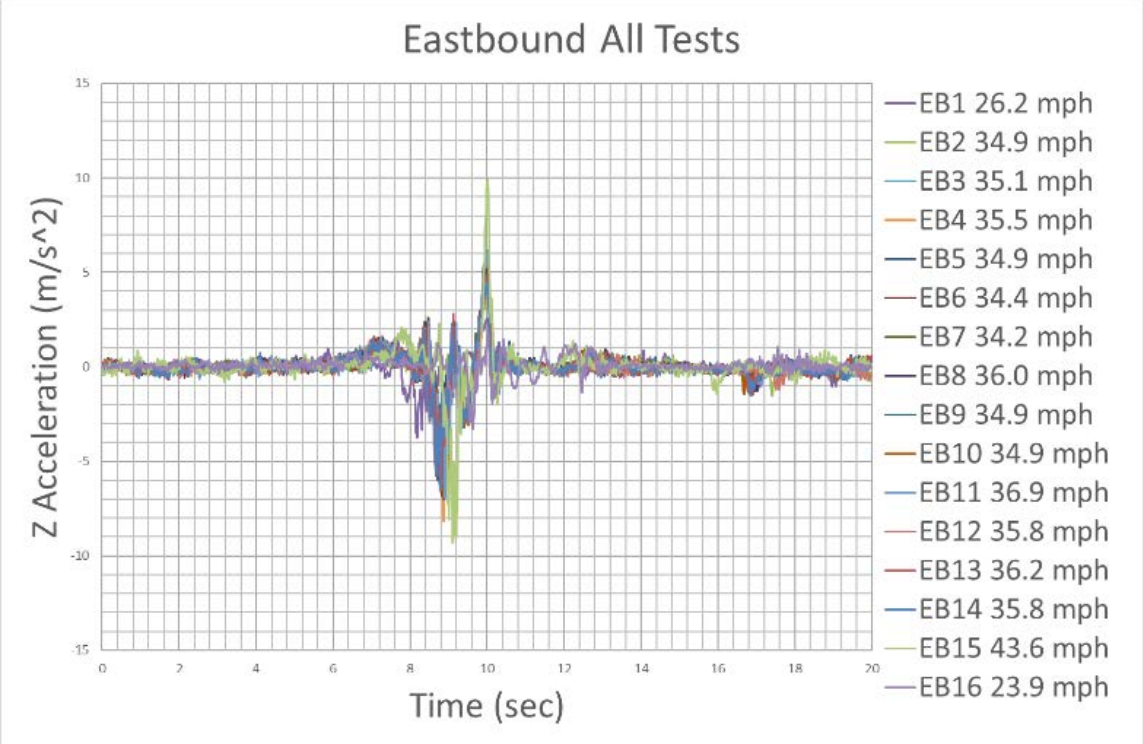

Figure 4.5 Eastbound acceleration tests.

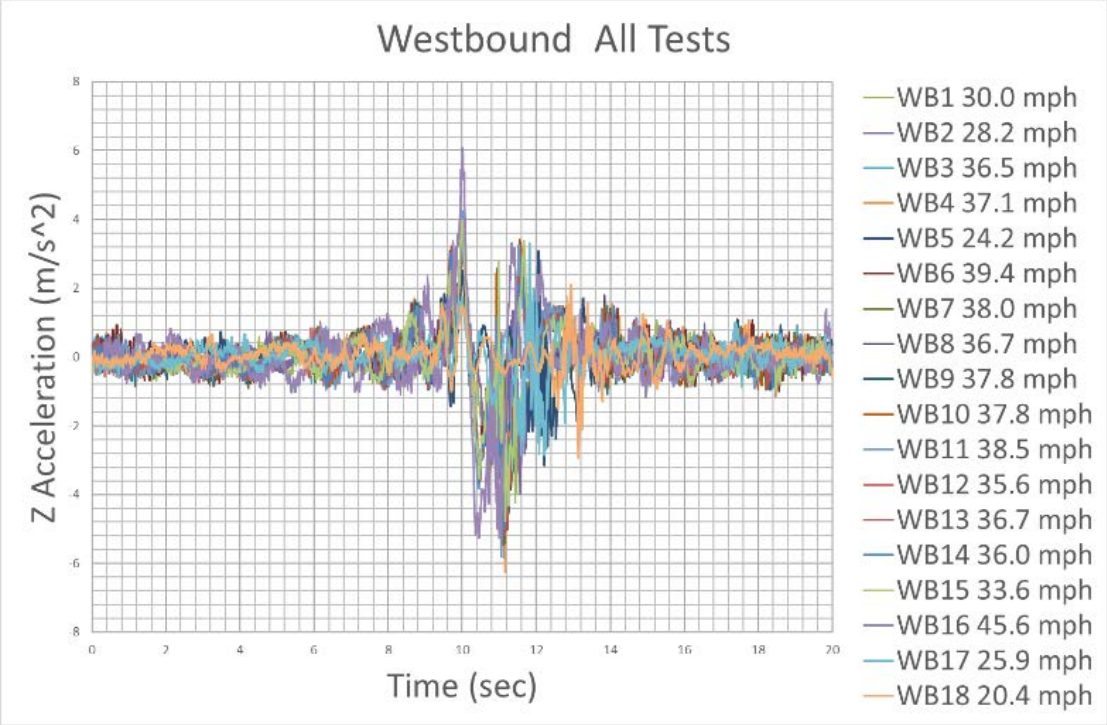

Figure 4.6 Westbound acceleration tests.

For each of the eastbound and westbound groups, 10 tests with speeds closest to 35 mph were selected. Results are shown in Figures 4.7 and 4.8.

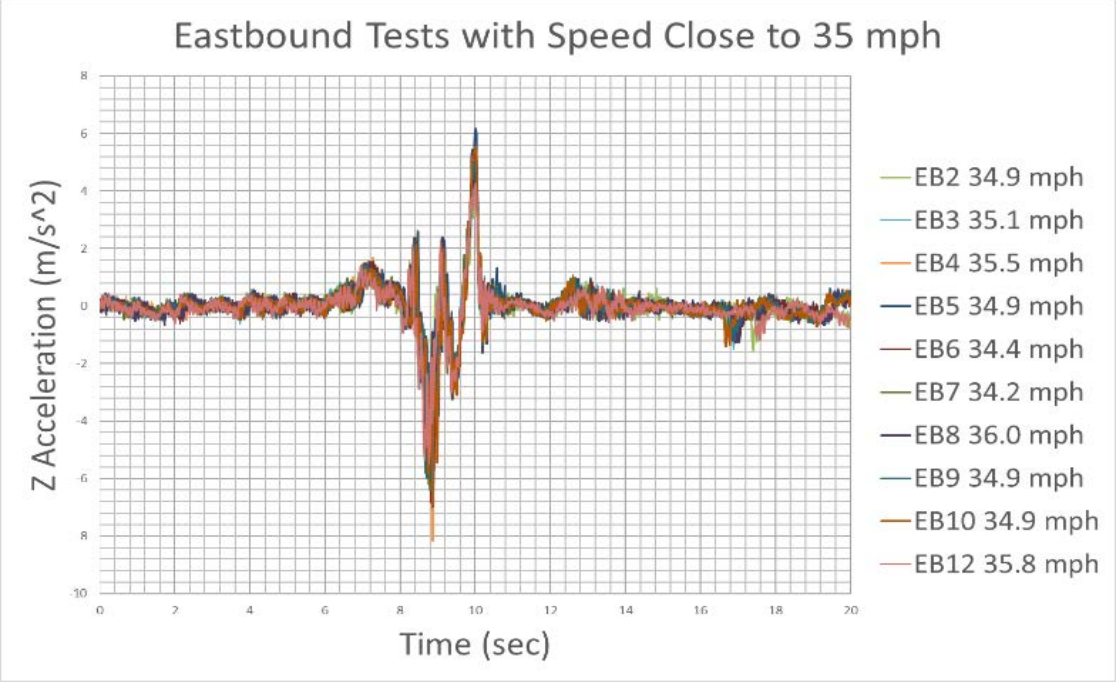

Figure 4.7 Eastbound tests with speed close to 35 mph.

Figure 4.8 Westbound tests with speed close to 35 mph.

Figures 4.7 and 4.8 both indicate that, when the test speed is held nearly constant (35 mph), both the frequency and amplitude of acceleration from one test are very close. This indicates that the test is highly repeatable and method is reliable for future work.

To test the effect of speed variation on accelerations, several bidirectional tests were performed at various speeds. Results of these tests are shown in Figures 4.9 and 4.10.

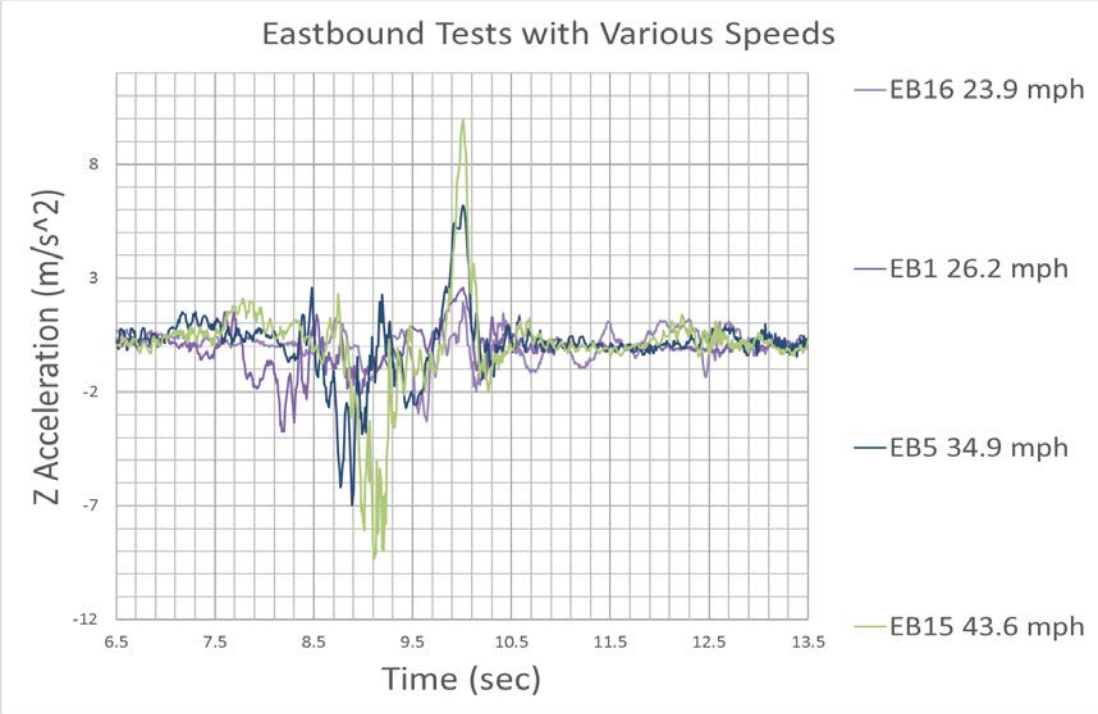

Figure 4.9 Eastbound tests with various speeds.

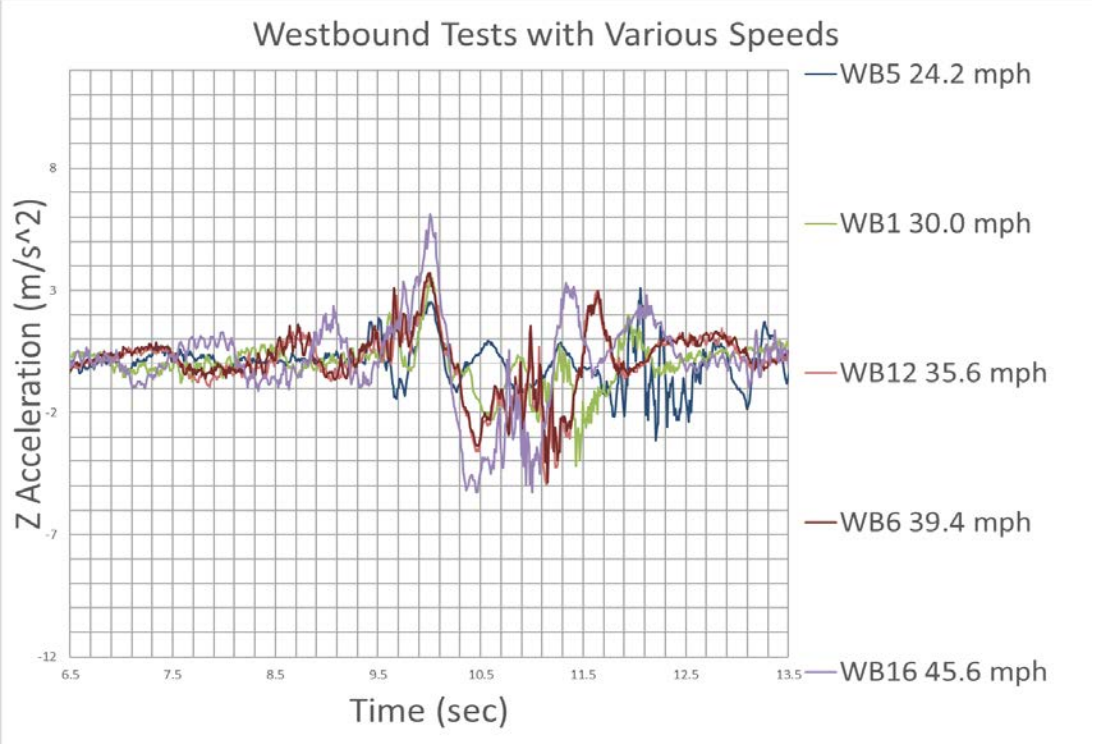

Figure 4.10 Westbound tests with various speeds.

From Figures 4.9 and 4.10, it can be seen that, as expected, acceleration amplitudes and frequencies increase with increasing speeds.

Overall, tests with accelerometers are shown to be repeatable and sensor reliability and accuracy appear to be sufficient for developing an acceleration-based metric for quantifying rideability at crossings.

4.4 Speed Bump Tests and Data Collection

Preliminary testing indicated that accelerometers are reliable and repeatable using one vehicle at one crossing. To be of practical value, the procedure must be tested using multiple vehicles, as the Impala used will not be available to others desiring to use the methodology. To develop a procedure to calibrate any vehicle for use as a test vehicle, a standard road profile was desired. A portable speed bump provided such a standard profile. A portable standard free-standing rubber speed bump with dimensions of 2.5" H by 18" W by 120"L was used for the research as shown in figure 4.11.

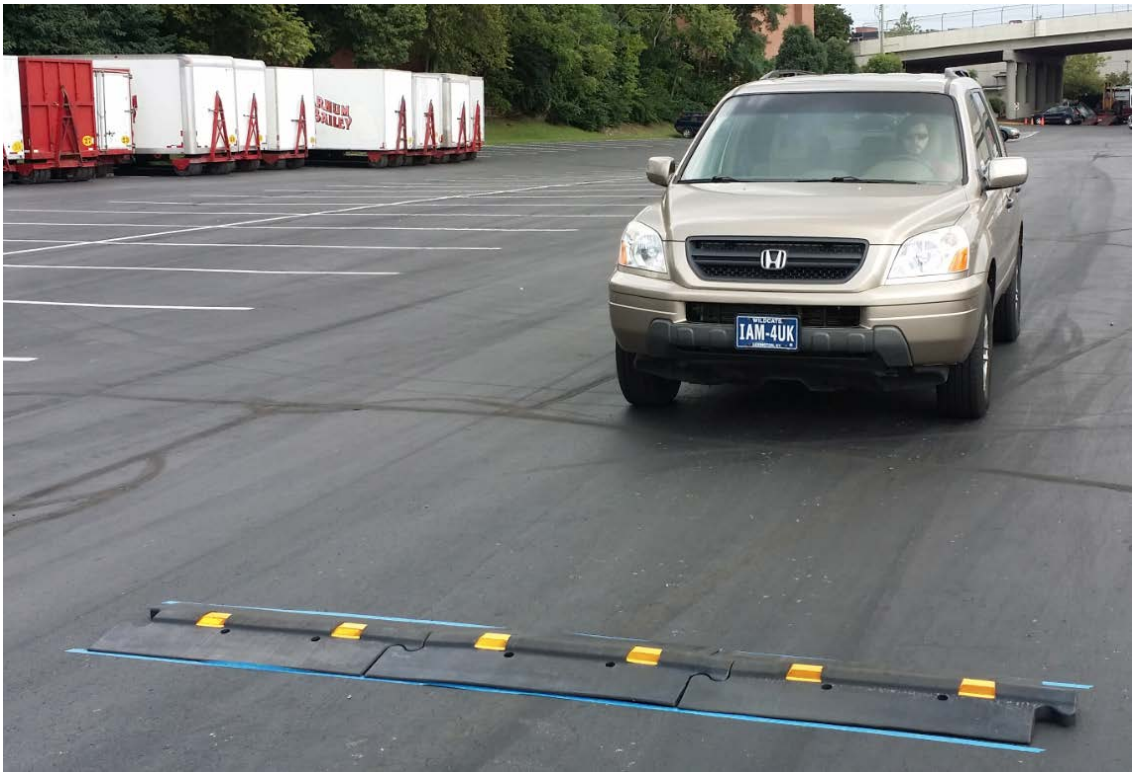

Figure 4.11 Acceleration collection test at a speed bump.

This section discusses the testing of multiple vehicles at the speed bump, attempting to provide a controlled, simplified and repeatable condition for calibrating various vehicles. With a constant profile, variation in acceleration between vehicles is assumed to be a function of the vehicle only.

Six different vehicles of types ranging from passenger vehicles to SUVs and trucks were used to perform tests at different speeds. The vehicles selected were:

1) 2004 BMW 530i sedan
2) 2006 Ford F150 truck
3) 2011 Chevrolet Impala sedan
4) 2005 Honda Pilot SUV
5) 2006 Jeep Grand Cherokee SUV
6) 2002 Toyota Tacoma truck

The vehicles were selected based on availability, but represent a good variation in vehicle weight and suspension.

All tests were performed at an empty, level, ground parking lot with enough runway distance before and after the speed bump to accelerate to the desired speed and decelerate safely. The same accelerometer and testing protocol were used as described in section 4.3. Vehicles were driven at speeds ranging from 10 mph to 45 mph at 5 mph intervals. All vehicles were driven in a straight line, perpendicular to the speed bump, and at a constant speed. Several runs of each vehicle-speed combination were performed to check repeatability and to average out small variations in speed. Multiple runs also provided more data when speed varied. Over 340 speed bump tests were conducted in all. After the acceleration data were collected, analysis of vehicle performance was conducted. That analysis is presented in the following sections.

4.5 Railroad Crossing Field Tests and Data Collection

After acceleration data for the six vehicles were collected using the speed bump, tests were conducted for the same six vehicles at five different rail highway crossings near the city of Lexington, Kentucky. These crossings are described in table 4.1 below.

Table 4-1 Railroad crossings in the acceleration test.

Location	Bryan Station Rd	Briar Hill Rd	Hatton Rd	Bridgeport-Benson Rd	Devil's Hollow Rd
USDOT ID No.	346839X	346842F	346726S	346730G	346732V
Highway speed mph	55	55	55	55	55
Posted speed mph	30	35	20	25	35

Aerial photos of each crossing were obtained from Google Maps® and are shown below in Figures 4.12 to 4.16.

Figure 4.12 Bryan Station Road crossing.

Figure 4.13 Briar Hill crossing.

Figure 4.14 Hatton Road crossing.

Figure 4.15 Bridgeport-Benson Road crossing.

Figure 4.16 Devil's Hollow Road crossing.

Testing followed the same protocol detailed above in section 4.2. The six vehicles were driven over these crossings from both directions at speeds of 20 mph, 25 mph, 30 mph, 35 mph and 40 mph (if it was safely achievable). At least two tests were performed

for each vehicle, speed, and direction at each crossing. In total, over 450 tests were completed.

4.6 Analysis and Results

The sections above reported that acceleration measurements for the same crossing, vehicle and speed are repeatable, both in magnitude and shape of response. Acceleration data were collected at a speed bump and at five crossings using six vehicles at varying speeds. Based on these data, the following sections present the development and analysis of two metrics of crossing rideability: 1) maximum positive or negative acceleration reading, and 2) root mean square (RMS) of acceleration readings.

4.6.1 Maximum Positive or Negative Acceleration

The maximum positive or negative acceleration experienced by a particular type of vehicle could be proposed as a metric with which to compare the rideability of crossings. However, it may not always be possible to use one particular type of vehicle to obtain readings for every crossing. Therefore, it is desirable to have a method of calibrating any "test" vehicle, such that its readings could be converted to those of a common "design" vehicle.

4.6.1.1 Using Maximum Accelerations at a Speed Bump to Calibrate a Test Vehicle

The kinetic energy of a vehicle translates to vertical acceleration when a tire crosses the uneven profile of a crossing. Accelerations are therefore expected to monotonically increase with increasing speed. The maximum positive and negative accelerations for different vehicles and speeds crossing the speed bump are plotted below in Figure 4.17 and Figure 4.18.

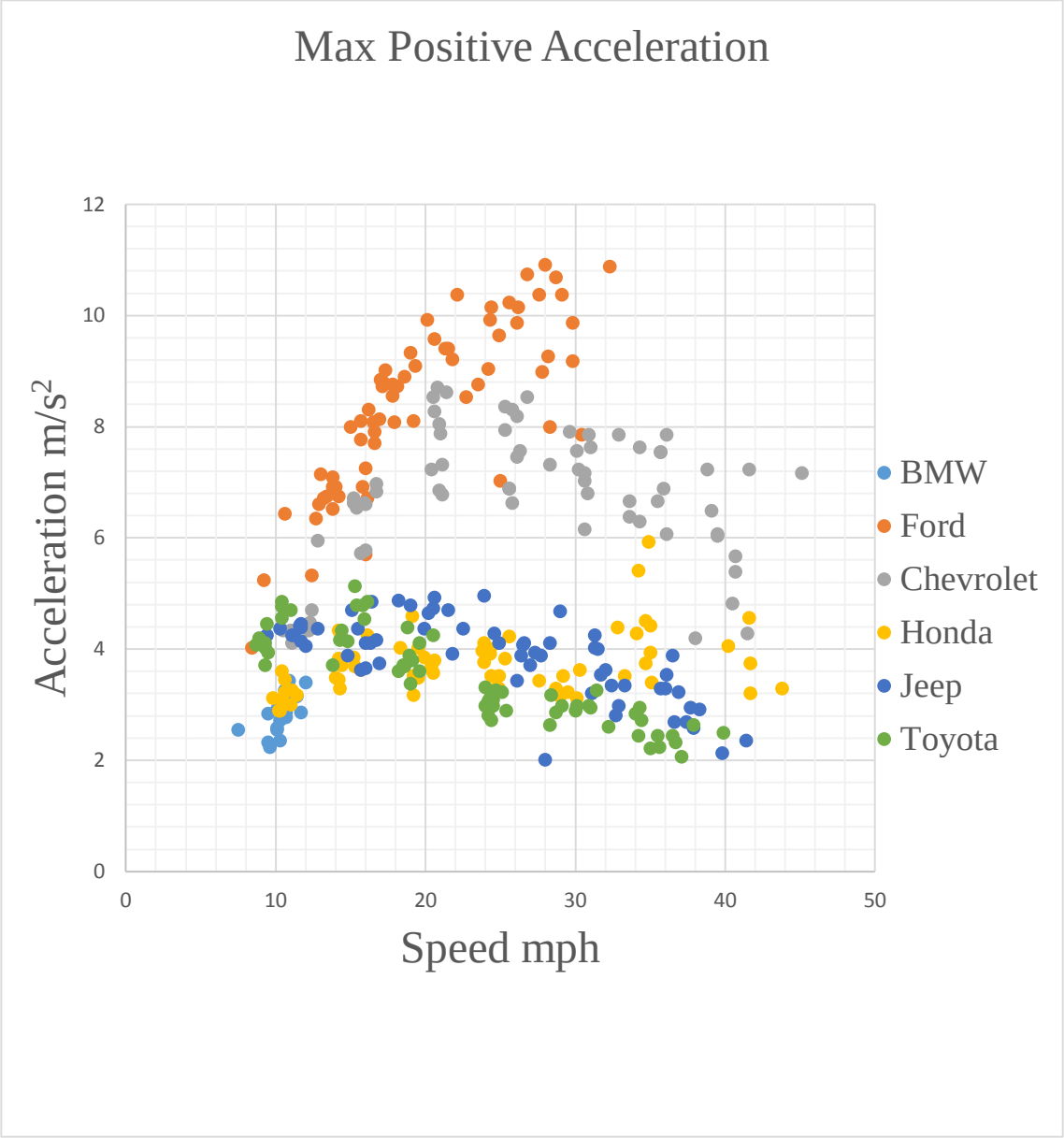

Figure 4.17 Max positive acceleration at the speed bump.

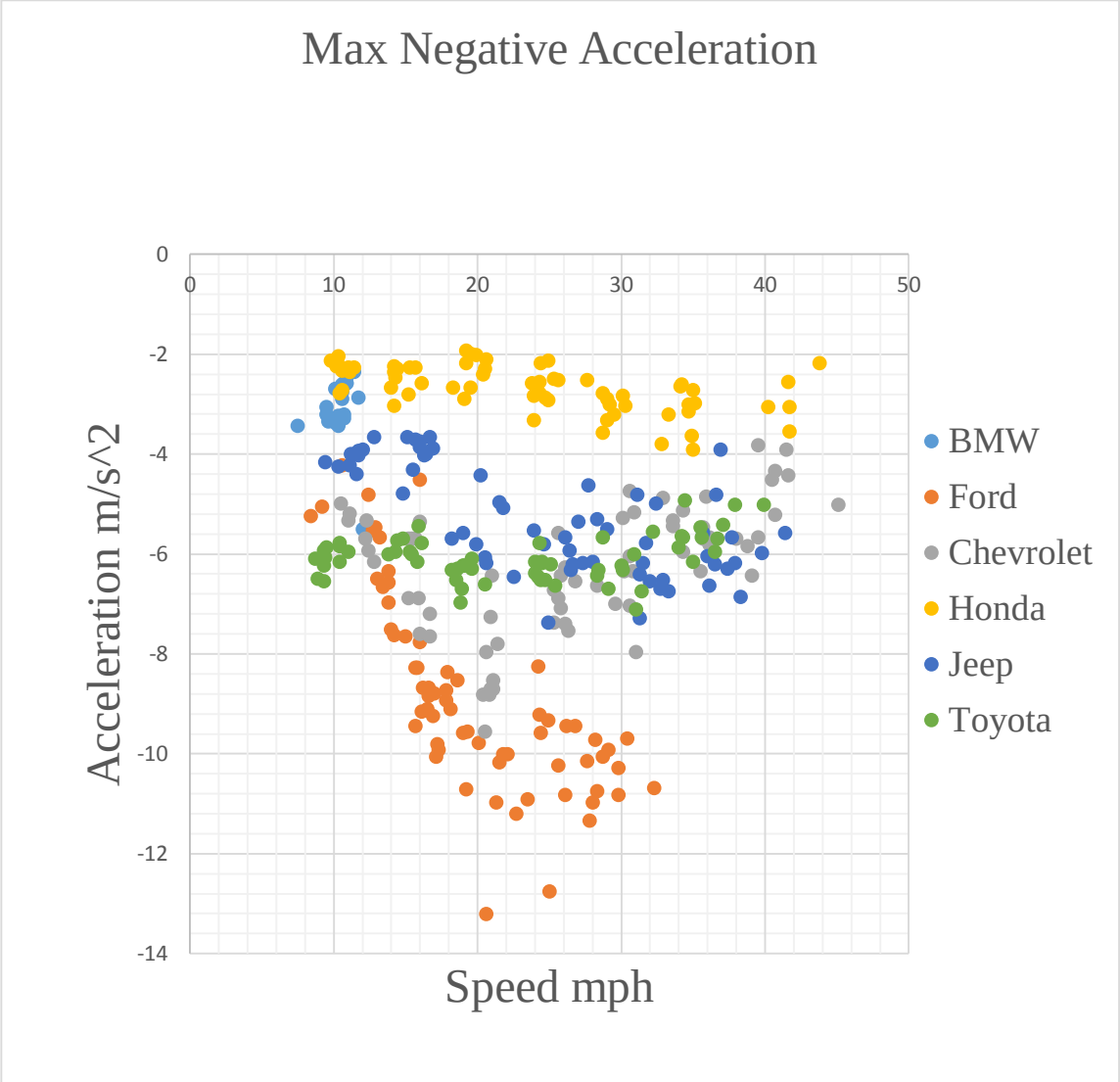

Figure 4.18 Max negative acceleration at the speed bump.

From Figure 4.17 and Figure 4.18, it can be seen that, for the same vehicle, the relationship between the maximum acceleration on the Z axis and speed is not as expected! Higher speeds do not always lead to higher acceleration. It turns out that the relationship between speed and vertical acceleration is more complicated than expected, probably due to nonlinear damping due to a combination of vehicle tires, suspensions, frame, body and interior cabin isolations. Even for vehicles of the same type, such as sedan, SUV and trucks, different vehicles performed quite differently.

The maximum positive and negative accelerations of a test vehicle are used to predict the accelerations that may be experienced by a design vehicle at various crossings

using accelerations at a speed bump as a control. The predicted design vehicle acceleration is computed by multiplying the acceleration experienced by the test vehicle by the ratio of accelerations experienced by the design and test vehicles at the speed bump, as follows:

Equation 4-1

$$a_{D,C} = a_{T,C} \times \left(\frac{a_{D,S}}{a_{T,S}}\right)$$

Where,

$a_{D,C}$ = The predicted design vehicle acceleration at the crossing.

$a_{T,C}$ = The test vehicle acceleration at the crossing.

$a_{D,S}$ = The design vehicle acceleration at the speed bump.

$a_{T,S}$ = The test vehicle acceleration at the speed bump.

Two tests were conducted. First, the data from the Jeep (test vehicle) were used to predict the accelerations of the Impala (design vehicle) for different speeds at the study crossings. Results of those predictions for maximum positive accelerations can be seen in Table 4-2 and Figure 4.19.

Table 4-2 Using Jeep maximum acceleration to predict Impala maximum acceleration.

Actual Jeep MAX Positive Acc. @ Speed		Highway Rail Crossing					
		Bryan Station	Briar Hill	Hatton	Bridgeport-Benson	Devil's Hollow	Speed Bump
Speed mph	15	--	--	--	--	--	4.3
	20	1.2	1.3	2.3	2.7	2.3	4.3
	25	1.2	2.2	4.4	3.5	3.3	4.1
	30	1.6	3.9	--	3.3	3.9	3.8
	35	2.6	4.4	--	3.4	2.6	3.2
	40	3.5	--	--	--	--	2.5
Actual IMPALA MAX Positive Acc. @ Speed		Highway Rail Crossing					
		Bryan Station	Briar Hill	Hatton	Bridgeport-Benson	Devil's Hollow	Speed Bump
Speed mph	15	--	--	--	--	--	6.1
	20	1.4	1.4	2.8	5.0	4.0	7.1
	25	2.7	3.0	6.8	3.6	4.4	7.6
	30	3.6	4.6	--	3.4	6.0	7.6
	35	4.9	4.8	--	--	6.5	7.1
	40	3.9	8.2	--	--	--	6.0
Predicted IMPALA MAX Positive Acc. @ Speed		Highway Rail Crossing					
		Bryan Station	Briar Hill	Hatton	Bridgeport-Benson	Devil's Hollow	Speed Bump
Speed mph	15	--	--	--	--	--	N/A
	20	2.0	2.1	3.8	4.4	3.8	N/A
	25	2.2	4.0	8.1	6.4	6.1	N/A
	30	3.2	7.9	--	6.6	7.9	N/A
	35	5.7	9.6	--	7.4	5.7	N/A
	40	8.3	--	--	--	--	N/A

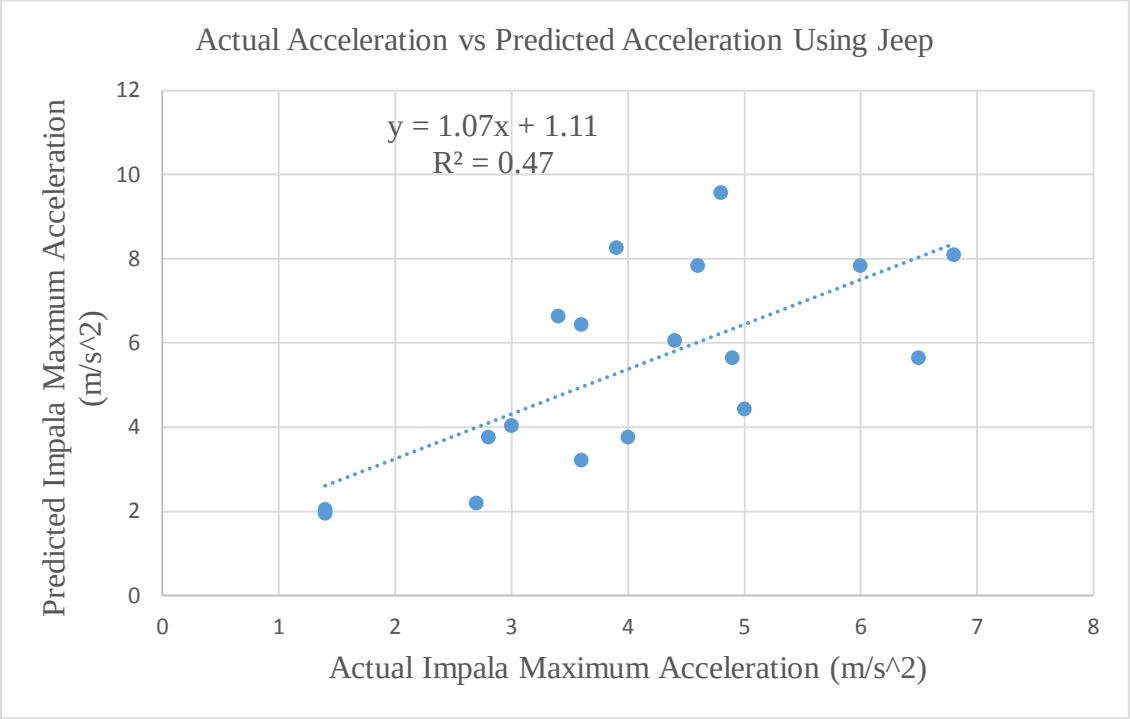

Figure 4.19 Impala actual acceleration vs predicted acceleration using Jeep as the test vehicle.

A second test was conducted using the F150 to predict the performance of the Impala. Results are similar and are shown in Table 4-3 and Figure 4.20.

Table 4-3 Using F150 maximum acceleration data to predict Impala maximum acceleration.

Actual F150 MAX Positive Acc. @ Speed		Highway Rail Crossing					
		Bryan Station	Briar Hill	Hatton	Bridgeport-Benson	Devil's Hollow	Speed Bump
Speed mph	15	--	--	--	--	--	7.4
	20	--	1.3	1.8	4.4	4.0	8.9
	25	1.9	2.2	3.1	2.7	4.2	9.7
	30	2.2	3.9	--	2.1	4.6	9.7
	35	2.0	4.4	--	--	3.8	9.0
	40	3.0	--	--	--	3.6	7.6
Actual IMPALA MAX Positive Acc. @ Speed		Highway Rail Crossing					
		Bryan Station	Briar Hill	Hatton	Bridgeport-Benson	Devil's Hollow	Speed Bump
Speed mph	15	--	--	--	--	--	6.1
	20	1.4	1.4	2.8	5.0	4.0	7.1
	25	2.7	3.0	6.8	3.6	4.4	7.6
	30	3.6	4.6	--	3.4	6.0	7.6
	35	4.9	4.8	--	--	6.5	7.1
	40	3.9	8.2	--	--	--	6.0
Predicted IMPALA MAX Positive Acc. @ Speed		Highway Rail Crossing					
		Bryan Station	Briar Hill	Hatton	Bridgeport-Benson	Devil's Hollow	Speed Bump
Speed mph	15	--	--	--	--	--	N/A
	20	--	1.0	1.4	3.5	3.2	N/A
	25	1.5	1.7	2.4	2.1	3.3	N/A
	30	1.7	3.0	--	1.6	3.6	N/A
	35	1.6	3.4	--	--	3.0	N/A
	40	2.4	--	--	--	2.8	N/A

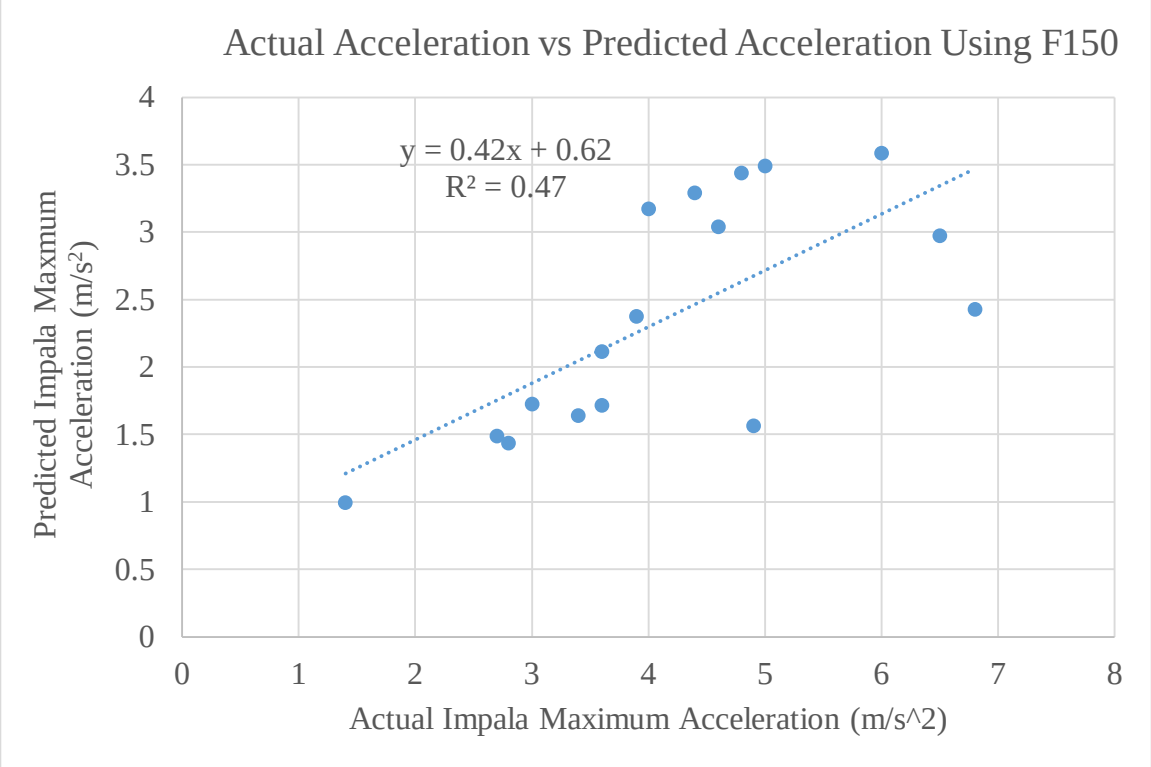

Figure 4.20 Impala actual acceleration vs predicted acceleration using F150 as the test vehicle.

This section demonstrated the use of a speed bump to calibrate test vehicles using maximum positive and negative acceleration as performance metrics. Results were promising, but inconclusive with a relatively low R squared value as shown in Figure 4.19 and Figure 4.20. Because speed bumps are designed to warn drivers of excessive speeds, not damage vehicles, and because vehicle and their suspensions behave nonlinearly with regards to accelerations crossing speedbumps, it is thought that vehicle accelerations at actual crossings may behave more predictably. That is, accelerations should be higher for increasing speeds at a given crossing. Therefore, a “reference crossing” might be better able to calibrate test vehicles.

4.6.1.2 Using Maximum Accelerations at a Crossing to Calibrate a Test Vehicle

To test the theory that a reference crossing may work better than a speed bump for calibration, multiple tests were performed at crossings using the six test vehicles. Maximum positive and negative accelerations are plotted for five crossings in each direction. Figure 4.21 shows the performance of various vehicles at Briar Hill Rd. For this crossing, results are as expected, as higher speeds induce higher accelerations. However, Figure 4.22 shows that for a different crossing, Devil's Hollow Rd., accelerations are not related to speed. This is because while the Devil's Hollow crossing appears to be in much worse condition than the Briar Hill Rd., crossing, it is relatively flatter in overall profile. Calibrating a vehicle at such a crossing will not work. Plots for the other crossings are provided in **APPENDIX B**.

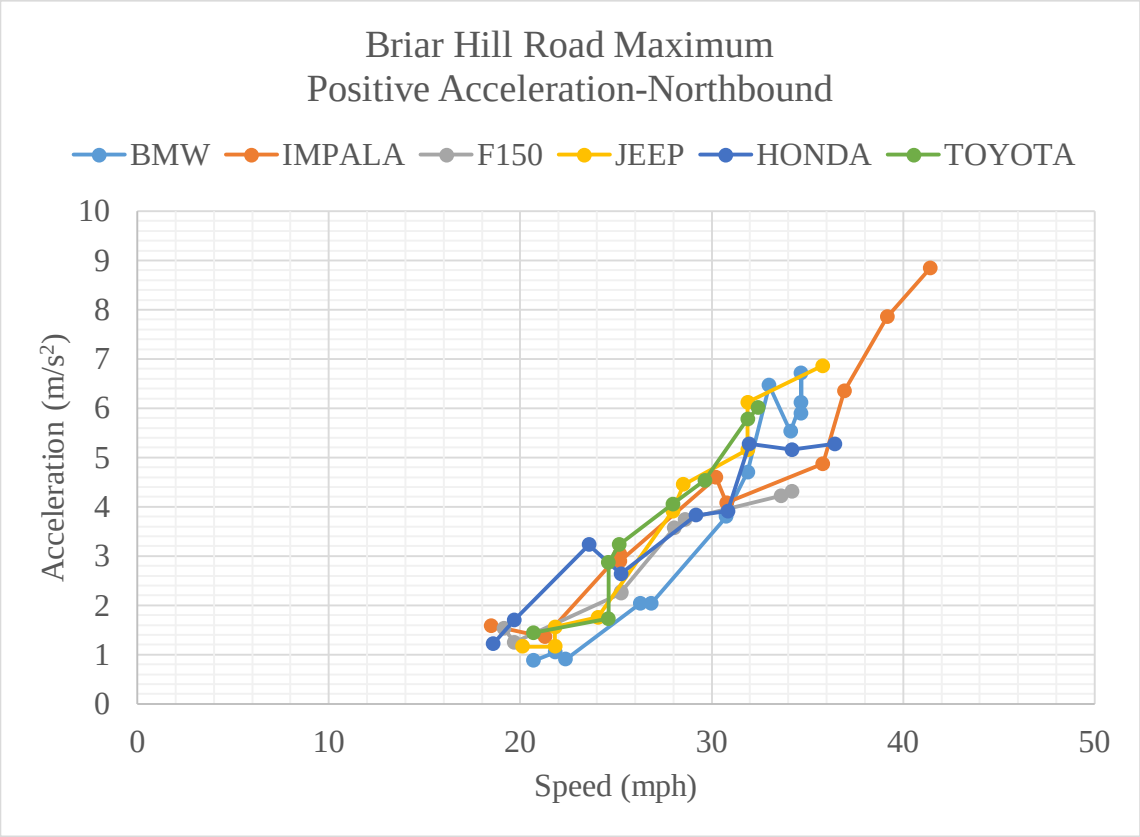

Figure 4.21 Briar Hill Road maximum positive acceleration-northbound.

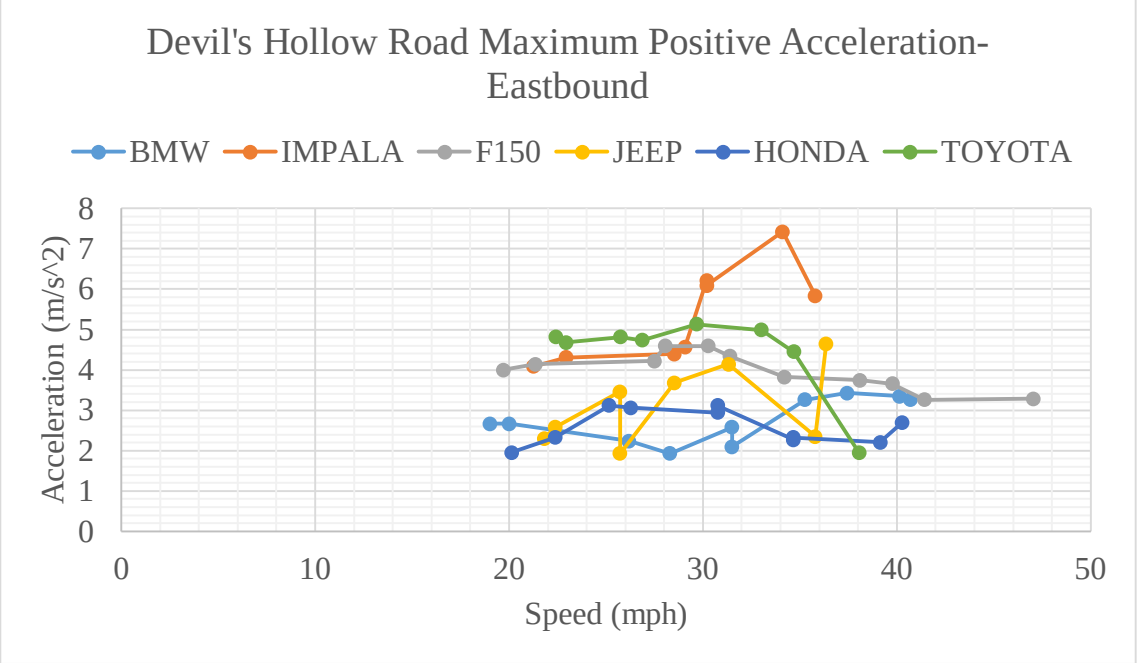

Figure 4.22 Devil's Hollow Road maximum positive acceleration-eastbound.

The response of individual vehicles was also tested across various crossings. Figure 4.23 shows the response of the BMW at various crossings by direction. Results are as expected, as at the crossings with more terrain change, accelerations increase with increasing speeds. Similar plots are provided in **APPENDIX C** for the other vehicles.

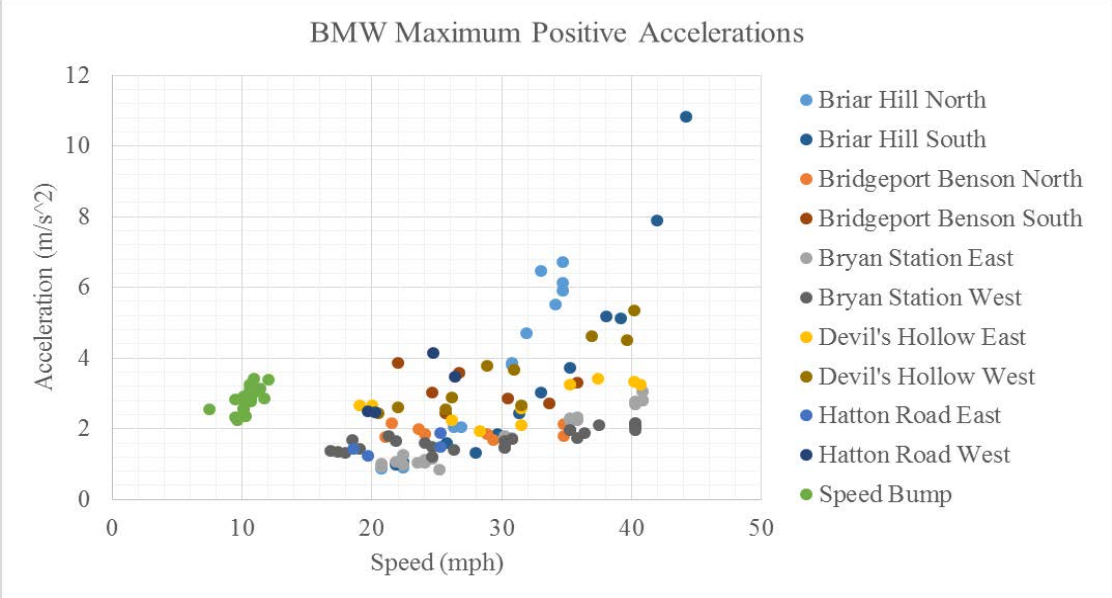

Figure 4.23 BMW maximum positive acceleration.

Upon careful examination of the data presented in these series of plots, it was determined that *maximum positive or negative accelerations* at a reference crossing would not be any more useful than the speed bump for calibrating test vehicles. Improvement is desired, and the next section presents a strategy that is not based simply on the maximum positive or negative acceleration.

4.6.2 Root Mean Squares (RMS)

In the previous section, only two data points (maximum positive or negative acceleration) were used to calibrate test vehicles. However, much more data are available, as vehicle accelerations were measured at 100Hz. To make use of this *rich* data source and improve the performance of the test vehicle calibration technique, more of the data are used in this section to compute a new metric of accelerations. To do this, six seconds of high frequency data are used (three seconds before, to three seconds after, the time of maximum acceleration—600 data points). The root mean squares (RMS) of these readings are computed using Equation 4-2. RMS has the advantage not only of addressing problems with negative values cancelling positive values, but the metric is also proportional to the total energy dissipated by the vehicle when passing the crossing.

Equation 4-2

$$RMS = \sqrt{\frac{1}{N}\sum_{i=1}^{N} a_i^2}$$

Where:

N= the total number of acceleration data points, 600.

a = acceleration in m/s^2.

4.6.2.1 Using RMS of Accelerations at a Speed Bump to Calibrate a Test Vehicle

The RMS of accelerations (RMS) for different vehicles and speeds crossing the speed bump are plotted below in Figure 4.24.

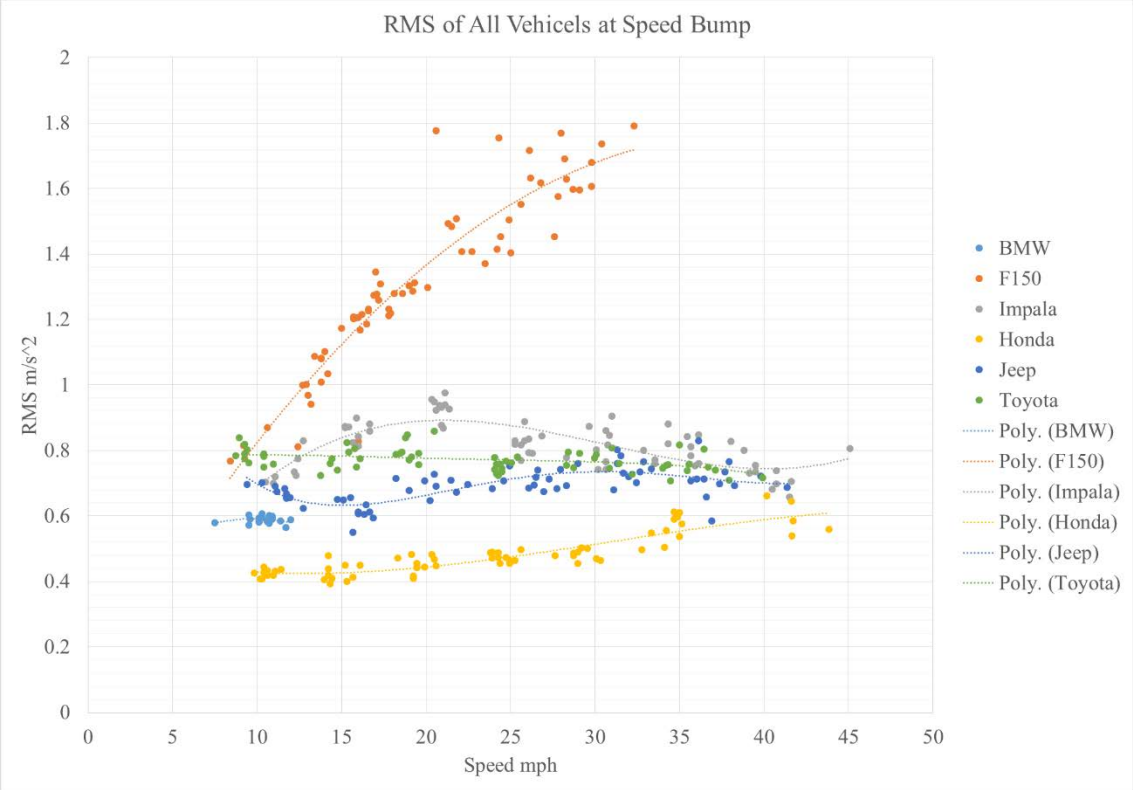

Figure 4.24 RMS of all vehicles at speed bump.

Figure 4.24 shows that for most vehicles, RMS is relatively insensitive to speed. However, the large pickup does exhibit the expected response (higher speed, higher acceleration). This is likely due to the stiffer suspension of the truck as compared to the smaller vehicles.

RMS was tested for its ability to calibrate a test vehicle for predicting the response of a design vehicle. Using the speed bump, five tests were conducted to see if four of the test vehicles could be used to accurately predict the remaining vehicle's response (the BMW was not used in this series of tests due to the hard suspension).

For example, the RMS from the Jeep (test vehicle) were used to predict the RMS of the Honda (design vehicle) for different speeds at various crossings. Results of those predictions can be seen in Table 4-4 and Figure 4.25.

Table 4-4 Using Jeep acceleration RMS to predict Honda acceleration RMS.

Actual Jeep RMS @ Speed		Highway Rail Crossing										
		Bryan Station E	Briar Hill N	Hatton E	Bridgeport-Benson N	Devil's Hollow E	Speed Bump	Bryan Station W	Briar Hill S	Hatton W	Bridgeport-Benson S	Devil's Hollow W
Speed mph	15	--	--	--	--	--	0.63	--	--	--	--	--
	20	0.38	0.56	0.99	0.70	0.56	0.66	0.39	0.62	1.04	0.88	0.57
	25	0.54	0.98	1.45	0.96	0.60	0.71	0.50	0.90	--	1.12	0.64
	30	0.71	1.41	--	1.23	0.64	0.74	0.59	1.40	--	1.29	0.65
	35	0.88	1.84	--	1.50	0.68	0.72	0.68	1.85	--	1.60	0.53
	40	1.05	--	--	--	--	0.70	0.78	2.31	--	--	--
Actual HONDA RMS @ Speed		Highway Rail Crossing										
		Bryan Station E	Briar Hill N	Hatton E	Bridgeport-Benson N	Devil's Hollow E	Speed Bump	Bryan Station W	Briar Hill S	Hatton W	Bridgeport-Benson S	Devil's Hollow W
Speed mph	15	--	--	--	--	--	0.43	--	--	--	--	--
	20	0.40	0.75	0.75	0.76	0.50	0.44	0.36	0.64	0.80	0.95	0.52
	25	0.55	0.95	1.00	0.95	0.44	0.48	0.50	0.90	1.00	1.00	0.57
	30	0.65	1.20	--	1.13	0.50	0.51	0.56	1.33	--	1.12	0.59
	35	0.95	1.67	--	1.32	0.54	0.55	0.72	1.84	--	1.50	0.55
	40	1.15	--	--	--	0.57	0.59	0.97	--	--	--	0.63
Predicted HONDA RMS @		Highway Rail Crossing										
		Bryan Station E	Briar Hill N	Hatton E	Bridgeport-Benson N	Devil's Hollow E	Speed Bump	Bryan Station W	Briar Hill S	Hatton W	Bridgeport-Benson S	Devil's Hollow W
Speed mph	15	--	--	--	--	--	N/A	--	--	--	--	--
	20	0.25	0.37	0.67	0.47	0.37	N/A	0.26	0.41	0.70	0.59	0.38
	25	0.36	0.66	0.97	0.64	0.40	N/A	0.33	0.60	--	0.75	0.43
	30	0.50	0.99	--	0.86	0.45	N/A	0.41	0.98	--	0.90	0.45
	35	0.67	1.41	--	1.15	0.52	N/A	0.52	1.42	--	1.23	0.41
	40	0.88	--	--	--	--	N/A	0.66	1.94	--	--	--

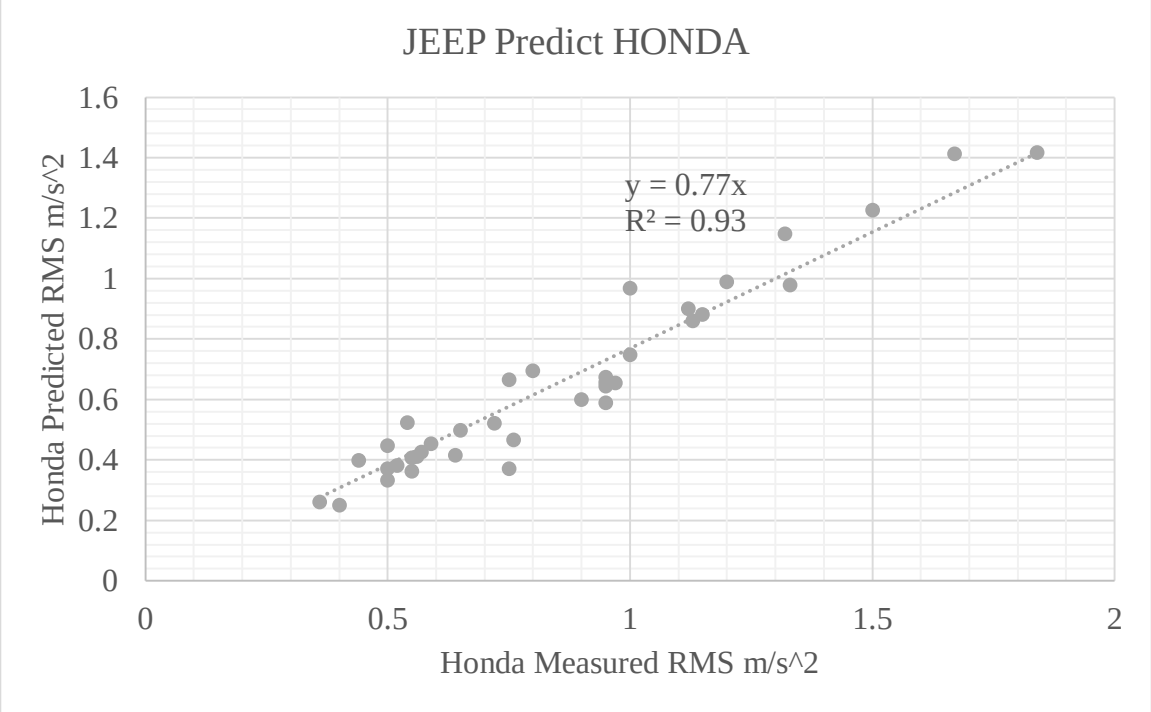

Figure 4.25 Honda actual RMS vs predicted RMS using Jeep as the test vehicle.

Visually, one can see the improvement in calibration capability offered by the used of RMS as opposed to the use of maximum accelerations only. To compare the results of each test, several goodness of fit measures may be calculated: root mean square error (RMSE), normalized root-mean-square or error (NRMSE) and coefficient of variation of the RMSE (CV(RMSE)), as follows:

Equation 4-3

$$RMSE = \sqrt{\frac{\sum_{t=1}^{n}(\bar{y}_t - y)^2}{n}}$$

Equation 4-4

$$NRMSE = \frac{RMSE}{y_{max} - y_{min}}$$

Equation 4-5

$$CV(RMSE) = \frac{RMSE}{\bar{y}}$$

For the example combination of vehicles shown in Figure 4.25, RMSE is 0.23, NRMSE is 15.4% and CV (RMSE) is 0.27. And while these results are good, the predictions can be further improved by normalizing the data, realizing the ideal line should intercept the origin and have a slope of 1:1. Because the original best fit line has a slope of 0.77, estimated values may be calibrated (adjusted) by multiplying by 1/0.77 or 1.30. The revised results are shown in Figure 4.26. Goodness of fit measures improve to 0.11, 7.2% and 0.12 respectively.

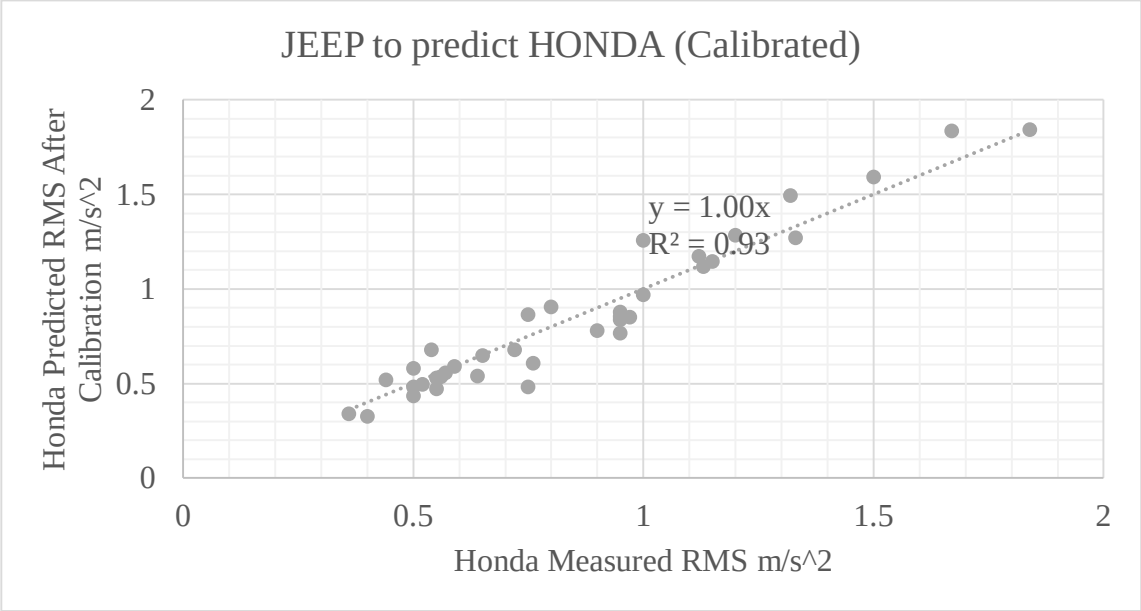

Figure 4.26 Honda actual RMS vs predicted RMS using Jeep as the test vehicle after calibration.

Normalized (adjusted) prediction results are summarized in Table 4-5**Error! Reference source not found.** through Table 4-7.

Table 4-5 RMSE of RMS-based predictions (speed bump).

RMSE after Calibration		Use the vehicle				
		F150	IMPALA	JEEP	HONDA	TOYOTA
To predict the vehicle	F150	-	0.17	0.20	0.16	0.19
	IMPALA	0.19	-	0.21	0.24	0.17
	JEEP	0.19	0.18	-	0.12	0.13
	HONDA	0.14	0.19	0.11	-	0.16
	TOYOTA	0.21	0.16	0.14	0.19	-

Table 4-6 NRMSE of RMS-based predictions (speed bump).

NRMSE after Calibration		Use the vehicle				
		F150	IMPALA	JEEP	HONDA	TOYOTA
To predict the vehicle	F150	0.0%	16.7%	20.0%	16.4%	18.9%
	IMPALA	16.4%	0.0%	11.9%	16.6%	9.6%
	JEEP	17.7%	9.3%	0.0%	8.1%	6.6%
	HONDA	14.0%	12.8%	7.2%	0.0%	10.8%
	TOYOTA	17.3%	9.2%	8.0%	15.6%	0.0%

Table 4-7 CV(RMSE) of RMS-based predictions (speed bump).

CV (RMSE) after Calibration		Use the vehicle				
		F150	IMPALA	JEEP	HONDA	TOYOTA
To predict the vehicle	F150	0.00	0.18	0.21	0.17	0.20
	IMPALA	0.18	0.00	0.19	0.22	0.16
	JEEP	0.22	0.19	0.00	0.13	0.14
	HONDA	0.18	0.23	0.12	0.00	0.19
	TOYOTA	0.21	0.16	0.13	0.19	0.00

From Table 4-5, Table 4-6, and Table 4-7, the test vehicle which best predicts each design vehicle is highlighted in green, for the three measures. The Jeep, Honda and Toyota show up most frequently, although the Jeep and Toyota provide the best predictions (lowest errors).

For all plots of speed bump RMS tests, refer to **APPENDIX D**.

4.6.2.2 Using RMS of Accelerations at a Reference Crossing to Calibrate a Test Vehicle

To explore whether the use of a reference crossing to calibrate test vehicles is superior to the use of a speed bump, the acceleration RMS for different vehicles and speeds at each crossing are plotted below from Figure 4.27 to Figure 4.32. The data are also summarized in Table 4-8.

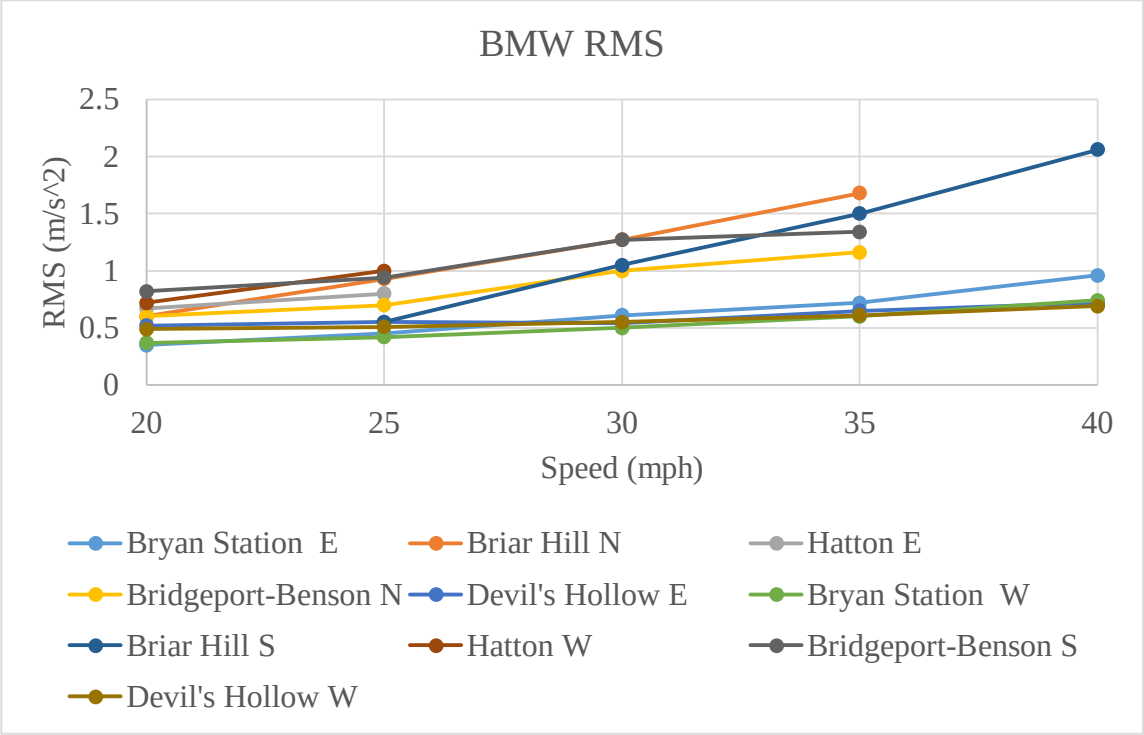

Figure 4.27 BMW RMS of accelerations at all crossings.

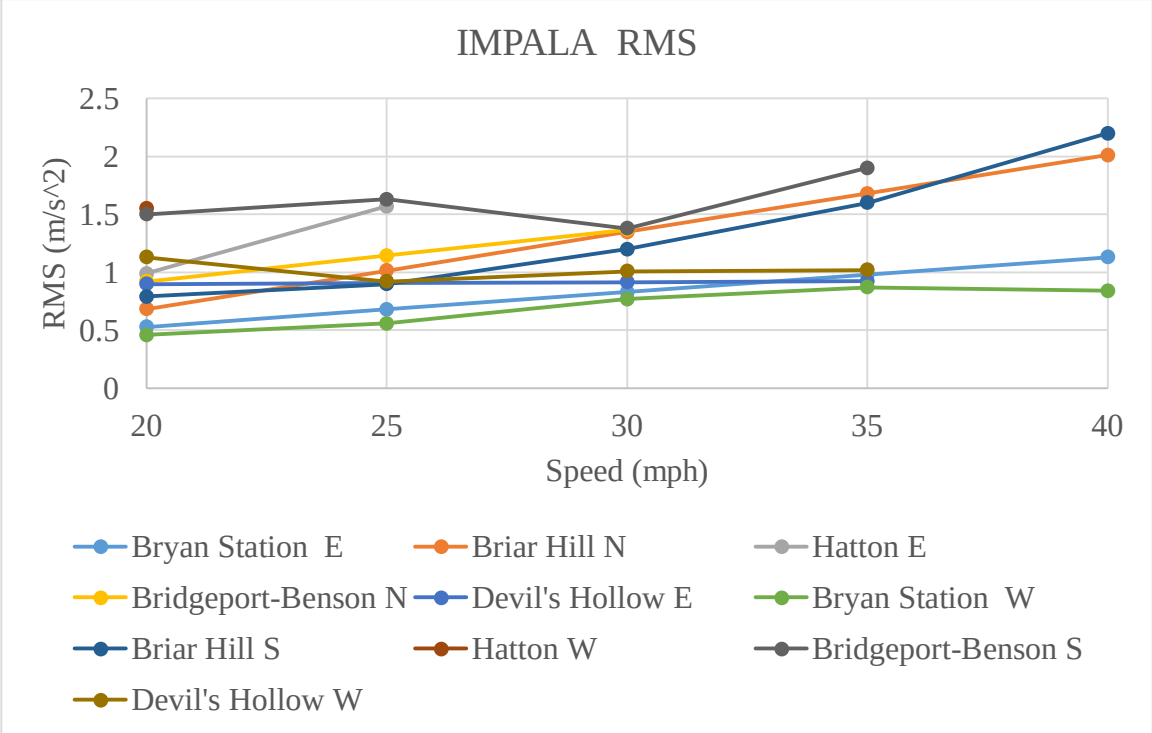

Figure 4.28 Impala RMS of accelerations at all crossings.

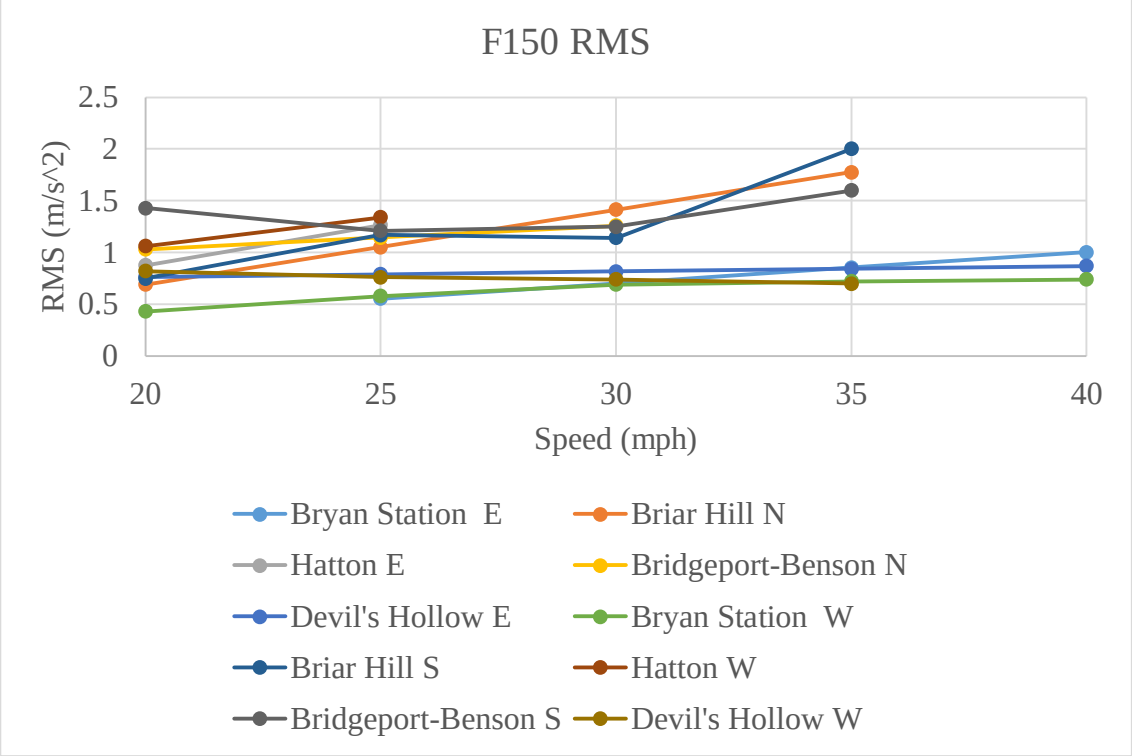

Figure 4.29 F150 RMS of accelerations at all crossings.

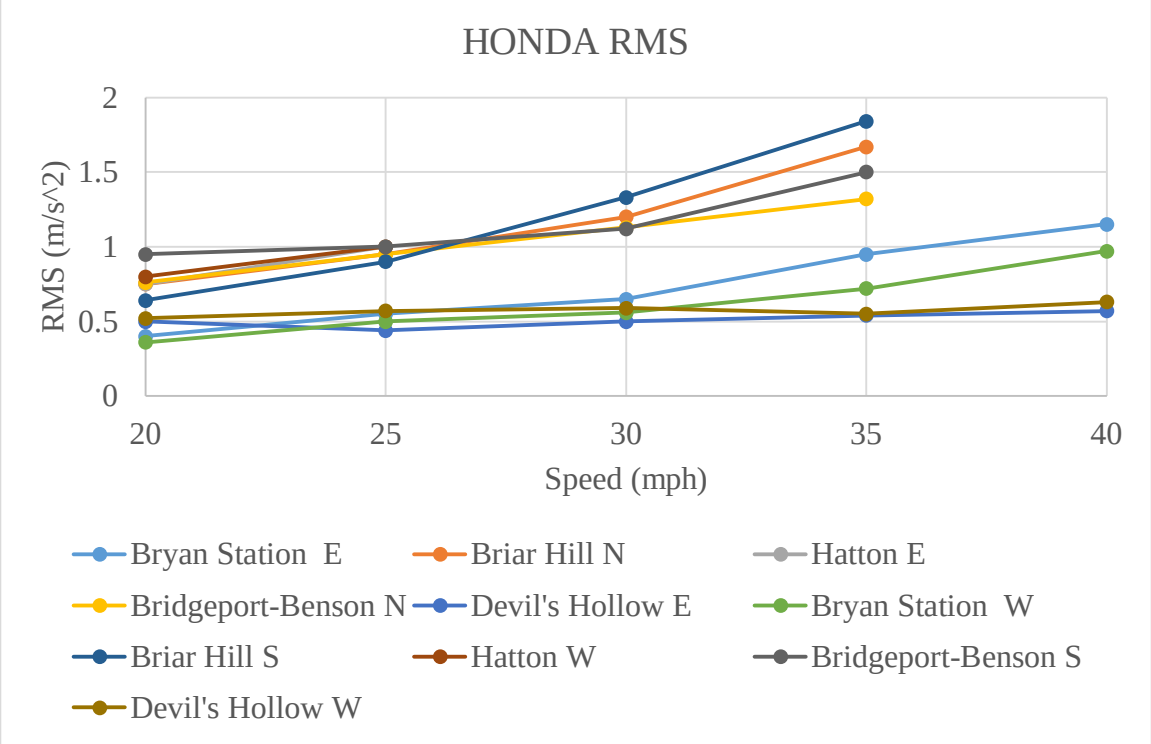

Figure 4.30 Honda RMS of accelerations at all crossings.

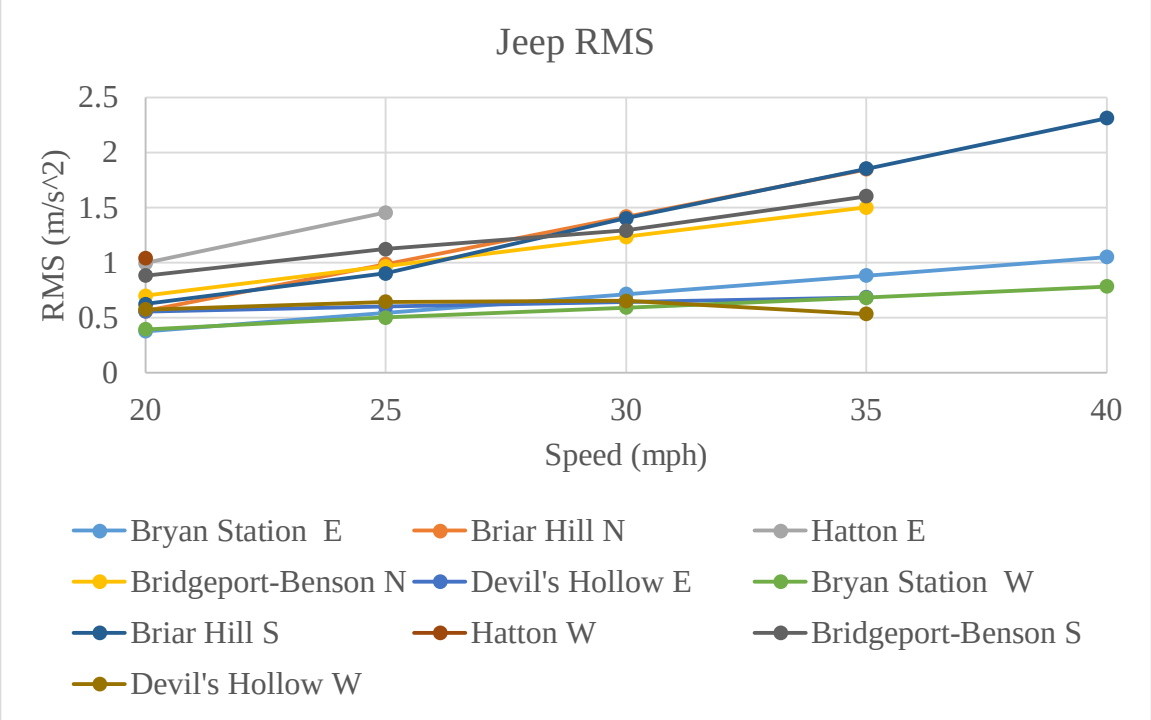

Figure 4.31 Jeep RMS of accelerations at all crossings.

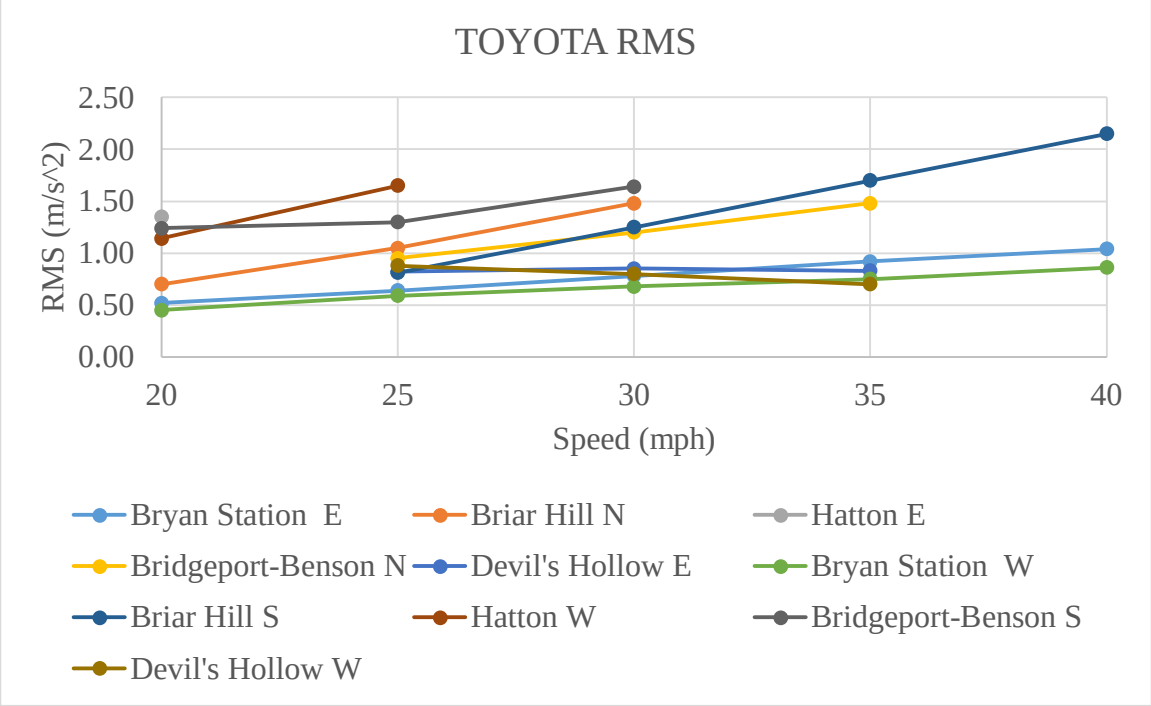

Figure 4.32 Toyota RMS of accelerations at all crossings.

Table 4-8 All vehicles RMS of accelerations at different crossings and speeds.

F150 RMS @ Speed		Bryan Station E	Briar Hill N	Hatton E	Bridgeport-Benson N	Devil's Hollow E	Bryan Station W	Briar Hill S	Hatton W	Bridgeport-Benson S	Devil's Hollow W
Speed mph	20	--	0.69	0.88	1.03	0.76	0.43	0.75	1.06	1.43	0.82
	25	0.55	1.05	1.27	1.15	0.79	0.58	1.17	1.34	1.21	0.76
	30	0.70	1.41	--	1.26	0.82	0.69	1.14	--	1.25	0.74
	35	0.85	1.77	--	--	0.84	0.72	2.00	--	1.60	0.70
	40	1.00	--	--	--	0.87	0.74	--	--	--	--
IMPALA RMS @		Bryan Station E	Briar Hill N	Hatton E	Bridgeport-Benson N	Devil's Hollow E	Bryan Station W	Briar Hill S	Hatton W	Bridgeport-Benson S	Devil's Hollow W
Speed mph	20	0.53	0.68	0.99	0.92	0.90	0.46	0.79	1.55	1.50	1.13
	25	0.68	1.02	1.57	1.14	0.91	0.56	0.90	--	1.63	0.92
	30	0.83	1.35	--	1.37	0.92	0.77	1.20	--	1.38	1.01
	35	0.98	1.68	--	--	0.92	0.87	1.60	--	1.90	1.02
	40	1.13	2.01	--	--	--	0.84	2.20	--	--	--
Jeep RMS @ Speed		Bryan Station E	Briar Hill N	Hatton E	Bridgeport-Benson N	Devil's Hollow E	Bryan Station W	Briar Hill S	Hatton W	Bridgeport-Benson S	Devil's Hollow W
Speed mph	20	0.38	0.56	0.99	0.70	0.56	0.39	0.62	1.04	0.88	0.57
	25	0.54	0.98	1.45	0.96	0.60	0.50	0.90	--	1.12	0.64
	30	0.71	1.41	--	1.23	0.64	0.59	1.40	--	1.29	0.65
	35	0.88	1.84	--	1.50	0.68	0.68	1.85	--	1.60	0.53
	40	1.05	--	--	--	--	0.78	2.31	--	--	--
HONDA RMS @		Bryan Station E	Briar Hill N	Hatton E	Bridgeport-Benson N	Devil's Hollow E	Bryan Station W	Briar Hill S	Hatton W	Bridgeport-Benson S	Devil's Hollow W
Speed mph	20	0.40	0.75	0.75	0.76	0.50	0.36	0.64	0.80	0.95	0.52
	25	0.55	0.95	1.00	0.95	0.44	0.50	0.90	1.00	1.00	0.57
	30	0.65	1.20	--	1.13	0.50	0.56	1.33	--	1.12	0.59
	35	0.95	1.67	--	1.32	0.54	0.72	1.84	--	1.50	0.55
	40	1.15	--	--	--	0.57	0.97	--	--	--	0.63
TOYOTA RMS @		Bryan Station E	Briar Hill N	Hatton E	Bridgeport-Benson N	Devil's Hollow E	Bryan Station W	Briar Hill S	Hatton W	Bridgeport-Benson S	Devil's Hollow W
Speed mph	20	0.52	0.70	1.35	--	--	0.45	--	1.14	1.24	--
	25	0.64	1.05	--	0.95	0.82	0.59	0.81	1.65	1.30	0.88
	30	0.78	1.48	--	1.20	0.85	0.68	1.25	--	1.64	0.80
	35	0.92	--	--	1.48	0.83	0.75	1.70	--	--	0.70
	40	1.04	--	--	--	--	0.86	2.15	--	--	--
BMW RMS @ Speed		Bryan Station E	Briar Hill N	Hatton E	Bridgeport-Benson N	Devil's Hollow E	Bryan Station W	Briar Hill S	Hatton W	Bridgeport-Benson S	Devil's Hollow W
Speed mph	20	0.35	0.60	0.67	0.60	0.52	0.37	--	0.72	0.82	0.49
	25	0.45	0.93	0.80	0.70	0.55	0.42	0.55	1.00	0.94	0.51
	30	0.61	1.27	--	1.00	0.54	0.50	1.05	--	1.27	0.55
	35	0.72	1.68	--	1.16	0.65	0.60	1.50	--	1.34	0.61
	40	0.96	--	--	--	0.72	0.74	2.06	--	--	0.69

Similar to the analysis using the speed bump in the previous section, this section presents the use of a reference crossing to calibrate a test vehicle. The Bryan Station Road crossing is used as the reference. Normalized prediction results using the eastbound direction RMS are summarized in Table 4-9, Table 4-10, and Table 4-11.

Table 4-9 RMS prediction result RMSE based on Bryan Station Road crossing tests after calibration.

RMSE after Calibration		Use the vehicle					
		F150	IMPALA	JEEP	HONDA	TOYOTA	BMW
To predict the vehicle	F150	0.00	0.18	0.13	0.18	0.17	0.17
	IMPALA	0.19	0.00	0.22	0.27	0.17	0.25
	JEEP	0.13	0.19	0.00	0.13	0.12	0.15
	HONDA	0.16	0.21	0.16	0.00	0.17	0.14
	TOYOTA	0.17	0.18	0.13	0.21	0.00	0.13
	BMW	0.13	0.18	0.12	0.13	0.10	0.00

Table 4-10 RMS prediction result NRMSE based on Bryan Station Road crossing tests after calibration.

NRMSE after Calibration		Use the vehicle					
		F150	IMPALA	JEEP	HONDA	TOYOTA	BMW
To predict the vehicle	F150	0.0%	12.9%	9.4%	12.7%	11.7%	11.8%
	IMPALA	14.5%	0.0%	12.6%	18.9%	9.7%	14.4%
	JEEP	9.4%	10.0%	0.0%	8.7%	6.5%	7.7%
	HONDA	11.1%	14.5%	10.9%	0.0%	11.8%	9.7%
	TOYOTA	15.4%	10.5%	7.9%	17.1%	0.0%	7.7%
	BMW	10.6%	10.7%	7.3%	10.0%	5.6%	0.0%

Table 4-11 RMS prediction result CV(RMSE) based on Bryan Station Road crossing tests after calibration.

CV(RMSE) after Calibration		Use the vehicle					
		F150	IMPALA	JEEP	HONDA	TOYOTA	BMW
To predict the vehicle	F150	0.00	0.17	0.12	0.17	0.16	0.16
	IMPALA	0.17	0.00	0.19	0.24	0.16	0.22
	JEEP	0.13	0.20	0.00	0.14	0.13	0.15
	HONDA	0.17	0.25	0.19	0.00	0.20	0.17
	TOYOTA	0.16	0.17	0.13	0.20	0.00	0.12
	BMW	0.16	0.22	0.15	0.17	0.12	0.00

From Table 4-9 to Table 4-11, the test vehicle which best predicts each design vehicle is highlighted in green, for the three measures. Overall, the Toyota provides the best predictions (lowest errors).

For all plots of the Bryan Station Road RMS tests, refer to **APPENDIX E**.

4.7 Conclusion: Using RMS to Rank Crossings

This chapter has presented the collection and analysis of accelerometer readings and proposed several metrics of rideability based on those readings. Normalized RMS based on calibrated test vehicle data is suggested as a repeatable and reliable metric for rideability of crossings. For the study crossings, average and standard deviation of normalized RMS are presented in Table 4-12 and Figure 4.33.

Table 4-12 Average crossing RMS.

Speed	All Vehicles Average RMS ± Std. Dev. (m/s^2)					
(mph)	Bryan Station	Briar Hill	Hatton	Bridgeport-Benson	Devil's Hollow	Speed Bump
20	0.42±0.06	0.68±0.07	0.99±0.26	0.98±0.29	0.68±0.22	0.83±0.34
25	0.55±0.07	0.93±0.15	1.23±0.3	1.09±0.23	0.7±0.17	0.88±0.4
30	0.67±0.1	1.29±0.13	--	1.26±0.16	0.72±0.16	0.9±0.45
35	0.8±0.12	1.74±0.14	--	1.49±0.21	0.71±0.16	0.7±0.1
40	0.94±0.14	2.15±0.12	--	--	0.7±0.11	0.69±0.07

The same results are also shown in Figure 4.33.

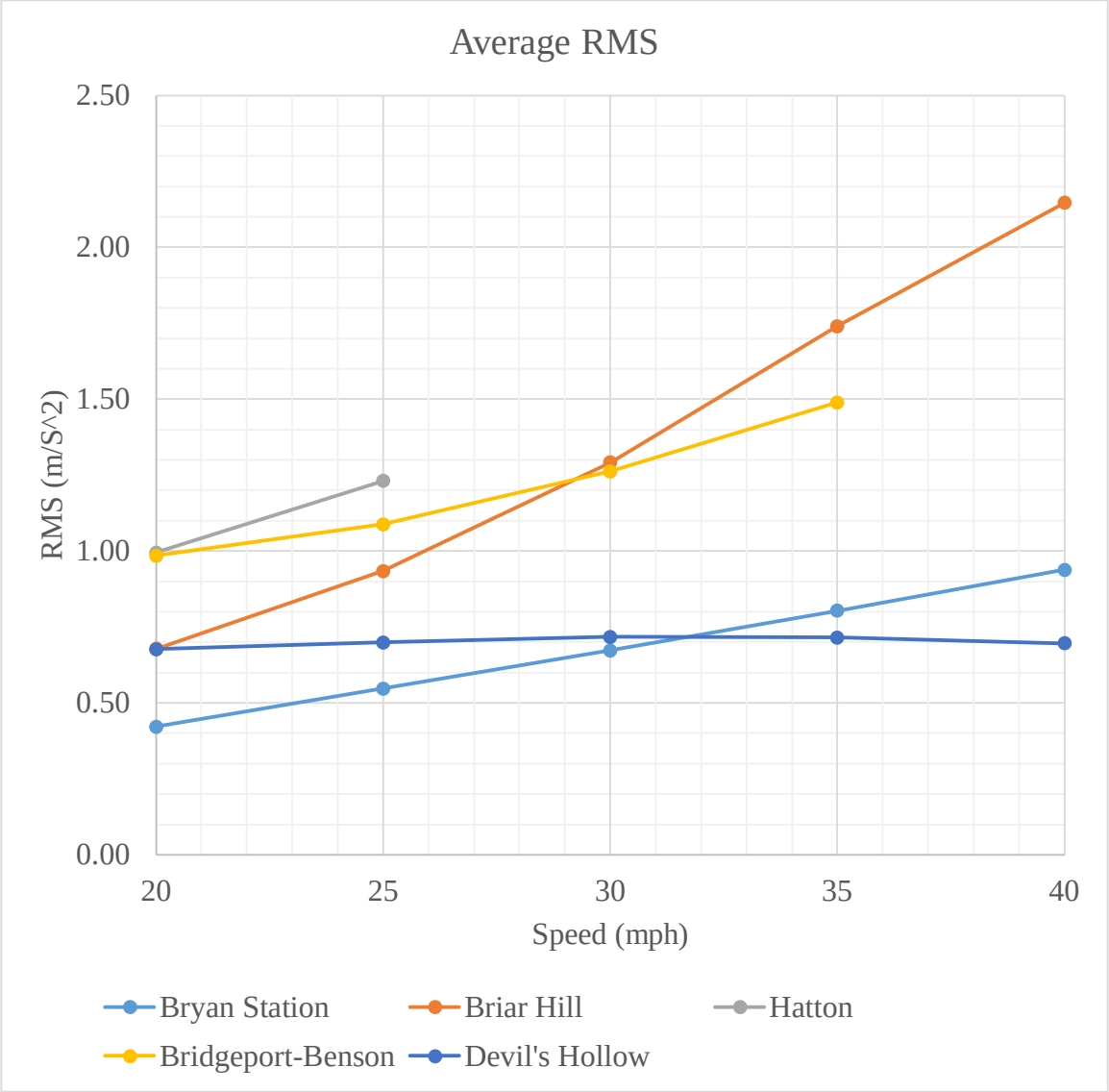

Figure 4.33 Average crossing RMS.

From Figure 4.33, the average RMS for each crossing is observed to linearly increase with speed, although Devil's Hollow Rd RMS is again seen to be insensitive to speed. Due to its relatively flat profile, this is as expected.

The rideability of each crossing can be ranked using RMS from individual vehicles at posted crossing speeds. The results are shown in Table 4-13.

Table 4-13 Ranking crossings based on RMS.

Crossing	Posted Speed	Ave. RMS	Rank based on Ave. RMS	Rank based on F150	Rank based on IMPALA	Rank based on JEEP	Rank based on HONDA	Rank based on TOYOTA	Rank based on BMW
Bryan Station	30	0.67	5	5	5	4	4	5	5
Briar Hill	35	1.74	1	1	1	1	1	1	1
Hatton	20	0.99	3	3	3	3	3	2	3
Bridgeport-Benson	25	1.09	2	2	2	2	2	3	2
Devil's Hollow	35	0.71	4	4	4	5	5	4	4

Crossing rideability rank based on normalized RMS is quite consistent. The ranking could be compared to subjective rankings by inspectors.

Two chief limitations for the use of normalized RMS in a statewide crossing program are identified. First, acceleration data must be collected by visiting every site. A number of runs is suggested to smooth out results, a calibrated test vehicle must be used, and accelerations may be sensitive to wheel path position for crossings with lateral surface variations. Second, rideability as a measure does not separate out the effects of crossing condition and as-built construction (including design profile and possibly crossing materials). Chapters 5 and 6 of this dissertation address these issues.

CHAPTER 5. VEHICLE DYNAMIC MODEL

5.1 Introduction

The rail-highway crossing represents a unique and problematic junction of two of the most ubiquitous transportation modes. While crashes at rail-highway crossings have diminished over recent decades, the problem continues. Increasing traffic (highway and rail), distraction, and reduced patience on the part of drivers suggest that the problem could increase in the future. Driver inattention and decision making in the vicinity of the at-grade crossing are important contributors to their safety as discussed in the previous chapter

To determine the potential safety effect, it is first necessary to quantify roughness. The overall objective of our research is to develop a method to quickly and inexpensively quantify the roughness of a crossing, and, based on correlations between roughness and safety, prioritize crossings for rehabilitation. A first step towards that objective is reported in Chapter 3. In that chapter, the development of a low-cost 3D data acquisition system (DAS) based on 3D structured light imaging technology was reported. As an extension of that research, a vehicle dynamic model was developed to use a 3D surface point cloud and vehicle wheel path to estimate accelerations.

The present chapter describes the continued development, calibration and validation of the dynamic simulation model for a single test vehicle, as applied to two different crossings for a number of vehicle speeds. Hence, the model is tested for both accuracy and repeatability across speeds and locations.

To quantify crossing roughness in the field, accelerations were measured from inside the passenger compartment of a passenger vehicle using a commercially available digital accelerometer. To estimate these accelerations without directly measuring with an accelerometer, a vehicle dynamic simulation model was modified. To run the model, a crossing terrain model is required.

This chapter is organized as follows: Following a section on development of terrain models used in this research, a section is presented on field measurement of acceleration. Next, the development of the dynamic simulation model is described. Following that section, calibration and validation documentation is presented. The chapter

concludes with a summary of our work, discussion of limitations and suggestions for future research.

5.2 Background

While track roughness may be evaluated by a railroad geometry car, highway crossings are usually qualitatively evaluated. However, previous work (Rose et al., 2009) investigated the use of a laser based inertial profiler and rolling dipstick to quantify rail crossing roughness. Results were of limited practicality, and investigation of alternative technology was recommended. A study of railroad crossing roughness classification in Indiana (Williams, 2003) and a report from Illinois (Illinois Department of Transportation, 2001) showed how railroad crossing roughness could be classified into different groups such as smooth, medium, and rough based on qualitative rideability evaluations (good, fair, poor) at different driving speeds. However, subjective ratings for crossings were found to be different for different vehicles. Further, the effect of crossing condition cannot be differentiated from effects of original geometric design using qualitative methods.

Roughness of highway pavements has long been studied. Various quantitative methods such as international roughness index (IRI) (Sayers, 1995), and profile index (PI) (Sayers & Karamihas, 1998) have been developed in the last 30 to 40 years. However, none of these technologies are applicable to measuring rail-highway crossing roughness due to the short distance and unique structure of the crossing.

Due to the various geometries that need to be accommodated at a highway rail crossing (grade of rail, elevation of rail, grade of highway, cross section of highway, drainage, …), it is difficult or impossible to field rate a crossing (by driving over it) and establish its performance for many combinations of crossing vehicle types, speeds and lateral placement of highway vehicle. A modelling approach is therefore desired. To model acceleration, an accurate 3D terrain model is required.

Technology exists to map crossing surfaces at different levels of precision and at various costs. For example, LiDAR (Light Detection Ranging) is a remote sensing technology that measures distance and other properties such as shapes and dimensions by illuminating a target with a laser and analyzing the reflected light (Olsen, 2013). LiDAR

and 3D sensing in general find many applications in civil, construction and transportation engineering. For example LiDAR has been used to verify highway bridge clearance (Rister et al., 2013) and modern pavement management systems use laser scanners to quantify highway surface condition ratings.

5.3 Development of Terrain Model

In this chapter, the same crossing location studied and presented in Chapter 4 is again used, Brannon Crossing Road. At that location, a 3D surface point cloud was collected using LiDAR (see Figure 5.1). The LiDAR data were collected using an Optech Lynx SG1 mobile LiDAR system. This 2-sensor system has a range precision of 5mm, 1σ (Optech Incorporated, 2015). The crossing is generally rough as can be seen in elevation changes on the highway approaches.

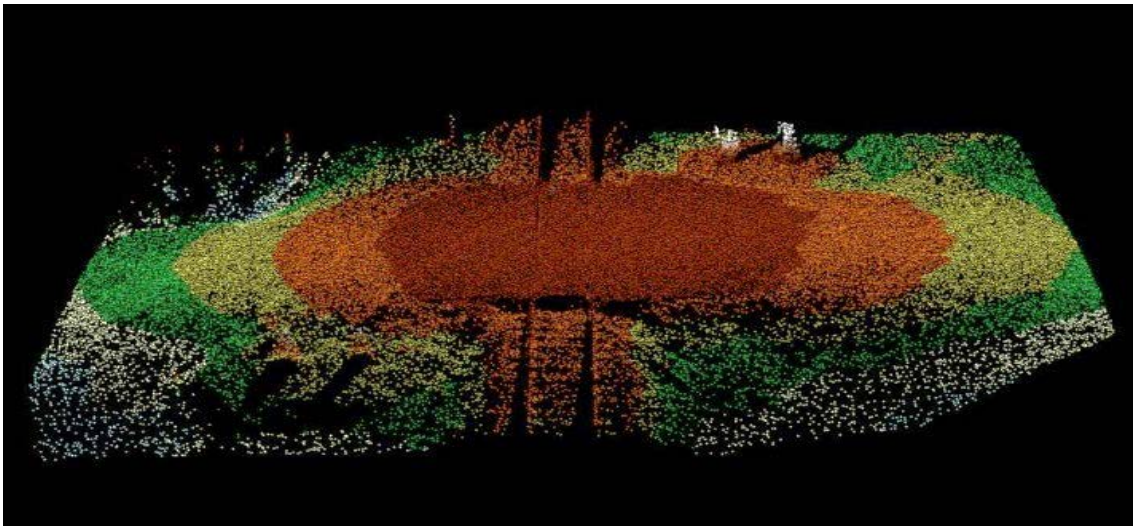

Figure 5.1 Brannon Road Crossing 3D point cloud. Green to red indicates increasing elevation.

For validation purposes, a terrain model was also developed for a second location along the RJ Corman Railroad at Bryan Station Road in Fayette County, KY, just north of Lexington (USDOT Crossing number 346839X).

5.4 Field Acceleration Data Collection

As reported in Chapter 4, accelerations were measured at close to the highway posted speed of 35 MPH. Figure 5.2 shows detail of the measured accelerations for 3 seconds as the vehicle negotiates the crossing.

Figure 5.2 Accelerations measured at speeds close to 35 mph.

Recall (and observe from Figure 5.2) that repeated tests had similar results in terms of the frequency and amplitude of vertical acceleration. However, different drivers may choose different paths where roughness may be different. That is, as the surface elevation varies horizontally, the ride experienced is a function of the chosen path. To illustrate, varying accelerations resulting from driving a sample crossing in different lateral positions using pneumatic road tube and video methods are presented (Fitzsimmons et al., 2013) and the result is shown in Figure 5.3. To minimize the effects of lateral placement,

all tests performed in this research were done within similar wheel paths over crossings with minimal lateral surface variation.

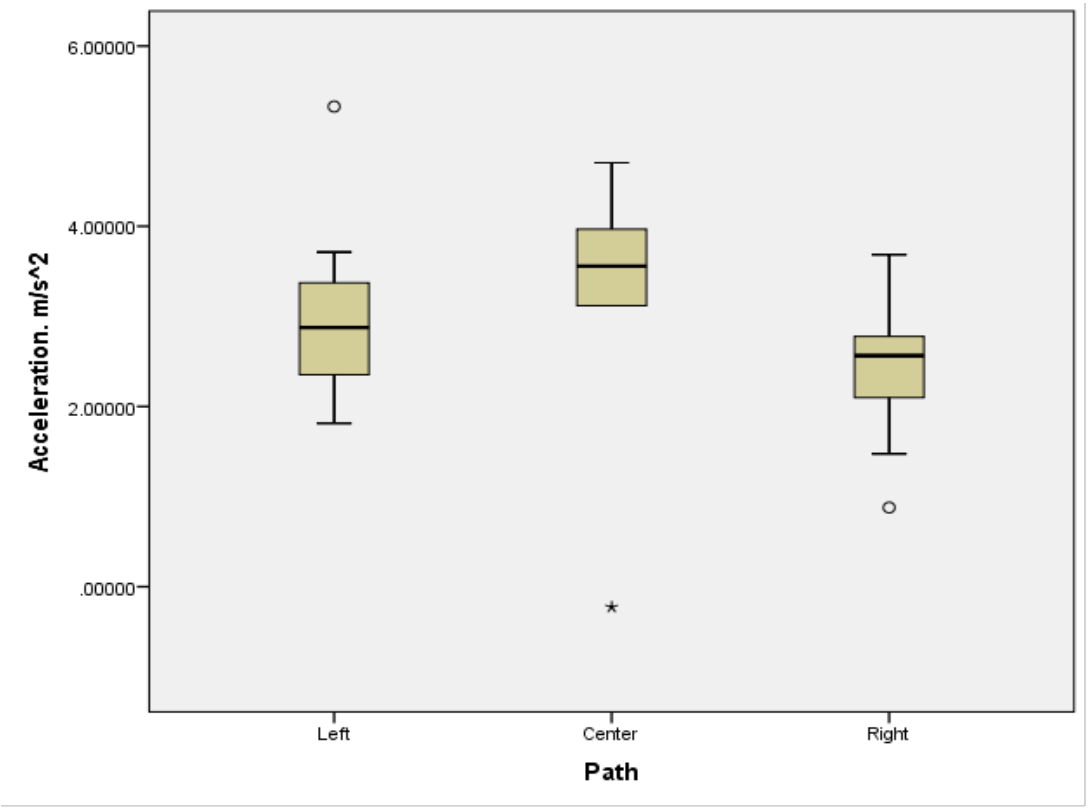

Figure 5.3 Effect of lateral wheel path position on measured accelerations.

5.5 Development of the Dynamic Simulation Model

In order to simulate the highway vehicle driving over a crossing and estimate accelerations, a highway vehicle dynamic model was developed based on the computer code ATTIF (Analysis of Train/Track Interaction Forces) (Dynamic Simulation Laboratory (DSL), 2013). The model was developed at the Dynamic Simulation Laboratory (DSL) of the University of Illinois at Chicago (UIC). Its original purpose was to simulate train and track interaction (Shabana et al., 2012). ATTIF included a detailed wheel/rail contact model based on surface geometry (see Figure 5.4).

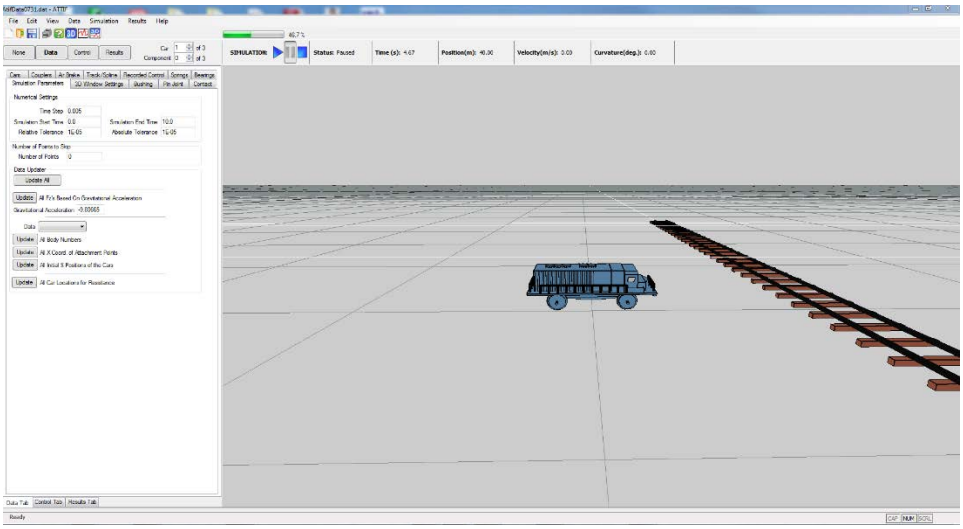

Figure 5.4 ATTIF based vehicle dynamic simulation model GUI.

The ATTIF vehicle dynamic model uses the 3D surface point cloud and realistic vehicle parameters for weight, velocity, wheel radius, wheel-base, and suspension characteristics to simulate a vehicle driving over the rail crossing. During the calibration process, initial simulated accelerations were observed to be about 3 times larger than field observations. The model also resulted in significant high frequency noise as shown in Figure 5.5.

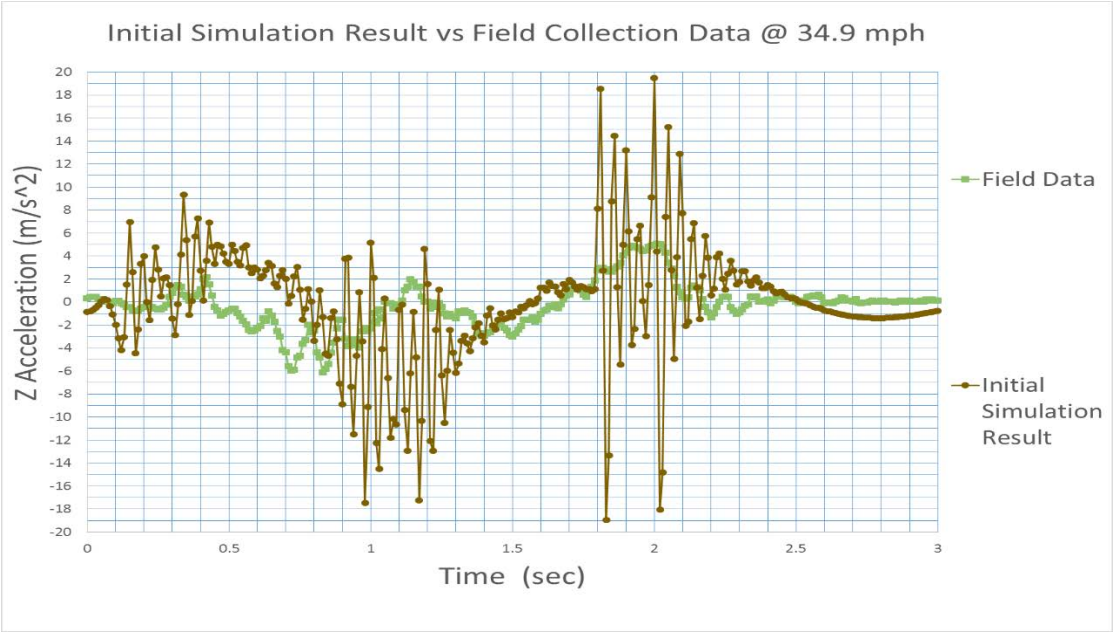

Figure 5.5 Initial simulation result vs field measured accelerations @ 34.9 mph.

The amplitude and frequency differences between the simulation and field observations were caused by differences in the stiffness and damping of the vehicle tires (significantly different from rail steel wheels). As the basic model was initially designed to analyze a steel-on-steel, wheel-to-track model, only four springs were used to model the suspension between the frame and car body. An additional four springs were added to represent the flexibility tires.

5.6 Model Calibration and Validation

To calibrate the model, a trial and error process was used to modify vehicle component parameters to best match the mid-range speed, 34.9mph. Tire stiffness was decreased by a factor of 12.5 and its damping factor was increased by a factor of 3.5. Suspension stiffness was increased by a factor of 4 and its damping factor was increased by a factor of about 2. Simulated accelerations were then compared to field observations for various speeds. These comparisons can be seen in Figure 5.6 and Figure 5.7.

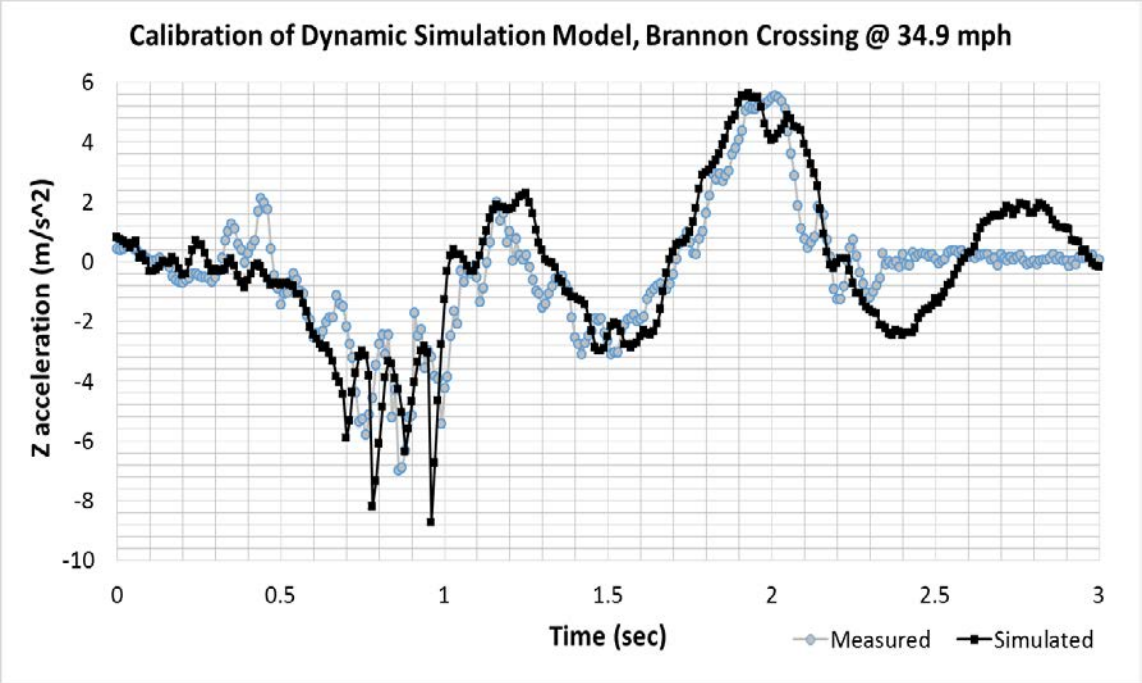

Figure 5.6 Calibration of dynamic simulation model, Brannon Crossing @ 34.9 mph.

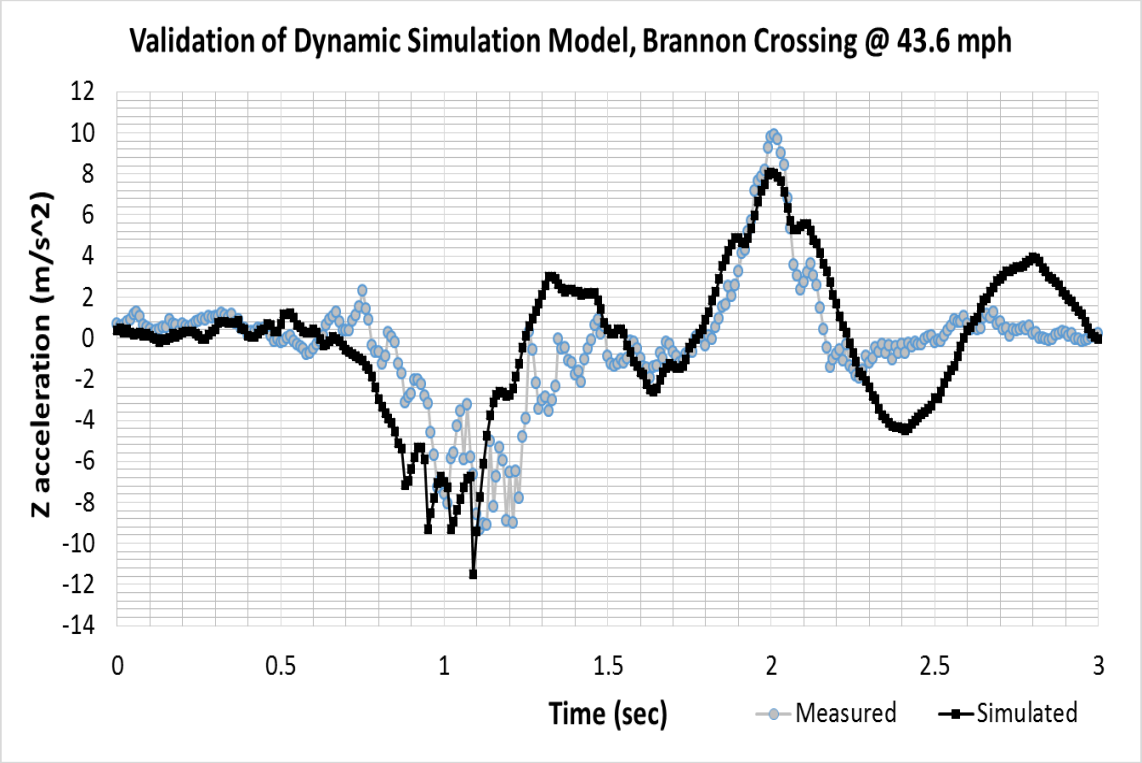

Figure 5.7 Validation (different speed) of Dynamic Simulation Model, Brannon Crossing @ 43.6 mph.

The relationship between estimated and field observed accelerations are generally similar (peaks align, overall magnitudes of accelerations are similar). Table 1 presents a numerical comparison of simulated and field-observed results. Maximum accelerations at all speeds are quite similar. For the higher speeds (at or above 34 mph) minimum accelerations are also quite similar. Peak differences vary from a low 0.09 m/s^2 to a high of 4.98 m/s^2. Estimation errors are higher at lower speeds and are likely due to nonlinear behaviors of vehicle suspensions. For example, when a car "bottoms out" (springs fully compress or shocks reach their maximum compression or extension), calibration of the model across all speeds will be impossible.

To quantify the goodness-of-fit and similarity of the two waves in the plot, a MATLAB script was developed to compute a cross correlation index (P in Equation 5-1) and mean squared error (MSE), and the results are shown in Table 5-1.

Table 5-1 Calibration of dynamic simulation model (Brannon Crossing).

Speed	P(A:B) A=field B=simulated	MSE (normalized to maximum acceleration)	MAX(A):MAX(B) in m/s2	MIN(A):MIN(B) in m/s2
23.9 mph	0.645	0.352	1.96 : 2.55	-3.29 : -8.27
26.2 mph	0.468	0.278	2.58 : 2.38	-3.74 : -7.01
34.9 mph	0.786	0.063	5.56 : 5.65	-7.00 : -8.70
43.6 mph	0.801	0.086	9.92 : 8.02	-9.32 : -11.57

Equation 5-1

$$\text{cross correlation index } P(A:B) = \frac{\text{cross correlation (A:B)}}{\text{cross correlation (A:A)}}$$

A and B are time series waves with the same number of points, and P(A:B) = 1, when wave A and B are the same shape.

The simulation model, calibrated for the Brannon Road crossing, was then used, without further calibration, to estimate the accelerations at a second crossing (Bryan Station). These "location validation" results are similar to those obtained during calibration (see Figure 5.8 and Table 5-2).

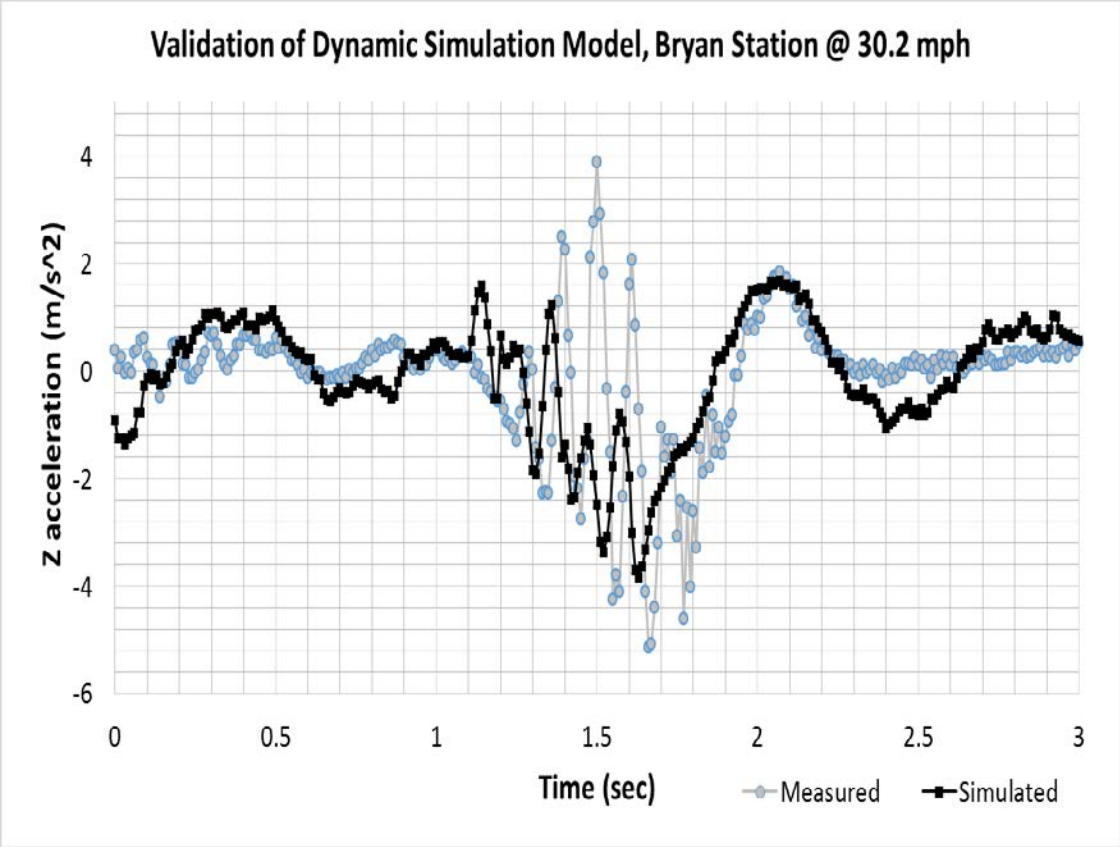

Figure 5.8 Validation of dynamic simulation model, different location, Bryan Station @ 30.2 mph.

Table 5-2 Validation of Dynamic Simulation Model (Bryan Station)

Speed	P(A:B) A=field B=simulated	MSE (normalized to maximum acceleration)	MAX(A):MAX(B) in m/s2	MIN(A):MIN(B) in m/s2
30.2 mph	0.842	0.363	3.88 : 1.68	-5.13 : -3.86
36.0 mph	1.189	0.187	5.22 : 2.53	-7.54 : -4.17
40.3 mph	1.155	0.159	3.91 : 3.67	-6.09 : -5.35

5.7 Conclusions and Recommendations

In this chapter, a vehicle dynamic model was developed to simulate vehicle accelerations using only a crossing terrain model and vehicle parameters as inputs. Accelerometer data were used to field calibrate and validate the model. Model repeatability and data accuracy was verified, suggesting that the vehicle dynamic model can be used to quantify vehicular accelerations at various speeds and different locations.

For the results of the approach to be useful in decision making, one must consider that the accelerations (modeled or measured) at a rail crossing location can derive from either condition or construction (design) of the crossing. That is to say, a crossing constructed on the level but in poor condition may induce less acceleration than a crossing in good condition that was poorly constructed or designed. In the next chapter, a procedure to separate the effects of condition and design/construction is introduced.

CHAPTER 6. QUANTITATIVE CROSSING ASSESSMENT INDICES

6.1 Introduction

Previous chapters presented the development of a low cost 3D sensor for data collection, a technique to use accelerometers to evaluate crossing rideability, and a dynamic model to assess crossing rideability based on a surface model and detailed vehicular characteristics. This chapter presents the development of a simple, scalable, and readily deployable surface-based method of crossing evaluation. This method also has the advantage of differentiating performance effects due to a) crossing surface condition/deterioration, and b) original/as-built design of the crossing.

This chapter first presents the development of a crossing roughness measure, estimated solely from a 3D point cloud and using established surface roughness parameters. Second, a crossing rideability measure is derived from smoothed 3D point cloud data and simple differentiation (smoothed rideability index). This measure of rideability is compared to field accelerometer measurements and can be used, in conjunction with functional or design classification to prioritize crossing improvements. Lastly, by subtracting the theoretical accelerations a vehicle would experience for the crossing were it in perfect condition, from field measured accelerations, a different crossing rideability index (profile-relative rideability index) is developed which can be used to prioritize crossing improvement based on condition alone.

6.2 Data Collection

Using the same Optech Lynx SG1 mobile LiDAR system used to collect the data for the Brannon Road crossing, 3Ddata were collected for four additional Lexington, KY area crossings. Raw data were first processed to provide a bare earth model. Points related to vegetation, gates and signs were all removed. The processed point clouds are visualized in Figure 6.1, through Figure 6.4.

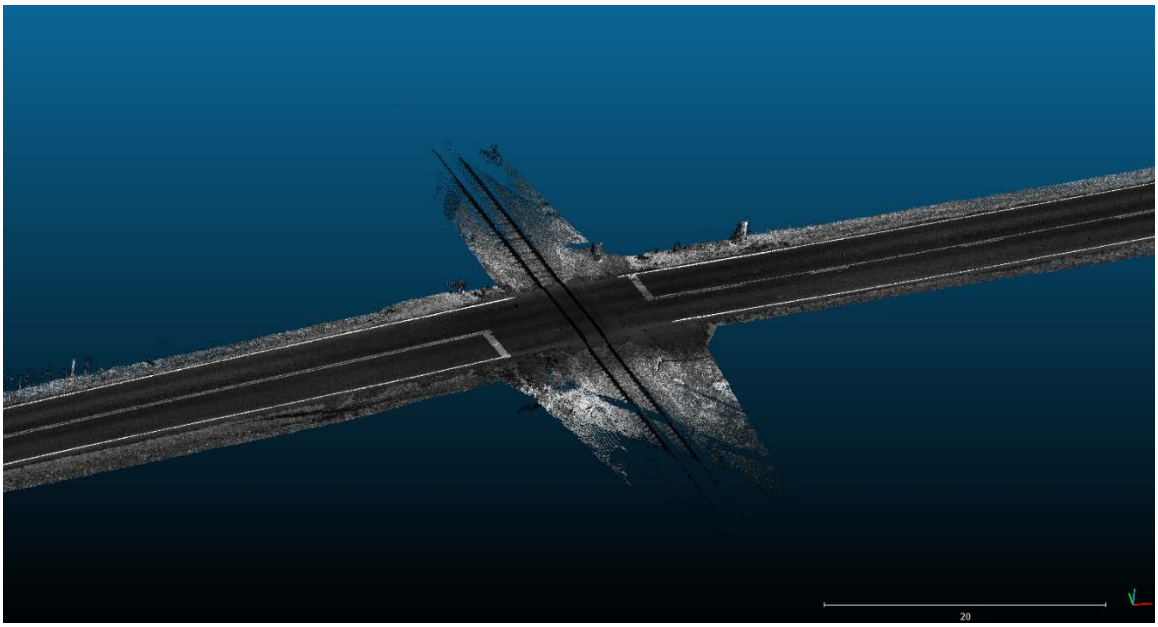

Figure 6.1 Bryan Station Road crossing.

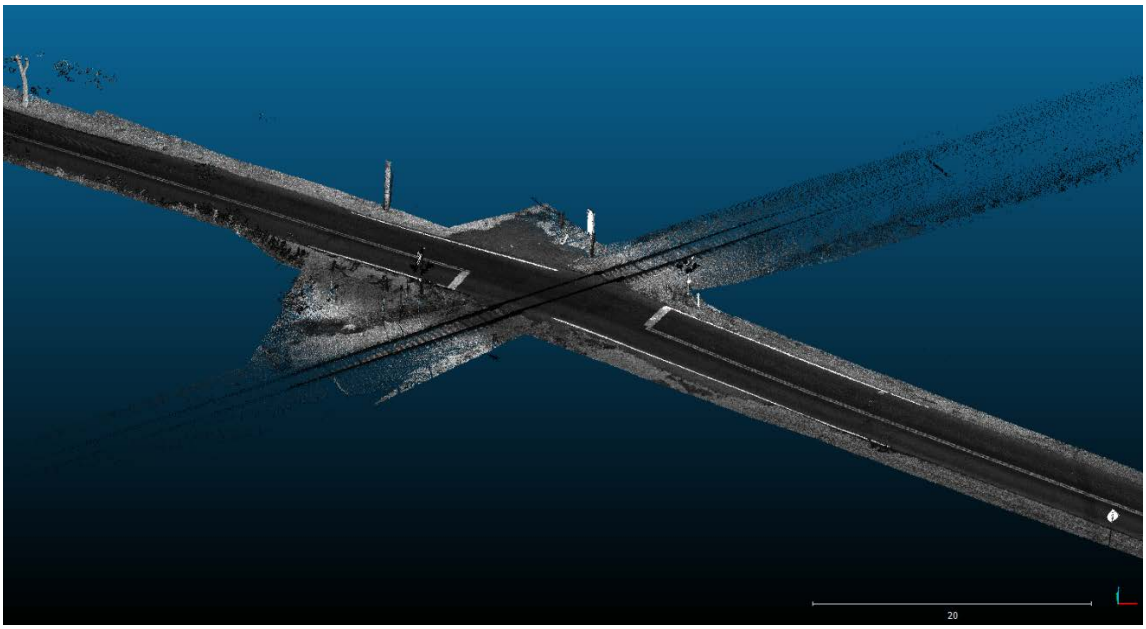

Figure 6.2 Briar Hill crossing.

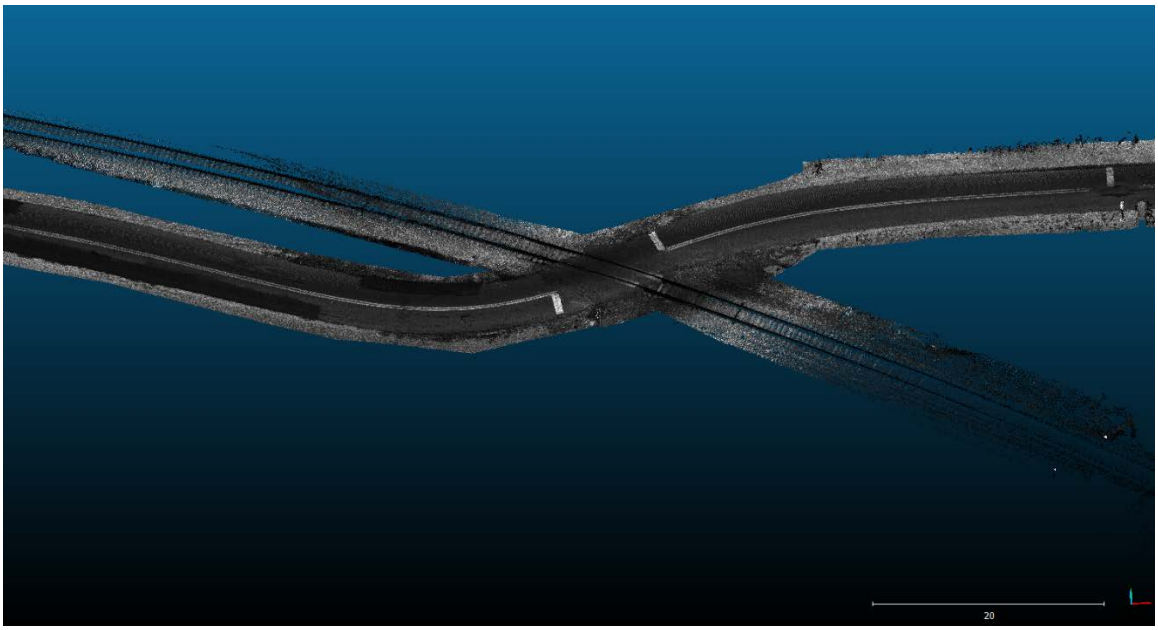

Figure 6.3 Hatton Road crossing.

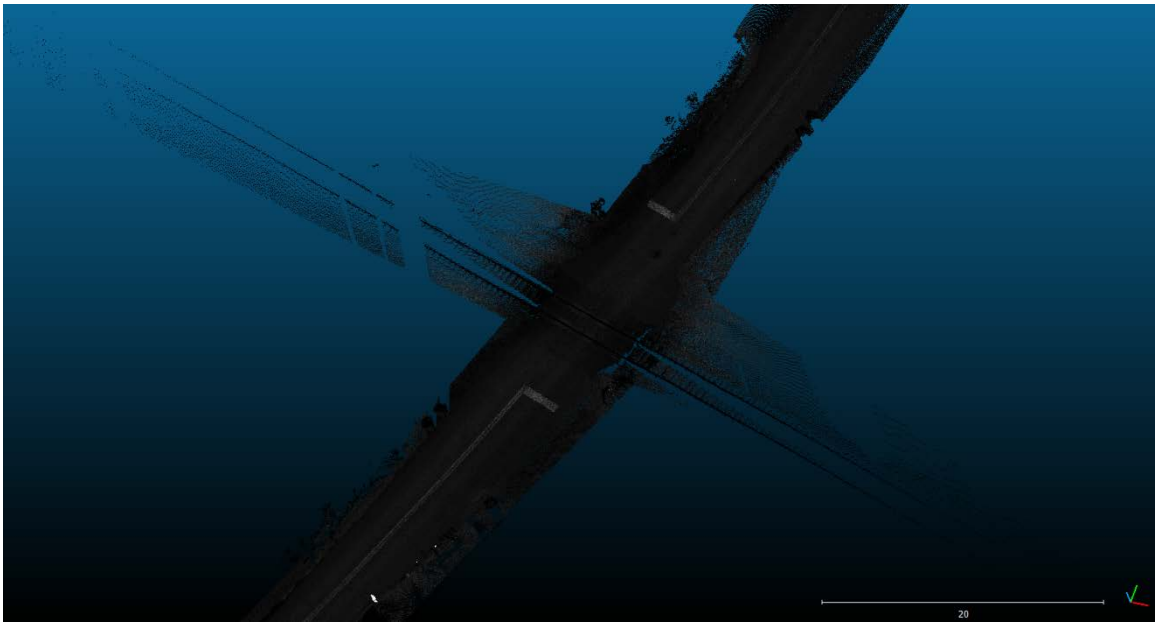

Figure 6.4 Bridgeport-Benson Road crossing.

Because the raw LiDAR data have sub-centimeter resolution, there are over two million points in each crossing data file. To reduce the size of the data file for more efficient processing, the point clouds were cropped to dimensions of 70 feet along the centerline of the highway and 20 feet in width. The intersection of the centerlines of rail and highway

were used to define the center of a local coordinate system for each crossing. Further, the density of each point cloud was thinned to five inch spacing, as passenger vehicle and larger tires have at least five by five inch contact areas, and finer deviations in surface are not likely to affect vehicle ride. This reduced the size of each point cloud from approximately two million points to just over 8,000 points—a much more manageable data set for analysis and presentation.

6.3 Crossing Roughness Index

Several standard measures of surface roughness are available. These measures are used for applications ranging from industrial manufactured surfaces texture (Lonardo et al., 1996) to characterization of surface deposits from volcanic eruptions (Whelley et al., 2014). Two basic measures are relevant to the current work.

First, areal arithmetic mean height (Sa) (Abouelatta, 2010) may be computed from Equation 1-1 as the average of absolute differences between a surface and its mean plane:

Equation 6-1

$$S_a = \frac{1}{MN}\sum_{j=1}^{N}\sum_{i=1}^{M}\left|z(x_i, y_j)\right|$$

Where:

M = total number of points along the X axis.

N = total number of points along the Y axis.

z = the elevation of point (xi, yj) at the XY plane.

Figure 1.5 presents a physical interpretation of this measure.

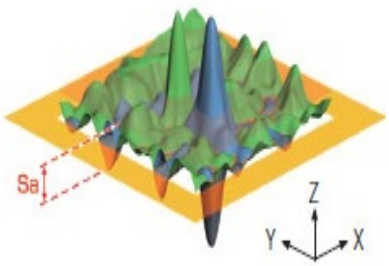

Figure 6.5 Arithmetic mean height (Olympus Corporation, 2016).

Second, areal root mean squared height (Sq) (Abouelatta, 2010) may be computed from Equation 1-2. Figure 2.9 presents a physical interpretation of this second measure. which is always greater than or equal to Sa.

Equation 6-2

$$S_q = \sqrt{\frac{1}{MN}\sum_{j=1}^{N}\sum_{i=1}^{M} z^2(x_i, y_j)}$$

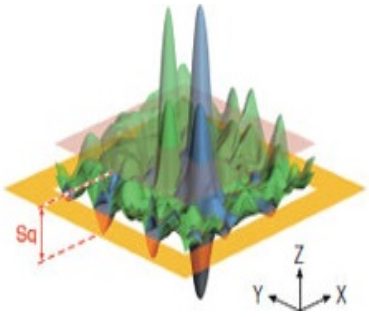

Figure 6.6 Root mean squared height (Olympus Corporation, 2016).

Both of these measures are calculated for each of the four crossings. Two surfaces are used in these computations. First, the entire 70-foot by 20-foot area is used (all 5”x5” grid cells). Next, only the approximate wheel paths of the crossings are used. For each crossing, there are four wheel paths, two in each direction. Table 6-1 presents the computed roughness indices for each crossing and each parameter for both total surface and wheel paths only. The ordered rank of crossings is the same for all measures. However, if there were significant variation (more extreme values) between wheel paths and entire surfaces (e.g., potholes, rutting, etc.), rank is more likely to be affected by choice of parameter.

Table 6-1 Crossing Roughness Index

Crossing	Entire Surface Area		Wheel path Area	
	Sa	Sq	Sa	Sq
Bryan Station	4.9	5.6	4.8	5.6
Briar Hill	7.7	9.5	7.7	9.5
Hatton	4.2	5.3	4.2	5.4
Bridgeport-Benson	5.2	6.3	5.1	6.2

Figure 6.7 shows that for the four study crossings, relative surface roughness measures are similar whether computed along the wheel path or across the entire crossing surface.

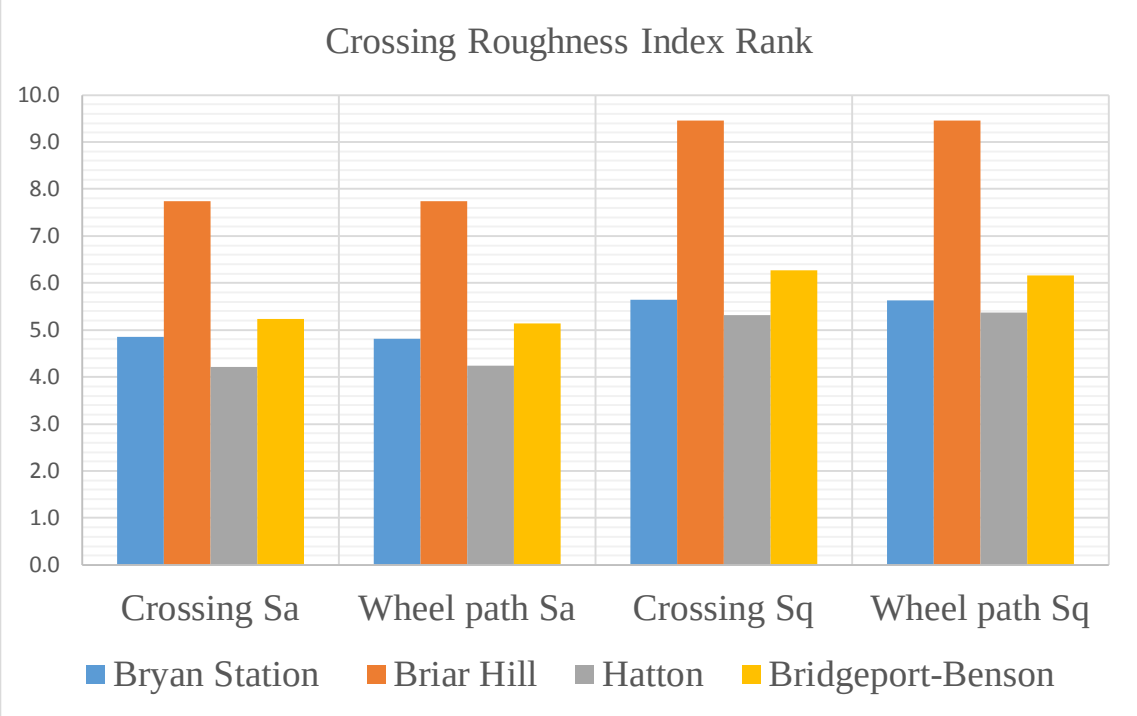

Figure 6.7 Crossing Roughness Index rank

To validate the relative measures provided by the surface roughness index, they can be normalized on a scale of 100 and compared to normalized field measured accelerations (those reported in chapter 4). Figure 6.8 shows there is little similarity between computed Sa and field measures of acceleration.

To explain, recall that simple computations of the Sa or Sq index makes use of a flat reference plane to determine the index. The use of such a plane limits the ability of the index to differentiate the effects of surface and profile, potentially creating absurd characterizations of smoothness. For example, Figure 6.9 illustrates a case where relative crossing "smoothness" would not be properly represented by these metrics. While Sa computed for surface A of the figure would be much greater than that computed for surface B, surface A is clearly smoother. In fact, the only cases where the use of a flat reference plane to calculate the measures would be correct, would be where both crossings had identical as-built profiles. Clearly, this is not realistic, as almost all crossings are different. This explains why Bryan Station has the lowest measured acceleration, but not the smoothest surface.

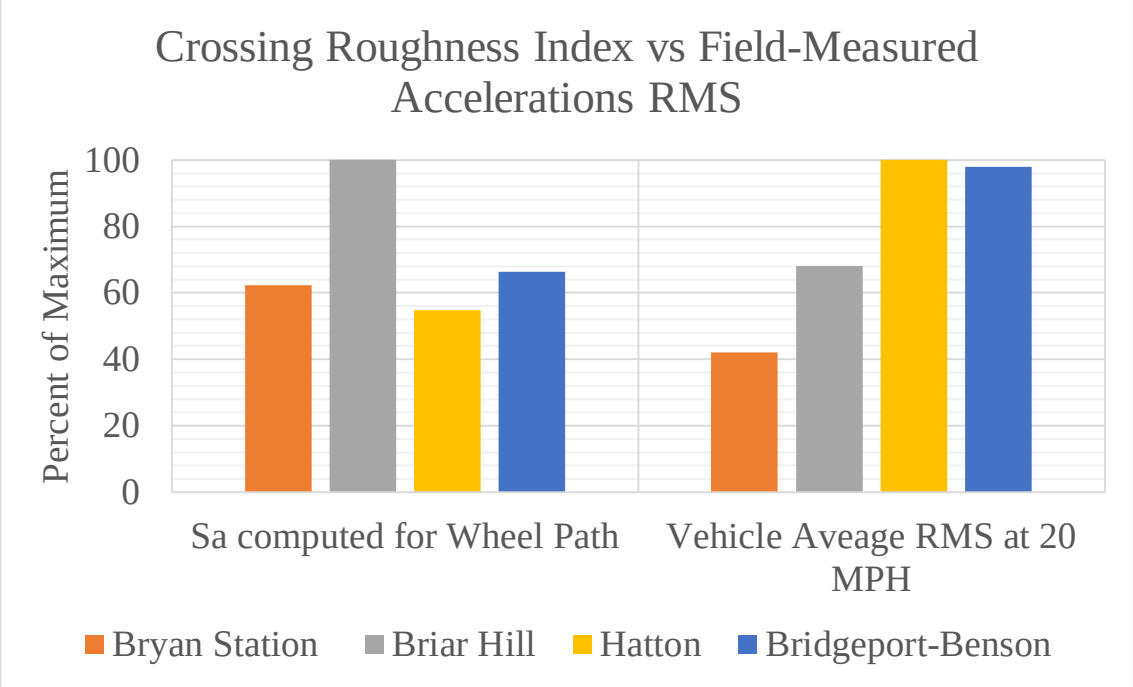

Figure 6.8 Normalized Crossing Roughness Index vs normalized field accelerations.

Crossing Profile A

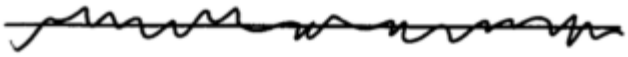

Crossing Profile B

Figure 6.9 Effect of profile only

A potential solution to the problem caused by the flat plane may be to compute the metrics based on the actual surface compared to a locally-smoothed surface (a "de-noised" profile). Section 4 of this chapter presents an approach based on this general concept.

Another possible solution to the problem would be to calculate the metrics based on differences between as-built and current surface models (Figure 6.10). Section 5 of this chapter demonstrates the potential utility of such an approach.

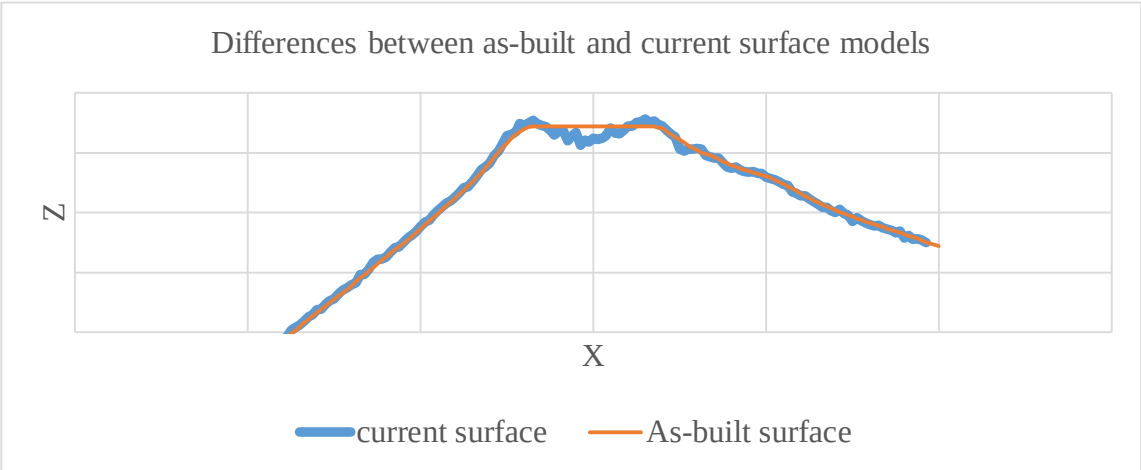

Figure 6.10 Differences between as-built and current surface models.

6.4 Crossing Rideability Index

The previous section developed measures which can be used to compare crossings based on surface model only, but that do not reliably predict the accelerations experienced by vehicles (rideability). This section presents a method which can be used to rank crossings with regards to their rideability as well. Predicting accurate values of acceleration is difficult (refer to previous chapter on vehicle dynamic modeling). However, prediction of relative accelerations is more feasible, and can be estimated using first principles of physics (vertical acceleration is the second derivative of vertical position with respect to time in the direction of travel). This can be readily computed based only upon the 3D surface model and an assumption off constant speed.

Initially, the second derivative of the sequential points on the actual surface were used to calculate accelerations. However, this resulted in exceedingly high estimates of acceleration as it would neglect the effect of vehicle suspension which smooths out the effects of small deviations. Therefore, a moving average along the surface profile was used to capture only more significant variations in surface (see Figure 6.11). A five-point moving average (20 inches) was used to compute relative accelerations in this work. Further investigations of moving average spacing could be a subject of future research.

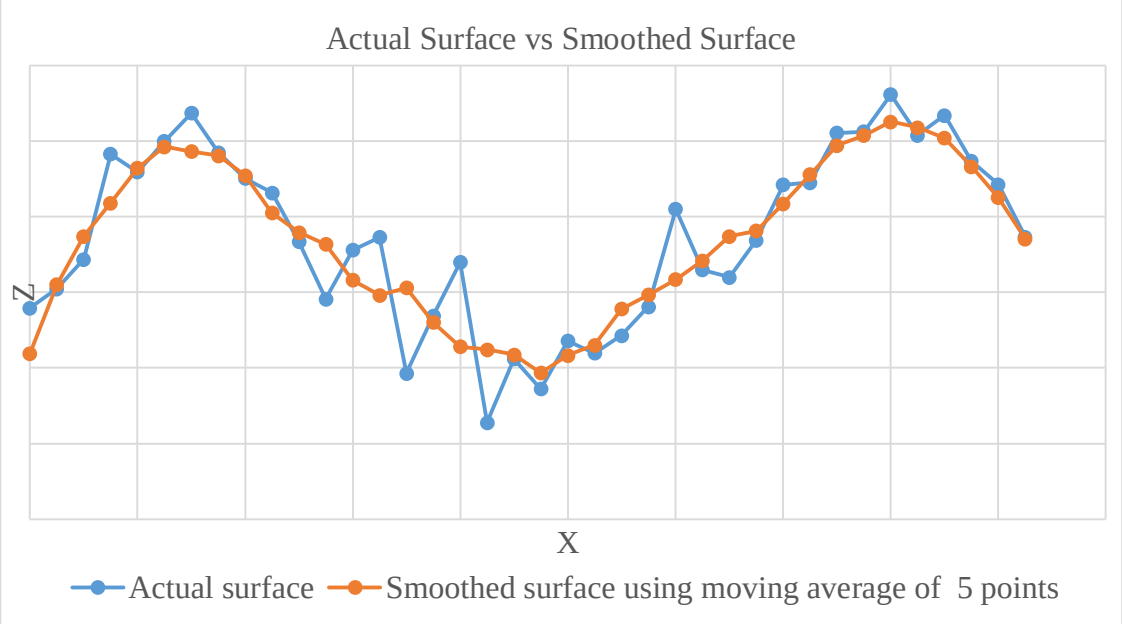

Figure 6.11 Actual surface vs smoothed surface.

In this section, computed accelerations are averaged by the root mean square method to determine a metric which can be compared to the field measured acceleration-derived RMS. This proposed metric (RMS of computed acceleration) is referred to as the "crossing rideability index." To establish a baseline relationship between crossing rideability and actual vehicle field-measured accelerations, the crossing rideability indices estimated by this method are compared to field readings for a common vehicle speed (20 MPH). Results are presented in Table 6-2.

There are two important observations to be made from these results. First, the accelerations predicted by the rideability index are still an order of magnitude higher than field readings. However, this is to be expected due to the damping effects of the vehicle suspension. Second, the relative ranking of crossing accelerations is closely approximated by the index. That is, the crossings with highest field readings are also those that are estimated to be highest by the index. Figure 6.12 shows the relative ratings of acceleration RMS normalized to maximum levels. For the four crossings evaluated, the Crossing Rideability Index reflects relative real-world observations.

Table 6-2 Crossing Rideability Index vs. measured accelerations at 20 MPH.

	Crossing Rideability Index (Entire Crossing Surface)	Crossing Rideability Index (Wheel path)	Accelerometer Measured Acceleration (average of all vehicles)
Bryan Station	8.5	7.9	0.42
Briar Hill	7.9	7.1	0.68
Hatton	14.2	13.4	1.00
Bridgeport-Benson	13.6	12.2	0.98

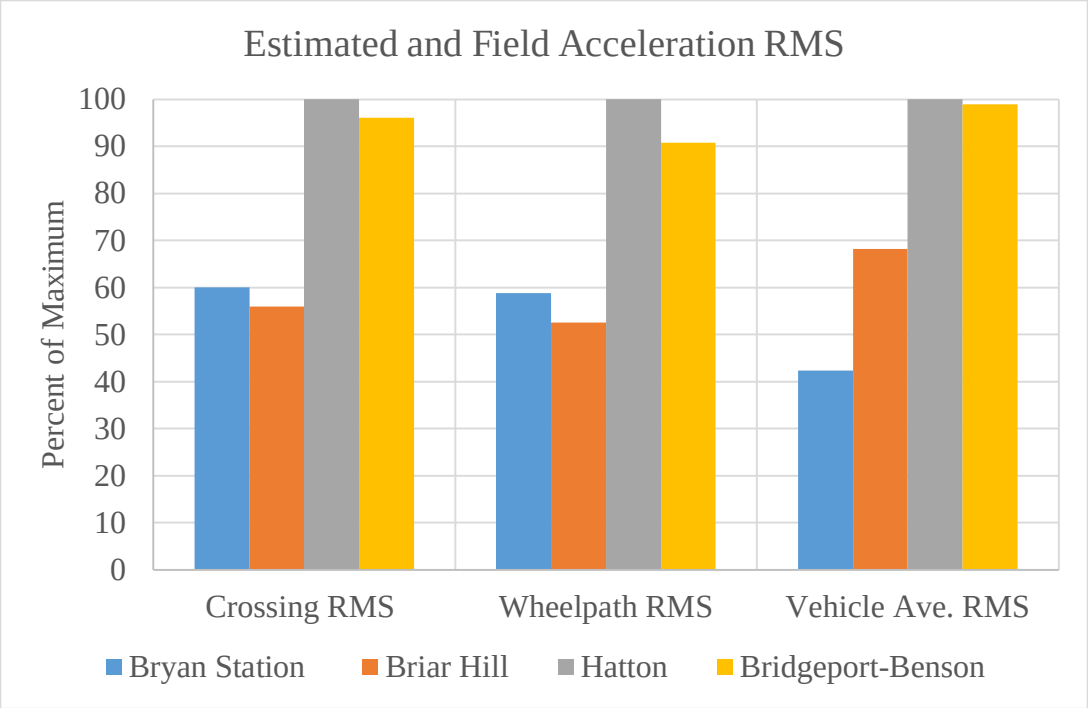

Figure 6.12 Normalized accelerations at 20 MPH.

The analysis to this point assumes a constant speed to compare crossings (in this case, 20 MPH). Generally, roads designed for mobility will have higher design speeds than those provided for access. While the public expects to slow down for railroad crossings, they also expect to be able to maintain higher speeds for higher functionally classed roads. Slowing vehicles to 20 MPH or even lower to comfortably negotiate a rail crossing on a major highway is not acceptable. Therefore, posted speed at the crossing relative to design speed of the highway should be taken into account when prioritizing improvements.

To address the importance of the crossing and therefore the practical aspects of ranking crossings for improvement, accelerations are calculated for the posted (desirable) highway speed. These accelerations are again compared to field readings as shown in Table 6-3. Again, there are two observations to be made from these results. As with the analysis of accelerations at 20 MPH, the accelerations predicted by the Crossing Rideability Index at posted speed are also an order of magnitude higher than field readings. And again, the relative ranking of crossing accelerations is closely approximated by the index. Figure 6.13 shows the relative ratings of acceleration RMS normalized to maximum levels.

Table 6-3 Crossing Rideability Index vs. measured accelerations at posted speeds.

	Crossing Rideability Index (Entire Crossing Surface)	Crossing Rideability Index (Wheel path)	Accelerometer Measured Acceleration (average of all vehicles)
Bryan Station (30mph)	19.1	17.8	0.67
Briar Hill (35mph)	24.3	21.6	1.74
Hatton (20mph)	14.2	13.4	0.99
Bridgeport-Benson (25mph)	21.3	19.1	1.09

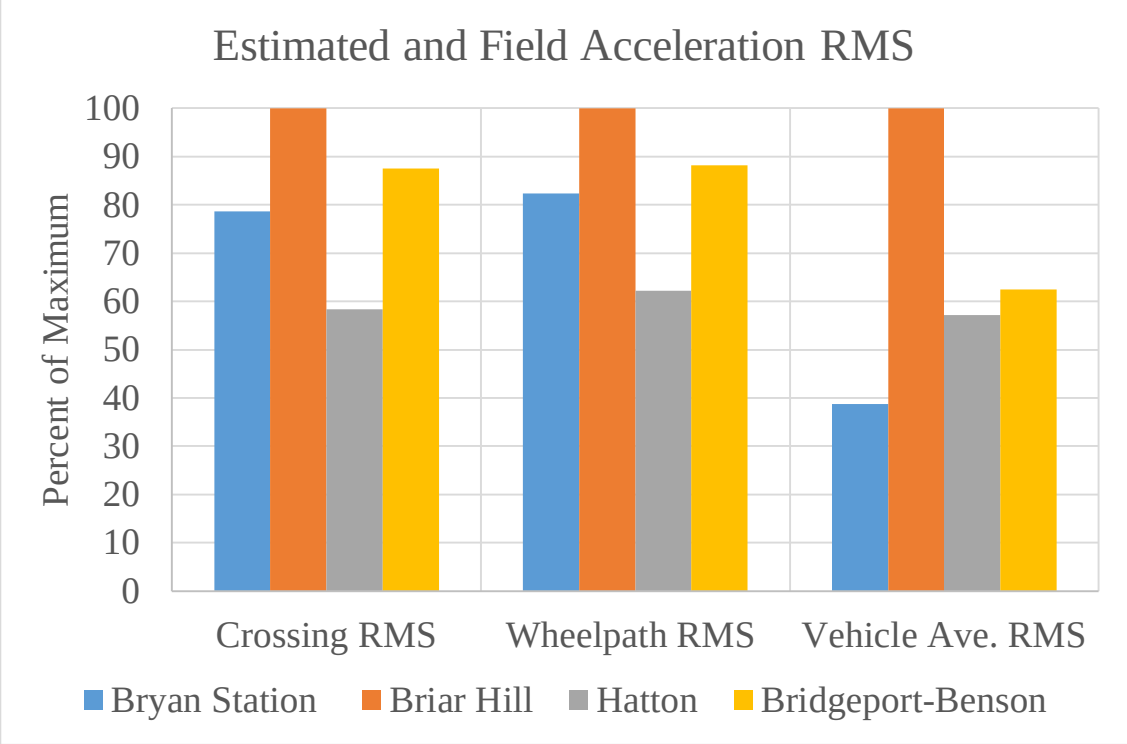

Figure 6.13 Normalized accelerations at posted speeds.

6.5 Crossing Condition Index (Separating the Effects of Condition and Design)

In previous chapters and sections of this dissertation, various approaches were developed and presented to quantify the overall roughness and rideability of the railroad crossing. It is now desired to resolve this performance into its principle components, which are: 1) effect of surface condition and 2) effect of as-built design profile. This section uses the field measured accelerations from Chapter 4 as the total (surface plus design) accelerations experienced at the crossing.

To estimate the design component of acceleration, accelerations are estimated to be those that would be experienced by a vehicle if the crossing were in its original condition. How was the crossing originally designed? Many, especially local road crossings are simply *constructed* rather than designed. If crossings are designed, vertical curves on the highway are based on a parabola. See Figure 6.14.

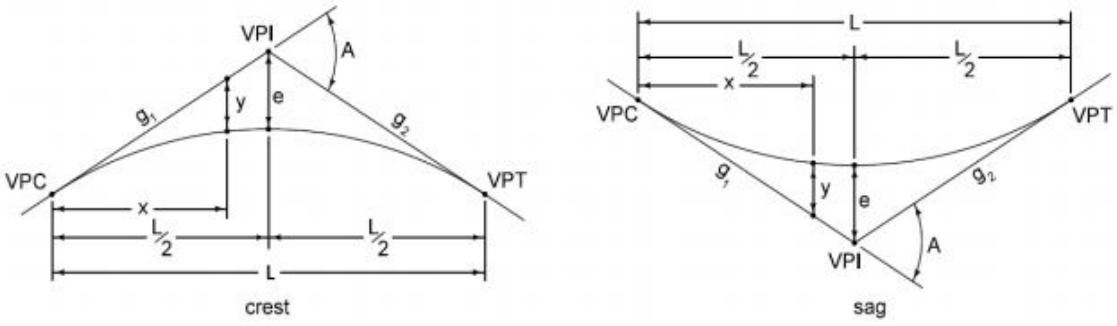

Figure 6.14 Vertical Curve Design

The equation which describes the parabolic shape of the highway vertical curve is:

Equation 6-3

$$y = \frac{G_2 - G_1}{200L}x^2 + \frac{G_1}{100}x + E_{VPC}$$

Where:

VPC = Vertical Point of the Curvature.

VPT = Vertical Point of Tangency.

y = Elevation of a point on the curve at a distance x from the VPC in feet.

x = horizontal distance to any point on the curve from the VPC in feet.

G1 and G2 = gradients of a slop in percent.

L = total length of vertical curve in feet.

E_{VPC} = elevation of VPC in feet.

When the vehicle is driven at a constant speed the following equation is obtained:

Equation 6-4 $$x = vt$$

Where:

t = travel time in second.

v = speed in ft/s.

Then,

Equation 6-5

$$y = \frac{G_2 - G_1}{200L}(vt)^2 + \frac{G_1}{100}(vt) + E_{VPC}$$

Taking the second derivative, one obtains:

Equation 6-6

$$a = \frac{d^2y}{dt^2} = \frac{G_2 - G_1}{100L}v^2$$

Where:

a = acceleration on the vertical direction in ft/s^2.

Setting "a" equal to 1.0 fps^2 results in:

Equation 6-7

$$L = \frac{G_2 - G_1}{100} v^2$$

When speed v is converted from ft/s into mph, Equation 1-7 becomes

Equation 6-8

$$L = \frac{G_2 - G_1}{46.5} v^2$$

Where:

L = total length of vertical curve in feet.

G1 and G2 = gradients of a slop in percent.

v =horizontal speed in mph

Reordering the terms produces:

Equation 6-9

$$v = \sqrt{\frac{46.5L}{G_2 - G_1}}$$

Where v is the vehicle longitudinal (speedometer) speed v and vertical acceleration is held to 1 ft/s^2.

To demonstrate the estimation of acceleration due to as-built profile, the Briar Hill road centerline crossing profile (extracted from the 3D point cloud surface model) is plotted as shown in Figure 6.15. A hypothetical as-built crossing profile is fit to this profile by establishing VPC and VPT and best-fit tangent lines.

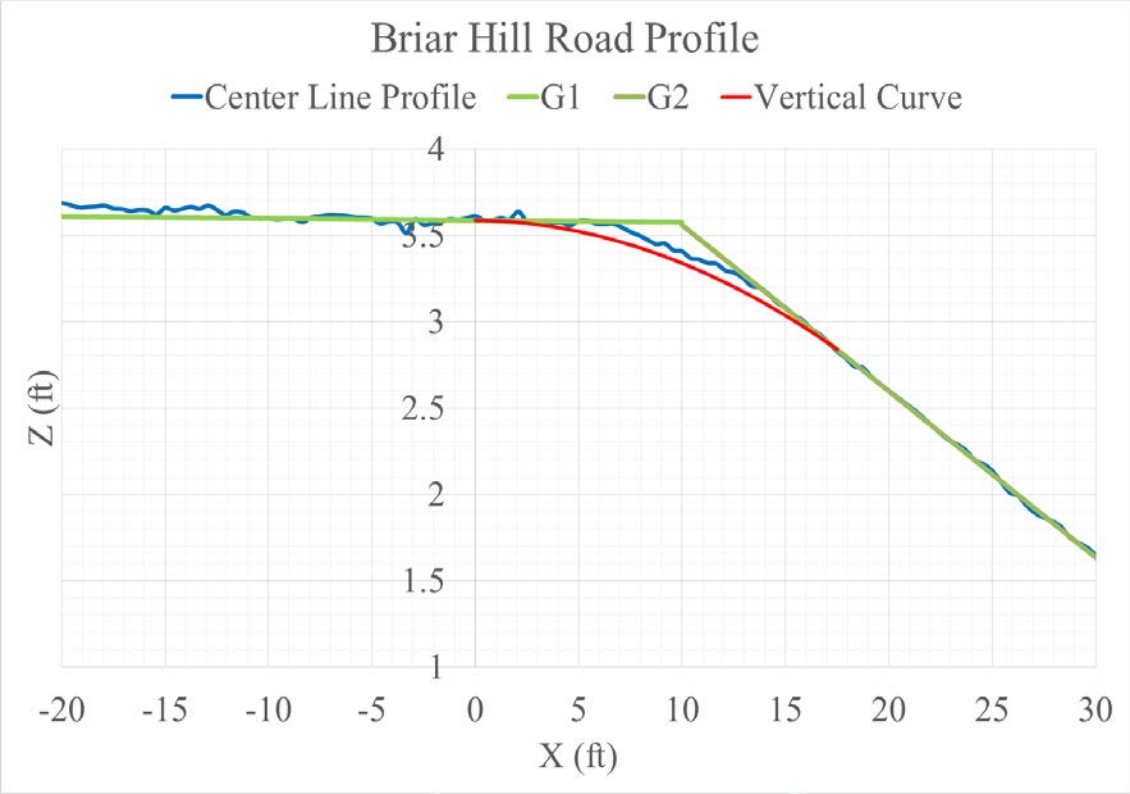

Figure 6.15 Briar Hill Road profile and fitted vertical curve.

From the plot, G1, G2 and L are measured as -0.10%, -0.96% and 17.5 feet, respectively. It is interesting to note that the length of vertical curves for this and many railroad crossings are much less than that that recommended for open road design. For example, the length of vertical curve needed to accommodate 35 mph operations at 1.0 fps^2 or 0.3 m/s^2 is 250 feet! However, in practice such long curves are not practical to construct at many locations.

It is interesting to recall the high accelerations experienced by vehicles crossing Briar Hill at the 35 mph posted speed (see Figure 6.16) suggesting that the highway agency may wish to reconsider the recommended speed at this location.

Figure 6.16 Briar Hill has a posted speed of 35 mph.

Using Equation 1-9, the speed at which a vehicle may be driven over the theoretical as-built vertical curve at Briar Hill while limiting the vertical acceleration to a comfortable 1.0 fps^2 is calculated as 9.3 mph.

From Equation 6-6, it can be seen that acceleration is proportional to the square of velocity, and thus,

Equation 6-10

$$\frac{a_1}{a_2} = \left(\frac{v_1}{v_2}\right)^2$$

Therefore, the vertical acceleration when the vehicle is driving over this curve at the 35 mph posted speed can be calculated as 14.3 fps^2 or 4.4 m/s^2.

Based on the field-measured acceleration data from chapter 4, the average acceleration of all vehicles crossing Briar Hill Road at 35 mph is 7.0 m/s^2. Clearly, most of this acceleration is caused by the vehicle negotiating the as-built profile. However, 2.6 m/s^2 of acceleration is unexplained. It is proposed that this residual is due to the surface condition of the crossing (and rail crossing surface geometry/materials), mitigated by the suspension of the vehicle. This residual may be defined as the "condition index" of the

crossing. The condition index for the Briar Hill Road crossing is therefore 2.6 m/s^2. Table 6-4 presents the condition indices calculated for the four study crossings. Figure 6.17 illustrates the two components of crossing rideability (profile-related acceleration and condition-related acceleration). Profiles fitted to all crossings as well as calculations are presented in **APPENDIX F**.

Table 6-4 Condition Index for study crossings

Crossing	Posted Speed mph	Field Measured Maximum Negative Acceleration (m/s^2)	Acceleration estimated from profile (m/s^2)	condition index (m/s^2)
Bryan Station	30	4.0	1.1	2.9
Briar Hill	35	7.0	4.4	2.6
Hatton	20	5.0	1.4	3.6
Bridgeport-Benson	25	6.0	1.7	4.3

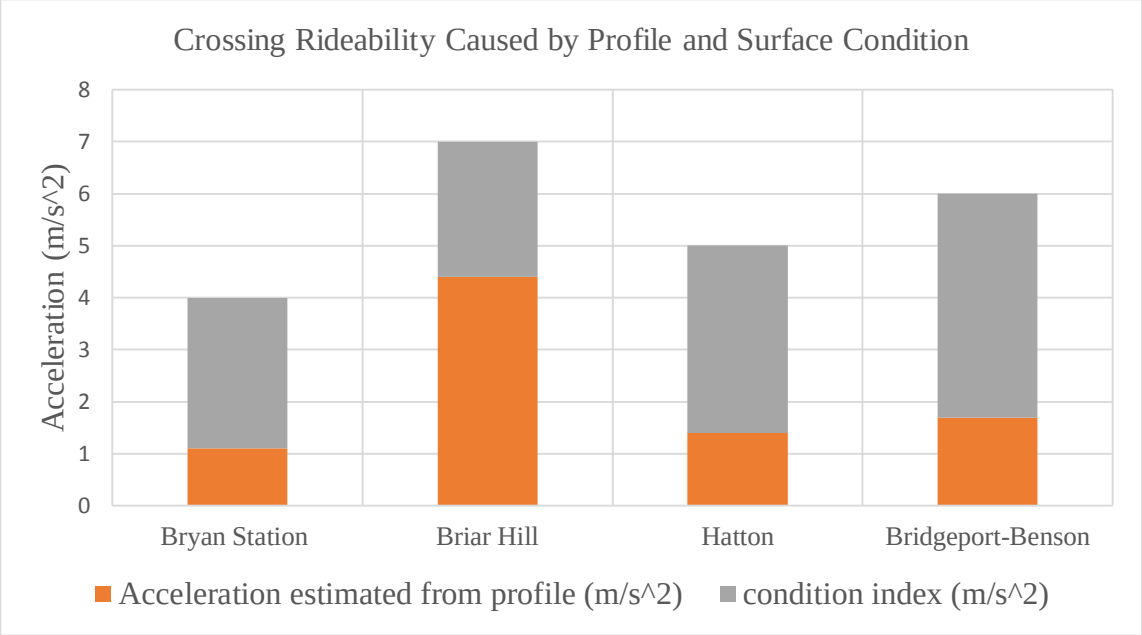

Figure 6.17 Two components of crossing rideability

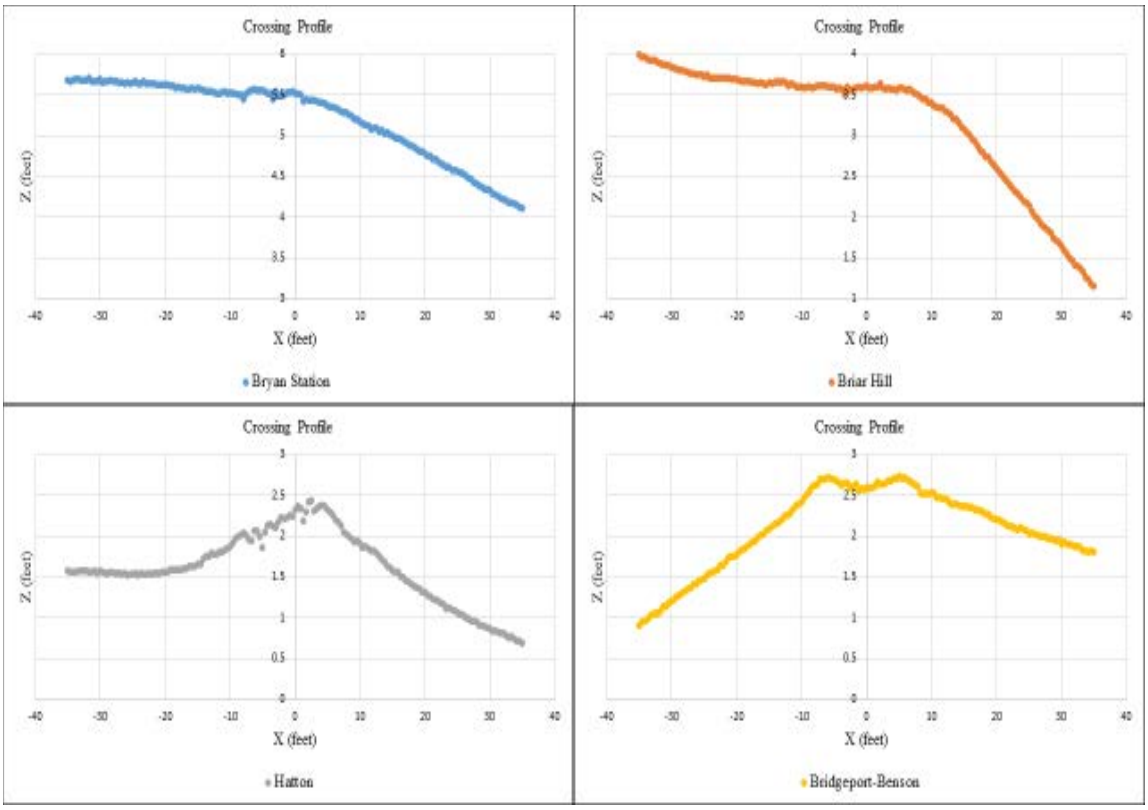

Figure 6.18 General shapes of crossing profiles.

The resulting condition indices seem consistent with the general shapes of each crossing profile (see Figure 6.18). For example, visually, Hatton Rd appears to be in the worst shape, surface-wise. However, amongst all crossings, it is clear that Bridgeport-Benson has the roughest profile.

There are several limitations of the proposed approach. These include:

- Field measured accelerations are quite variable, especially maximum accelerations (therefore, RMS was used for ranking)
- Rough condition produces both positive and negative accelerations, while profile generally will produce only positive (sag) or negative (crest) accelerations (assuming only one vertical curve in the design); as previously mentioned, crossings are not always designed, so their original profile may not be a simple vertical curve
- Complexity of vehicle response

- Unless as-built diagrams or 3D surface plots are available from the time of construction, judgment is required in the selection of points defining the as-built profile. Condition index, as defined, is sensitive to the selection of these points, especially the length of curve. For example, at Briar Hill, changing the estimated original curve length from 17.5 to 20 changes the condition index from 2.6 to 3.2 m/s^2.
- A crossing may appear to have been constructed with multiple slopes/curves (see Figure 6.19, Bridgeport-Benson). However, it is unlikely that such short vertical curves were actually constructed as such, It is more likely that the curvature observed in the current condition is caused by settlement or re-lining of the track, or buildup of asphalt at road approaches.

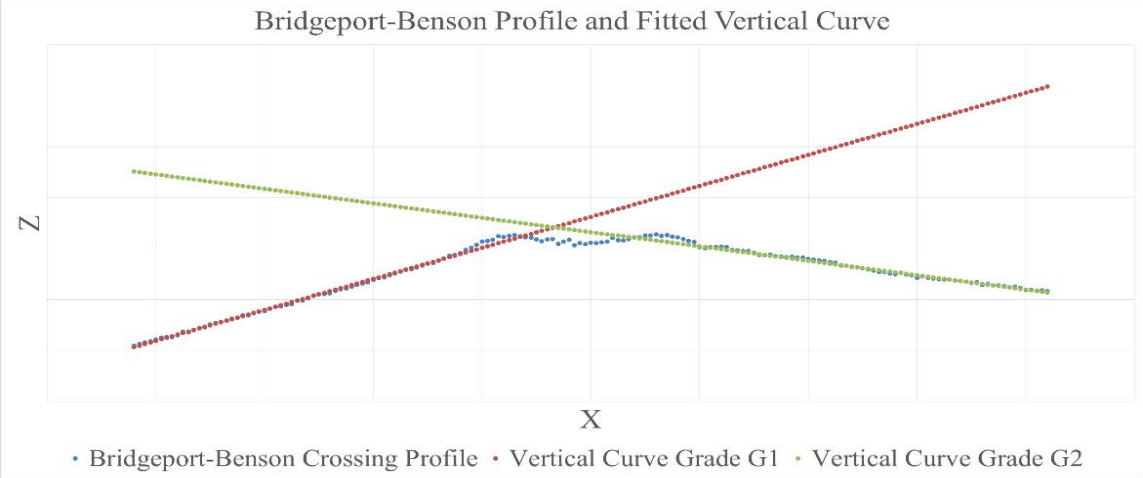

Figure 6.19 Bridgeport-Benson profile and fitted vertical curve.

6.6 Summary and Conclusion

In this chapter, three different quantitative crossing assessment indices were presented. The Crossing Roughness Index and the Crossing Rideability Index were both developed based on the crossing 3D point cloud only. The Crossing Roughness Index calculates the roughness due to geometric characteristics of actual crossing surface condition and profile grades of highway approaches. The Crossing Rideability Index estimates RMS of vertical accelerations as the second derivation of the crossing vertical

profile. The last, Crossing Condition Index separates the acceleration contribution of surface condition plus vehicle response from that of original vertical curve design.

The Crossing Roughness Index and the Crossing Rideability Index were used to rank the performances of four different crossings and the results compared to the accelerometer measurement method from Chapter 4. Depending on data availability and actual application needs, single or multiple indices could be chosen to perform the assessment of the existing crossing condition.

CHAPTER 7. RAIL CROSSING SAFETY: IDENTIFICATION AND ASSESSMENT OF HUMP CROSSINGS

7.1 Introduction

Quality of surface is an important aspect affecting both the safety and the performance of at-grade rail-highway crossings. A hump crossing, defined as a crossing where a vehicle with low ground clearance may become high-centered or stuck, may increase the risk of crashes for both trains and automobiles (Bauer, 1958). Crashes at hump crossings, besides being devastating, attract public attention, as the vehicles most likely to be involved are large trucks or mass transit vehicles. For example, video of a recent limousine-train crash at a hump crossing in New Paris, Indiana was posted on the Internet (StudioNoeProductions, 2015). Although in this case no one was injured, the video attracted over two million viewers and highlights the hump crossing safety issue. Figure 2.10 shows the catastrophic result of a train-truck collision at a hump crossing.

Design guidelines are available for constructing crossings in such a way as to reduce or eliminate the probability of a vehicle becoming high-centered (American Railway Engineering Maintenance-of-Way Association (AREMA), 2015). However, many crossings are not built to these standards. In Kentucky, assessment of hump crossings is limited. Based on an inspector's judgment, hump crossings are cataloged in a single field of the State's road inventory—a field which simply includes a yes or a no. Where crossings are assessed quantitatively (in Kentucky or elsewhere), a 2D approach is used (based on the road profile only, or, if based on a 3D pavement model, are still restricted to 2D for the vehicle). However, no methods exist to evaluate the potential impact of pavement cross section variation on all possible contact points of the vehicle and pavement. In part, the cost and difficulty of collecting 3D data has likely limited the development of tools for such analysis.

Today, 3D data are becoming widely available. Given a 3D point cloud, the distance between any two points of a crossing as well as and elevation differences between surfaces can be readily measured. Scenarios where vehicles with low ground clearance may become high-centered or hung-up on a crossing may be determined based on vehicle dimensions such as wheel base length and clearance height. Not only may such an

application of 3D technology identify hump crossings, it may also be possible to quantify the severity of potential interference (some trucks “drag” their loads across) and be used to proactively improve safety at crossings.

This chapter presents a method to quantify and evaluate the complex geospatial interaction between vehicles and crossings, and is organized as follows:

- The second section presents background including a discussion of current design guidelines for rail grade crossings, previous studies and applications of hump crossing identification and current research on and application of 3D data collection for rail grade crossings.
- The third section describes field test locations and data collection efforts
- The fourth section presents a detailed methodology for identifying and assessing hump crossings
- A fifth section details test results
- The sixth section provides a field validation of the hump crossing assessment methodology.
- The seventh and concluding section presents conclusions, advantages, limitations and future application of the proposed methodology.

7.2 Background

Crossing geometric design guidance is provided in AASHTO’s A Policy on Geometric Design of Highways and Streets (the Green book) (American Association of State Highway and Transportation Officials, 2011), US DOT Railroad-Highway Grade Crossing Handbook (US Department of Transportation, 2007) and American Railway Engineering and Maintenance-of-Way Association (AREMA) Manual for Railway Engineering (American Railway Engineering Maintenance-of-Way Association, 2015). These guides indicate that the surface of the highway should be neither more than 3 inches higher nor more than 6 inches lower than the top of the nearest rail at a point 30 feet from the rail, measured at a right angle, unless track superelevation dictates otherwise, as shown in Figure 7.1. Following these guidelines would prevent most all but the most extreme low and long vehicles from becoming hi-centered.

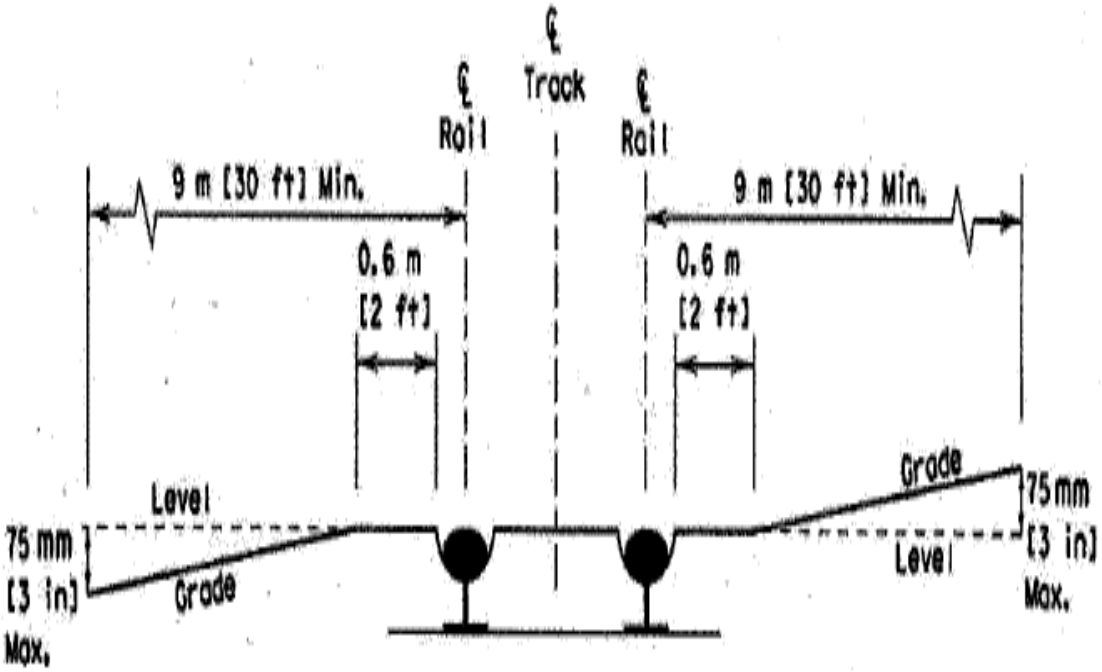

Figure 7.1 Rail-Highway grade crossing vertical alignment (AASHTO, 2011).

Previous efforts have been made to address the hump crossing issue. The "HANG-UP" software(Eck & Kang, 1992; Kang & Eck, 1991), developed in the early 1990s and later, related papers, (French et al., 2003) (Clawson, 2002), approach the hump crossing problem based on two dimensional geometric design. These dimensions include only the vehicle length and clearance as well as the crossing profile to identify conflict points, as shown in Figure 2.11. These solutions do not consider that actual field crossings vary in cross section due to highway or rail superelevation, construction abnormalities or conditions such as rutting or potholes. Wheel paths may incur different profiles, not to mention that pavement may vary between wheel paths where most conflicts are likely to occur (e.g, in the center of the wheels at the low part of axle or between front and rear wheels and again in the middle of the wheel path.) Also, previous work has examined only a very sparse grid of potential conflict points (e.g., every five feet) and computing power limited the extension of the application into three dimensions.

Another approach to the identification of hump crossings has been to build physical models with frame and wheels and "drive" the model over crossings as shown in Figure 2.12. Obviously, the physical model must be taken to each crossing and traffic control must be provided to conduct systematic evaluation. Such an evaluation is time consuming. Two additional disadvantages to the physical model approach are 1) the frame only represents a particular vehicle that may or may not be in the mix of vehicles that actually use the crossing, and 2) to assess the third dimension (cross section) of the crossing, the frame must be driven across the crossing multiple times.

Today, with the advent of low-cost and ubiquitous 3D technology and data, there are more analytical possibilities. Several methods exist to map crossing surfaces at varying levels of precision and cost as discussed in previous chapters of this dissertation. Data collected by these methods provide the basis for a modeling crossings, and when combined with 3D models of design vehicles, facilitate investigating potential conflicts in three dimensions for any hump crossing.

7.3 Acquisition 3D Data of Crossing Pavement

To develop and test the analytical methods proposed, data were collected for three crossings in Kentucky. These particular crossings were selected as representative of varying surface conditions, as-built profiles and single and double tracks.

For each of these, aerial imagery, LiDAR point clouds, and centerline profiles are visualized in Figure 7.2 through Figure 7.10.

Figure 7.2 Crossing A: Bryan Station Road (USDOT #346839X) aerial photo.

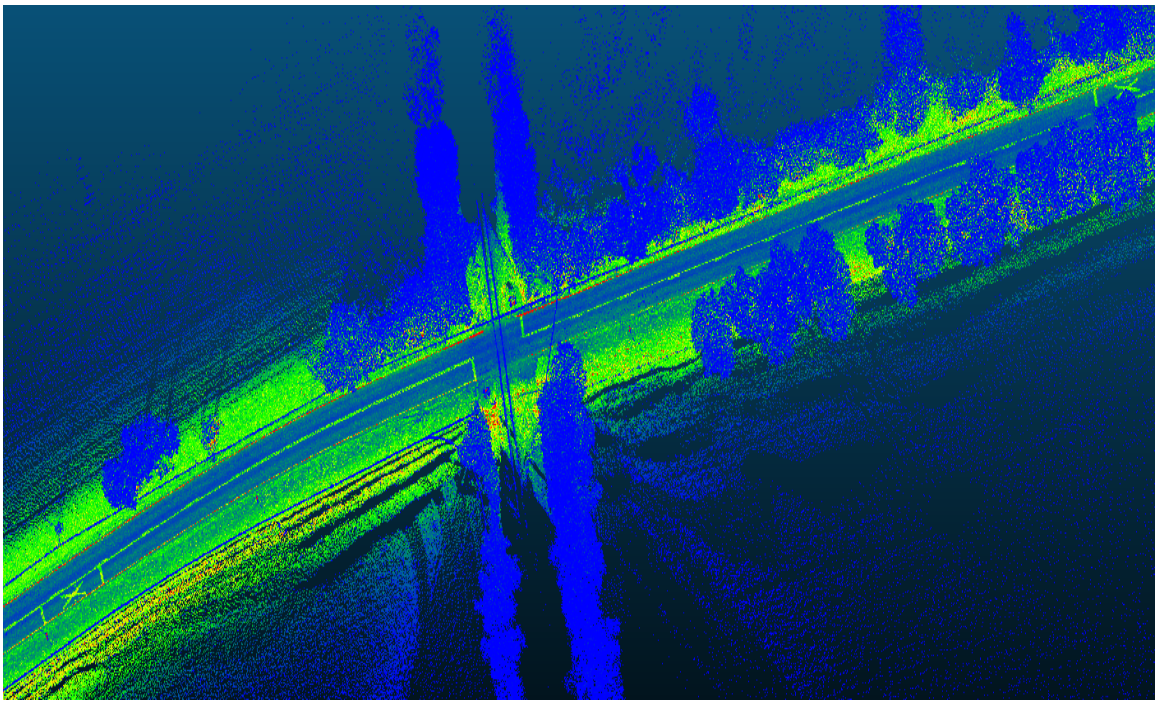

Figure 7.3 Crossing A: Bryan Station Road LiDAR point cloud.

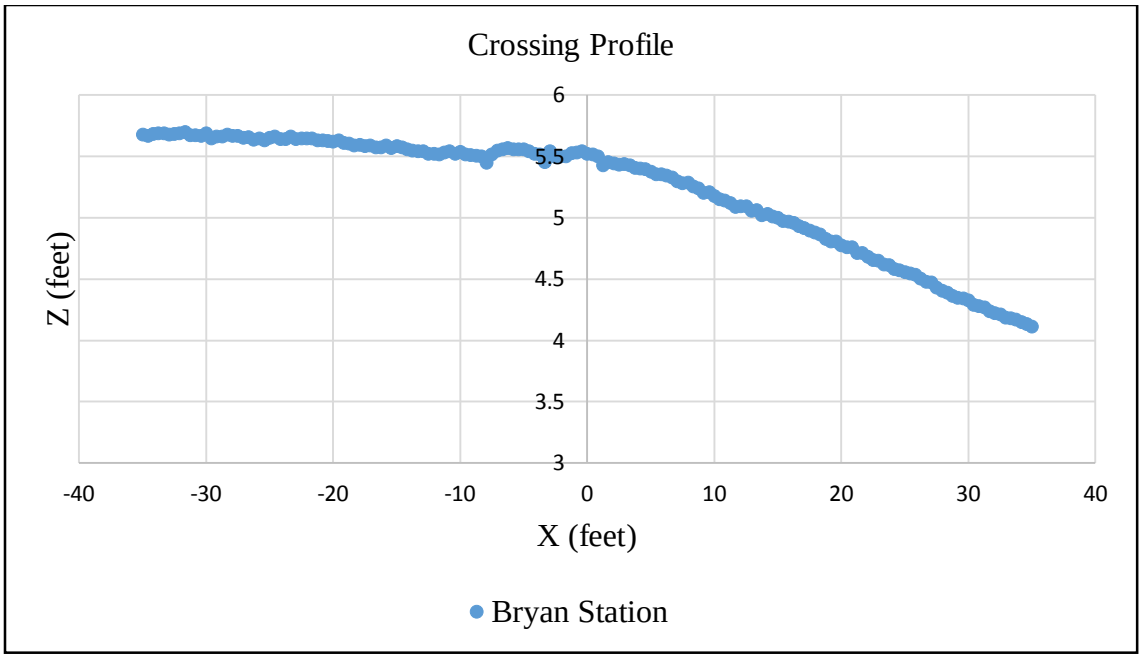

Figure 7.4 Crossing A: Bryan Station Road centerline profile.

Figure 7.5 Crossing B. Brannon Road crossing (USDOT # 841647U) aerial photo.

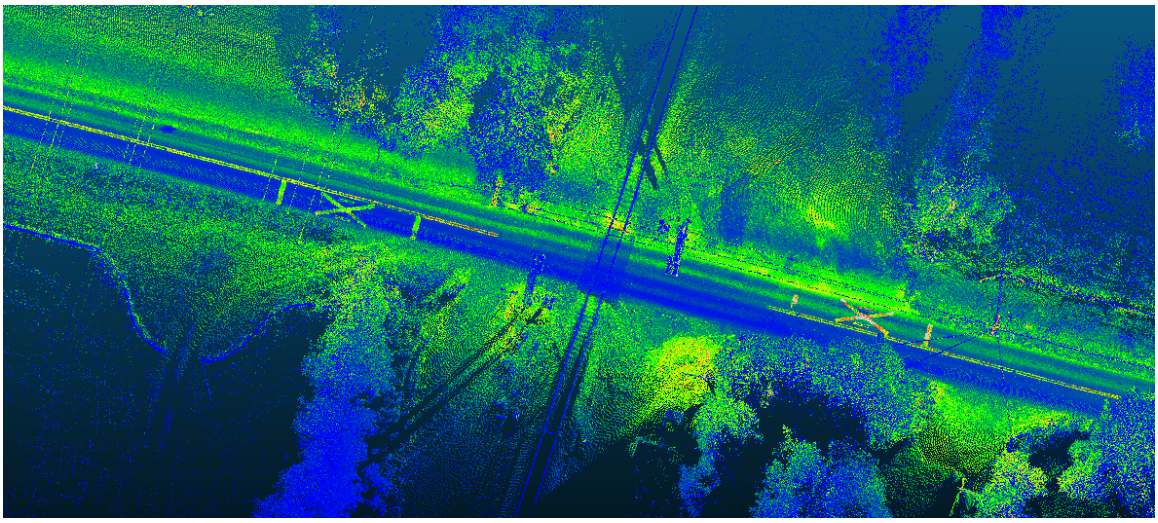

Figure 7.6 Crossing B. Brannon Road crossing LiDAR point cloud.

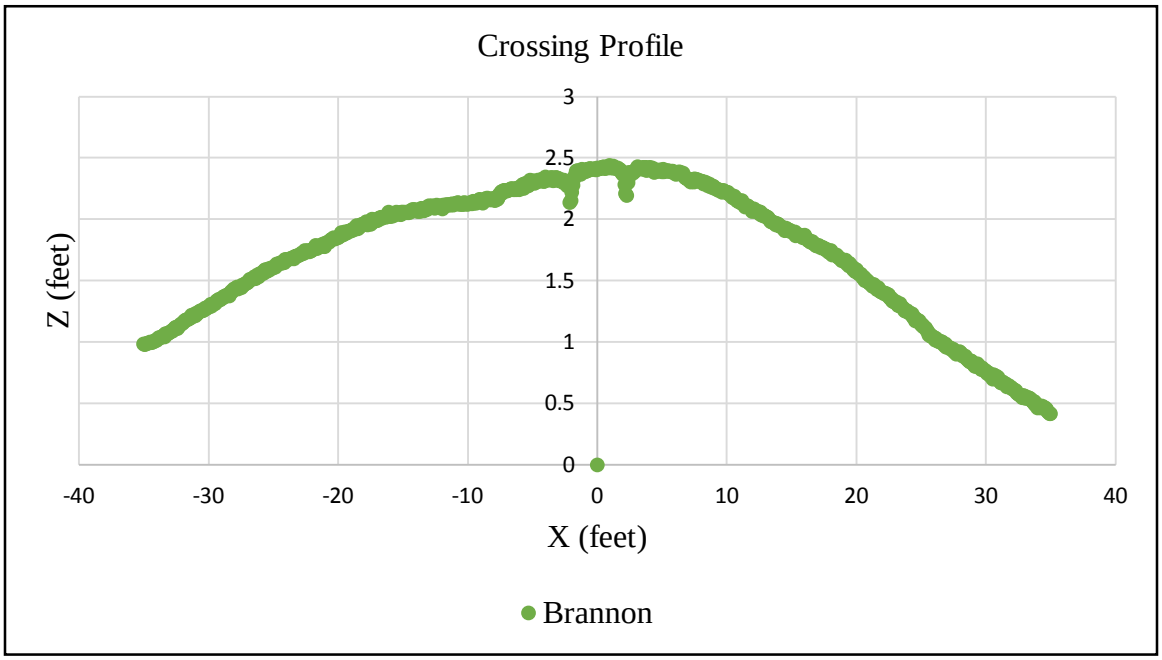

Figure 7.7 Crossing B. Brannon Road crossing centerline profile.

Figure 7.8 Crossing C. Briar Hill Road Army Depot Road crossing (USDOT # 346849D) aerial photo.

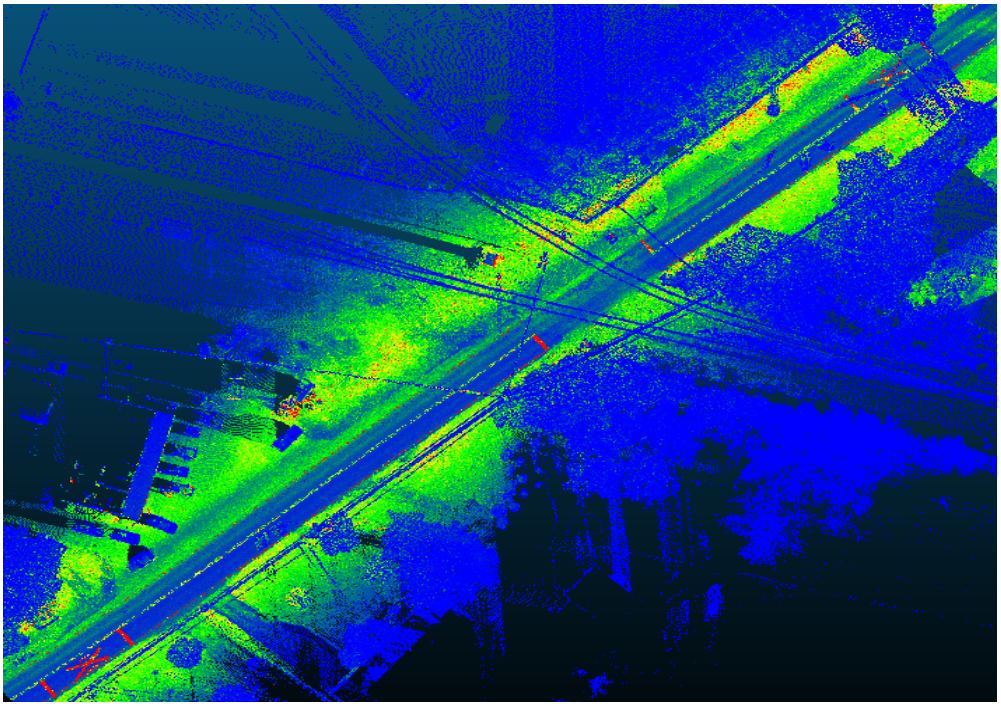

Figure 7.9 Crossing C. Briar Hill Army Depot Road crossing LiDAR point cloud

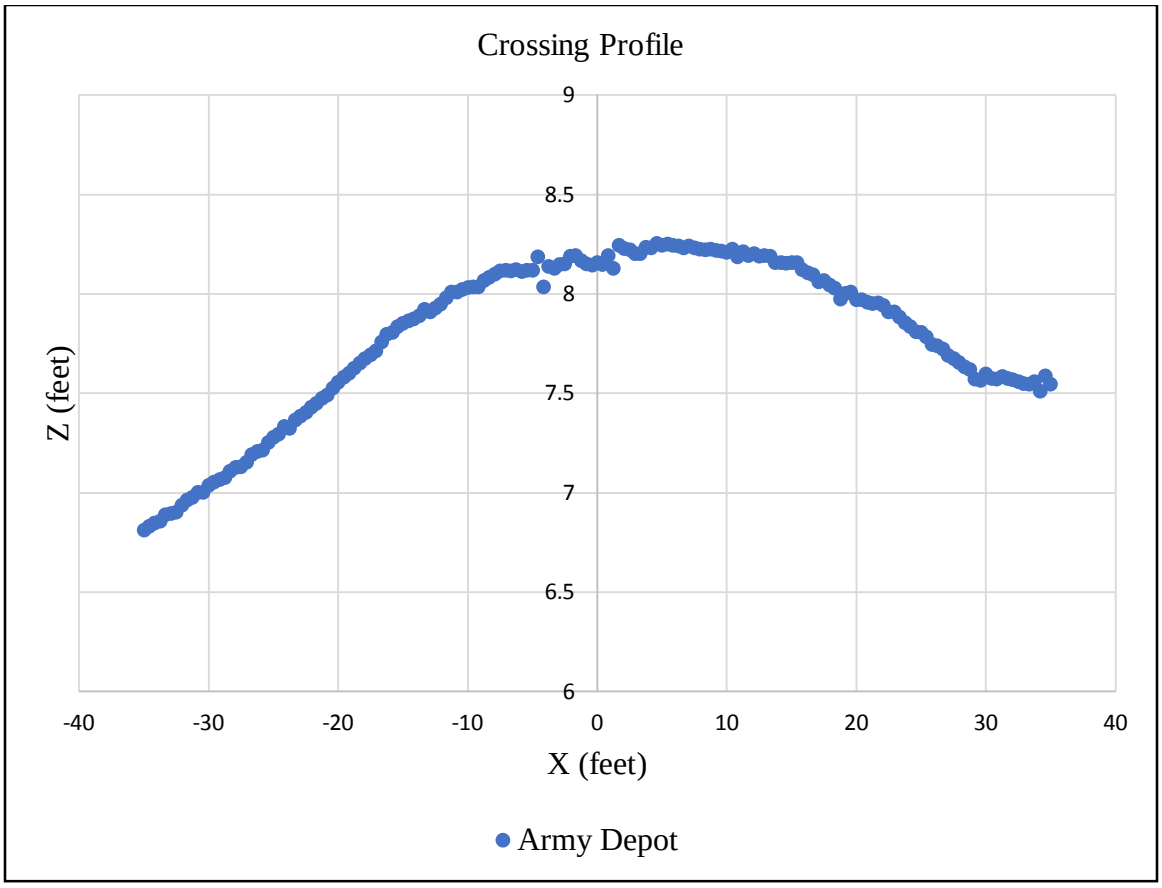

Figure 7.10 Crossing C. Briar Hill Army Depot Road crossing centerline profile.

7.4 Methodology for Quantifying Rail-Highway Hump Crossings

In this section, a novel method is developed to quantify rail-highway hump crossings using 3D data. To facilitate the explanation of the methodology and to establish a reference framework, conditions and assumptions are listed below:

1. The origin of the local coordinate system (center of the crossing) is set as the intersection of the highway and railroad centerlines (center of the two tracks if double-track). The X-axis refers to the highway centerline. (See Figure 7.11)
2. The highway portion of the crossing is straight and analysis of approach is limited to 120 feet in each direction of the highway.
3. The railroad portion of the crossing is limited to the width of the highway.
4. Vehicle are considered as a rigid frame with 4 wheels. No flexible suspension is accounted for. Generally, only three of the four wheels will be in contact with the

ground for an uneven surface (consider a table with four legs resting on an irregular surface).

5. The dimensions of vehicle wheel base, track width, front overhang, rear overhang and corresponding ground clearance are shown in Figure 7.12 and Table 7-1. The left front wheel is referred to as the number one wheel. The reference numbers for the other wheels and a local coordinate system for the vehicle are shown in Figure 7.12.
6. There are no deformation of the vehicle tire, frame or suspension, and so the worse-case condition is considered (at crawl speed). The frame bottom is considered to be formed by 3 plates, corresponding to the front overhang, area between the wheels and rear overhang.
7. Road pavement is considered as rigid (no appreciable deformation of the road under load).
8. The surface of the crossing is referenced on a 5×5 inch grid to reduce the density of the point cloud as well as number of calculations. Vehicle wheels are considered to move along grid cells. Although the actual contact area between the tire and pavement (contact patch) varies according to tire design, materials and pressure, the contact patch is assumed to occupy, at a minimum, 25 square inches. A typical truck tire will contact much more than 25 square inches (e.g., a maximum 9000 pound wheel load at 100 psi occupies 90 square inches.) The 5x5 inch grid used in the analysis is quite conservative (the 5 inch patch will be sufficient to identify potholes or ruts that will affect vehicle placement).
9. There is no contact point between vehicle and pavement except wheels.
10. When a wheel contacts the pavement, it will contact the highest point measured within the grid block.

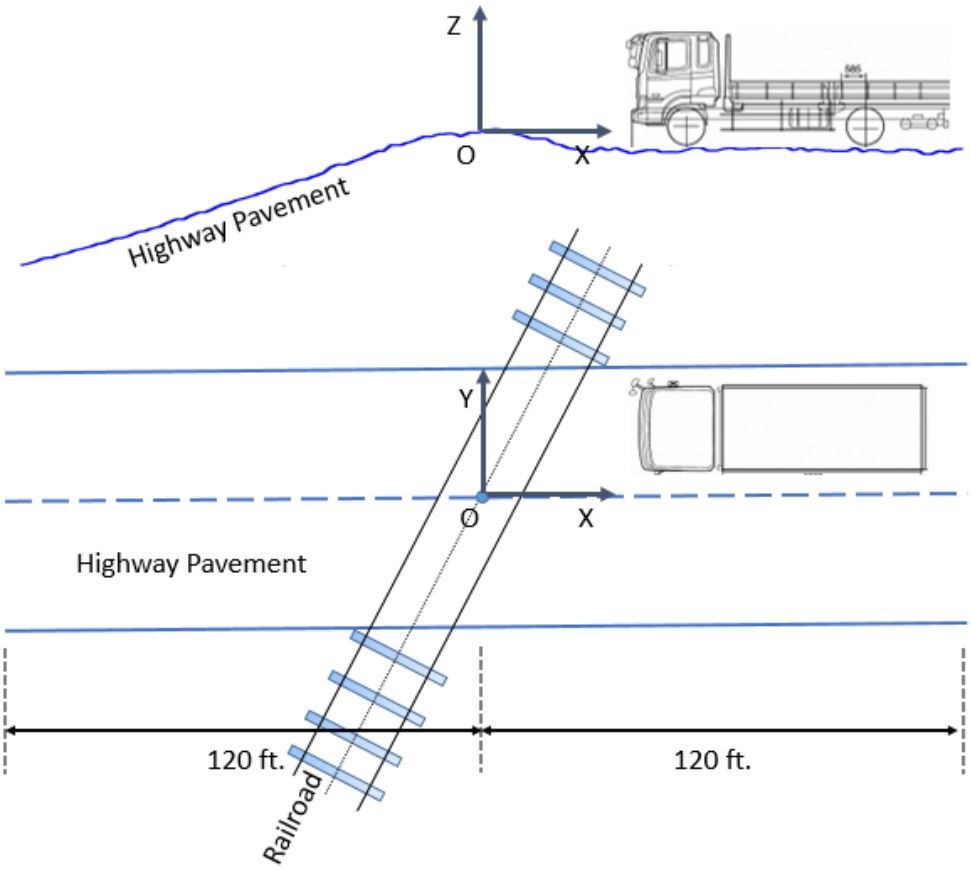

Figure 7.11 Hump crossing coordinate system (not to scale).

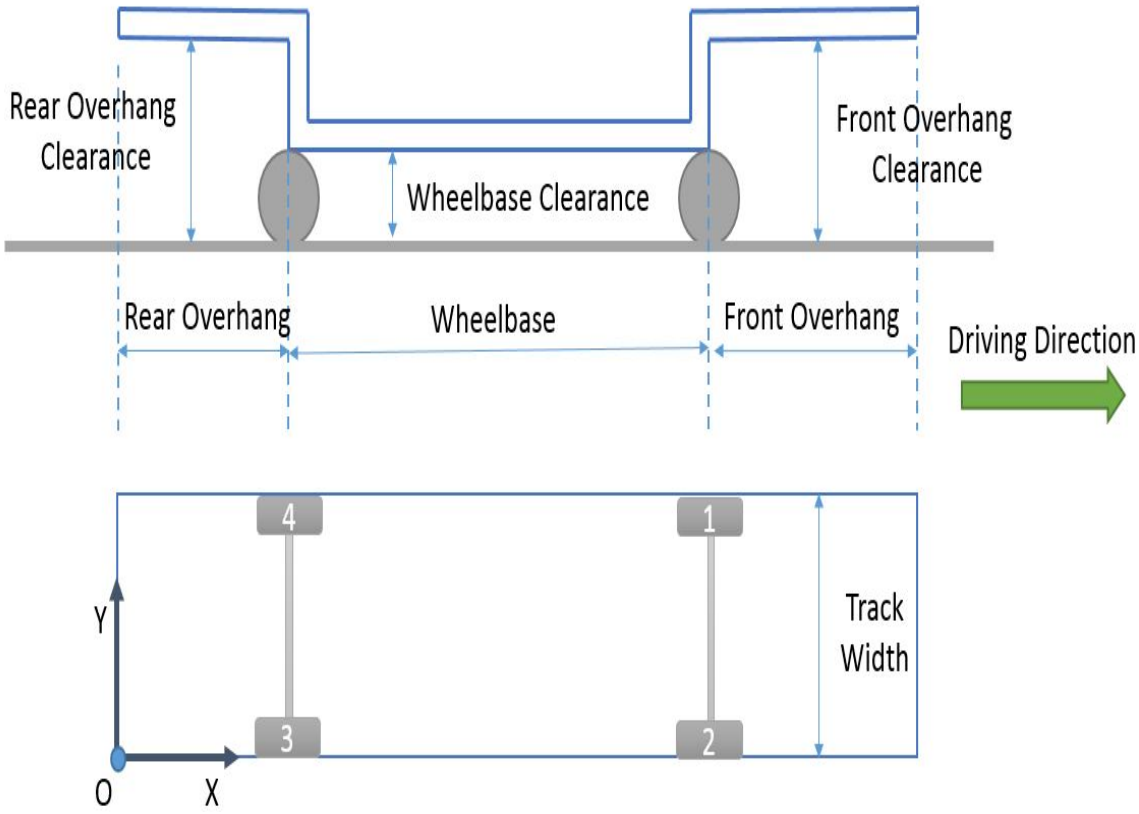

Figure 7.12 Vehicle model dimensions and coordinate system (not to scale).

Table 7-1 Parameters of typical low clearance vehicles

No.	Design Vehicle	Wheel base (ft)	Assumed Track Width (ft)	Front Overhang (ft)	Rear Overhang (ft)	Ground Clearance (inch)		
						Wheel base	Front Overhang	Rear Overhang
1	Rear-Load Garbage Truck	20	8.5	--	10.5	12	--	14
2	Aerial Fire Truck	20	8.5	7	12	9	11	10
3	Pumper Fire Truck	22	8.5	8	10	7	8	10
4	School Bus	23	8.5	--	13	7	--	11
5	Lowboy Trailers <53 feet	38	8.5	--	--	5	--	--
6	Car Carrier Trailer	40	8.5	--	14	4	--	6
7	Limousine	20	8.5	--	--	4	--	--

The basic approach of the methodology is to place specific vehicle models at every possible position on the highway portion of the crossing. At each position, the minimum elevation difference, δ_{min}, between vehicle base and highway pavement can be checked. If δ_{min} is greater than 0, there is no contact between the vehicle and pavement (assuming the vehicle is not bouncing). If δ_{min} is less than 0, conflict will occur. The minimum elevation difference, δ_{min}, and its position relative to both vehicle base and crossing are recorded to enable identification of worst conflict (highest elevation difference).

The analytical procedure is represented by the flowchart shown in Figure 7.13, which can be divided into three steps: preprocessing, processing and summarizing.

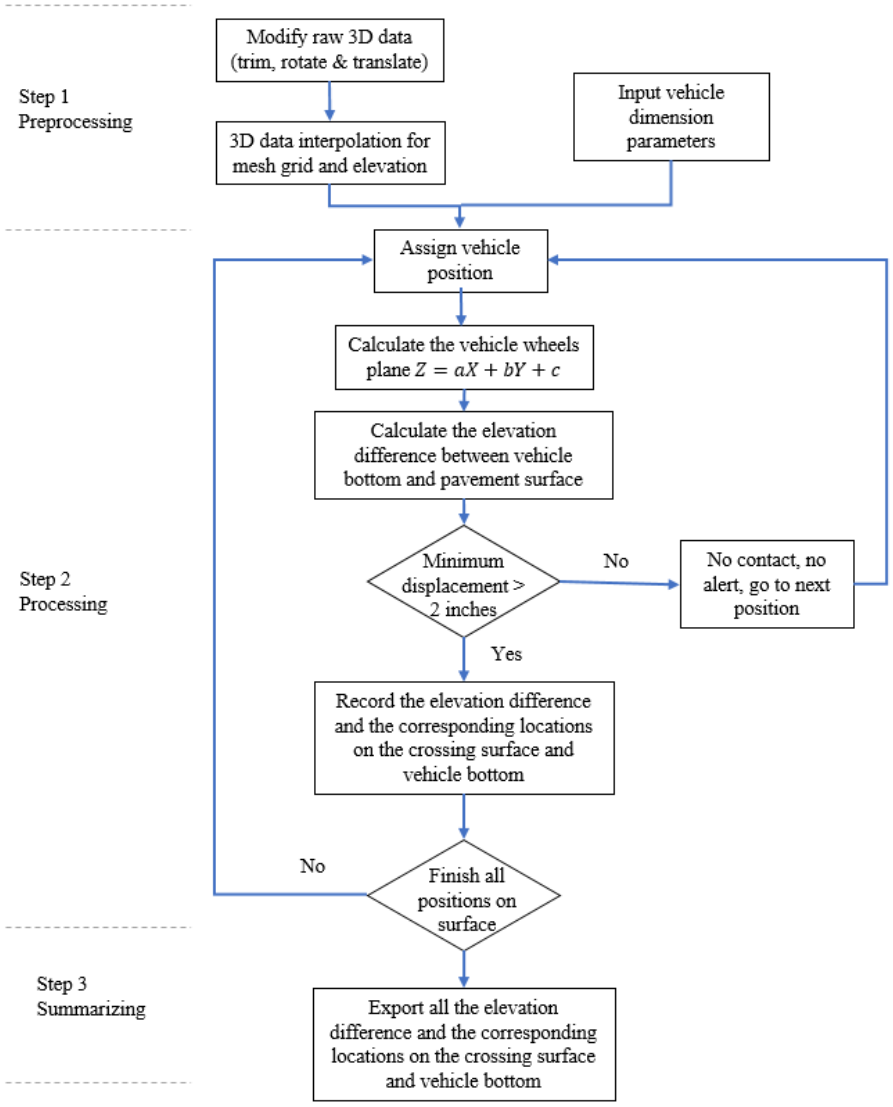

Figure 7.13 Analysis procedure flow chart.

In the first step, data are pre-processed. 3D raw data are trimmed, offset and rotated to align with the local coordinate system. Next, the point cloud is resampled and thinned to a 5×5 inch XY grid, producing surface P which is defined by a set of points P(i) with coordinates ($x_{P(i)}$,$y_{P(i)}$,$z_{P(i)}$) for all i *where i = 1, 2,….n,* and *n* is the number of points comprising the surface. Preprocessed 3D data of for the KY-57 Briar Hill Army Depot Crossing is shown in Figure 7.14.

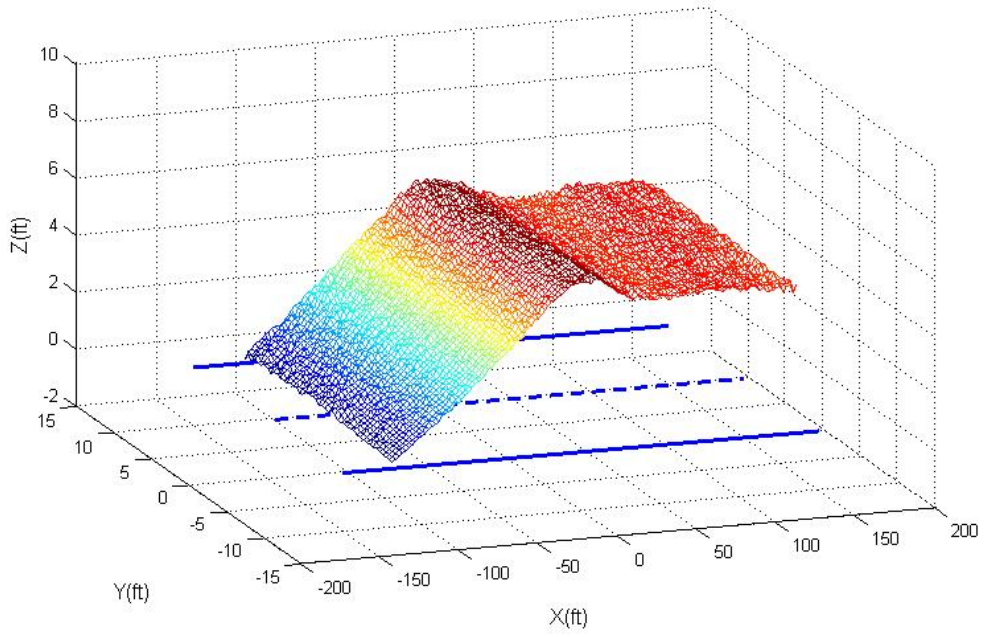

Figure 7.14 Preprocessed 3D data of KY-57 Briar Hill Army Depot crossing.

In the second step, a vehicle is "moved" to a location on the crossing surface. W can be defined as the set of points comprising the bottom of the wheels of the vehicle. Each wheel bottom W(j) has coordinates ($x_{W(j)}$,$y_{W(j)}$,$z_{W(j)}$) for all *j*=1-4) (wheel order 1-4 as shown on Figure 7.12). For example, when wheel 1 is moved to the assigned position P(1) with surface coordinates $x_{P(1)}$,$y_{P(1)}$,$z_{P(1)}$, the x, y position of all four wheels is defined as:

$$x_{\mathrm{W}(1)} = x_{\mathrm{P}(1)},\ y_{\mathrm{W}(1)} = y_{\mathrm{P}(1)}; \qquad x_{\mathrm{W}(2)} = x_{\mathrm{P}(1)}, y_{\mathrm{W}(2)} = y_{\mathrm{P}(1)} - t;$$

$$x_{\mathrm{W}(3)} = x_{\mathrm{P}(1)} - L, y_{\mathrm{W}(3)} = y_{\mathrm{P}(1)} - t;\ \ x_{\mathrm{W}(4)} = x_{\mathrm{P}(1)} - L, y_{\mathrm{W}(4)} = y_{P(1)}.$$

Where t is the track width and L is the wheel base length.

For the rigid frame vehicle models on an irregular surface, there are 4 wheel contact patterns to be evaluated:

I. Wheel No. 2, 3 and 4;
II. Wheel No. 1, 3 and 4;
III. Wheel No. 1, 2 and 4;
IV. Wheel No. 1, 2 and 3.

Take pattern I for example. At the initial x, y position of the vehicle wheels (shown above), the Z coordinates of wheels 2, 3 and 4 are simply the Z coordinates of the surface at these locations. These known points define a plane parallel to the vehicle base. The elevations of any plane can be expressed by the equation:

$$\mathrm{Z} = a\mathrm{X} + b\mathrm{Y} + c$$

Where *a*, *b* and *c* are undetermined coefficients. These coefficients can be solved for using a system of equations defined by three points:

$$a = \frac{\begin{vmatrix} z_2 & y_2 & 1 \\ z_3 & y_3 & 1 \\ z_4 & y_4 & 1 \end{vmatrix}}{\begin{vmatrix} x_2 & y_2 & 1 \\ x_3 & y_3 & 1 \\ x_4 & y_4 & 1 \end{vmatrix}} \quad \mathrm{b} = \frac{\begin{vmatrix} x_2 & z_2 & 1 \\ x_3 & z_3 & 1 \\ x_4 & z_4 & 1 \end{vmatrix}}{\begin{vmatrix} x_2 & y_2 & 1 \\ x_3 & y_3 & 1 \\ x_4 & y_4 & 1 \end{vmatrix}} \quad \mathrm{c} = \frac{\begin{vmatrix} x_2 & y_2 & z_2 \\ x_3 & y_3 & z_3 \\ x_4 & y_4 & z_4 \end{vmatrix}}{\begin{vmatrix} x_2 & y_2 & 1 \\ x_3 & y_3 & 1 \\ x_4 & y_4 & 1 \end{vmatrix}}$$

The z coordinate value of wheel No.1 can be calculated as:

$\mathrm{z}_{\mathrm{W}(1)} = a\mathrm{x}_{\mathrm{W}(1)} + \mathrm{by}_{\mathrm{W}(1)} + \mathrm{c}$.

- If $\mathrm{z}_{\mathrm{W}(1)} \geq z_{P(i)\,[at\ x(W1),y(W1)]}$, wheel 1 is above the pavement. Patterns I and III are practical cases where this may occur.
- If $\mathrm{z}_1 < z_{P(i)\,[at\ x(W1),y(W1)]}$, wheel 1 is under the pavement. Therefore, only patterns II and IV are practical.

For the practical pattern combinations, the elevation difference δ between vehicle and crossing can be calculated for all points on the vehicle underbody surfaces.

$$\mathrm{z}\,(vehicle) = ax + by + c + Clearance_{Front\ overhang} \quad (\mathrm{x,y}) \in \mathrm{A}_{\text{front overhang}}$$

$$\mathrm{z}\,(vehicle) = ax + by + c + Clearance_{Wheelbase\ area} \quad (\mathrm{x,y}) \in \mathrm{A}_{\text{wheelbase area}}$$

$$\mathrm{z}\,(vehicle) = ax + by + c + Clearance_{rear\ overhang} \quad (\mathrm{x,y}) \in \mathrm{A}_{\text{rear overhang}}$$

$\delta =$ z $(vehicle) - z(crossing\ surface)$, for all vehicle underbody surface points

If $\delta_{min} < 0$, the vehicle will contact the pavement. For safety considerations, a minimum difference can be set as a warning value. If δ_{min} is less than the warning value, the corresponding position on both vehicle underbody and crossing pavement can be recorded.

The second step is then repeated for all possible vehicle positions along the crossing surface for both directions over the crossing. In the third step of the methodology, elevation differences are recorded and exported to a file for all crossing/vehicle underbody point combinations.

A MATLAB program was developed to implement and test the methodology described above. A typical car carrier trailer was selected as a test vehicle. For this vehicle, the wheelbase is 40 feet with a clearance of 6 inches. Its length of rear overhang is 14 feet with clearance of 4 inches. Figure 7.16 shows the results if the trailer passed the KY-57 Briar Hill army depot crossing. The top part of the figure present a plot of contact points referenced to the local crossing coordinate system. The dotted line in the plot represents the centerline of the road. The lower portion of the figure shows a plot of contact position on the underside of the vehicle. Severity of conflict (difference in elevation) is represented by color. Conflicts occurred both under the wheelbase and under the rear overhang. When the two axles of the truck are on the opposite sides of the crossing, wheelbase contact may occur. In this situation, δ_{min} = -4.91 inch, at a point located to the north of the crossing near the railroad. Rear overhang conflict occurs when the front axle approaches the railroad. The front of the vehicle will rise causing the rear overhang to scrape the ground. In this situation δ_{min} = -2.99 inch.

Figure 7.15 Car carrier trailer.

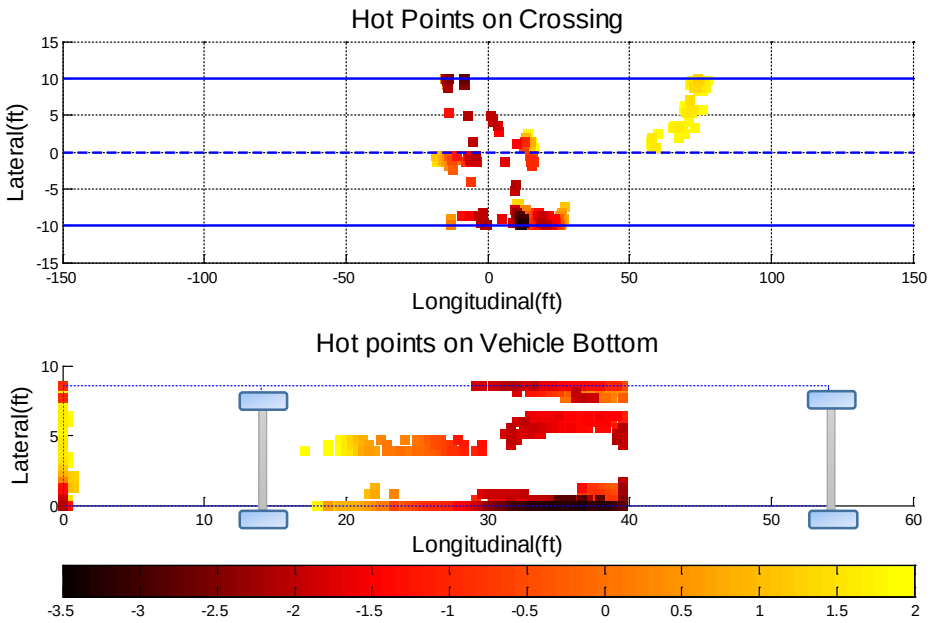

Figure 7.16 Car carrier trailer contact points at KY-57 Briar Hill Army Depot crossing.

7.5 Analysis and Results

For all three study crossings, seven vehicle types were selected for analysis, as shown in Table 7-1**Error! Reference source not found.**. Although many types of vehicles may use a particular crossing, it would be time consuming to assess all possible passing vehicles. Vehicles 1 through 5 are common for these crossings, where numbers 6 and 7 are less commonly seen on the types of highways.

The minimum distance δ_{min} represent the severity of humping. If δ_{min} is only slightly smaller than zero, the flexibility of the vehicle body and its suspension system may enable to vehicle to pass, perhaps only scraping the surface of crossing. However, if δ_{min} is much smaller, the vehicle may become stuck. Correspondingly, a five-level evaluation criterion is proposed:

$Level\ 1$: $\delta_{min} > 2$ inch

$Level\ 2$: $2\ inch \geq \delta_{min} > 0\ inch$

$Level\ 3$: $0\ inch \geq \delta_{min} > -1\ inch$

$Level\ 4$: $-1\ inch \geq \delta_{min} > -2\ inch$

$Level\ 5:\ \delta_{min} \leq -2\ inch$

Results for the crossings are presented in Table 7-2. Observations include:

1. Vehicle type 1 may safely negotiate all crossings
2. Vehicle types 2, 3, 5, and 7 crossings A and C are characterized mainly by L1 or L2 conflict (no contact), but for crossing B, some contact will be made front and/or rear overhangs.
3. Vehicle types 5 and 6 will have seriously problems negotiating all three crossings.

Table 7-2 Evaluation of Railroad – Highway crossing

	KY-57 Bryan Station (A)			Brannon Rd (B)			KY-57 Briar Hill Army Depot (C)		
Veh. type	Wheel base	Front Over hang	Rear Over hang	Wheel base	Front Over hang	Rear Over hang	Wheel base	Front Over hang	Rear Over hang
1	L1	-	L1.	L1	-	L1	L1.	-	L1
2	L1	L1	L1	L1	L1	L5	L1	L1	L1
3	L1	L1	L1	L2	L3	L4	L1	L1	L1
4	L1	-	L1	L2	-	L3	L1	-	L1
5	L3	-	-	L5	-	-	L4	-	-
6	L4	-	L1	L5	-	L5	L5	-	L3
7	L2	-	-	L4	-	-	L2	-	-

Figure 7.17 through Figure 7.19 depict contact points for the three crossings. The minimum values of elevation difference between vehicles and crossings are (-3.5) inches, (-7.0) inches and (-5.0) inches, respectively. According to these data, all can be considered to be hump crossings, while crossing B is most severe.

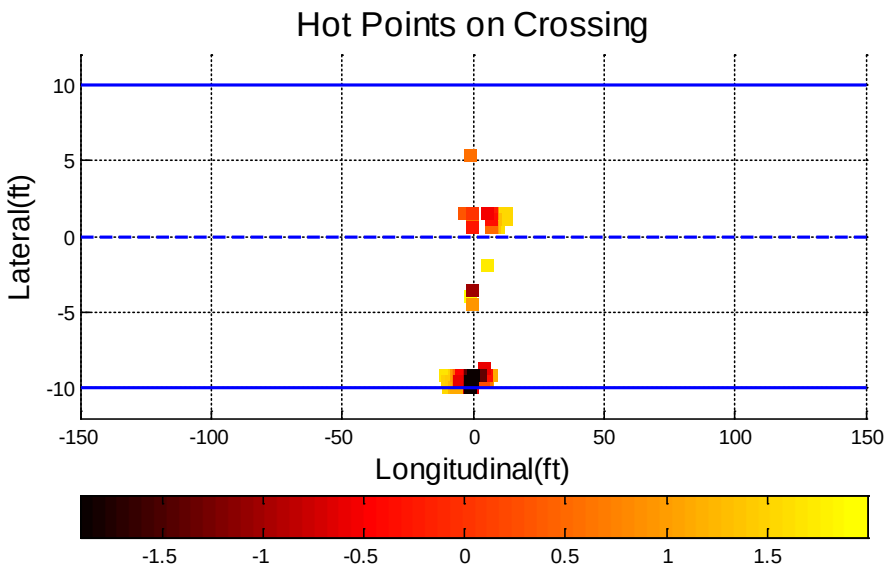

Figure 7.17 Contact points on KY-57 Bryan Station crossing (A)

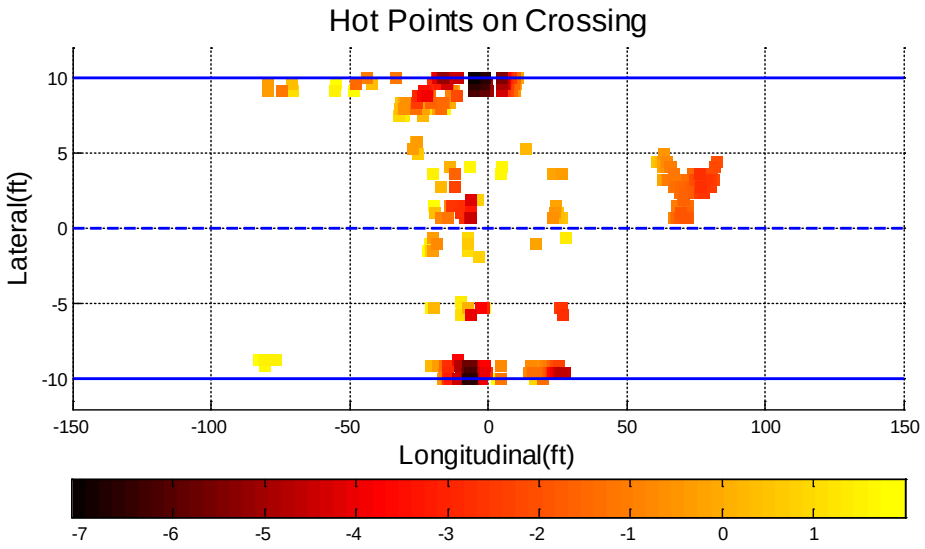

Figure 7.18 Contact points on Brannon Rd crossing (B)

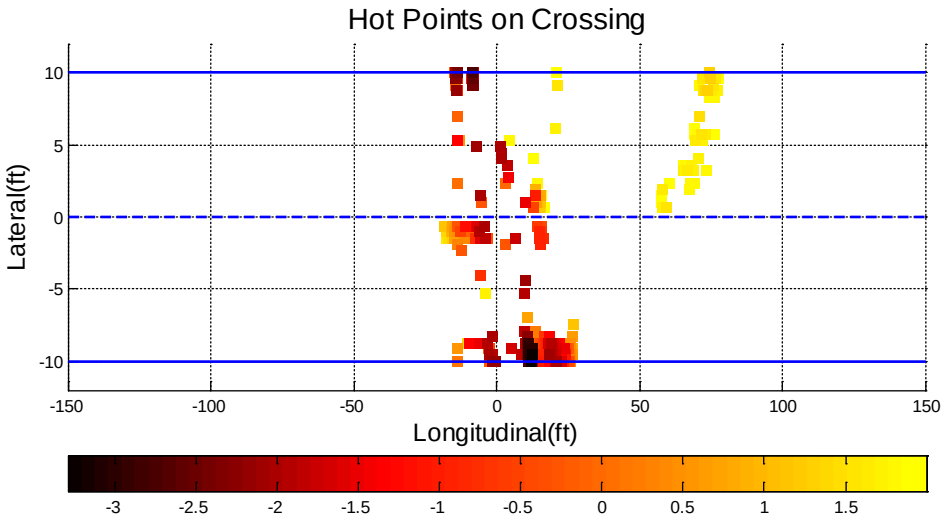

Figure 7.19 Contact points on KY-57 Briar Hill Army Depot (C)

7.6 Verification

After completing the analysis and examining the results, several field verification visits were conducted. In the field, a survey tape and level rods were used to measure elevations along the crossing. Different vehicle clearances were marked on the rods which were connected by tape to build a physical model. This model was used to sweep over the crossing surface from left to right and check for contact points as shown in Figure 7.20 and Figure 7.21. Scraping marks on the crossing pavement were compared with conflict maps. The verification concluded that while there was a correlation between modeled and observed conflicts (scrape marks), not all areas indicated by the methodology had scrape marks. This is likely due to the absence of some of the vehicle types at the actual locations, vehicle characteristic that are not similar to the ones used in the analysis, or deterioration of previous marks due to weathering. See Figure 7.22 and Figure 7.23.

Figure 7.20 Field verification A.

Figure 7.21 Field verification B.

Figure 7.22 Crossing scratch marks A.

Figure 7.23 Crossing scratch marks B.

7.7 Conclusions

This chapter presented the development and testing of a methodology to identify and quantify the potential severity of hump crossings. Results indicate promise for the use of 3D datasets to improve systems inventories and reduce potential risks of highway-rail collisions due to vehicles becoming stuck at crossings. With the proposed methodology, all possible contact areas between vehicle undersides and crossings can be investigated. The method provides a far richer database to road managers than a simple yes/no inventory. Warning areas are identified and can be customized to any vehicle with known geometry. Once a crossing 3D point cloud is obtained, any vehicle and any wheel path can be simulated to provide results without the need for field visits and concomitant risks. Of course, the practical application of such a methodology depends on the availability of 3D data. Future work could be to investigate the impact of dynamic forces on hump crossing conflict, incorporating aspects such as speed and suspension into the model.

CHAPTER 8. CLOSURE

8.1 Conclusions

This dissertation presented several methods to quantitatively assess the condition and performance of highway-rail crossings. The methods produce metrics that can be used to evaluate the performance of designs and construction methods, which in turn may be used to implement more cost-effective improvement programs. Safety should also benefit as smooth crossings may allow motorists to proceed more safely, allowing more focus on watching for trains rather than worrying about vehicle speed or navigating rough surfaces. Community livability may also be enhanced through reduced noise and delay for vehicles using or avoiding the crossings. Vehicle maintenance costs may also be reduced by implementation of more effective crossing renewal programs.

Where crossing rehabilitation is jointly (or entirely) funded by the railroad, economic benefits may accrue to the railroad as well, but the biggest benefit of the methods introduced in this dissertation may be to reduce the frequency of repair and reconstruction, with its commensurate benefit to maintenance off traffic. The proposed methods permit better and more objective management of crossings as assets, resulting in more effective preventative maintenance and reduction of overall life cycle costs.

The dissertation was presented in eight chapters. Following an introduction and literature review, a chapter is presented detailing the development of a prototype low-cost 3D scanner based on structured light technology. 3D surface data collected by using the scanner was used for both visual demonstration and preliminary surface roughness analysis.

Second, a crossing rideability ranking method based on field measured acceleration was developed. Results are consistent with rankings by inspectors indicating the method can be used to complement or even replace visual inspection. Measures based on acceleration should also be more reliable and repeatable than visual ratings.

Third, a vehicle dynamic model was developed to simulate vehicle accelerations using only a crossing terrain model and vehicle parameters as inputs. Accelerometer data were used to field calibrate and validate the model. Model repeatability and data accuracy

was verified, suggesting that the vehicle dynamic model can be used to quantify vehicular accelerations at various speeds and different locations.

Forth, three different quantitative crossing assessment indices were presented. A Crossing Roughness Index and a Crossing Rideability Index were developed. These may be computed based directly on a 3D terrain model of the crossing. The Crossing Roughness Index calculates roughness from geometric characteristics of current crossing surface conditions and profile grades of highway approaches. The Crossing Rideability Index is computed from the second derivation of the crossing vertical profile and is proportional to the root mean square of vertical accelerations as. Both indices are used to rank the performance of different crossings and results are compared to measures derived from accelerometer-based field measurements. Another metric, the Crossing Condition Index, is developed to separate the contributions to total acceleration from surface condition and as-built design. Depending on data availability and actual application needs, single or multiple indices may be chosen to assess crossing condition.

Lastly, a methodology to identify and quantify the potential severity of hump crossings was developed as another application of using 3D surface data and vehicle parameters. Results indicate promise for the use of 3D datasets to improve systems inventories and reduce potential risks of highway-rail collisions due to vehicles becoming stuck at crossings. With the proposed methodology, all possible contact areas between vehicle undersides and crossings can be investigated. The method provides a far richer database to road managers than a simple yes/no inventory. Warning areas are identified and can be customized to any vehicle with known geometry. Once a crossing 3D point cloud is obtained, any vehicle and any wheel path can be simulated to provide results without the need for field visits and their concomitant risks.

8.2 Limitations

Because the Structured Light scanner could not be fully developed and deployed under the scope of this study, LiDAR was used to obtain 3D surface point clouds for the remainder of the work presented in this dissertation. Note that the applications of 3D data for roughness and rideability analysis would be the same, no matter how the 3D data is collected.

Two chief limitations for the use of accelerometers to assess crossings in a state wide crossing program can be identified. First, the sheer number of sites for collection is daunting—acceleration data must be collected by visiting every site. In addition, a number of runs is suggested to smooth out results. A calibrated test vehicle must be used, and accelerations may be sensitive to wheel path position for crossings with lateral surface variations. Second, rideability as a single measure of performance based on the acceleration data cannot distinguish between accelerations caused by crossing condition and those induced by grade profiles as originally constructed.

Lastly, the practical applications of vehicle dynamic model, quantitative crossing assessment indices and hump crossing assessment methodologies highly depend on the availability of 3D data. It is likely that in part, due to technologies such as those explored in this dissertation, 3D data may become ubiquitous in the next five to ten years.

8.3 Recommendations for Future Research and Application

If system-wide LiDAR or other 3D data are available, application of the terrain-model based methodologies presented in this dissertation may provide a feasible alternative to field review. However, given present technology and costs, obtaining LiDAR data for the sole purpose of rail crossing condition assessment is not likely to be feasible. Field measurements of accelerations may be a more cost effective approach. The dissertation described and tested the use of several more-or-less common vehicles to collect acceleration data. A more repeatable and reliable approach may be to outfit a standard road roughness trailer with sensors for measuring acceleration and profile. Such an instrument could analyze rideability and surface condition for district or state-wide inventories of railroad-highway grade crossings.

For future application of the methodologies described in this dissertation, 3D data are obviously required. A more fully-developed structured light 3D scanner could provide a cost effective way for agencies to collect the needed data. Other technologies could also lower costs. For example, a relatively low cost UAV may be configured to collect 3D data using photogrammetric principles.

Both the vehicle dynamic simulation model and hump crossing assessment program can be improved. Future work should investigate the impact of dynamic forces on vehicle when driving over the crossing, incorporating aspects such as vehicle speed, suspension types and perhaps even movement of the rail track system under load.

This research has the potential for application to Section 3 of the FRA Railroad-Highway Grade Crossing Handbook if crossing roughness/rideability data are desired inventory elements.

Grade crossing crash prediction models do not currently explicitly incorporate roughness into risk calculations. It is possible that quantitative roughness measures could be used as independent variables in such models.

The roughness and rideability measurement and assessment methodologies developed in this dissertation could be used to measure and monitor system assets over time, and could be extended to other infrastructure components such as highway pavements and bridges. It is also possible that the methods and techniques developed in this research could be applied to precise 3D datasets and be useful to those analyzing long term performance of innovative rail track designs and materials, such as asphalt underlayment or tie cushioning.

Further, the data collection technology developed in this research may have the potential for application to other civil infrastructures that can be better represented or analyzed using 3D technology such as building information modelling (BIM) for road highway and building design. It is even possible that structured light could have applications in automated highway systems, or the development of other information and data applications such as Virtual Reality (VR), Augmented Reality (AR), and 3D printing, and to lower the cost of 3D data collection in general.

APPENDIX A

Chapter 4 Acceleration test plot

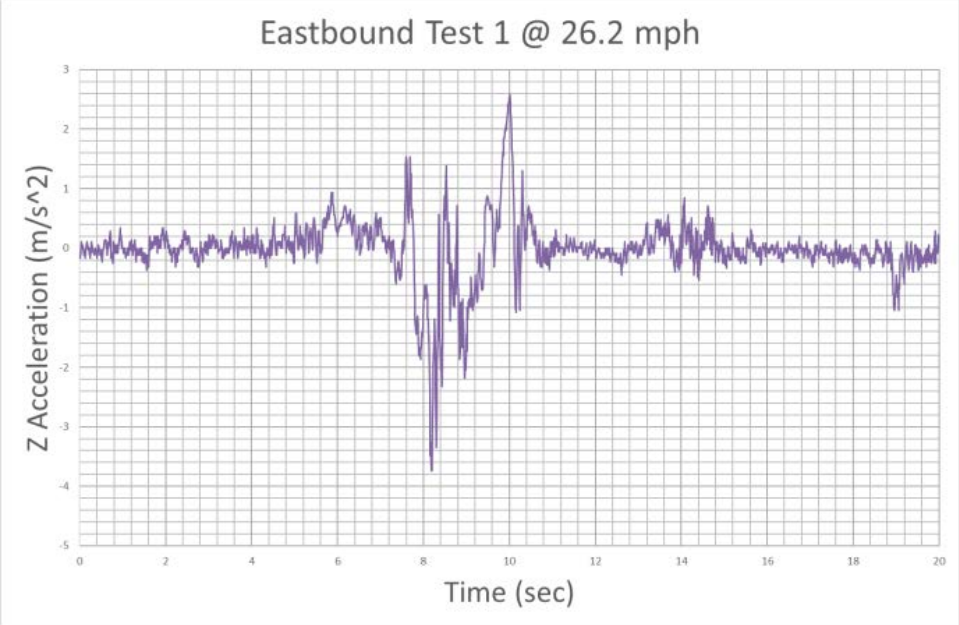

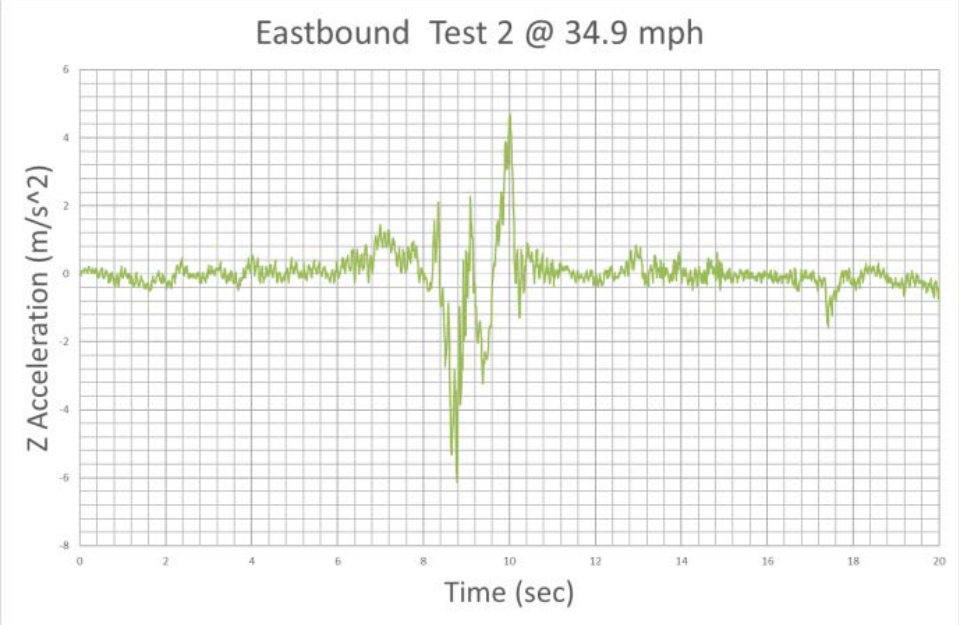

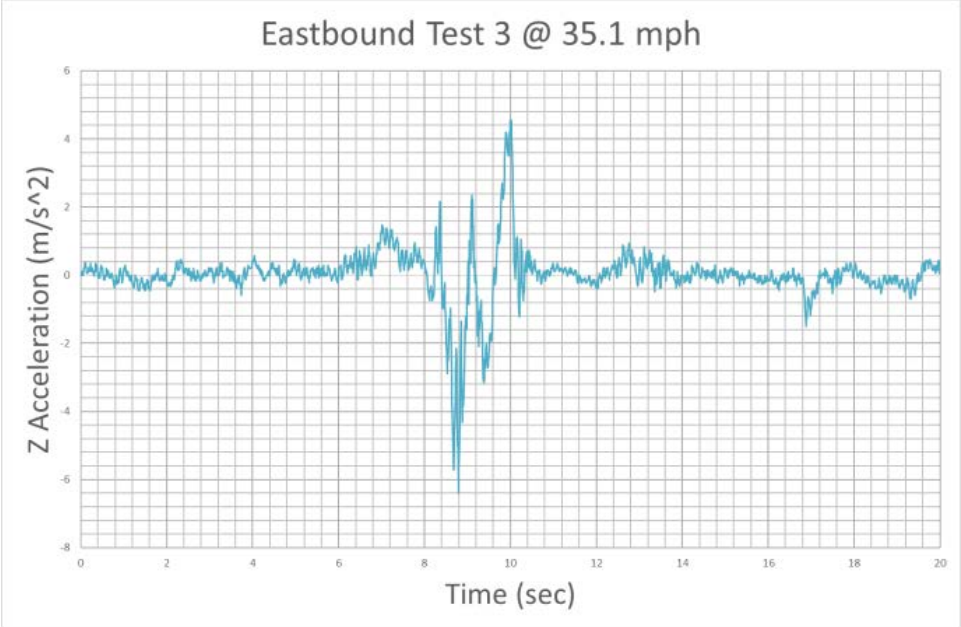
Eastbound Test 3 @ 35.1 mph
Z Acceleration (m/s^2)
Time (sec)

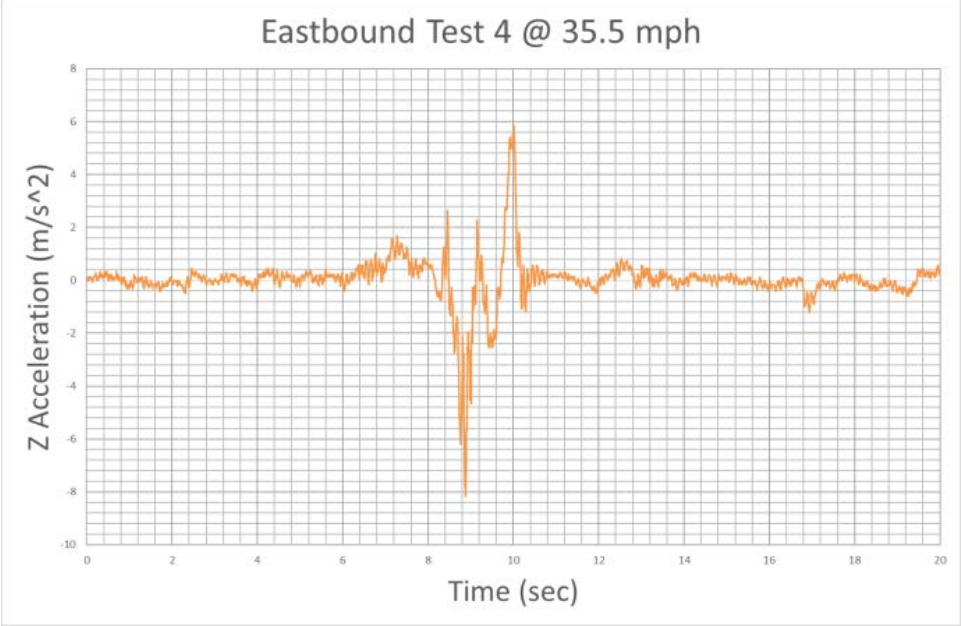
Eastbound Test 4 @ 35.5 mph
Z Acceleration (m/s^2)
Time (sec)

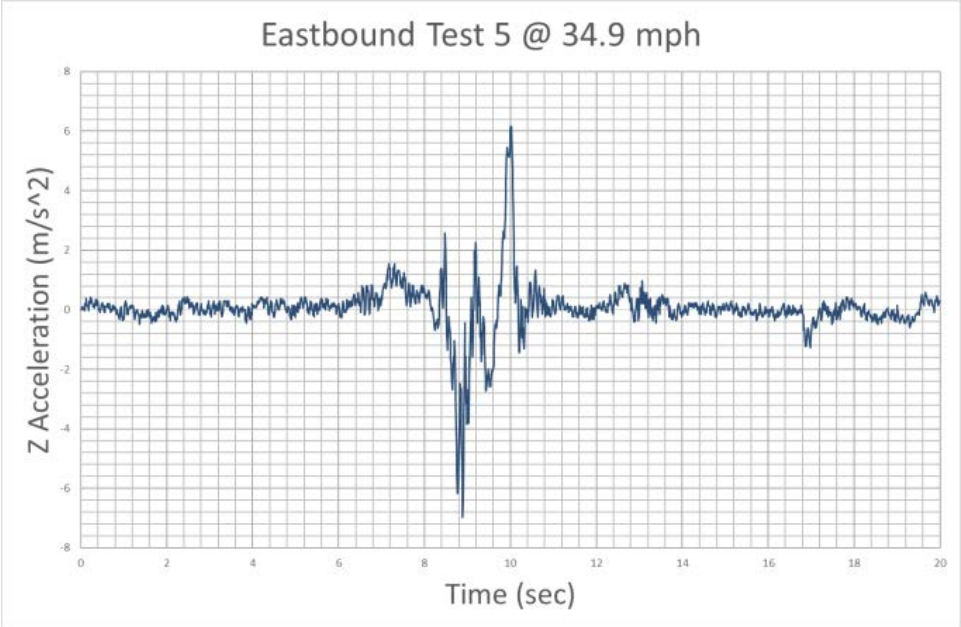
Eastbound Test 5 @ 34.9 mph
Z Acceleration (m/s^2)
Time (sec)

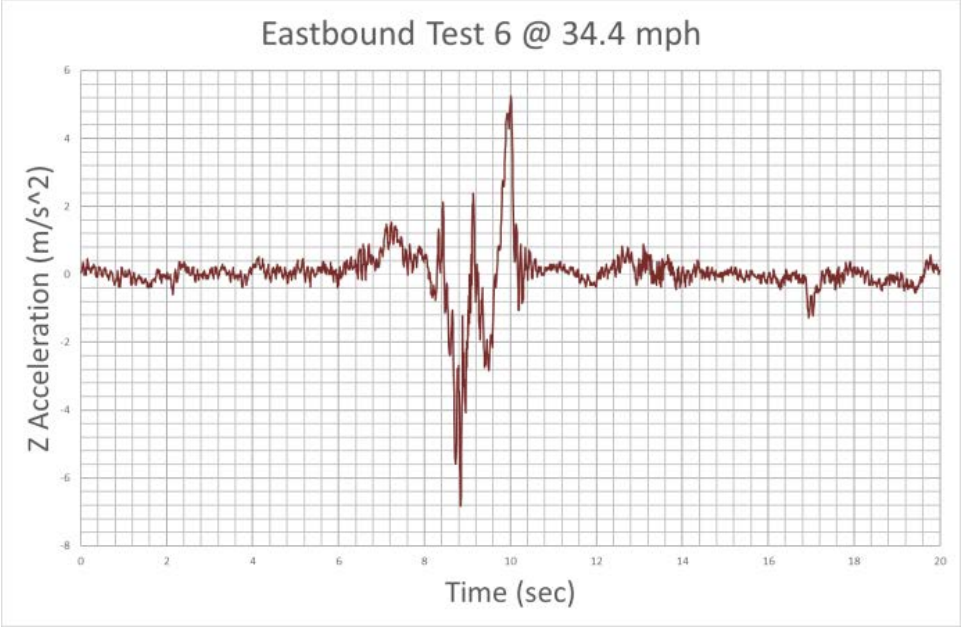
Eastbound Test 6 @ 34.4 mph
Z Acceleration (m/s^2)
Time (sec)

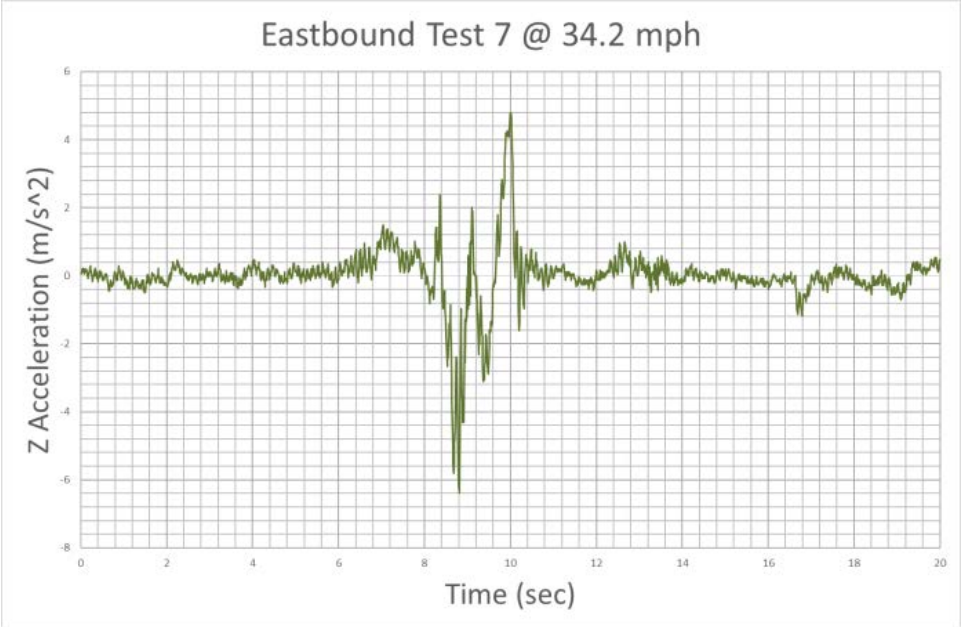
Eastbound Test 7 @ 34.2 mph
Z Acceleration (m/s^2)
Time (sec)

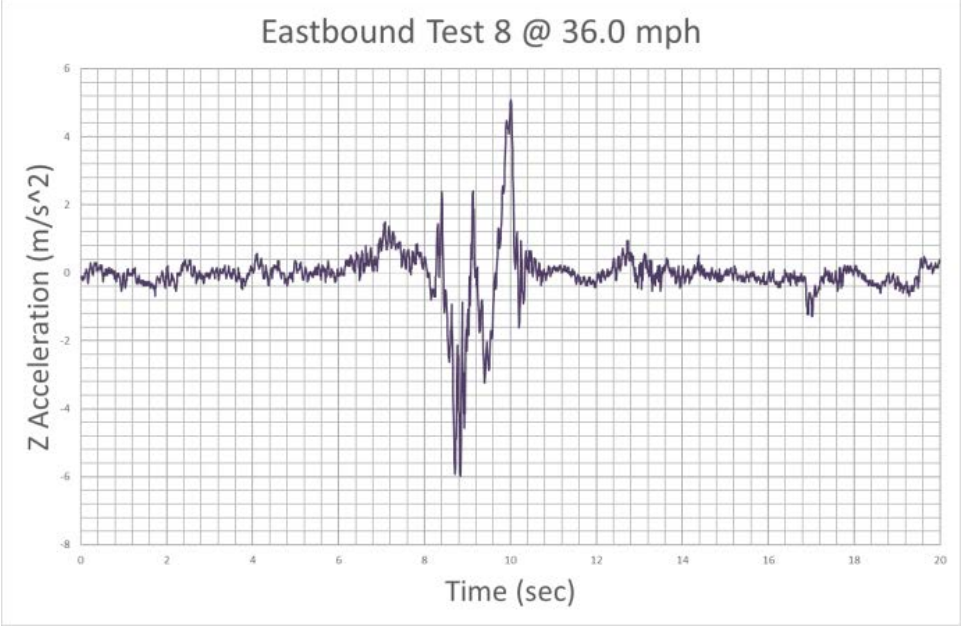
Eastbound Test 8 @ 36.0 mph
Z Acceleration (m/s^2)
Time (sec)

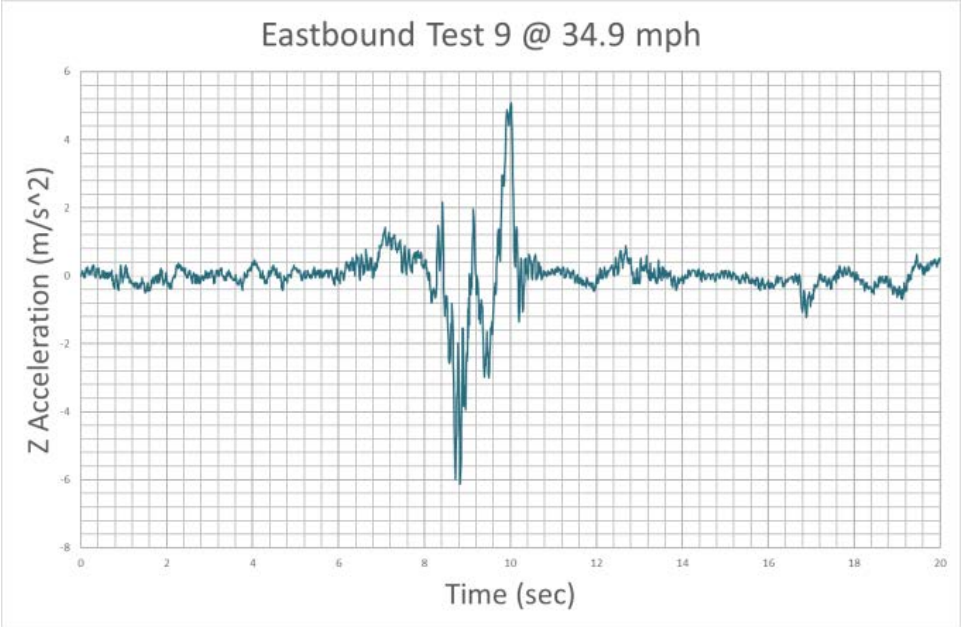
Eastbound Test 9 @ 34.9 mph
Z Acceleration (m/s^2)
Time (sec)

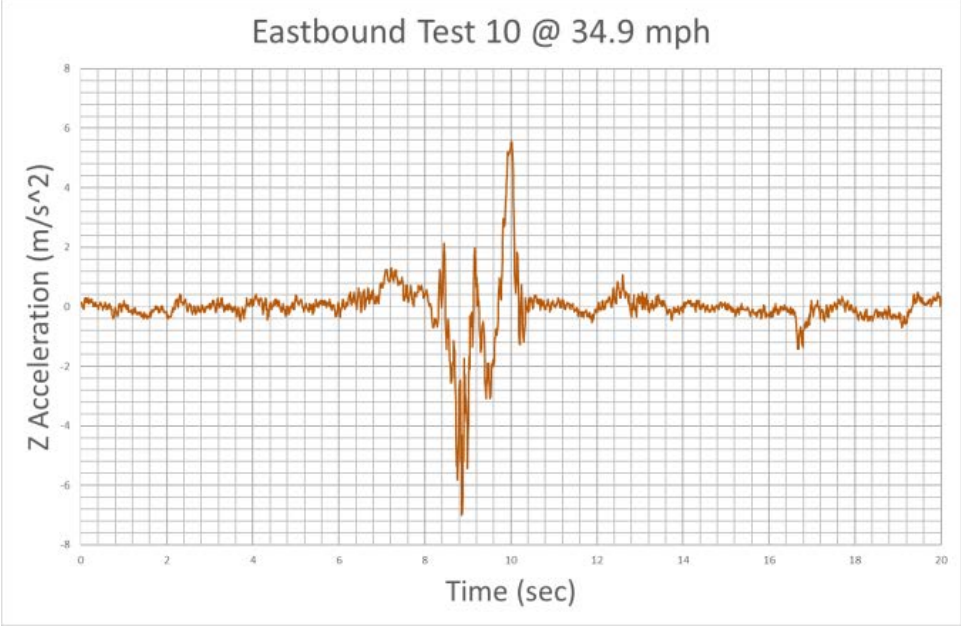
Eastbound Test 10 @ 34.9 mph
Z Acceleration (m/s^2)
Time (sec)

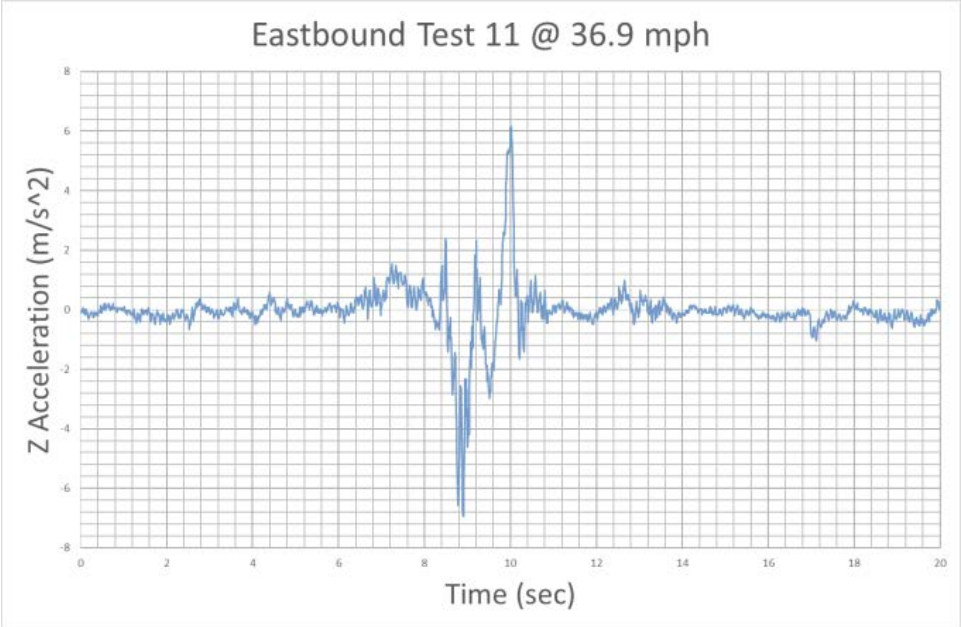
Eastbound Test 11 @ 36.9 mph
Z Acceleration (m/s^2)
Time (sec)

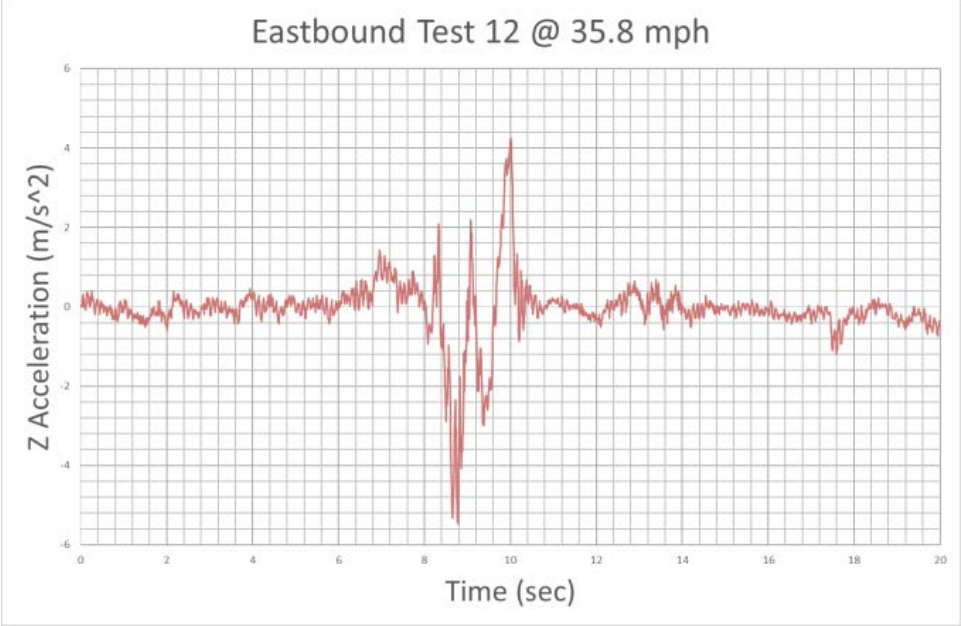
Eastbound Test 12 @ 35.8 mph
Z Acceleration (m/s^2)
Time (sec)

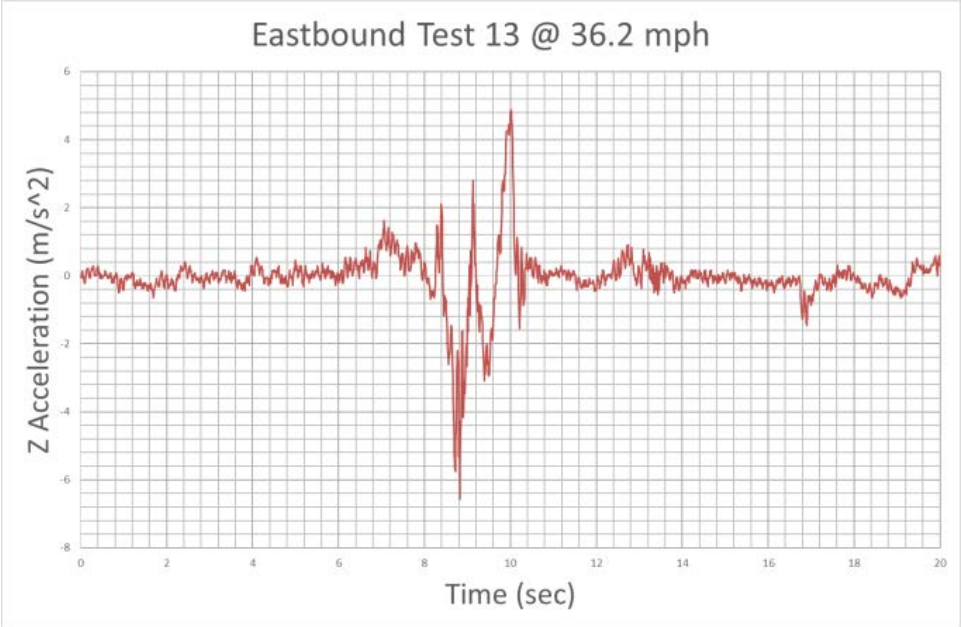
Eastbound Test 13 @ 36.2 mph
Z Acceleration (m/s^2)
Time (sec)

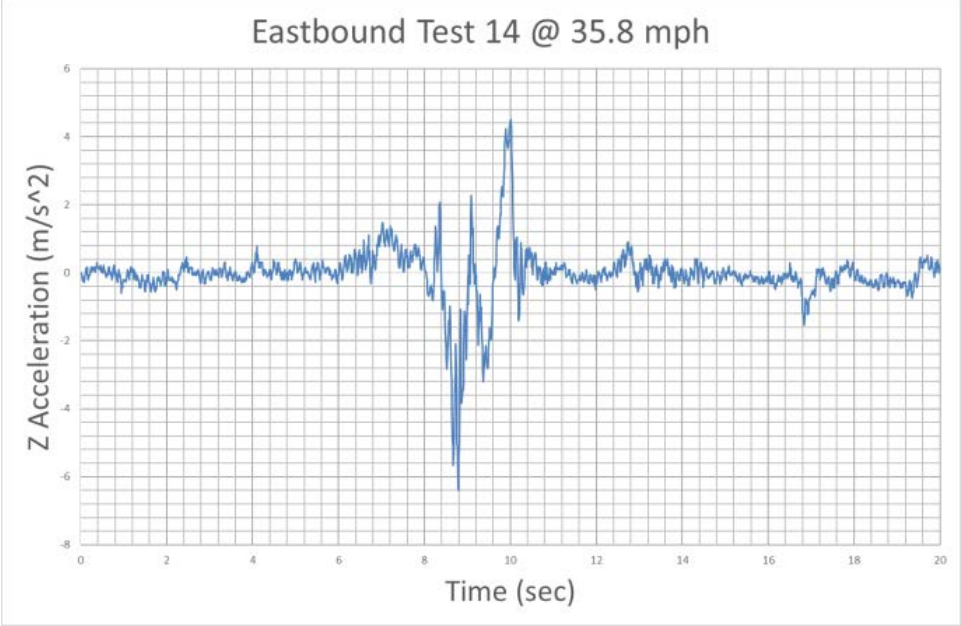
Eastbound Test 14 @ 35.8 mph
Z Acceleration (m/s^2)
Time (sec)


Eastbound Test 15 @ 43.6 mph
Z Acceleration (m/s^2)
15
10
5
0
-5
-10
-15
0
2
4
6
8
10
12
14
16
18
20
Time (sec)

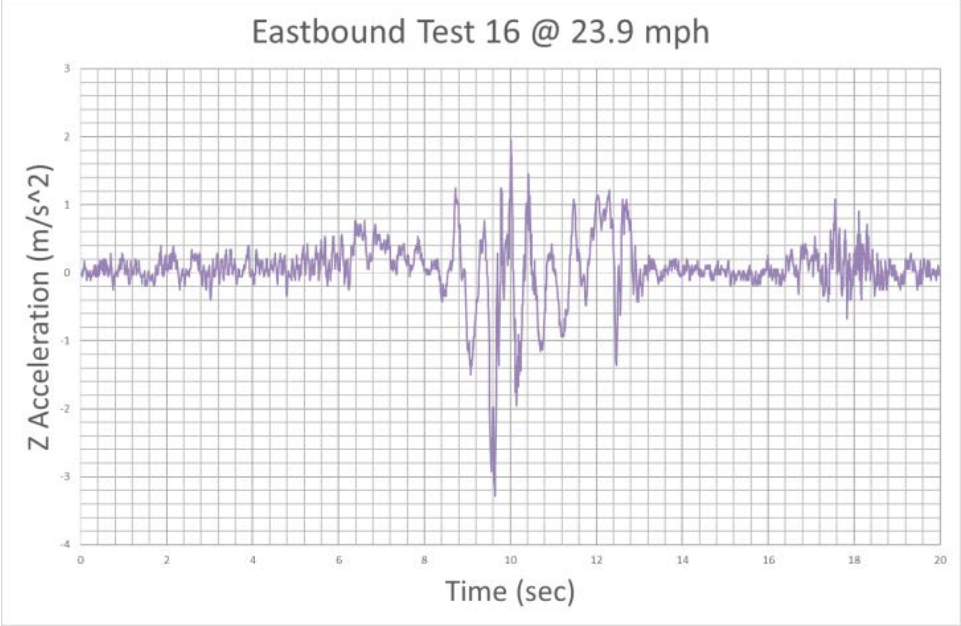
Eastbound Test 16 @ 23.9 mph
Z Acceleration (m/s^2)
3
2
1
0
-1
-2
-3
-4
0
2
4
6
8
10
12
14
16
18
20
Time (sec)


Westbound Test 1 @ 30.0 mph
Z Acceleration (m/s^2)
Time (sec)

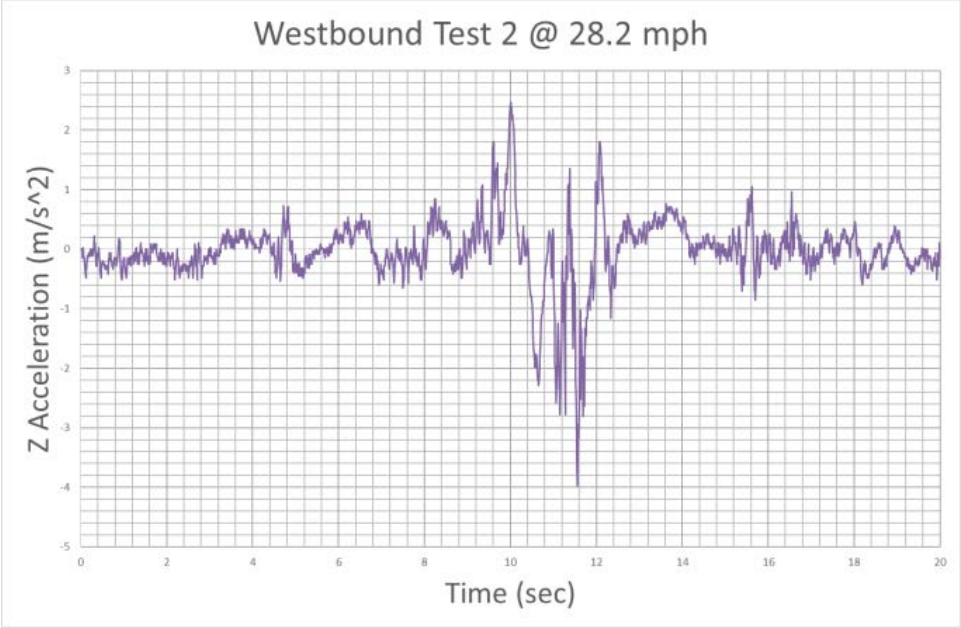
Westbound Test 2 @ 28.2 mph
Z Acceleration (m/s^2)
Time (sec)

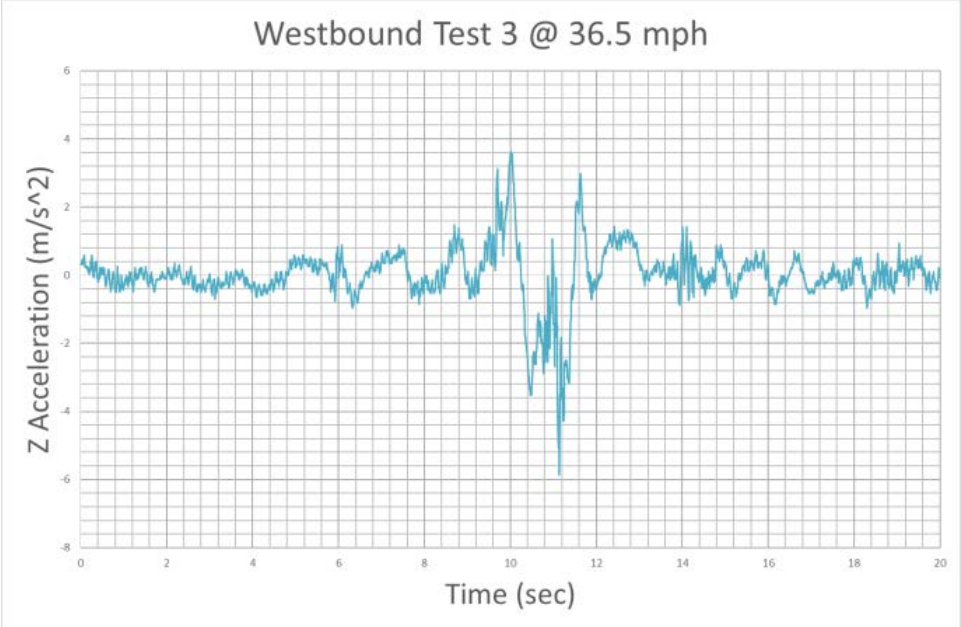
Westbound Test 3 @ 36.5 mph
Z Acceleration (m/s^2)
Time (sec)

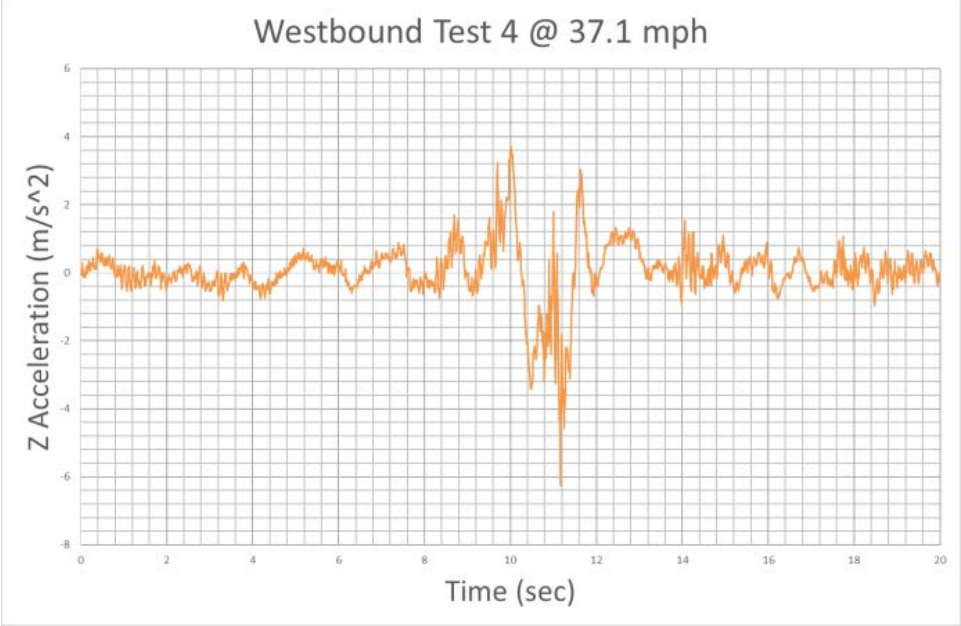
Westbound Test 4 @ 37.1 mph
Z Acceleration (m/s^2)
Time (sec)

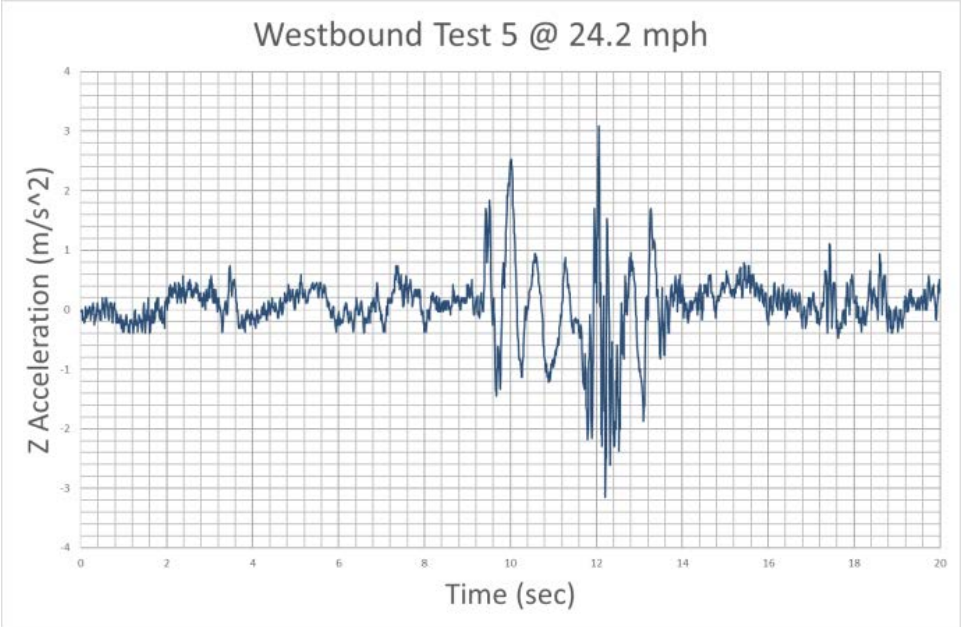
Westbound Test 5 @ 24.2 mph
Z Acceleration (m/s^2)
Time (sec)

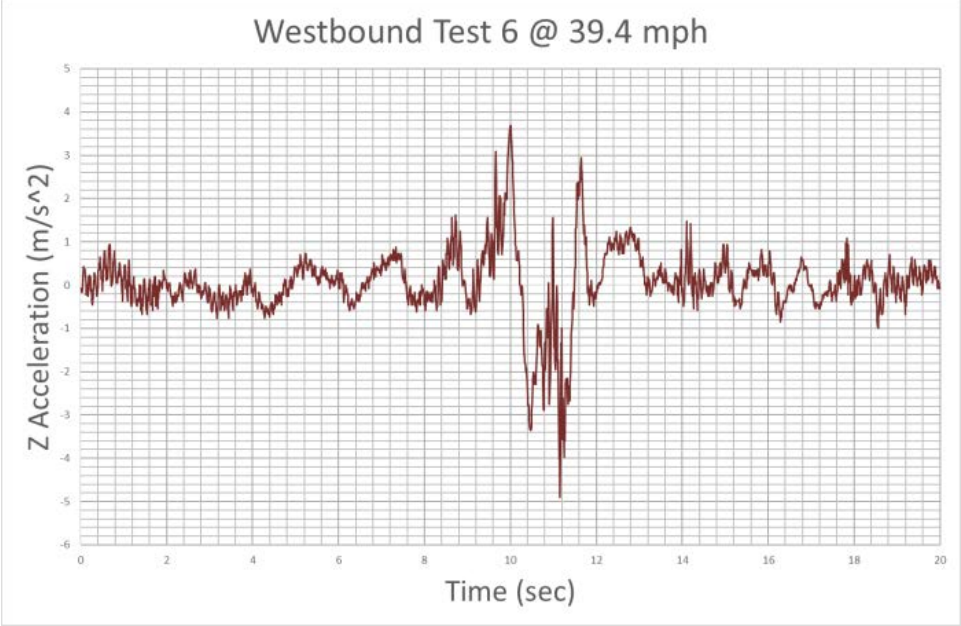
Westbound Test 6 @ 39.4 mph
Z Acceleration (m/s^2)
Time (sec)

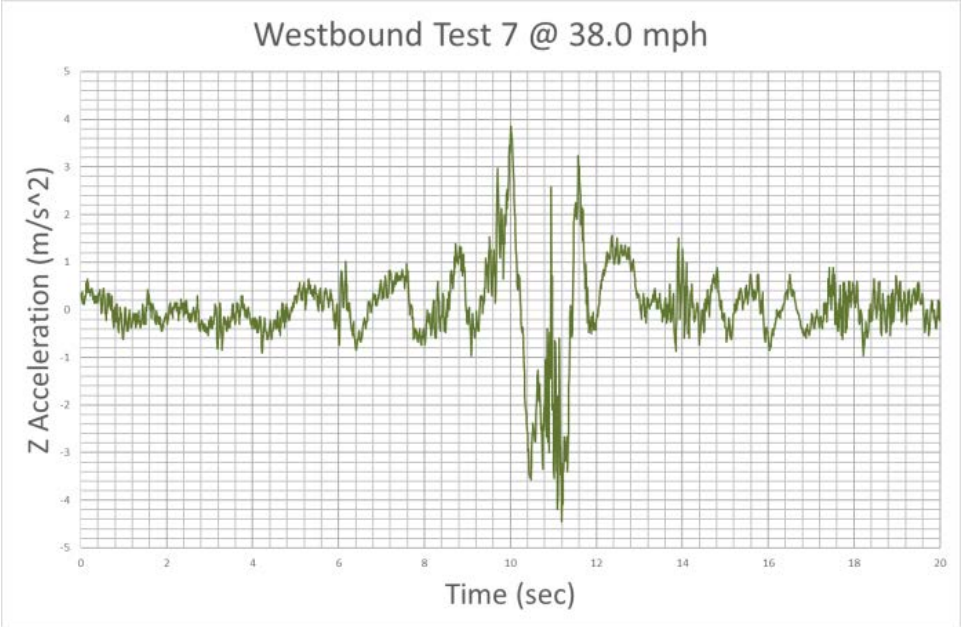
Westbound Test 7 @ 38.0 mph
Z Acceleration (m/s^2)
Time (sec)

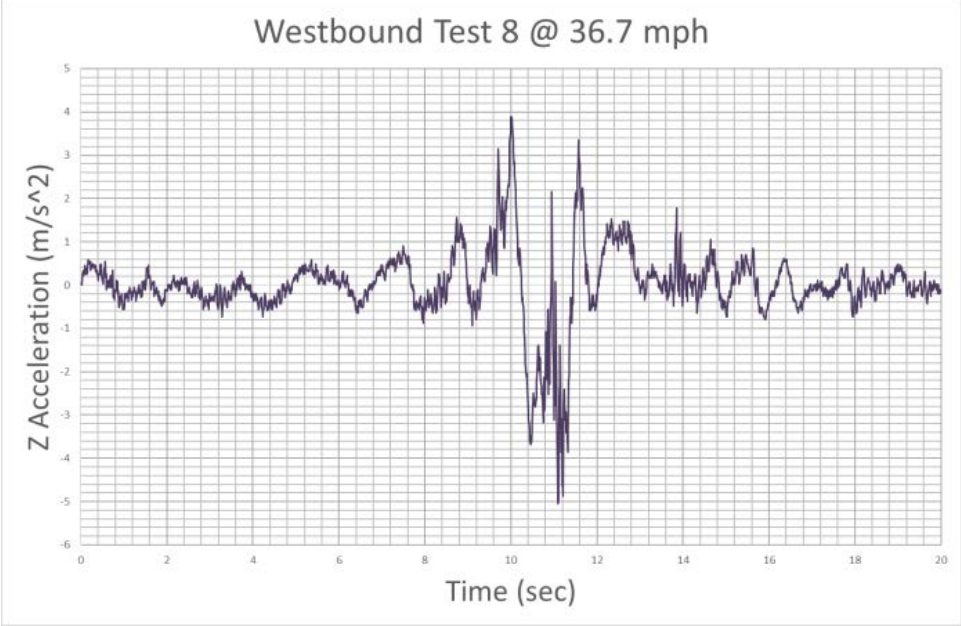
Westbound Test 8 @ 36.7 mph
Z Acceleration (m/s^2)
Time (sec)

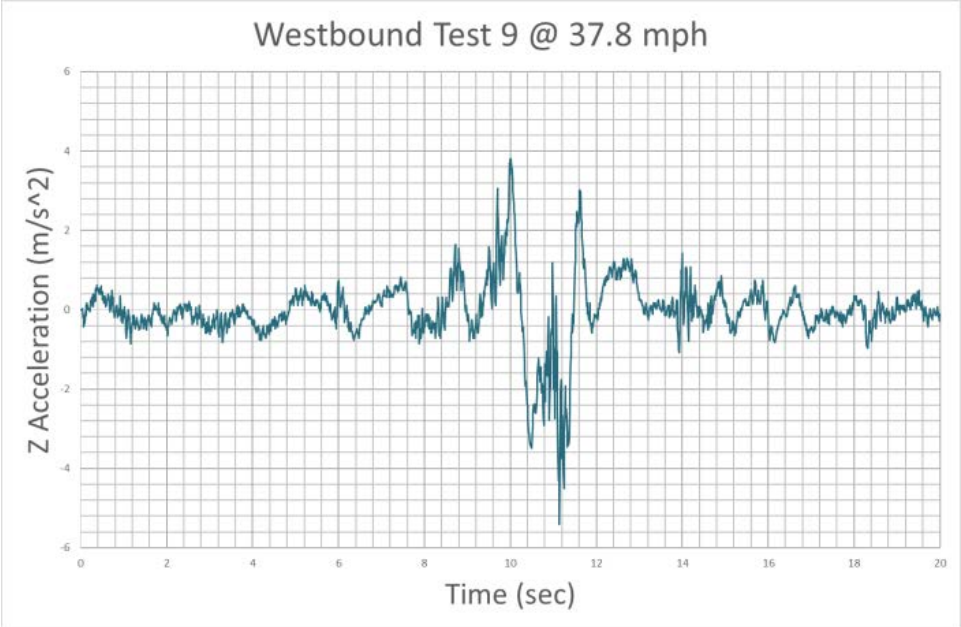
Westbound Test 9 @ 37.8 mph
Z Acceleration (m/s^2)
Time (sec)

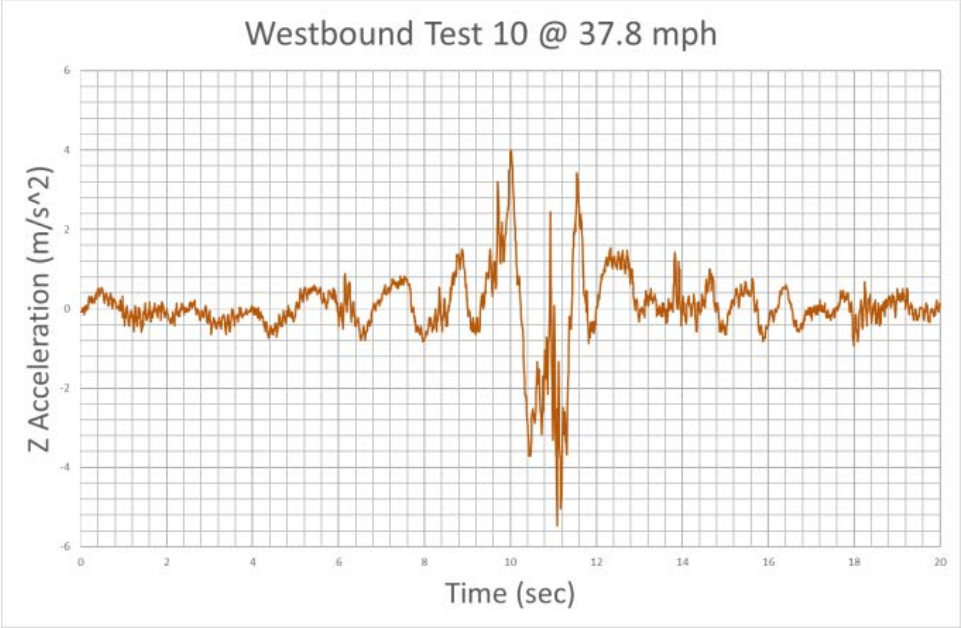
Westbound Test 10 @ 37.8 mph
Z Acceleration (m/s^2)
Time (sec)

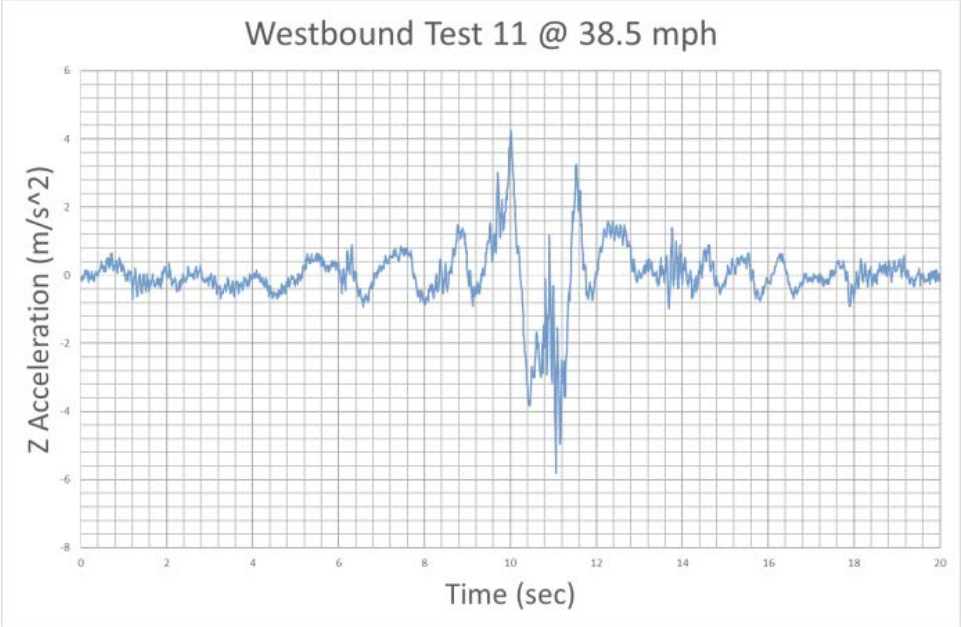
Westbound Test 11 @ 38.5 mph
Z Acceleration (m/s^2)
Time (sec)


Westbound Test 12 @ 35.6 mph
Z Acceleration (m/s^2)
Time (sec)

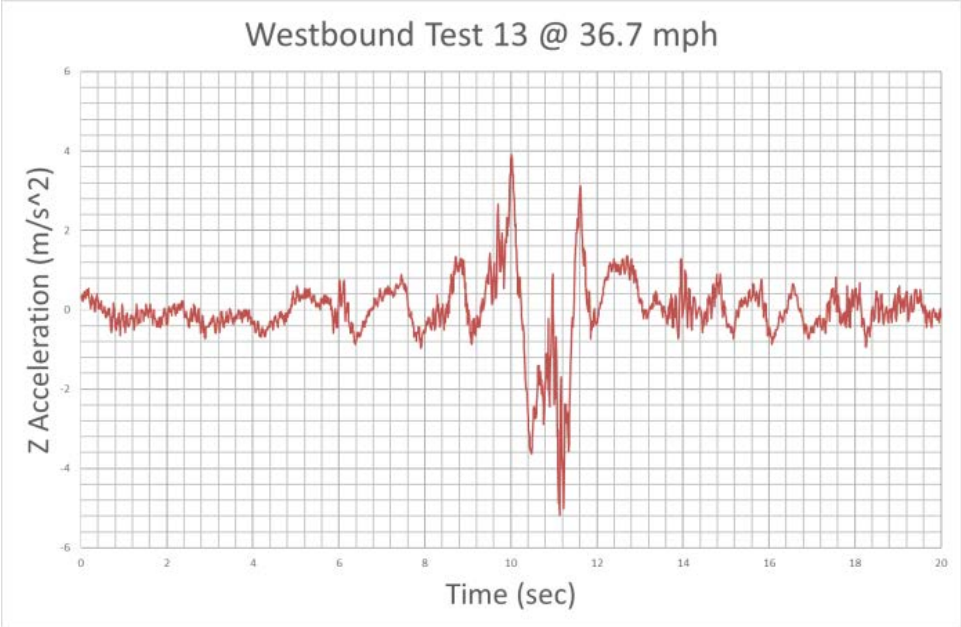
Westbound Test 13 @ 36.7 mph
Z Acceleration (m/s^2)
Time (sec)

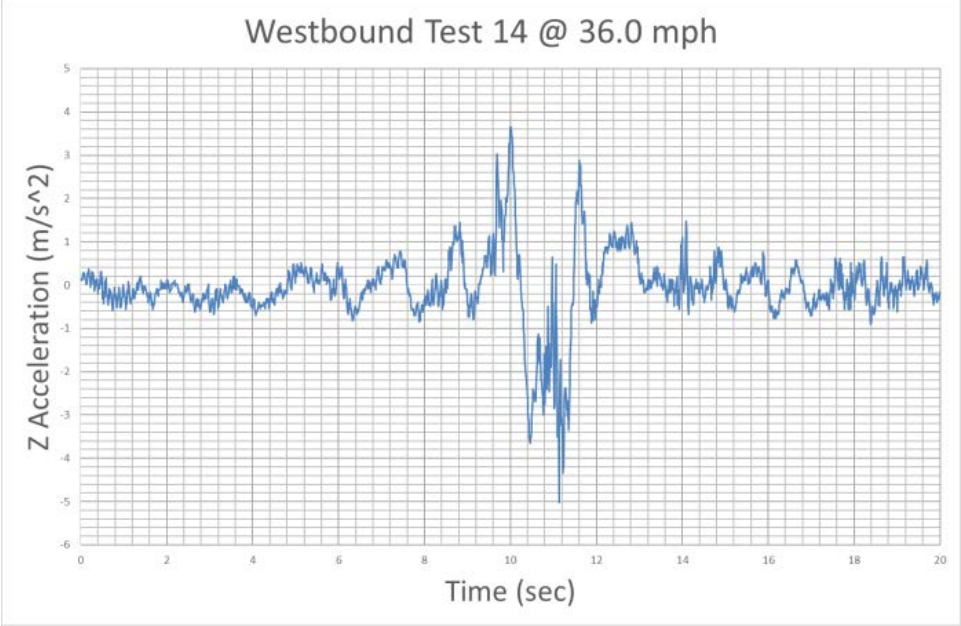
Westbound Test 14 @ 36.0 mph
Z Acceleration (m/s^2)
Time (sec)


Westbound Test 15 @ 33.6 mph
Z Acceleration (m/s^2)
Time (sec)

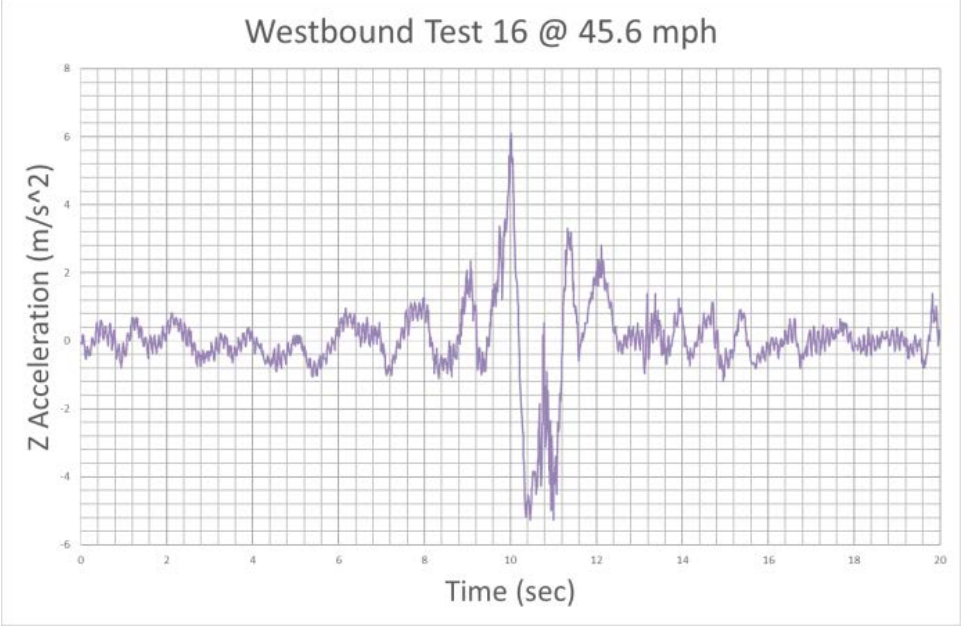
Westbound Test 16 @ 45.6 mph
Z Acceleration (m/s^2)
Time (sec)

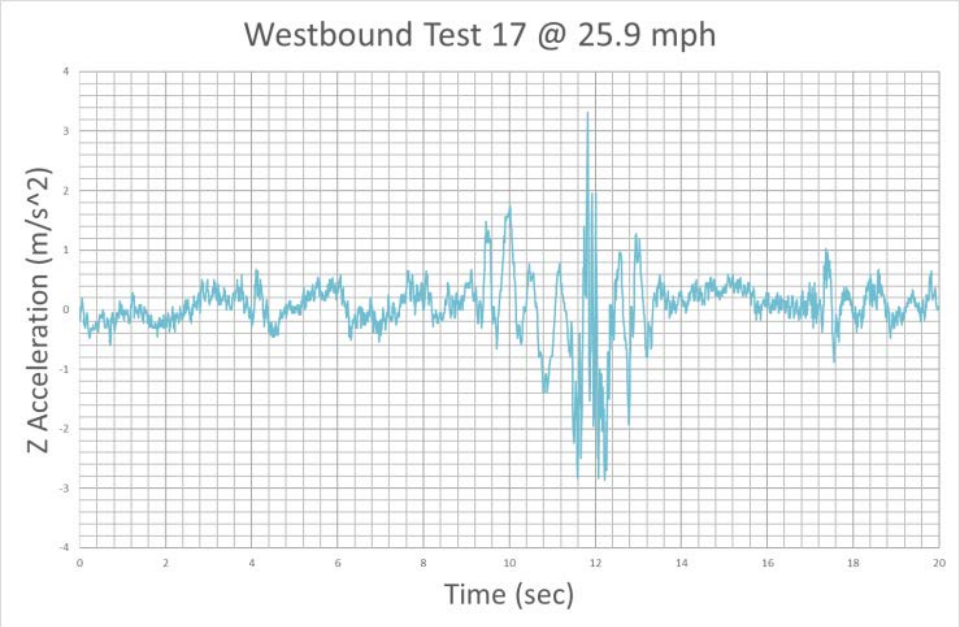
Westbound Test 17 @ 25.9 mph
Z Acceleration (m/s^2)
Time (sec)


Westbound Test 18 @ 20.4 mph
Z Acceleration (m/s^2)
Time (sec)

APPENDIX B

Chapter 4 1.6.1.2 Maximum Acceleration classified by crossing

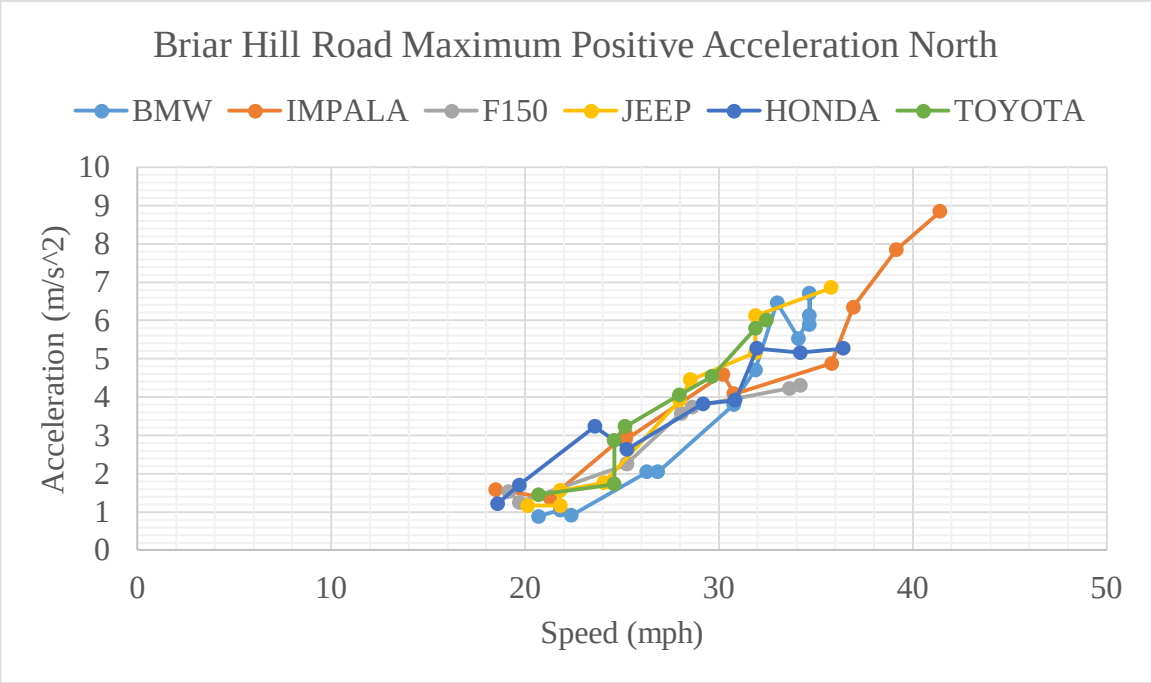

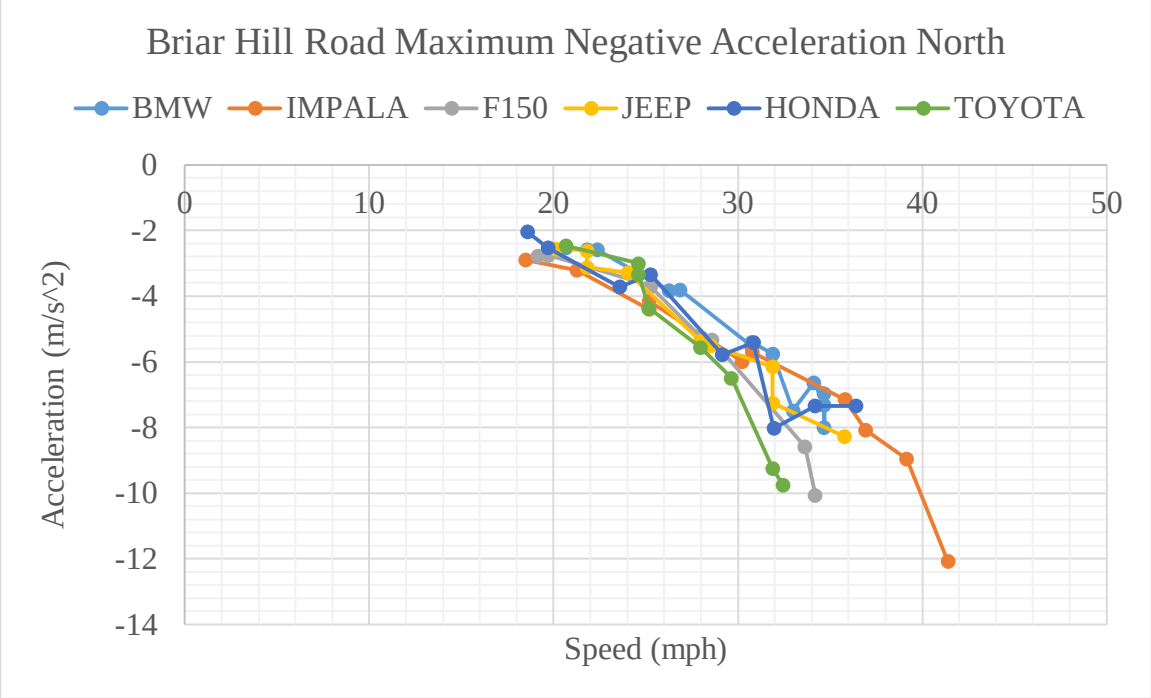

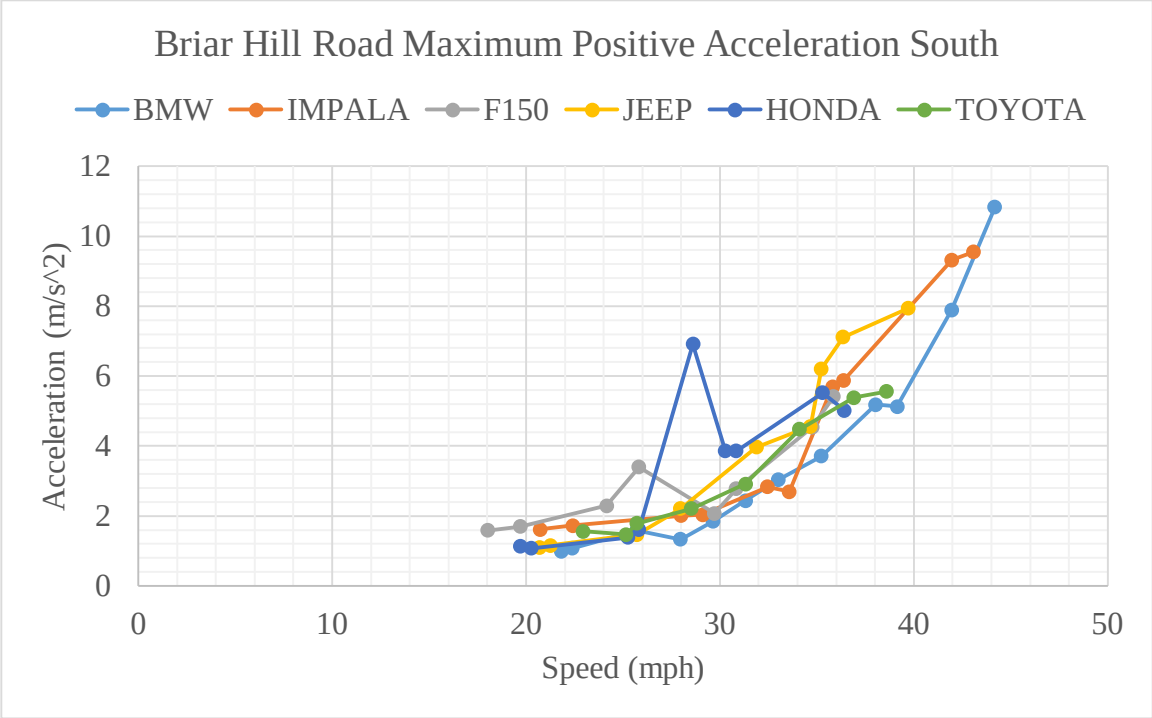
Briar Hill Road Maximum Positive Acceleration South
BMW
IMPALA
F150
JEEP
HONDA
TOYOTA
Acceleration (m/s^2)
12
10
8
6
4
2
0
0
10
20
30
40
50
Speed (mph)

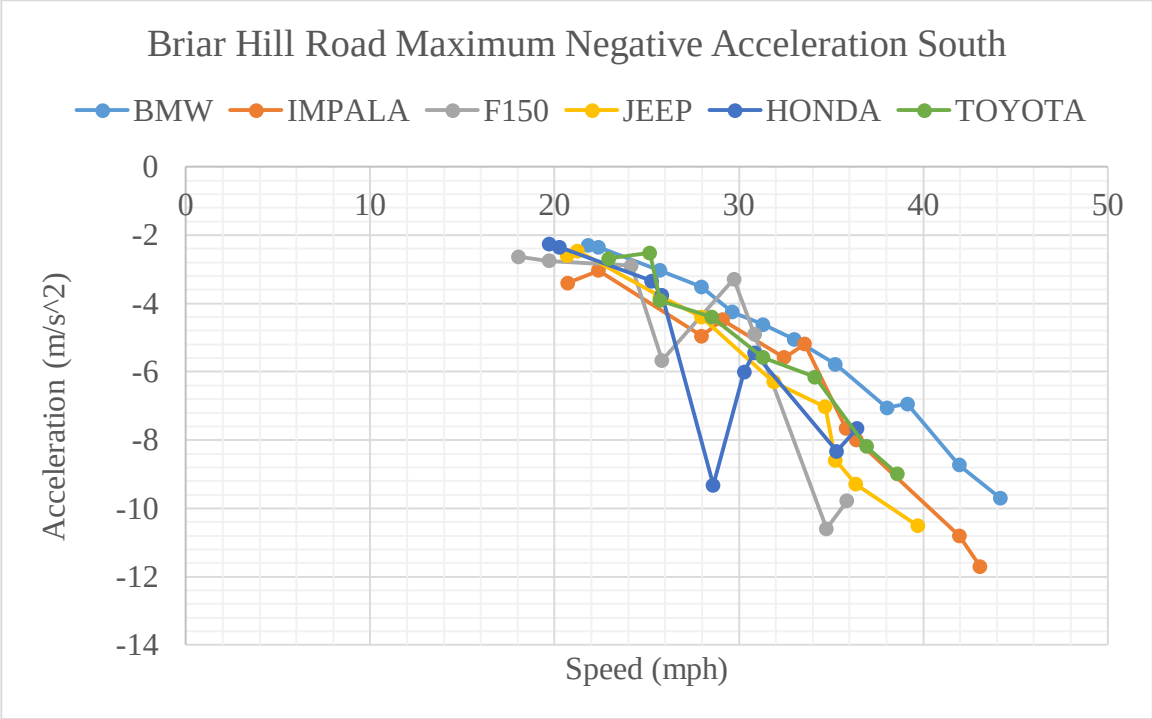
Briar Hill Road Maximum Negative Acceleration South
BMW
IMPALA
F150
JEEP
HONDA
TOYOTA
Acceleration (m/s^2)
0
-2
-4
-6
-8
-10
-12
-14
0
10
20
30
40
50
Speed (mph)

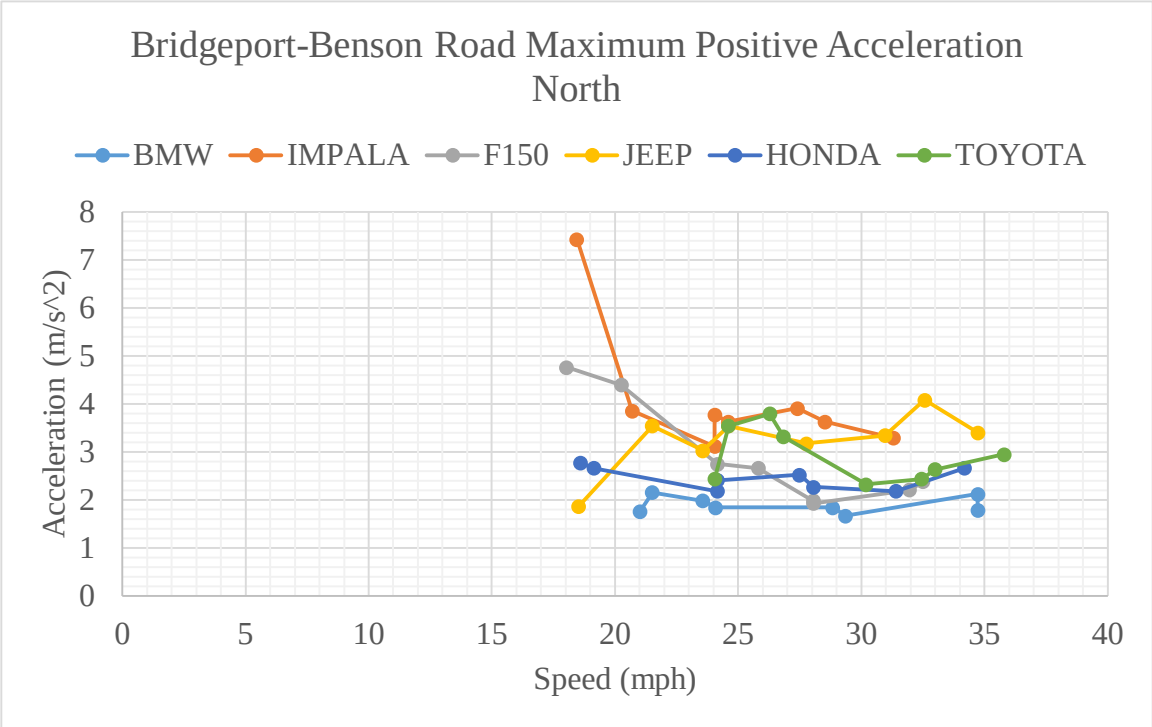
Bridgeport-Benson Road Maximum Positive Acceleration North
BMW
IMPALA
F150
JEEP
HONDA
TOYOTA
Acceleration (m/s^2)
8
7
6
5
4
3
2
1
0
0
5
10
15
20
25
30
35
40
Speed (mph)

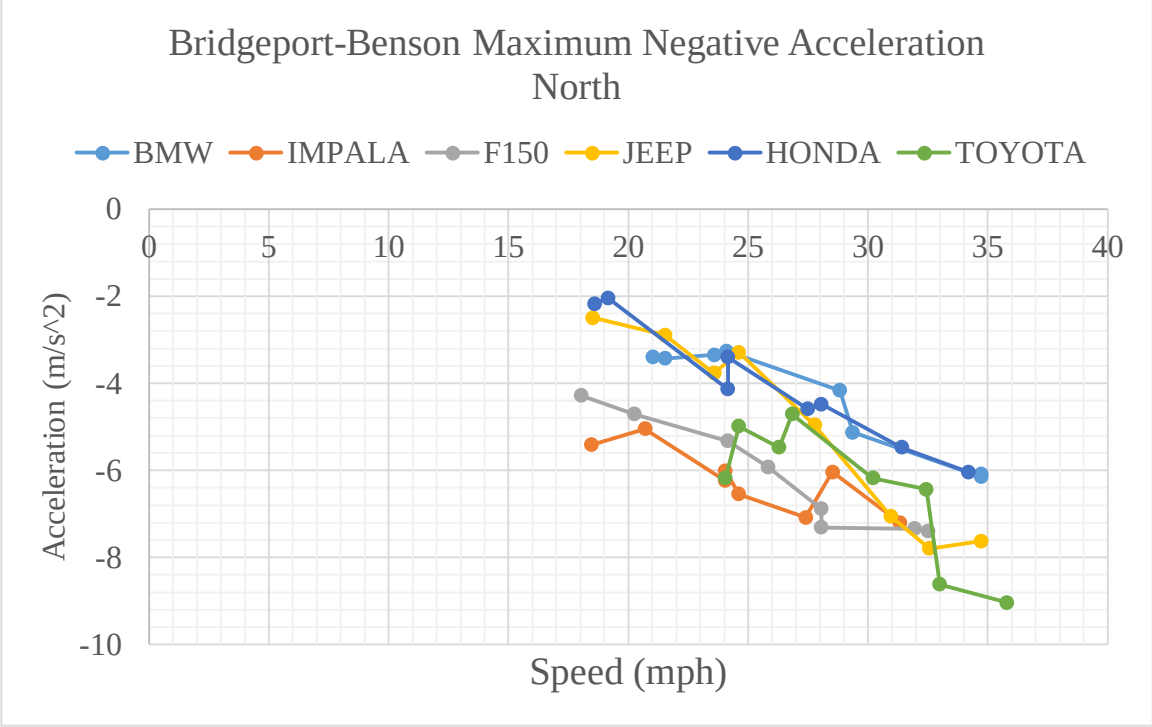
Bridgeport-Benson Maximum Negative Acceleration North
BMW
IMPALA
F150
JEEP
HONDA
TOYOTA
Acceleration (m/s^2)
0
-2
-4
-6
-8
-10
0
5
10
15
20
25
30
35
40
Speed (mph)

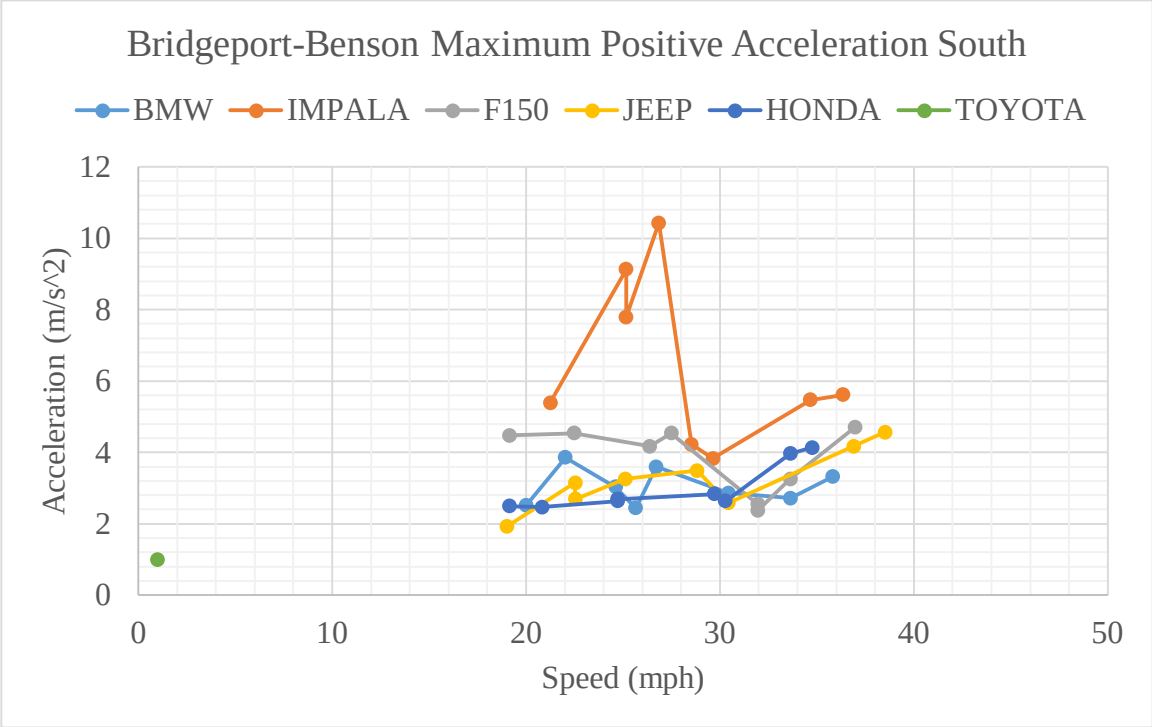
Bridgeport-Benson Maximum Positive Acceleration South
BMW
IMPALA
F150
JEEP
HONDA
TOYOTA
Acceleration (m/s^2)
12
10
8
6
4
2
0
0
10
20
30
40
50
Speed (mph)

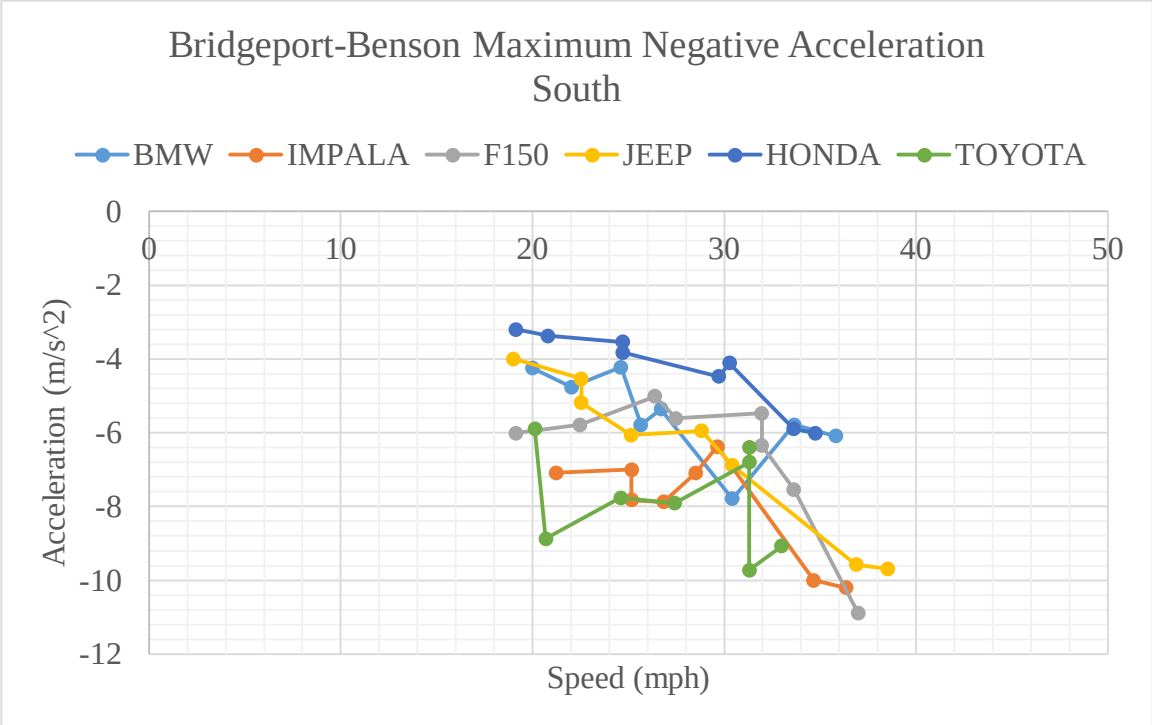
Bridgeport-Benson Maximum Negative Acceleration South
BMW
IMPALA
F150
JEEP
HONDA
TOYOTA
Acceleration (m/s^2)
0
-2
-4
-6
-8
-10
-12
0
10
20
30
40
50
Speed (mph)

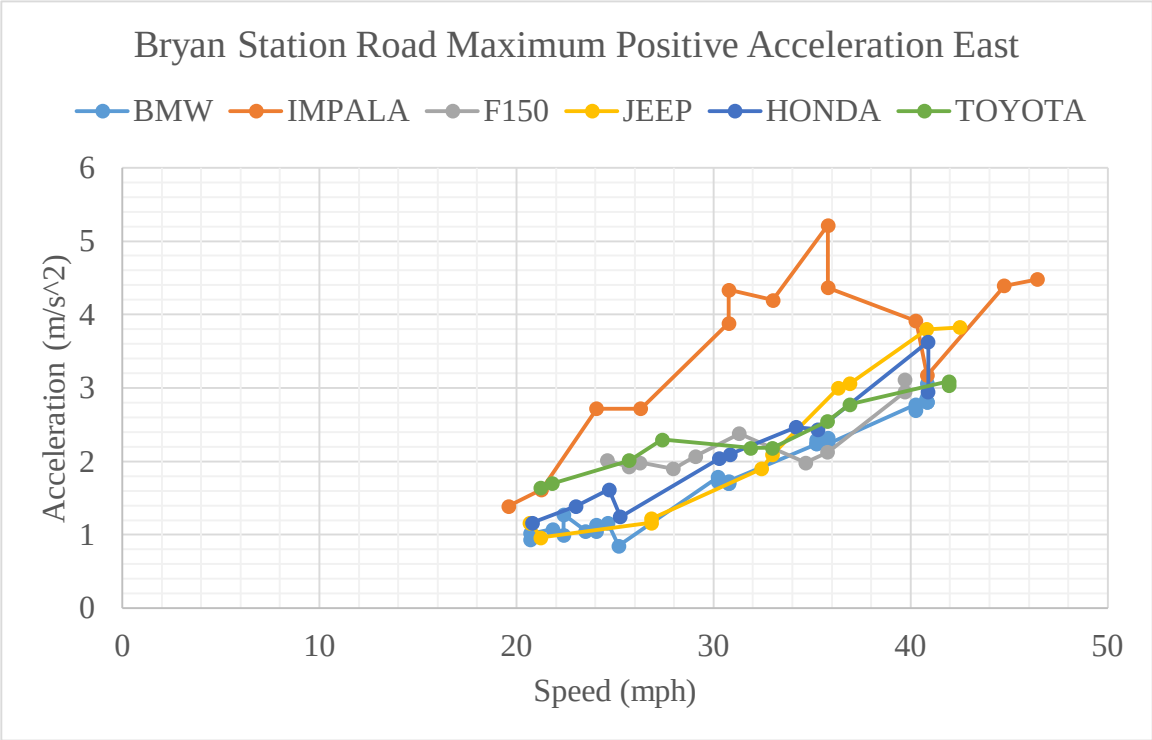
Bryan Station Road Maximum Positive Acceleration East
BMW
IMPALA
F150
JEEP
HONDA
TOYOTA
Acceleration (m/s^2)
0
1
2
3
4
5
6
0
10
20
30
40
50
Speed (mph)

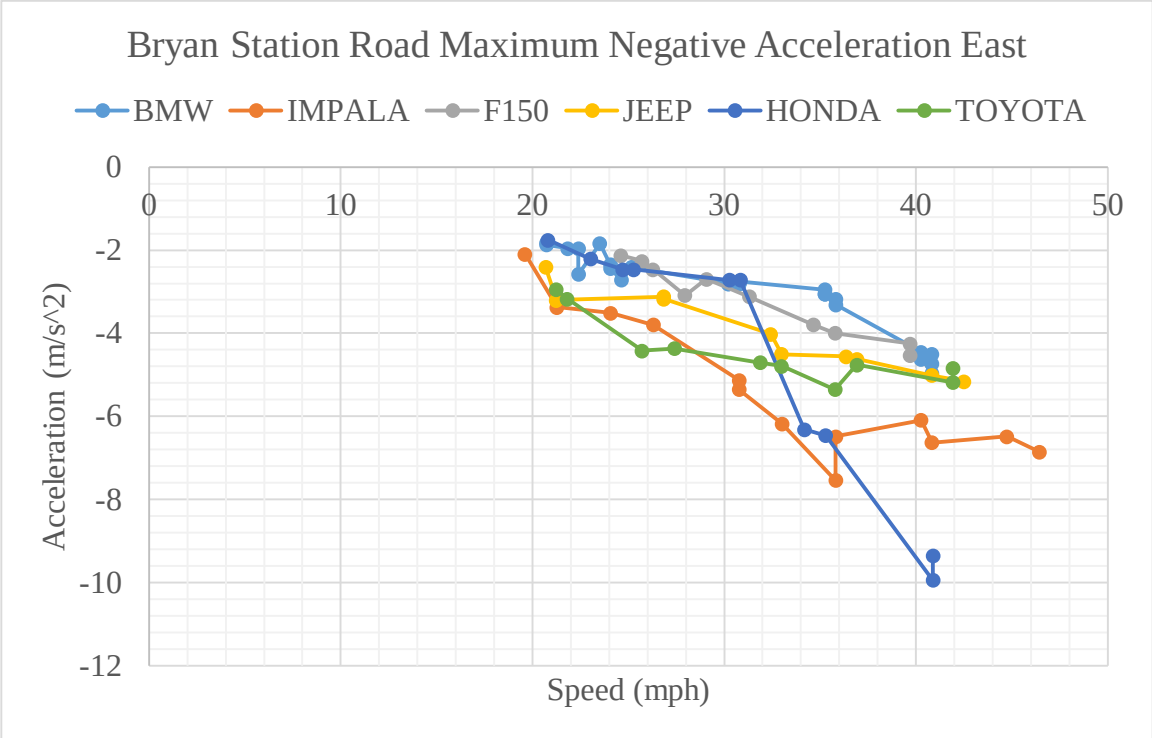
Bryan Station Road Maximum Negative Acceleration East
BMW
IMPALA
F150
JEEP
HONDA
TOYOTA
Acceleration (m/s^2)
0
-2
-4
-6
-8
-10
-12
0
10
20
30
40
50
Speed (mph)

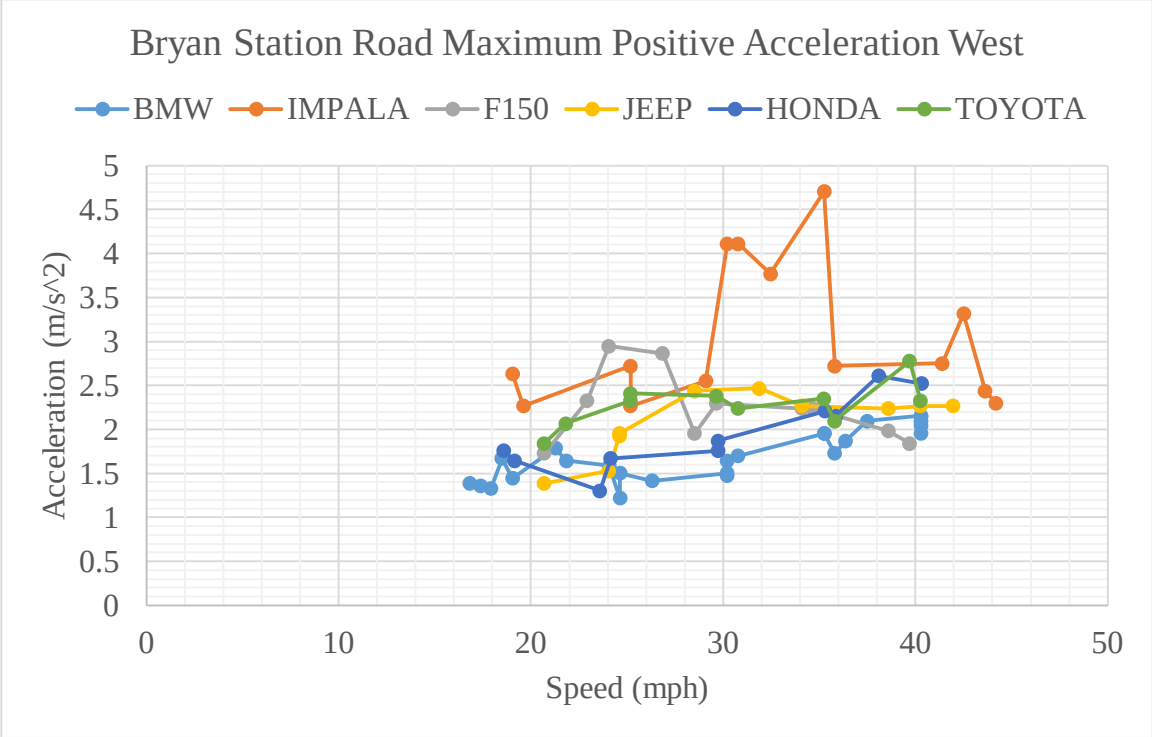
Bryan Station Road Maximum Positive Acceleration West
BMW
IMPALA
F150
JEEP
HONDA
TOYOTA
Acceleration (m/s^2)
5
4.5
4
3.5
3
2.5
2
1.5
1
0.5
0
0
10
20
30
40
50
Speed (mph)

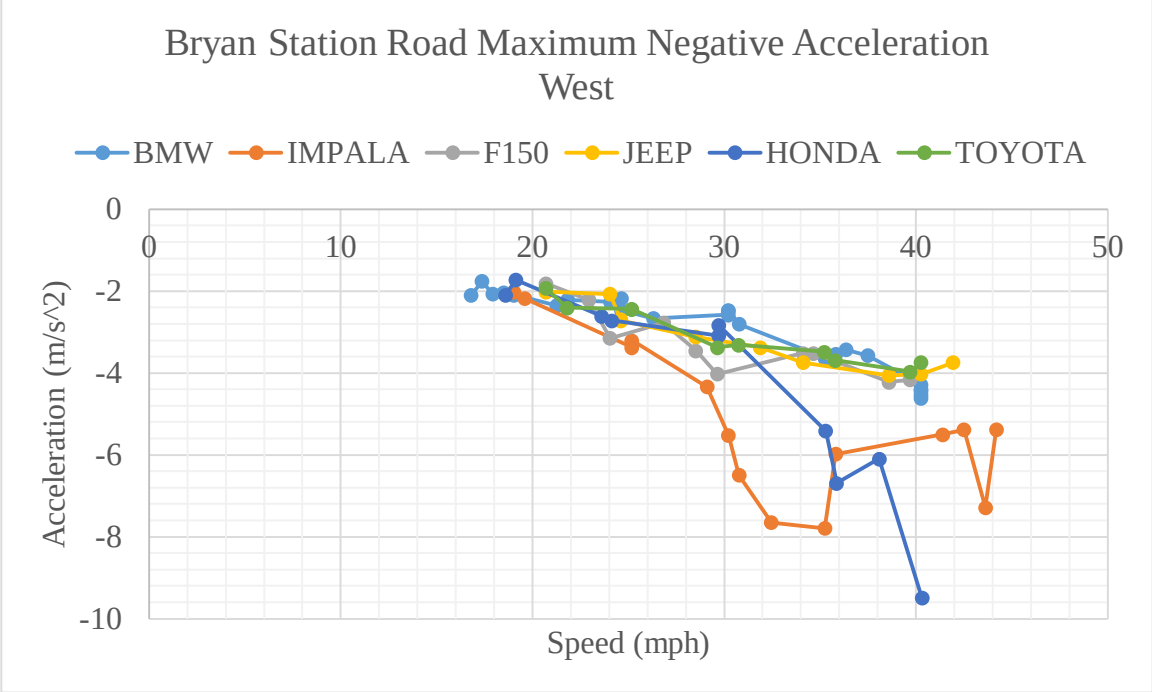
Bryan Station Road Maximum Negative Acceleration West
BMW
IMPALA
F150
JEEP
HONDA
TOYOTA
Acceleration (m/s^2)
0
-2
-4
-6
-8
-10
0
10
20
30
40
50
Speed (mph)

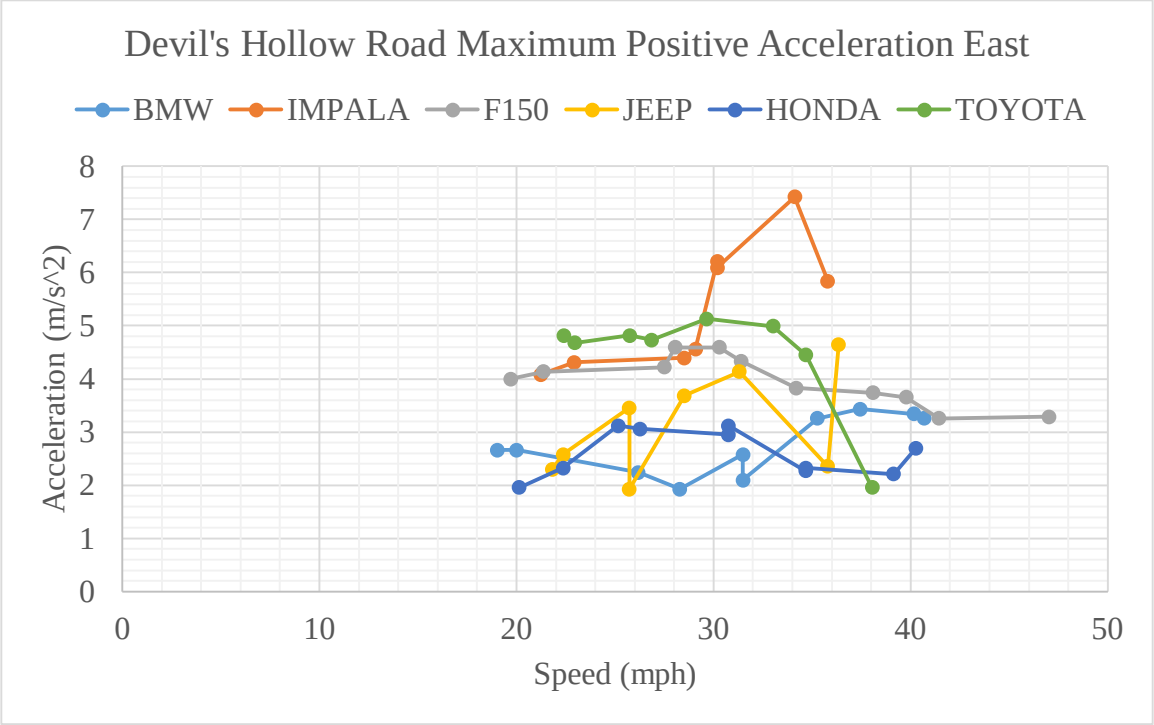
Devil's Hollow Road Maximum Positive Acceleration East
BMW
IMPALA
F150
JEEP
HONDA
TOYOTA
Acceleration (m/s^2)
8
7
6
5
4
3
2
1
0
0
10
20
30
40
50
Speed (mph)

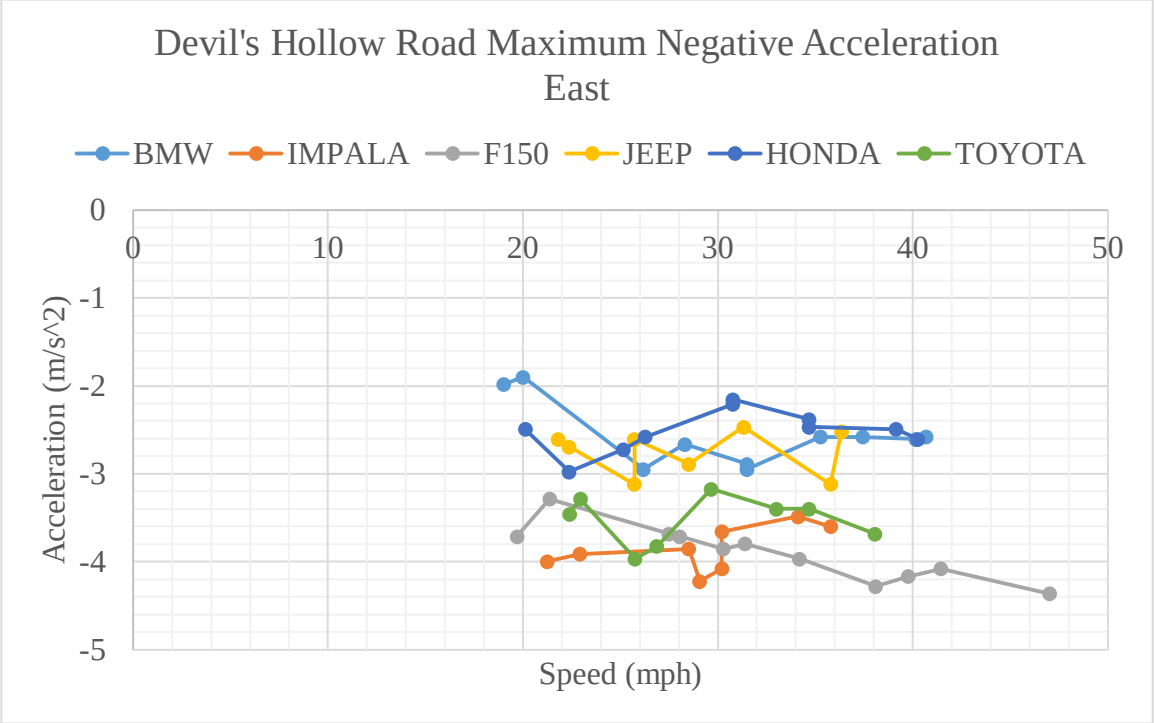
Devil's Hollow Road Maximum Negative Acceleration East
BMW
IMPALA
F150
JEEP
HONDA
TOYOTA
Acceleration (m/s^2)
0
-1
-2
-3
-4
-5
0
10
20
30
40
50
Speed (mph)

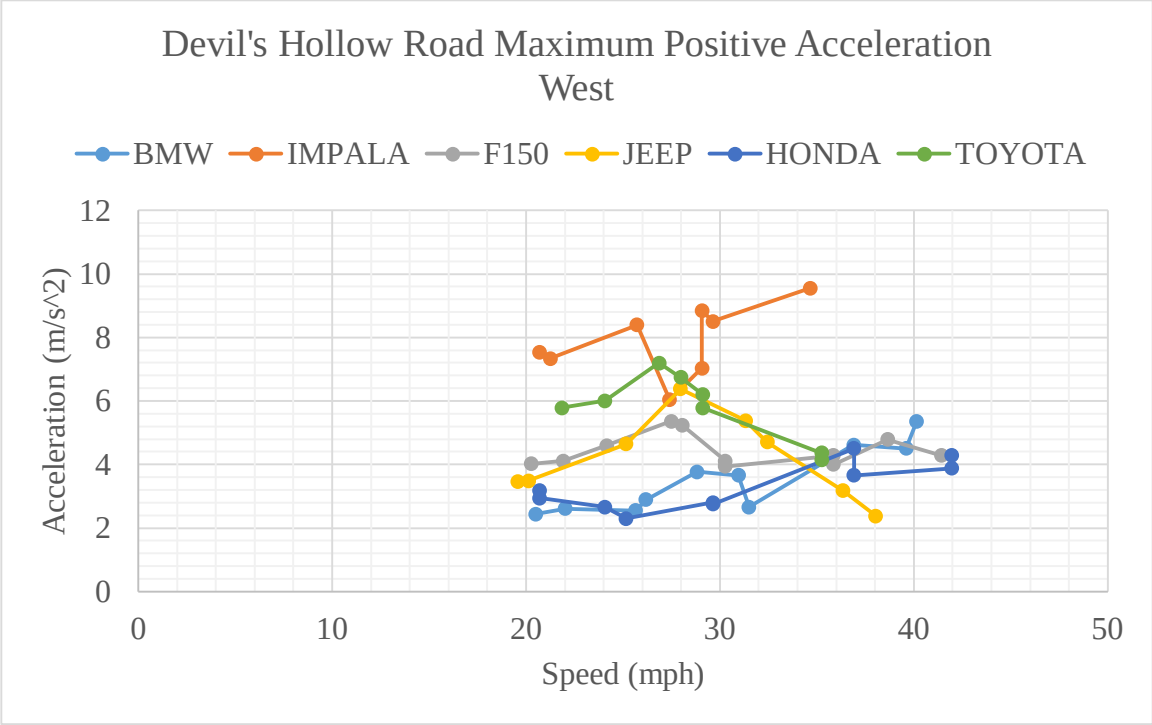
Devil's Hollow Road Maximum Positive Acceleration
West
BMW
IMPALA
F150
JEEP
HONDA
TOYOTA
Acceleration (m/s^2)
12
10
8
6
4
2
0
0
10
20
30
40
50
Speed (mph)

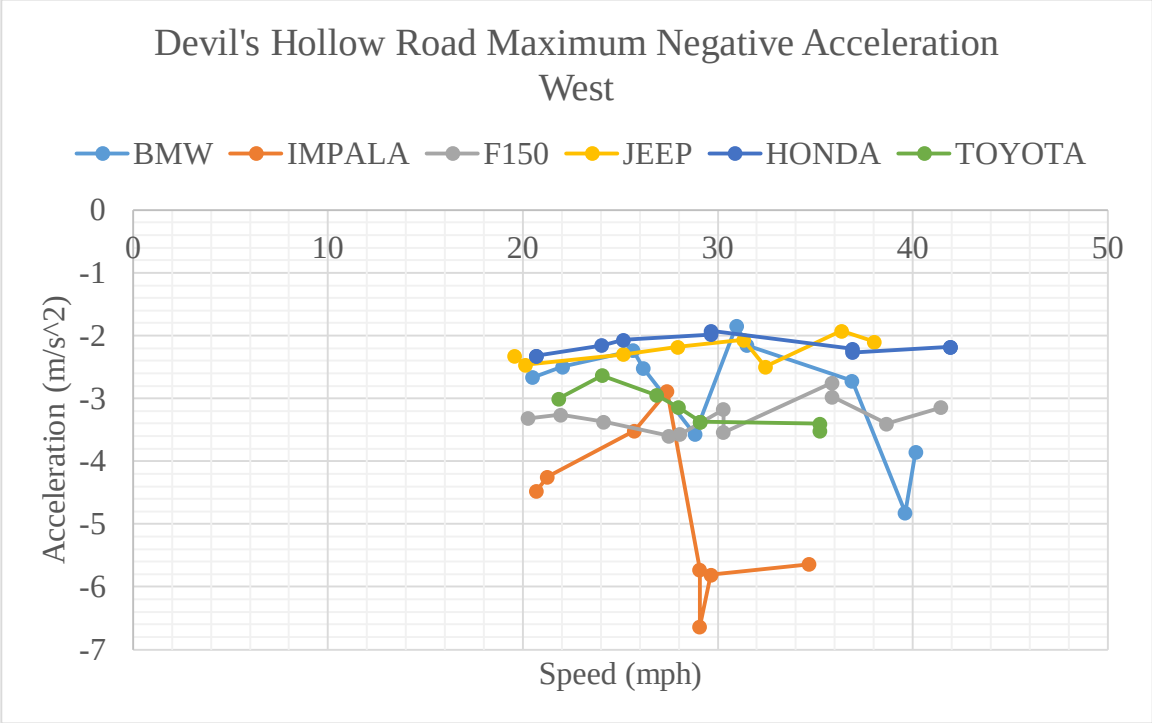
Devil's Hollow Road Maximum Negative Acceleration
West
BMW
IMPALA
F150
JEEP
HONDA
TOYOTA
Acceleration (m/s^2)
0
-1
-2
-3
-4
-5
-6
-7
0
10
20
30
40
50
Speed (mph)

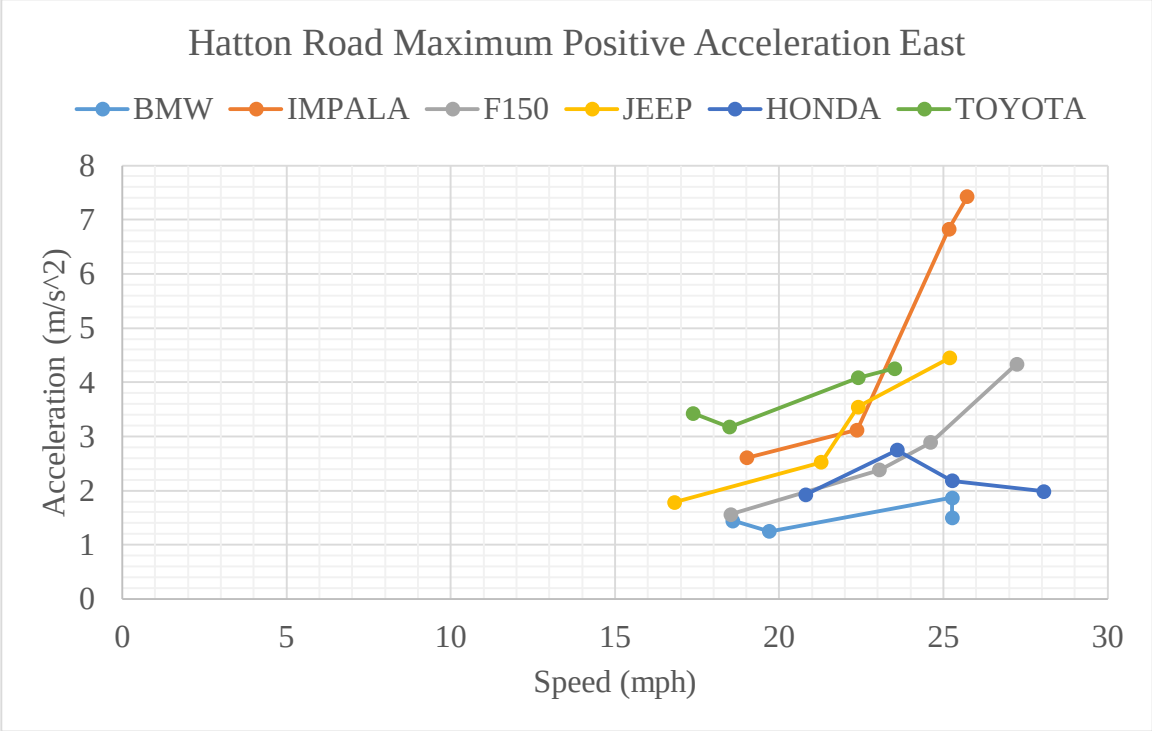
Hatton Road Maximum Positive Acceleration East
BMW
IMPALA
F150
JEEP
HONDA
TOYOTA
Acceleration (m/s^2)
8
7
6
5
4
3
2
1
0
0
5
10
15
20
25
30
Speed (mph)

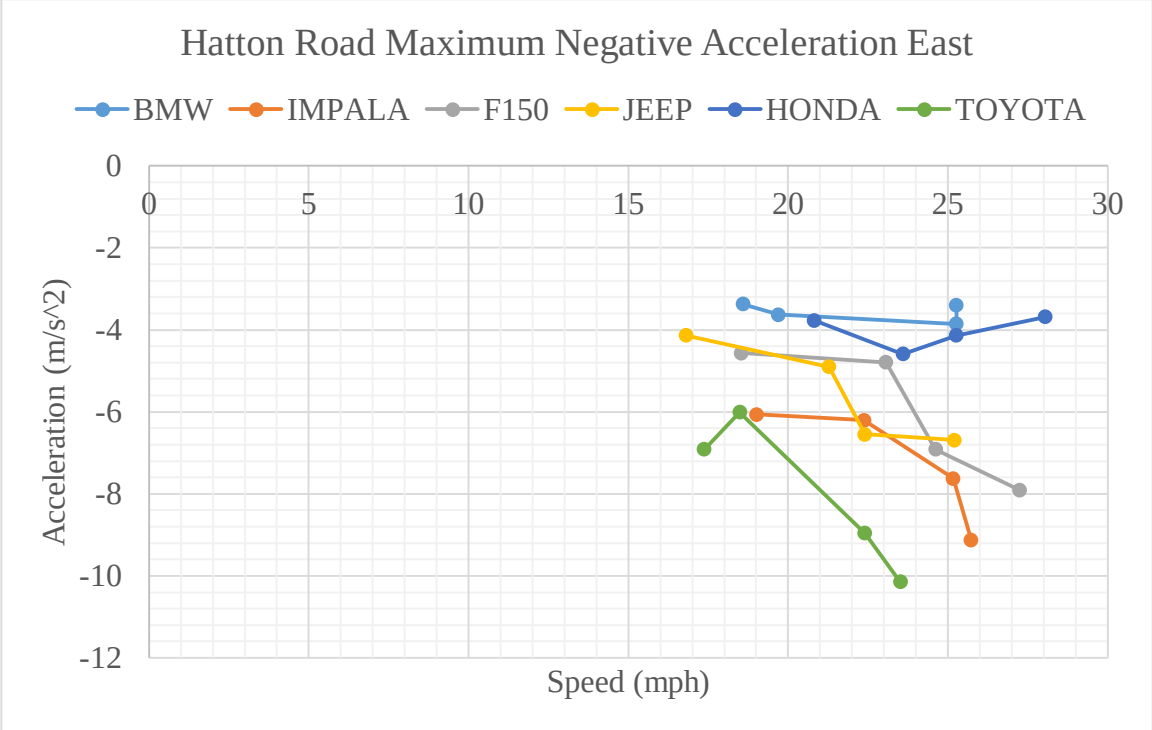
Hatton Road Maximum Negative Acceleration East
BMW
IMPALA
F150
JEEP
HONDA
TOYOTA
Acceleration (m/s^2)
0
-2
-4
-6
-8
-10
-12
0
5
10
15
20
25
30
Speed (mph)

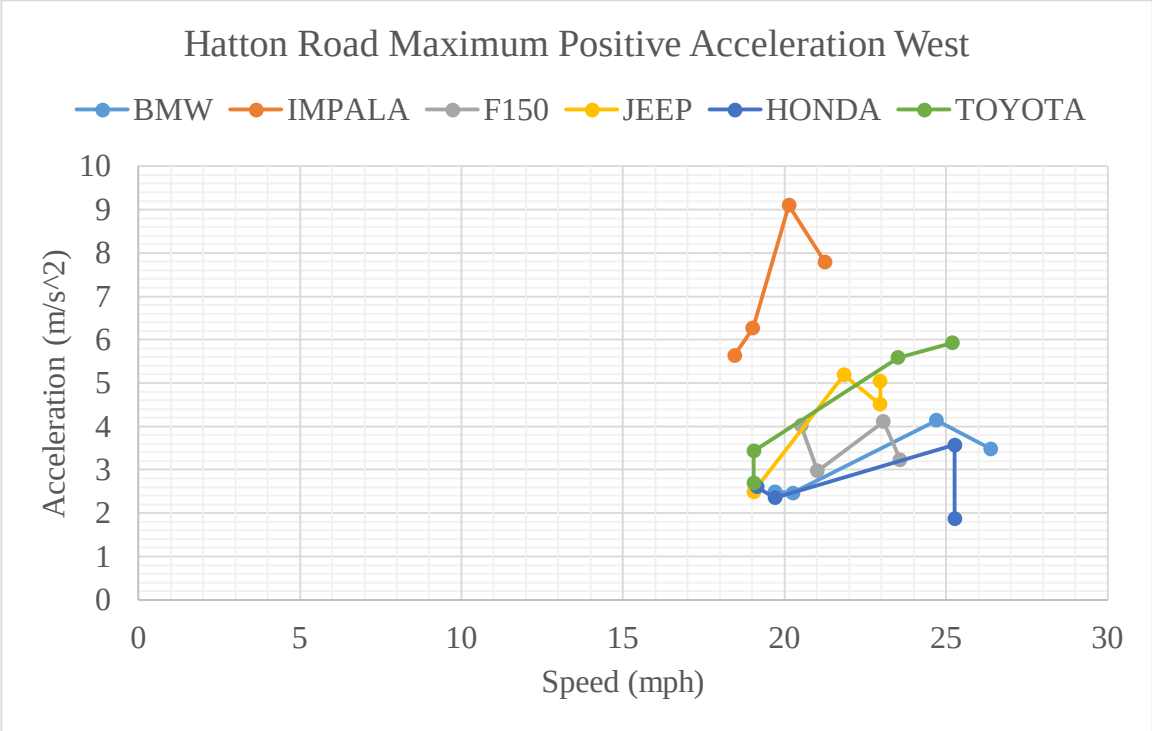
Hatton Road Maximum Positive Acceleration West
BMW
IMPALA
F150
JEEP
HONDA
TOYOTA
Acceleration (m/s^2)
10
9
8
7
6
5
4
3
2
1
0
0
5
10
15
20
25
30
Speed (mph)

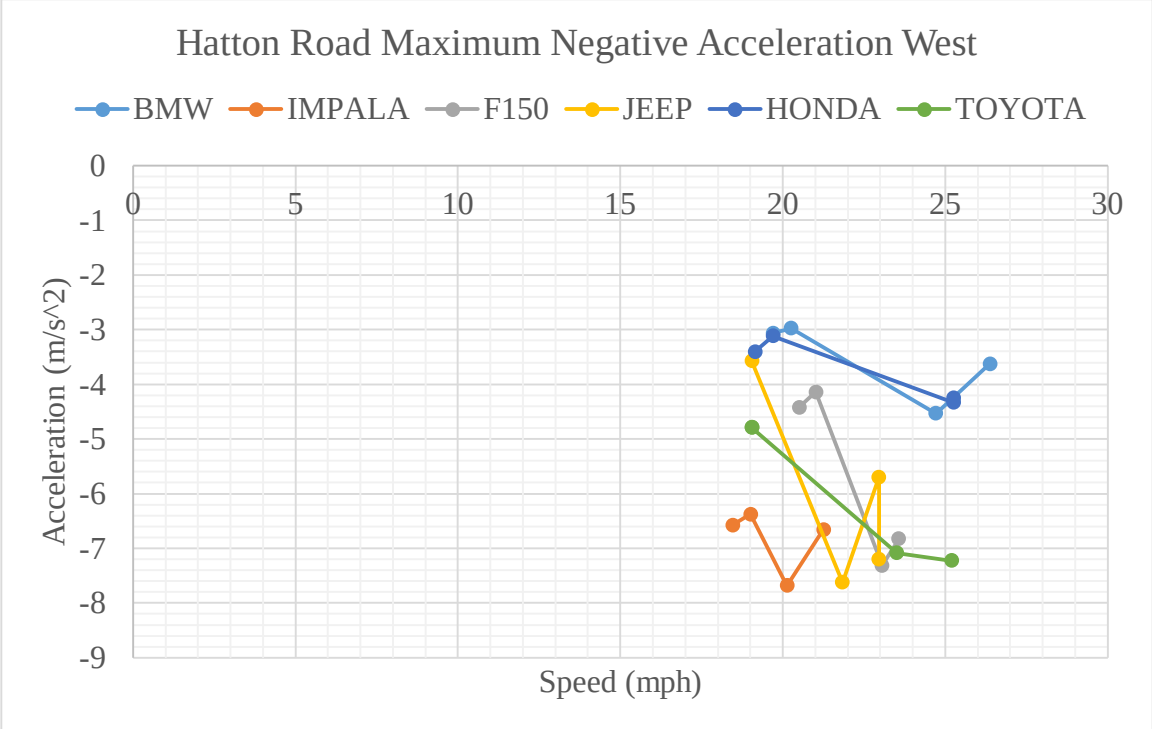
Hatton Road Maximum Negative Acceleration West
BMW
IMPALA
F150
JEEP
HONDA
TOYOTA
Acceleration (m/s^2)
0
-1
-2
-3
-4
-5
-6
-7
-8
-9
0
5
10
15
20
25
30
Speed (mph)

APPENDIX C

Chapter 4 Maximum Acceleration Classified by Vehicle

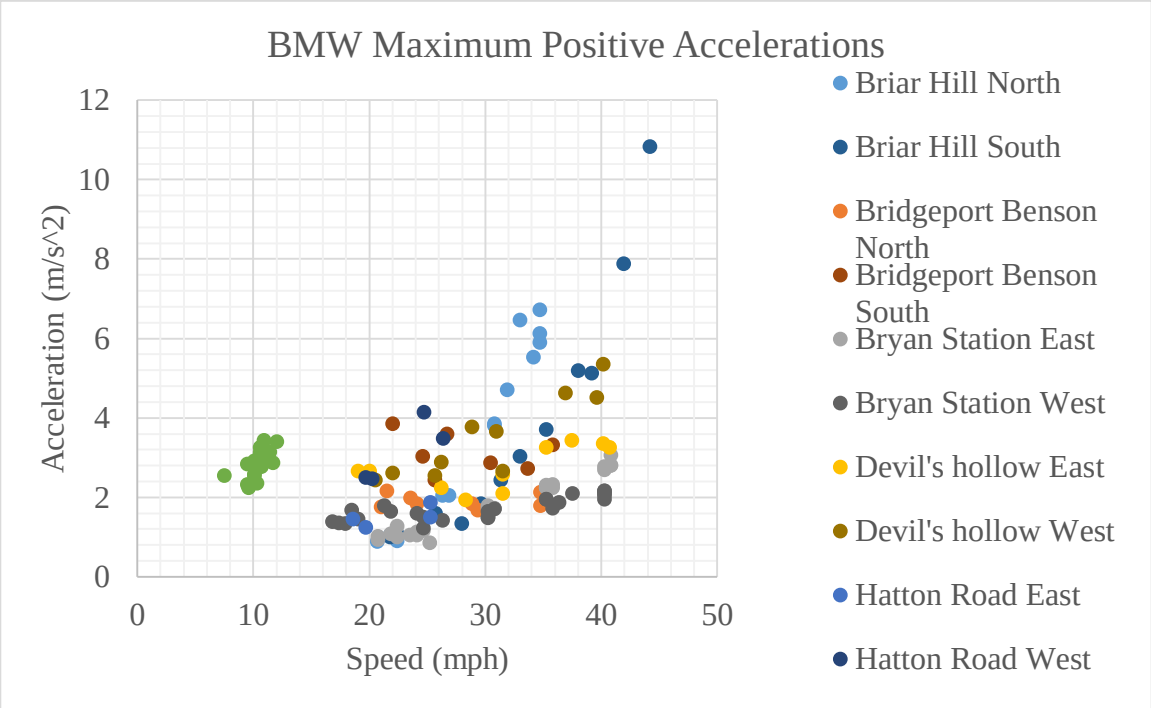

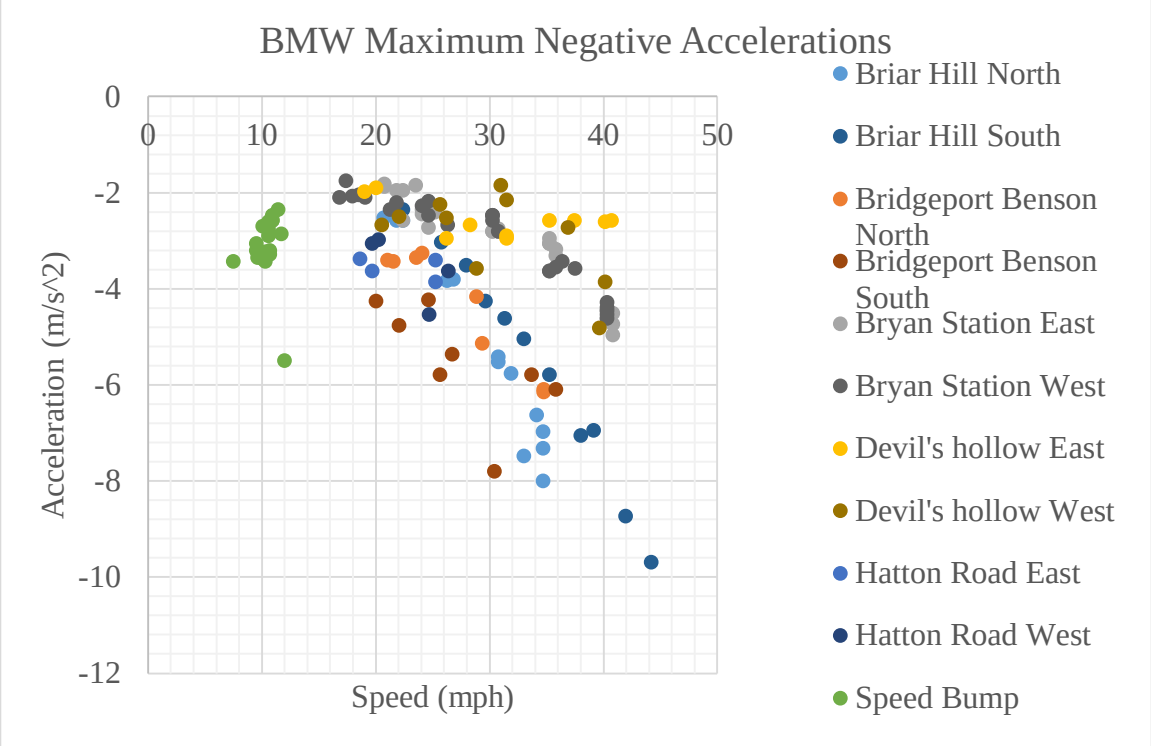

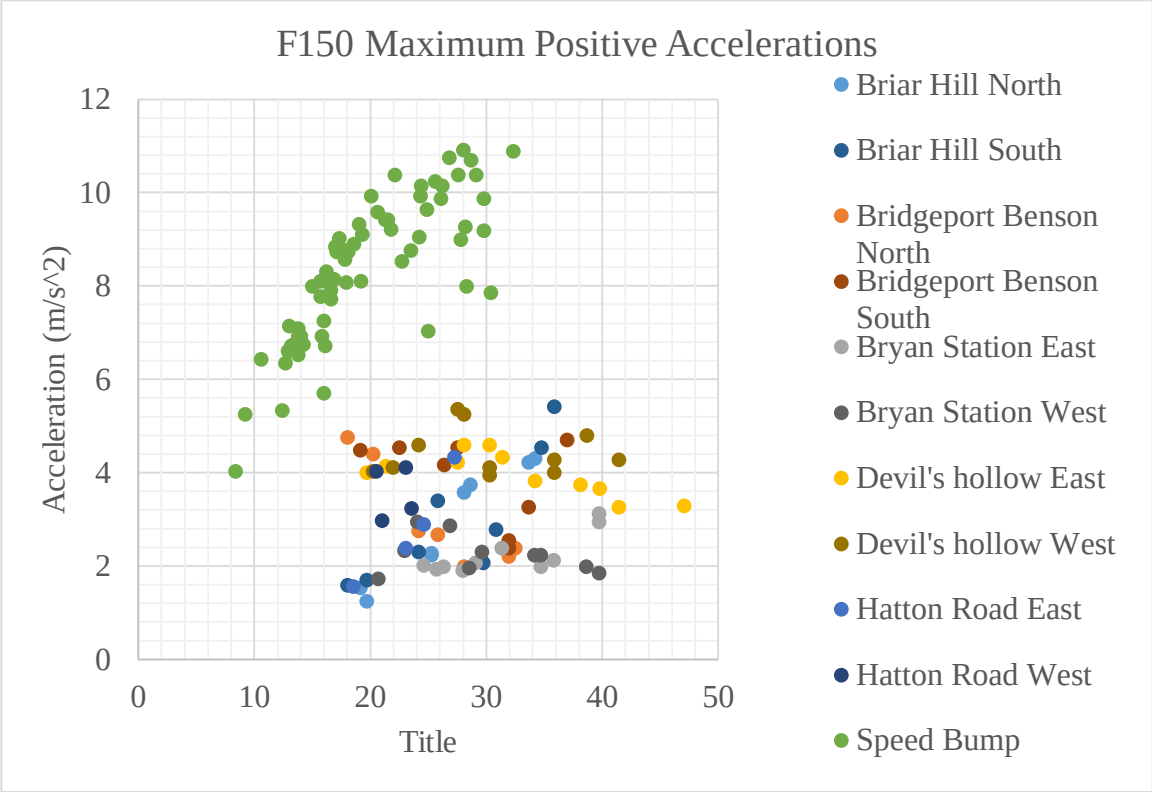
F150 Maximum Positive Accelerations
Acceleration (m/s^2)
12
10
8
6
4
2
0
0
10
20
30
40
50
Title
Briar Hill North
Briar Hill South
Bridgeport Benson North
Bridgeport Benson South
Bryan Station East
Bryan Station West
Devil's hollow East
Devil's hollow West
Hatton Road East
Hatton Road West
Speed Bump

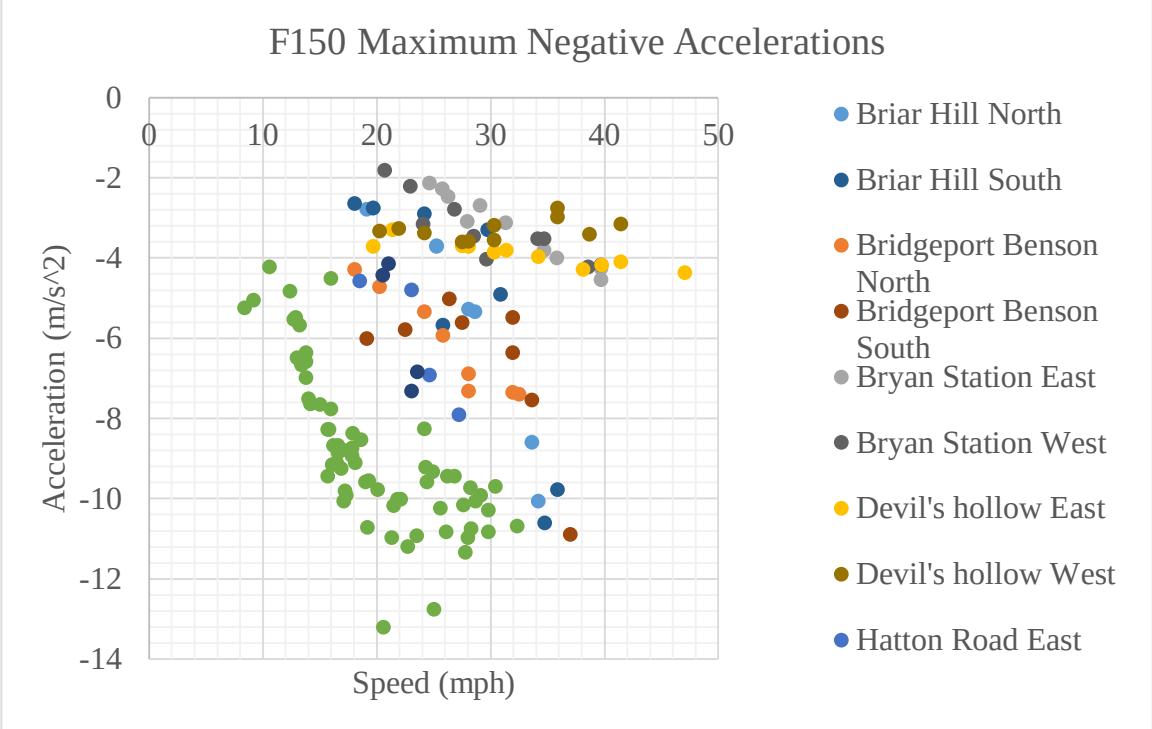
F150 Maximum Negative Accelerations
Acceleration (m/s^2)
0
-2
-4
-6
-8
-10
-12
-14
0
10
20
30
40
50
Speed (mph)
Briar Hill North
Briar Hill South
Bridgeport Benson North
Bridgeport Benson South
Bryan Station East
Bryan Station West
Devil's hollow East
Devil's hollow West
Hatton Road East

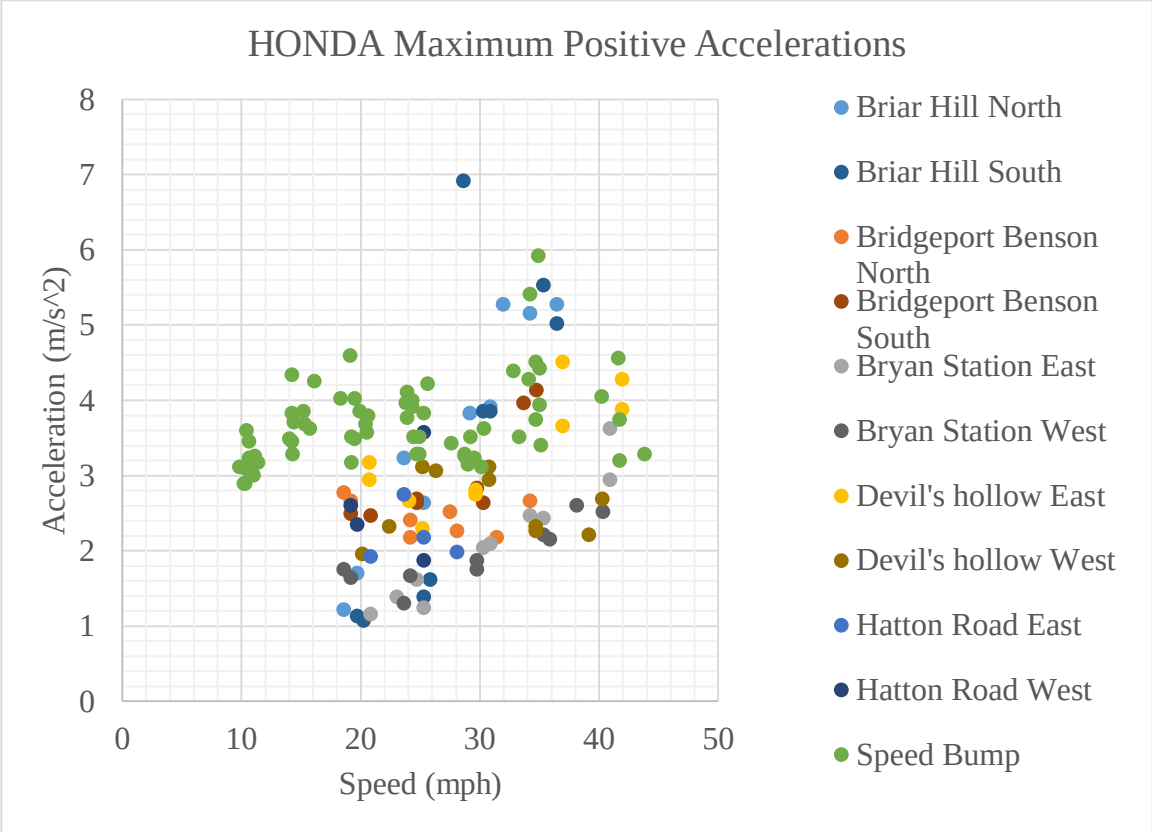
HONDA Maximum Positive Accelerations
Acceleration (m/s^2)
8
7
6
5
4
3
2
1
0
0
10
20
30
40
50
Speed (mph)
Briar Hill North
Briar Hill South
Bridgeport Benson North
Bridgeport Benson South
Bryan Station East
Bryan Station West
Devil's hollow East
Devil's hollow West
Hatton Road East
Hatton Road West
Speed Bump

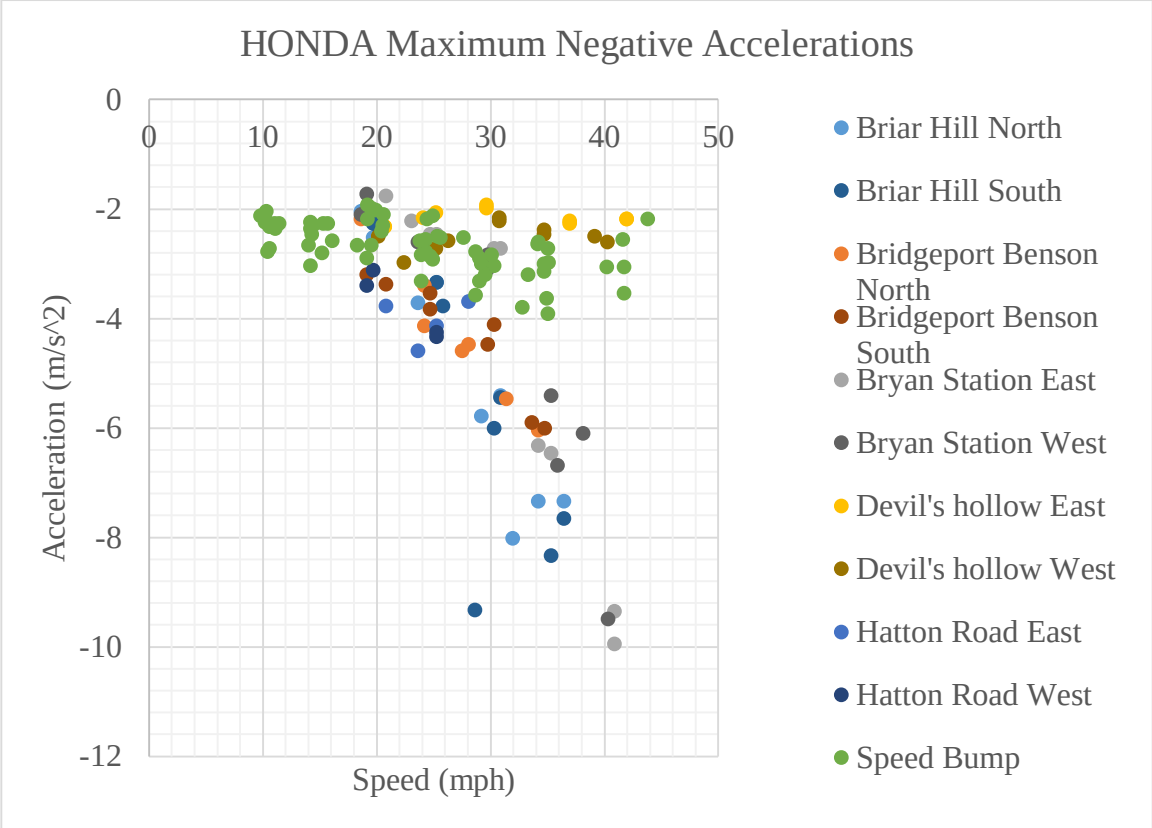
HONDA Maximum Negative Accelerations
Acceleration (m/s^2)
0
-2
-4
-6
-8
-10
-12
0
10
20
30
40
50
Speed (mph)
Briar Hill North
Briar Hill South
Bridgeport Benson North
Bridgeport Benson South
Bryan Station East
Bryan Station West
Devil's hollow East
Devil's hollow West
Hatton Road East
Hatton Road West
Speed Bump

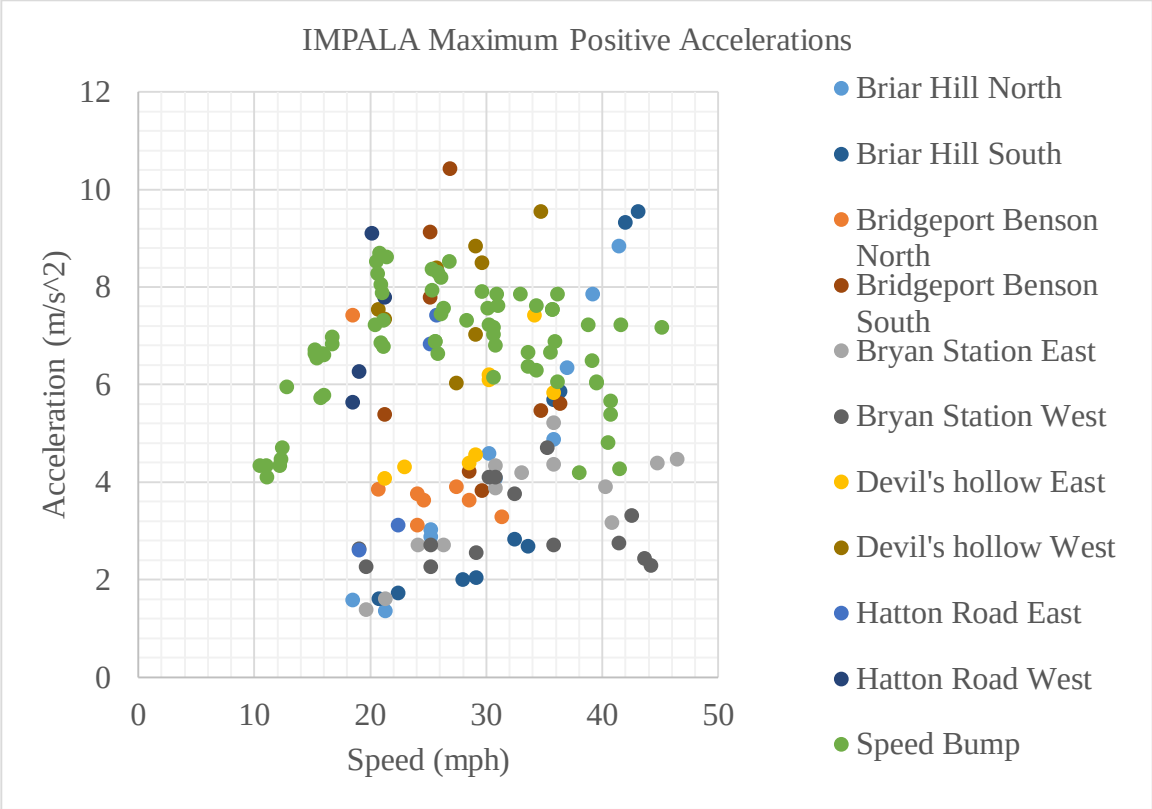
IMPALA Maximum Positive Accelerations
Acceleration (m/s^2)
12
10
8
6
4
2
0
0
10
20
30
40
50
Speed (mph)
Briar Hill North
Briar Hill South
Bridgeport Benson North
Bridgeport Benson South
Bryan Station East
Bryan Station West
Devil's hollow East
Devil's hollow West
Hatton Road East
Hatton Road West
Speed Bump

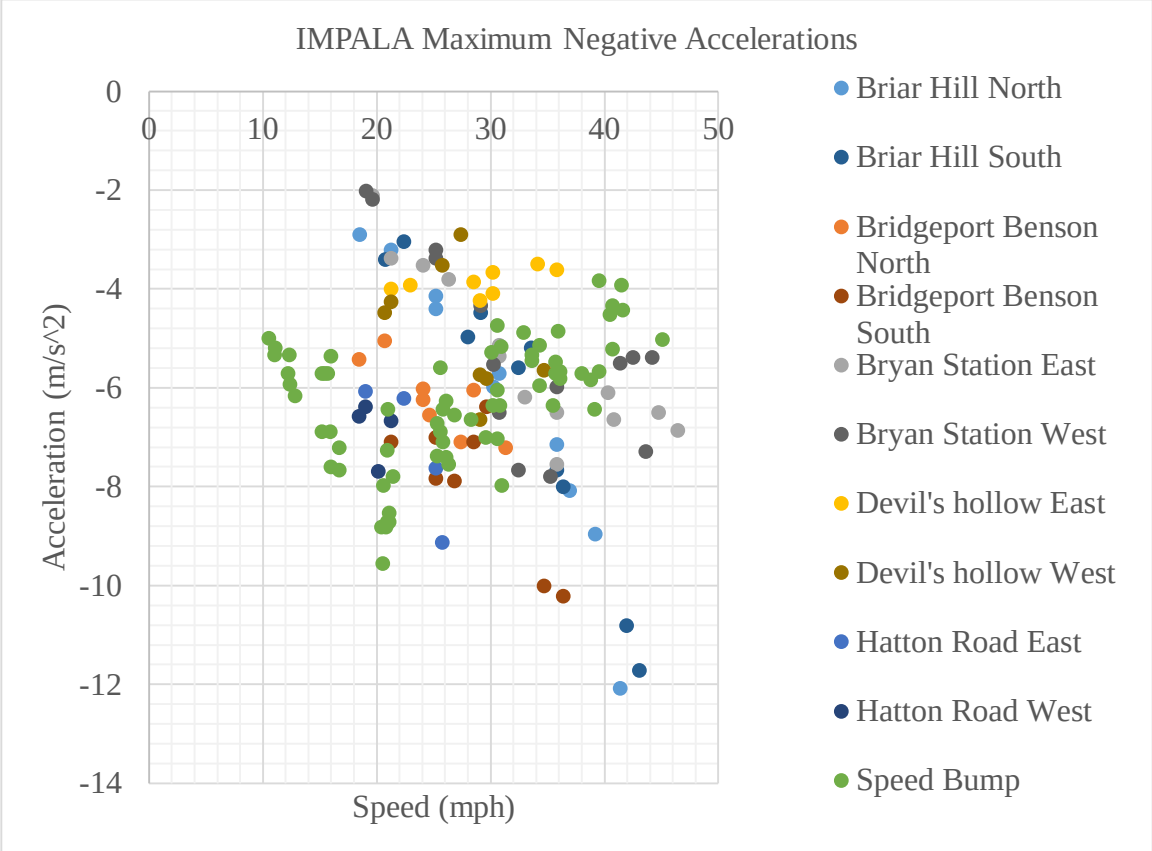
IMPALA Maximum Negative Accelerations
Acceleration (m/s^2)
0
-2
-4
-6
-8
-10
-12
-14
0
10
20
30
40
50
Speed (mph)
Briar Hill North
Briar Hill South
Bridgeport Benson North
Bridgeport Benson South
Bryan Station East
Bryan Station West
Devil's hollow East
Devil's hollow West
Hatton Road East
Hatton Road West
Speed Bump

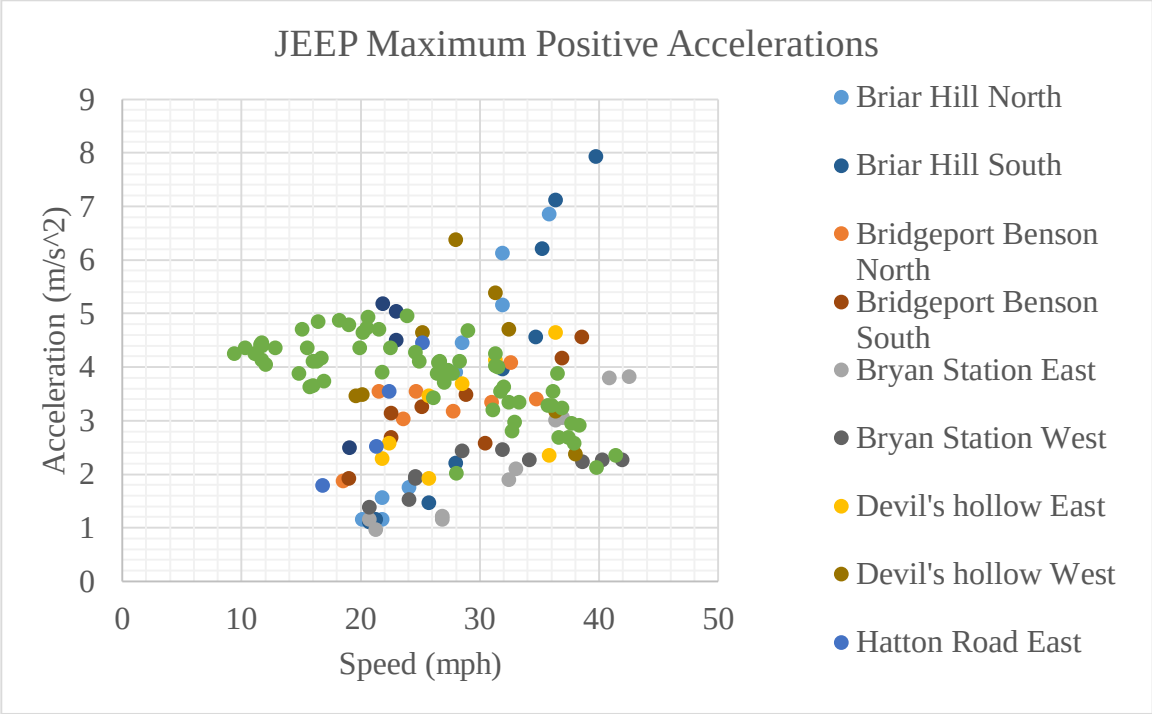
JEEP Maximum Positive Accelerations
Acceleration (m/s^2)
9
8
7
6
5
4
3
2
1
0
0
10
20
30
40
50
Speed (mph)
Briar Hill North
Briar Hill South
Bridgeport Benson North
Bridgeport Benson South
Bryan Station East
Bryan Station West
Devil's hollow East
Devil's hollow West
Hatton Road East

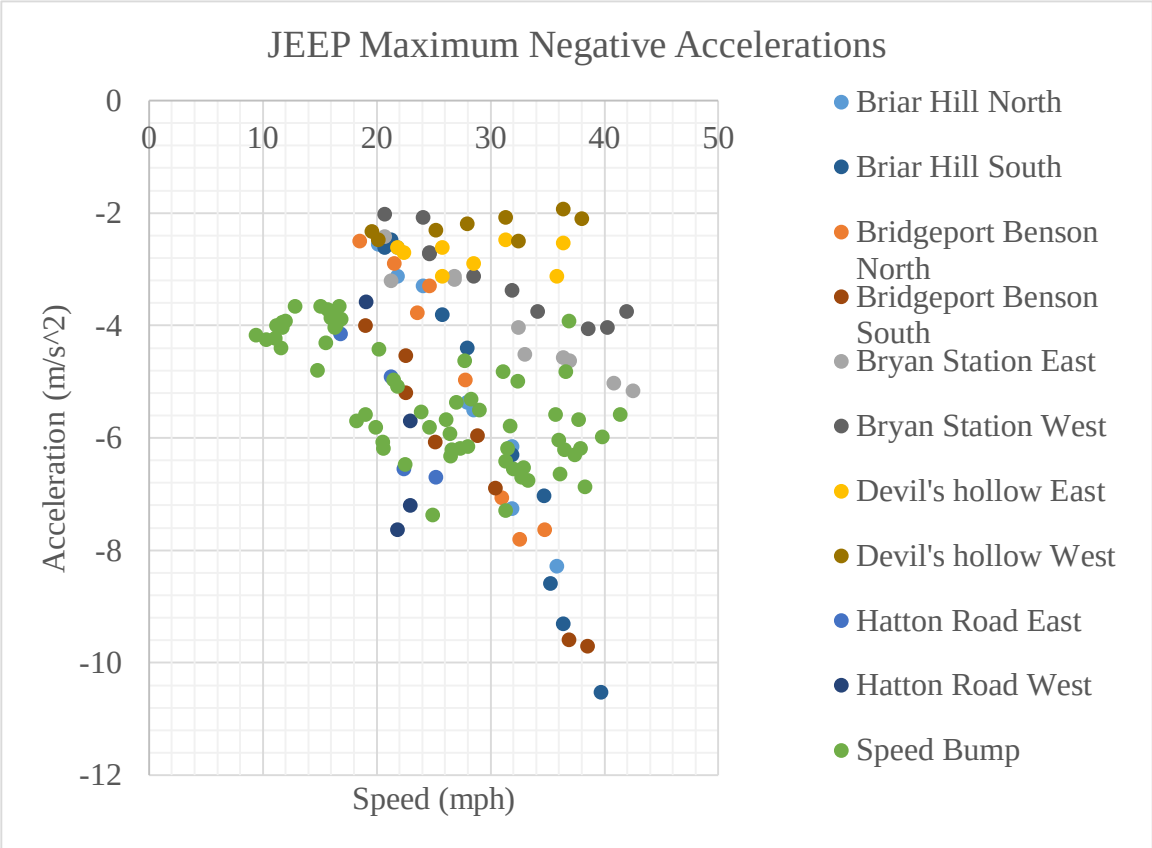
JEEP Maximum Negative Accelerations
Acceleration (m/s^2)
0
-2
-4
-6
-8
-10
-12
0
10
20
30
40
50
Speed (mph)
Briar Hill North
Briar Hill South
Bridgeport Benson North
Bridgeport Benson South
Bryan Station East
Bryan Station West
Devil's hollow East
Devil's hollow West
Hatton Road East
Hatton Road West
Speed Bump

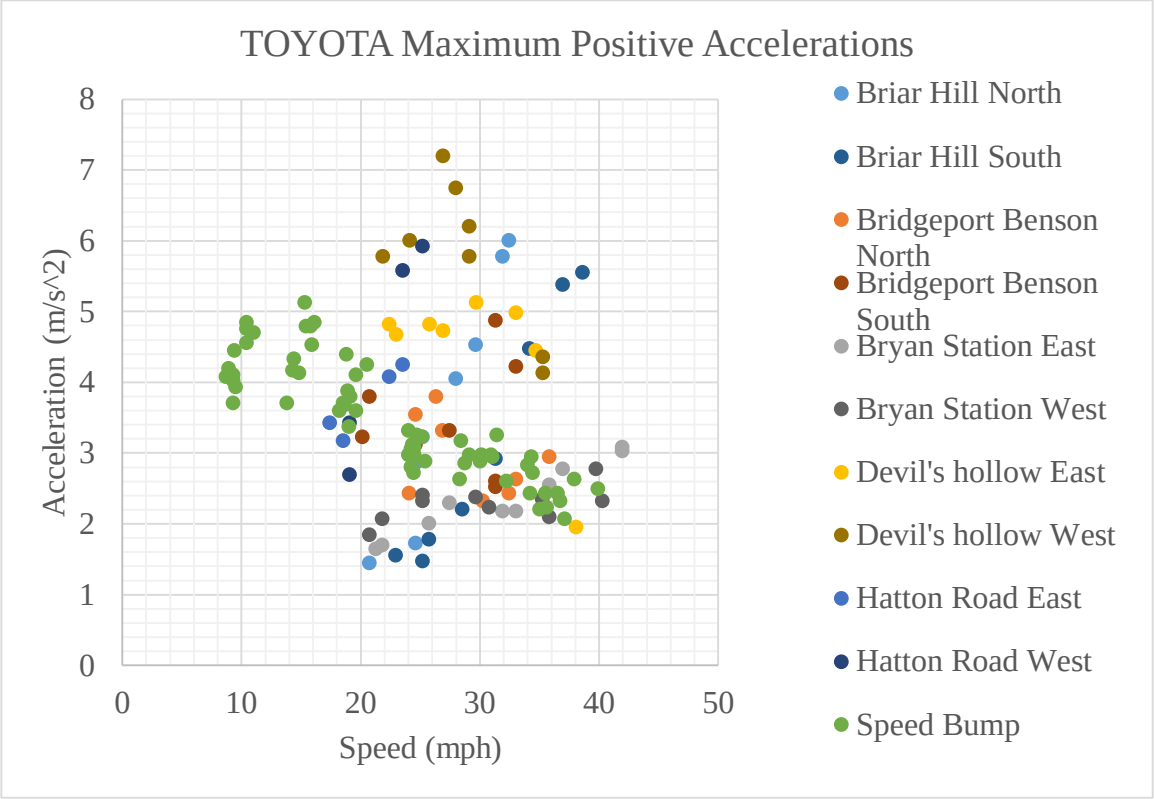
TOYOTA Maximum Positive Accelerations
Acceleration (m/s^2)
8
7
6
5
4
3
2
1
0
0
10
20
30
40
50
Speed (mph)
Briar Hill North
Briar Hill South
Bridgeport Benson North
Bridgeport Benson South
Bryan Station East
Bryan Station West
Devil's hollow East
Devil's hollow West
Hatton Road East
Hatton Road West
Speed Bump

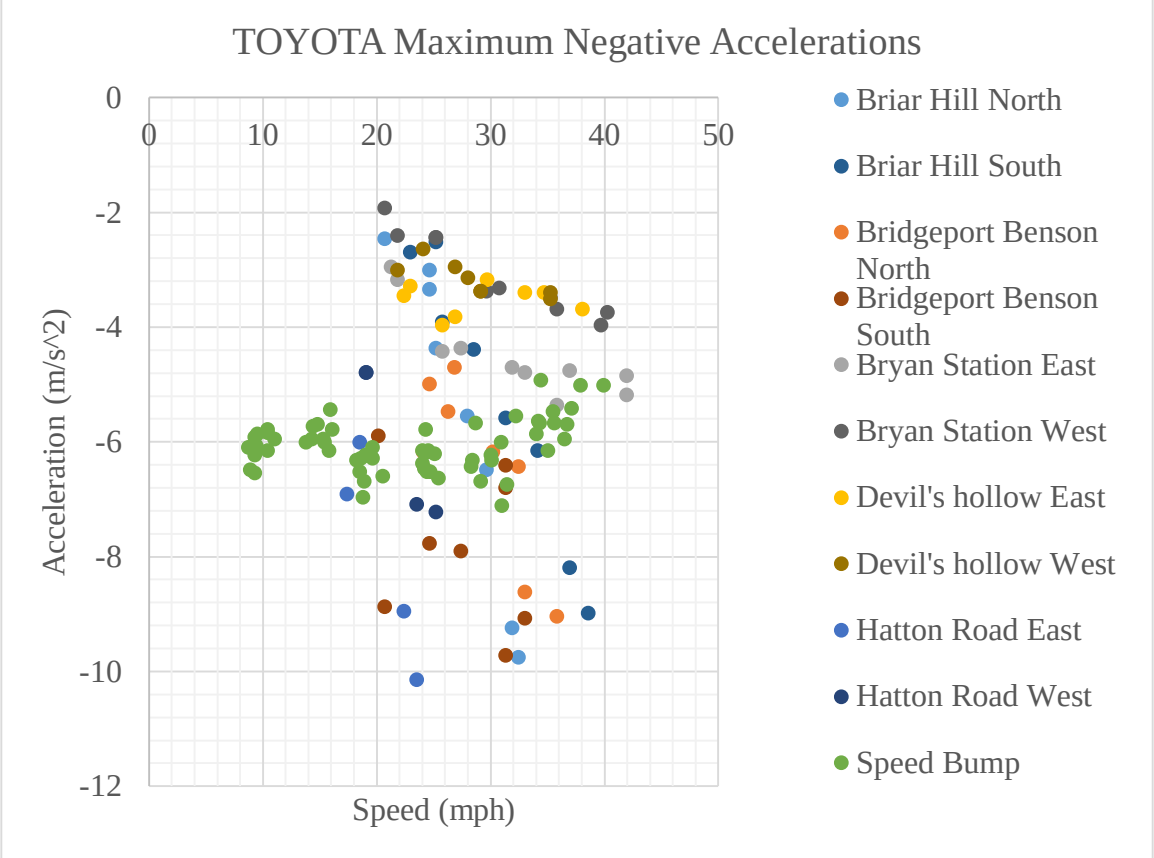
TOYOTA Maximum Negative Accelerations
Acceleration (m/s^2)
0
-2
-4
-6
-8
-10
-12
0
10
20
30
40
50
Speed (mph)
Briar Hill North
Briar Hill South
Bridgeport Benson North
Bridgeport Benson South
Bryan Station East
Bryan Station West
Devil's hollow East
Devil's hollow West
Hatton Road East
Hatton Road West
Speed Bump

APPENDIX D

Chapter 4 RMS before and after calibration prediction results plots USING Speed pump

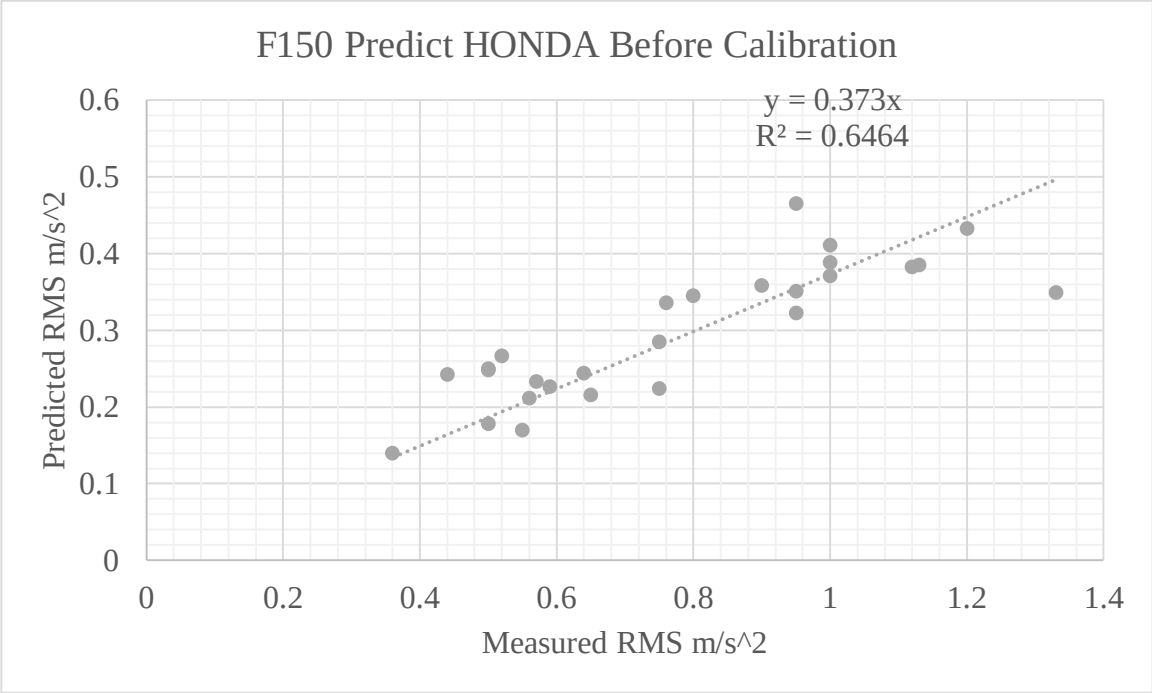

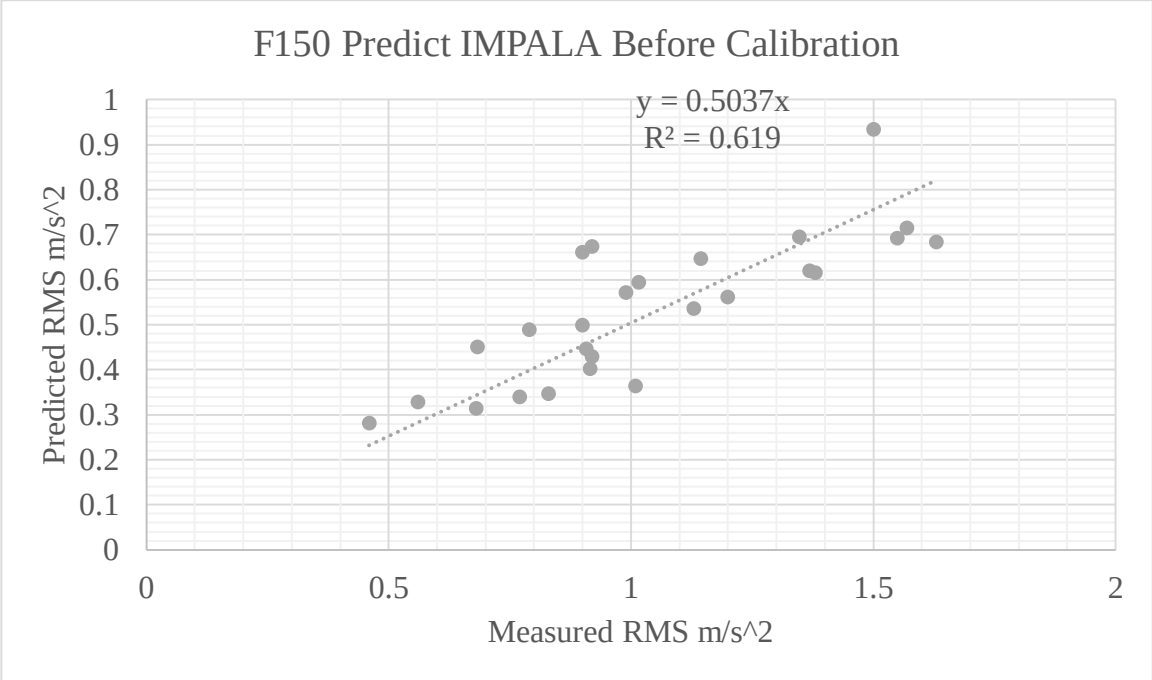

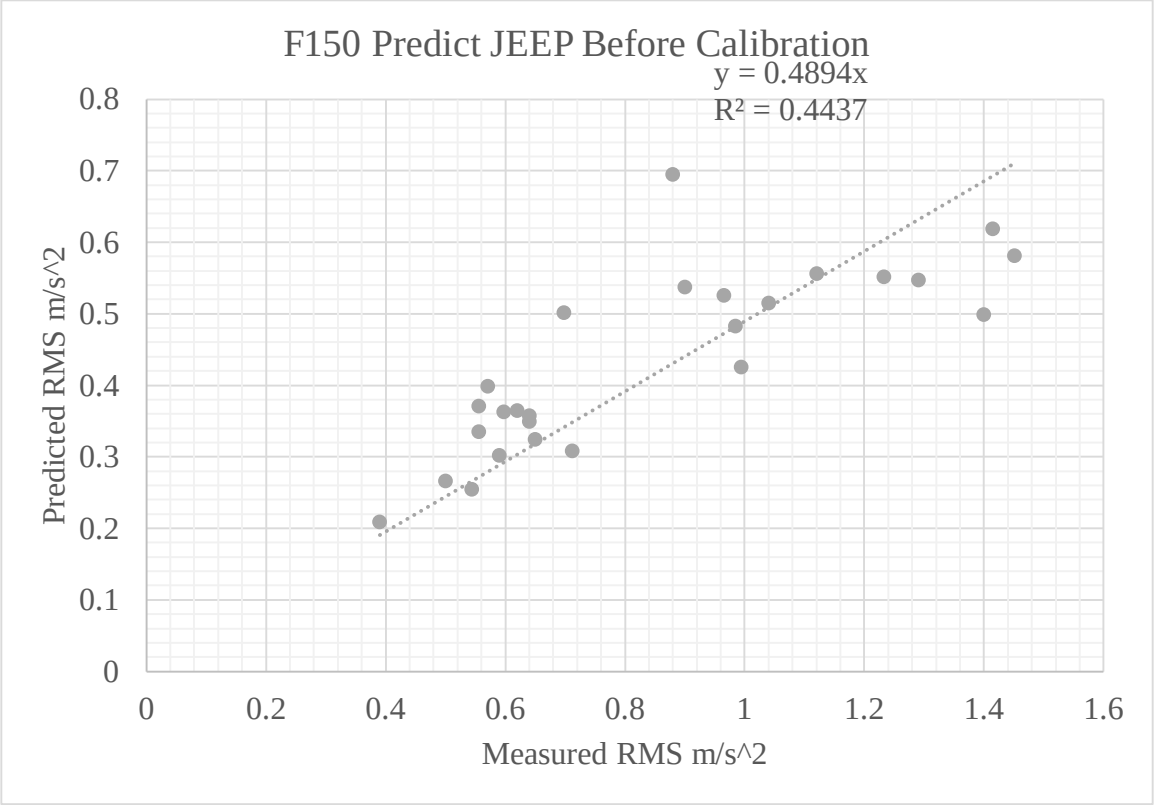
F150 Predict JEEP Before Calibration
y = 0.4894x
R² = 0.4437
Predicted RMS m/s^2
Measured RMS m/s^2
0
0.1
0.2
0.3
0.4
0.5
0.6
0.7
0.8
0
0.2
0.4
0.6
0.8
1
1.2
1.4
1.6

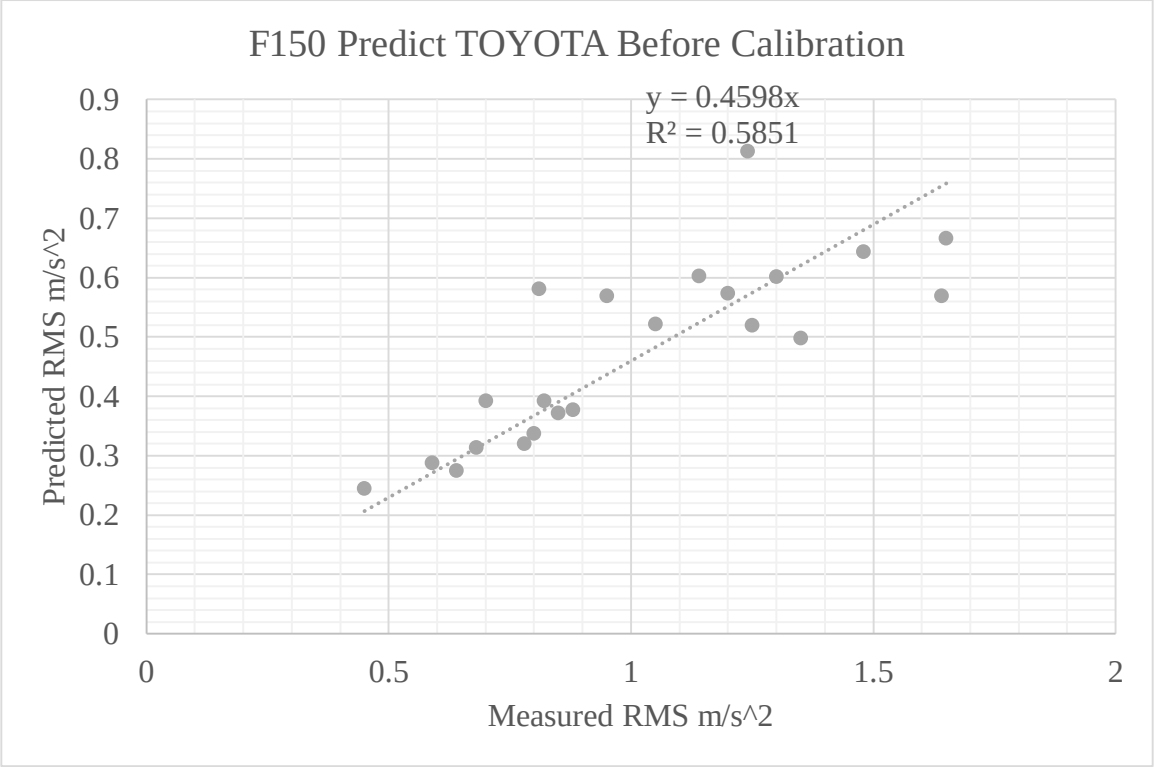
F150 Predict TOYOTA Before Calibration
y = 0.4598x
R² = 0.5851
Predicted RMS m/s^2
Measured RMS m/s^2
0
0.1
0.2
0.3
0.4
0.5
0.6
0.7
0.8
0.9
0
0.5
1
1.5
2

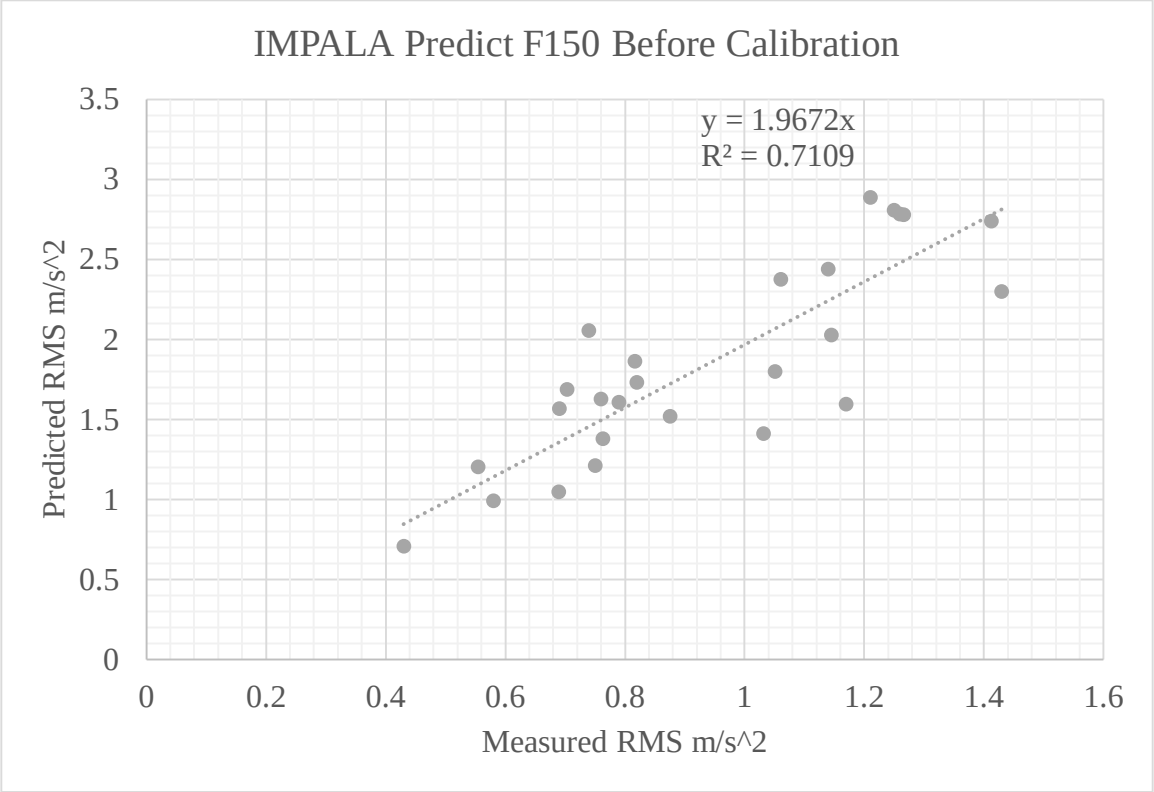
IMPALA Predict F150 Before Calibration
y = 1.9672x
R² = 0.7109
Predicted RMS m/s^2
Measured RMS m/s^2
0
0.5
1
1.5
2
2.5
3
3.5
0
0.2
0.4
0.6
0.8
1
1.2
1.4
1.6

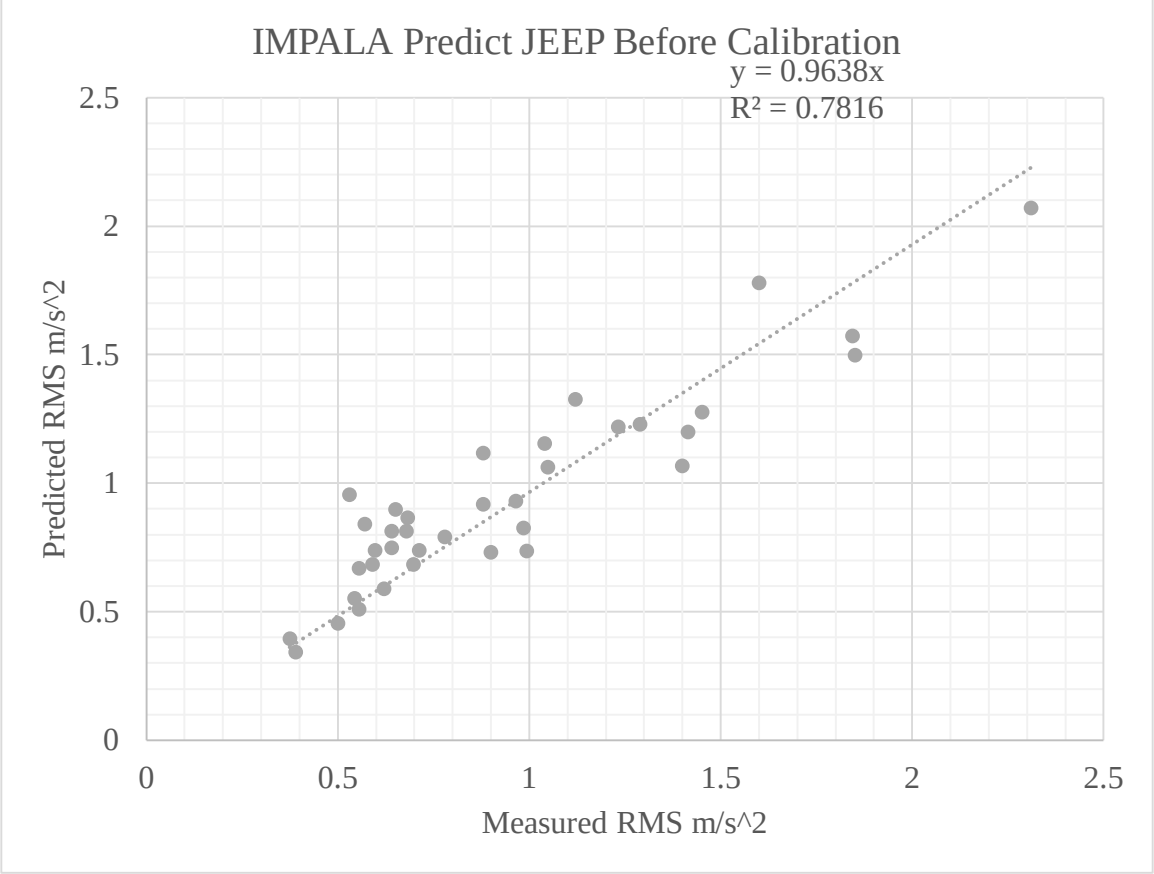
IMPALA Predict JEEP Before Calibration
y = 0.9638x
R² = 0.7816
Predicted RMS m/s^2
Measured RMS m/s^2
0
0.5
1
1.5
2
2.5
0
0.5
1
1.5
2
2.5

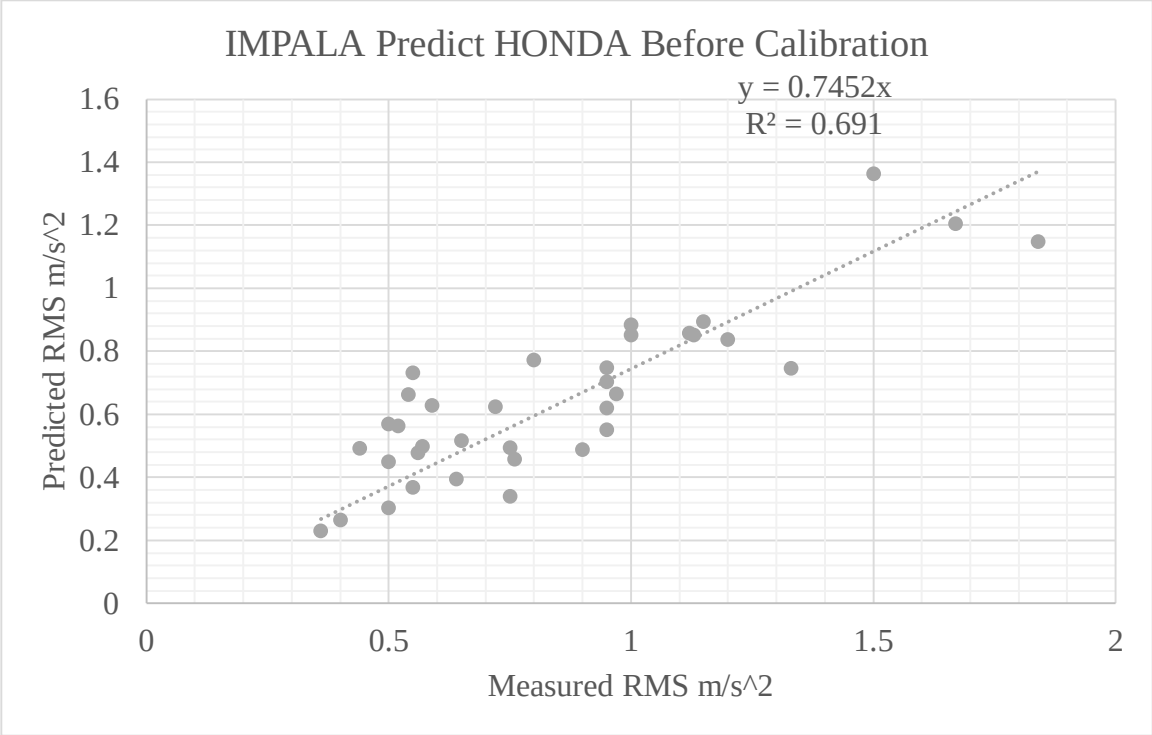
IMPALA Predict HONDA Before Calibration
y = 0.7452x
R² = 0.691
Predicted RMS m/s^2
Measured RMS m/s^2
0
0.2
0.4
0.6
0.8
1
1.2
1.4
1.6
0
0.5
1
1.5
2

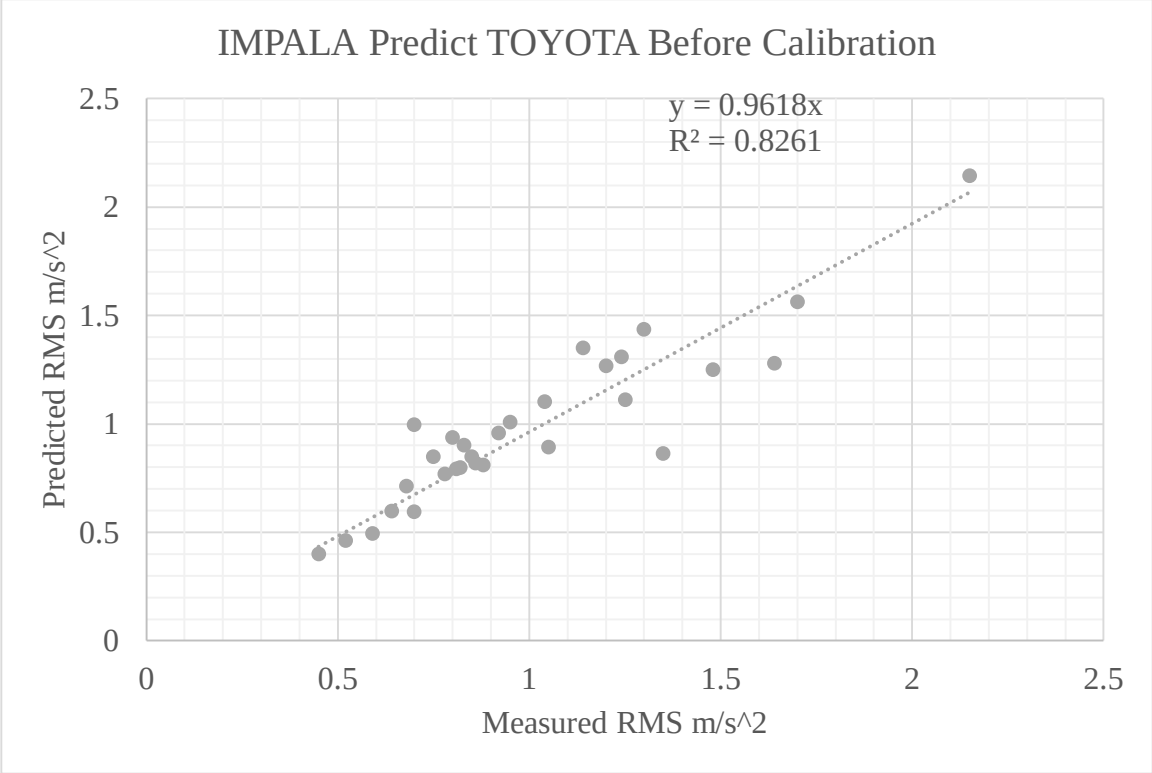
IMPALA Predict TOYOTA Before Calibration
y = 0.9618x
R² = 0.8261
Predicted RMS m/s^2
Measured RMS m/s^2
0
0.5
1
1.5
2
2.5
0
0.5
1
1.5
2
2.5

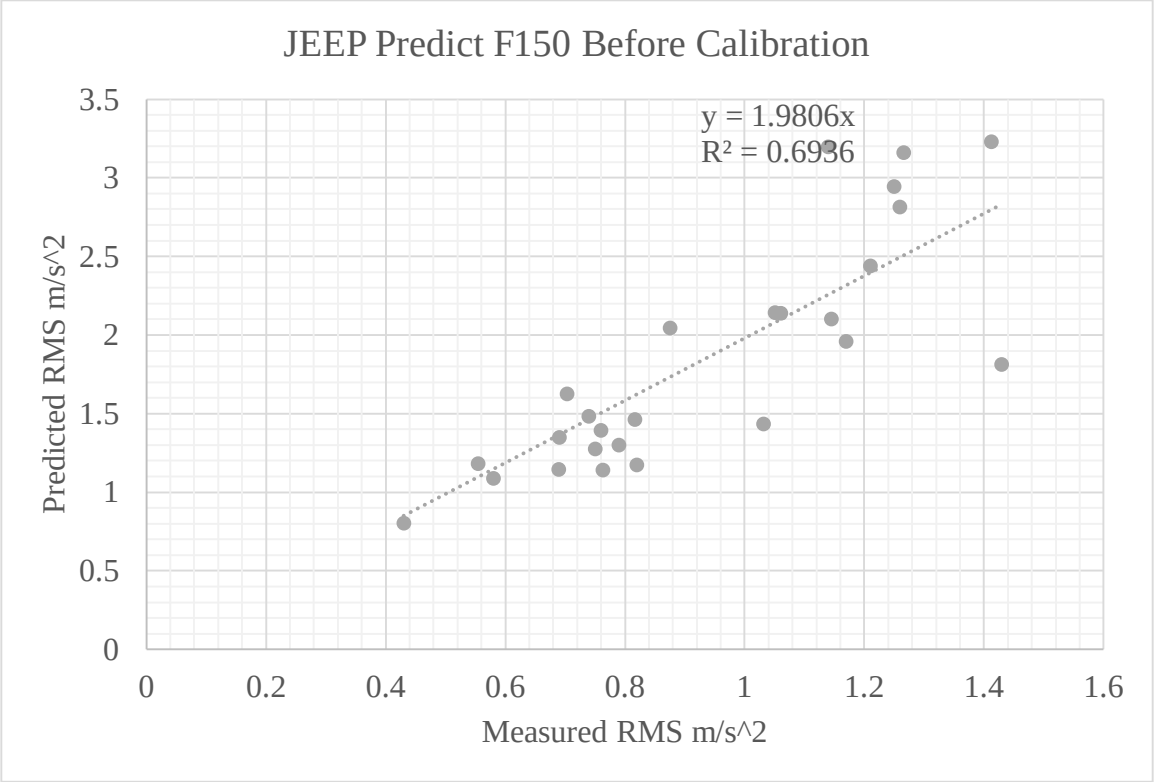
JEEP Predict F150 Before Calibration
y = 1.9806x
R² = 0.6936
Predicted RMS m/s^2
Measured RMS m/s^2
0
0.5
1
1.5
2
2.5
3
3.5
0
0.2
0.4
0.6
0.8
1
1.2
1.4
1.6

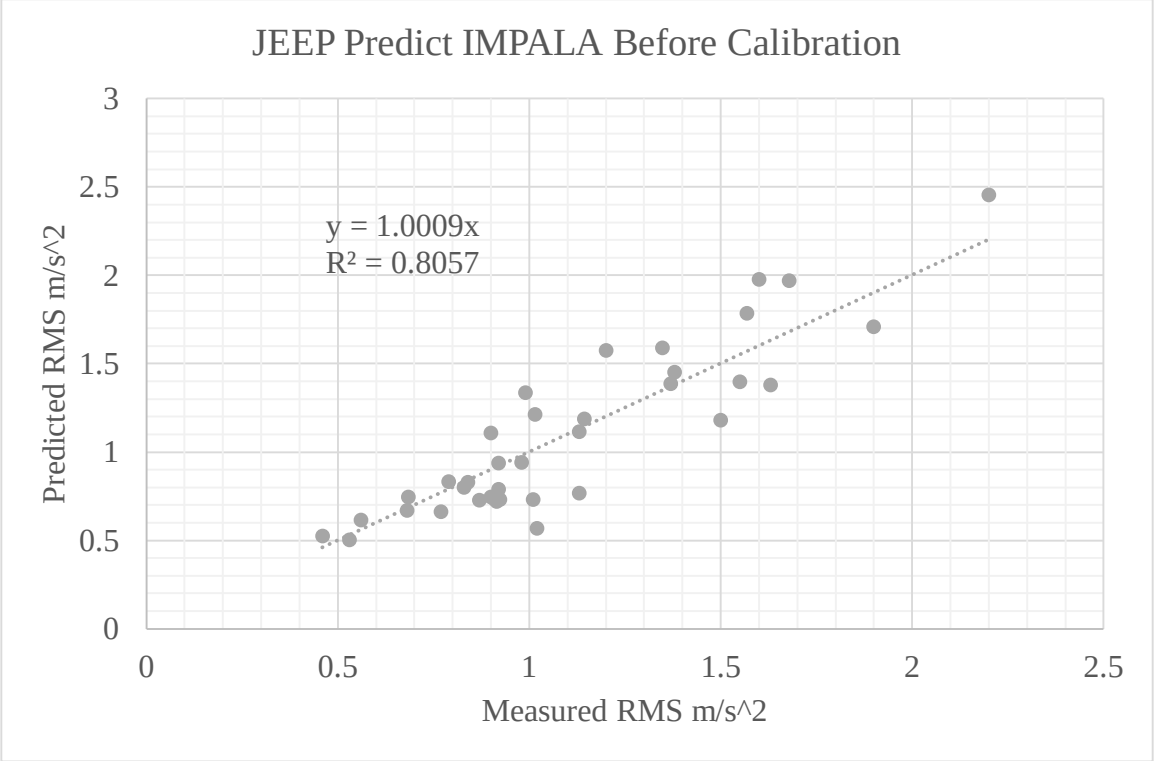
JEEP Predict IMPALA Before Calibration
y = 1.0009x
R² = 0.8057
Predicted RMS m/s^2
Measured RMS m/s^2
0
0.5
1
1.5
2
2.5
3
0
0.5
1
1.5
2
2.5

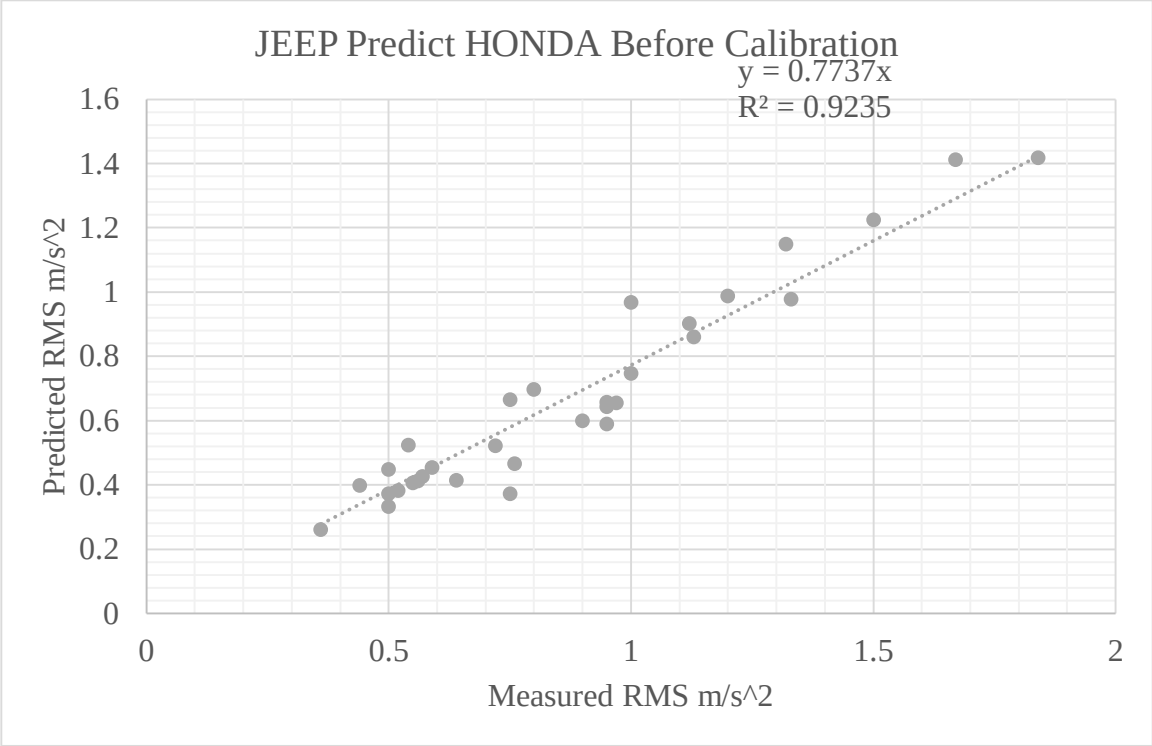
JEEP Predict HONDA Before Calibration
y = 0.7737x
R² = 0.9235
Predicted RMS m/s^2
Measured RMS m/s^2
0
0.2
0.4
0.6
0.8
1
1.2
1.4
1.6
0
0.5
1
1.5
2

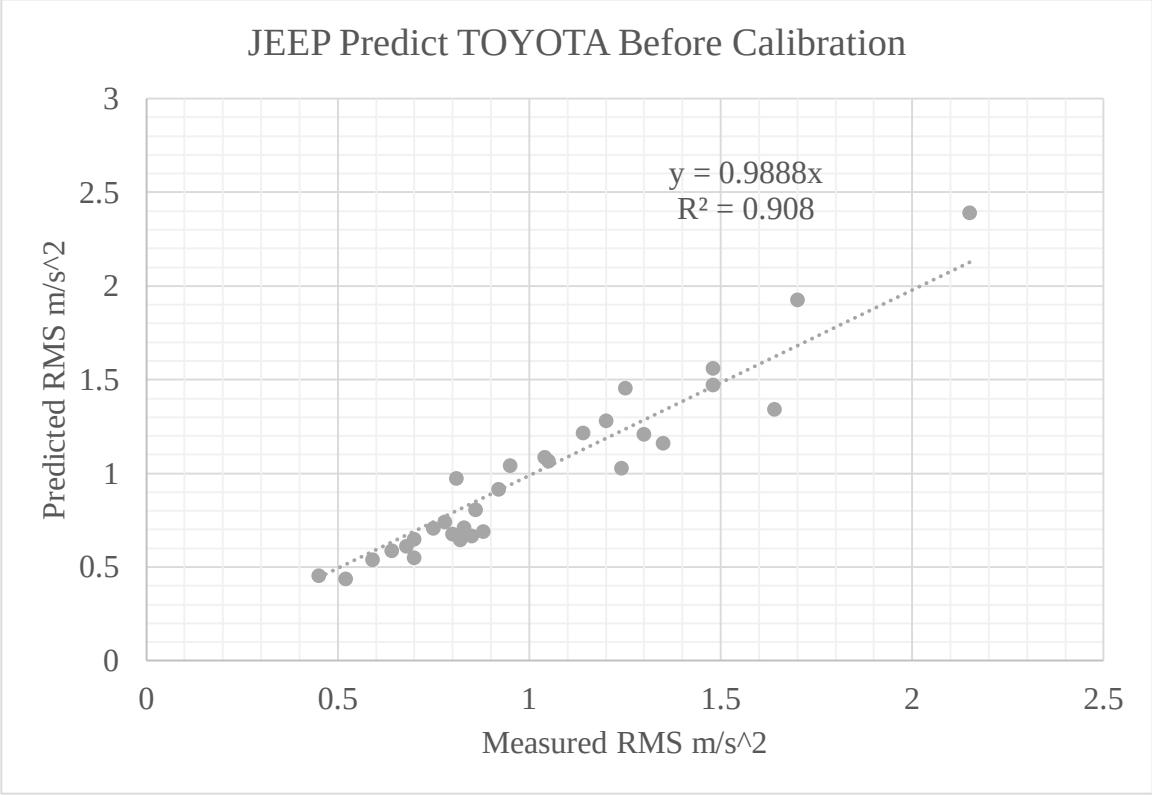
JEEP Predict TOYOTA Before Calibration
y = 0.9888x
R² = 0.908
Predicted RMS m/s^2
Measured RMS m/s^2
0
0.5
1
1.5
2
2.5
3
0
0.5
1
1.5
2
2.5

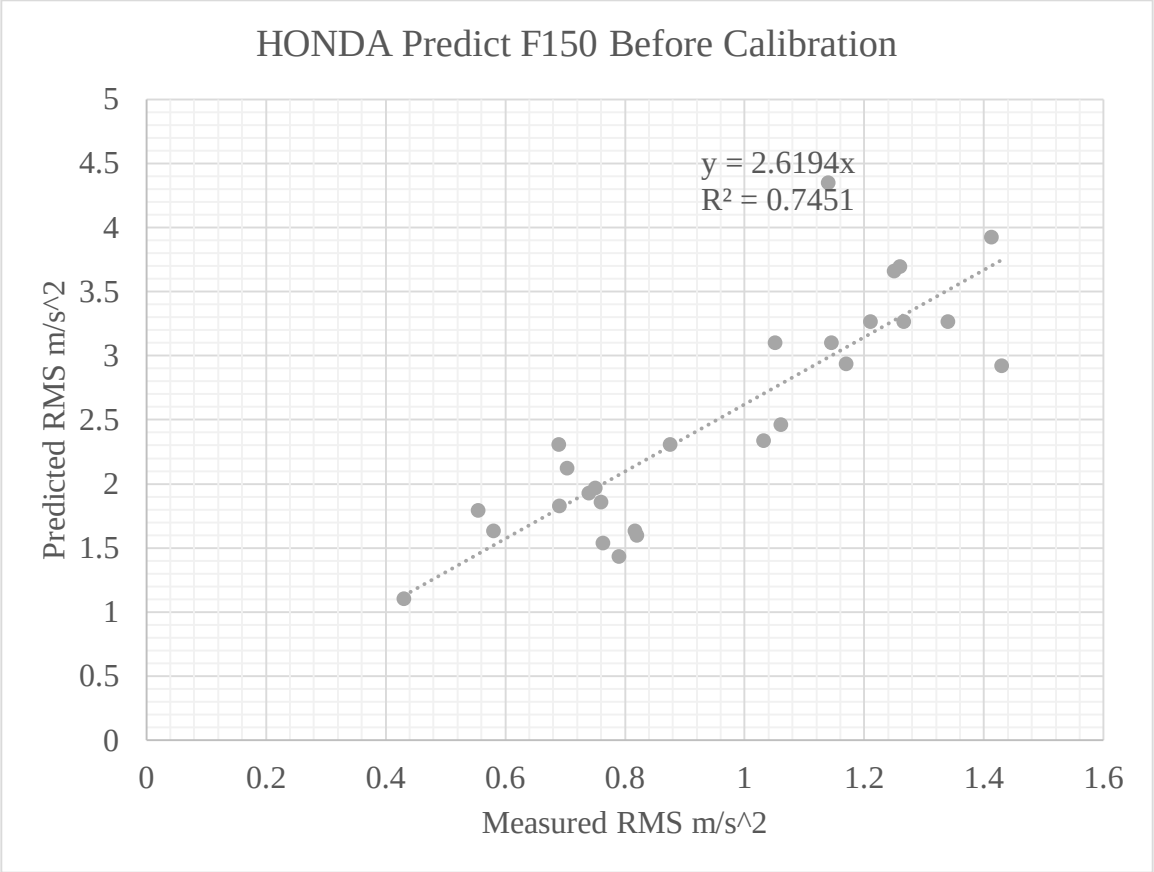
HONDA Predict F150 Before Calibration
y = 2.6194x
R² = 0.7451
Predicted RMS m/s^2
Measured RMS m/s^2
0
0.5
1
1.5
2
2.5
3
3.5
4
4.5
5
0
0.2
0.4
0.6
0.8
1
1.2
1.4
1.6

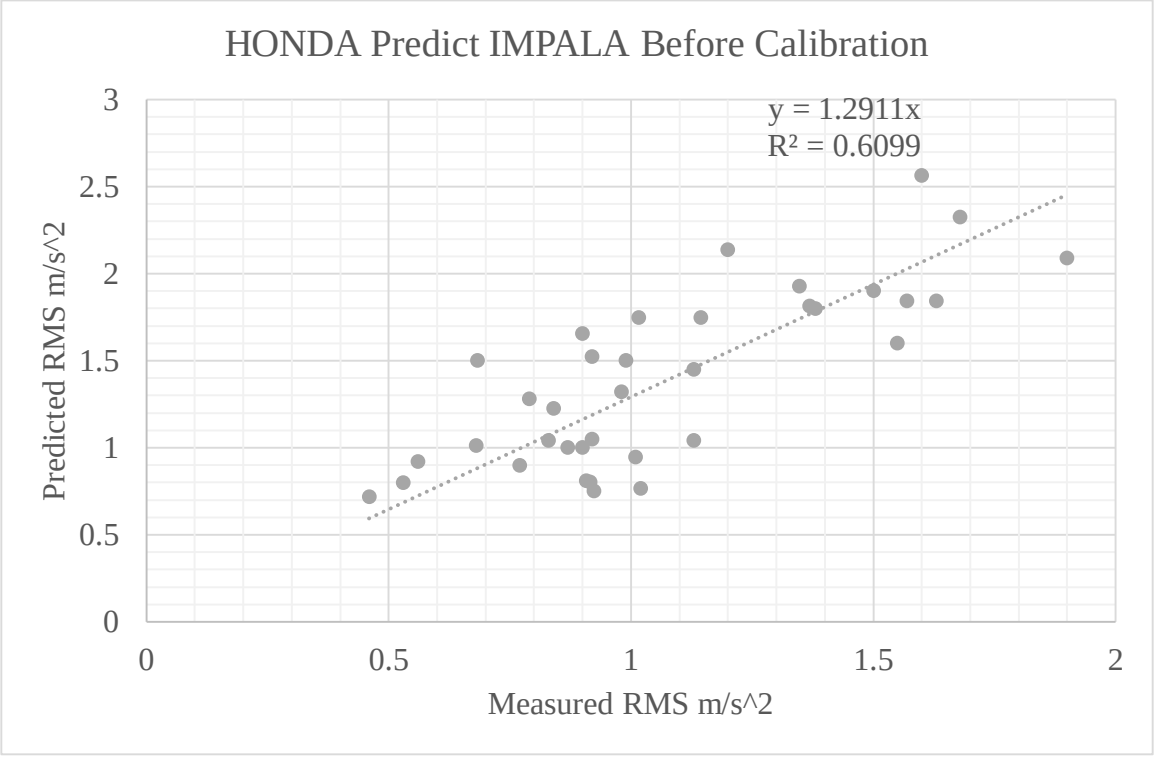
HONDA Predict IMPALA Before Calibration
y = 1.2911x
R² = 0.6099
Predicted RMS m/s^2
Measured RMS m/s^2
0
0.5
1
1.5
2
2.5
3
0
0.5
1
1.5
2

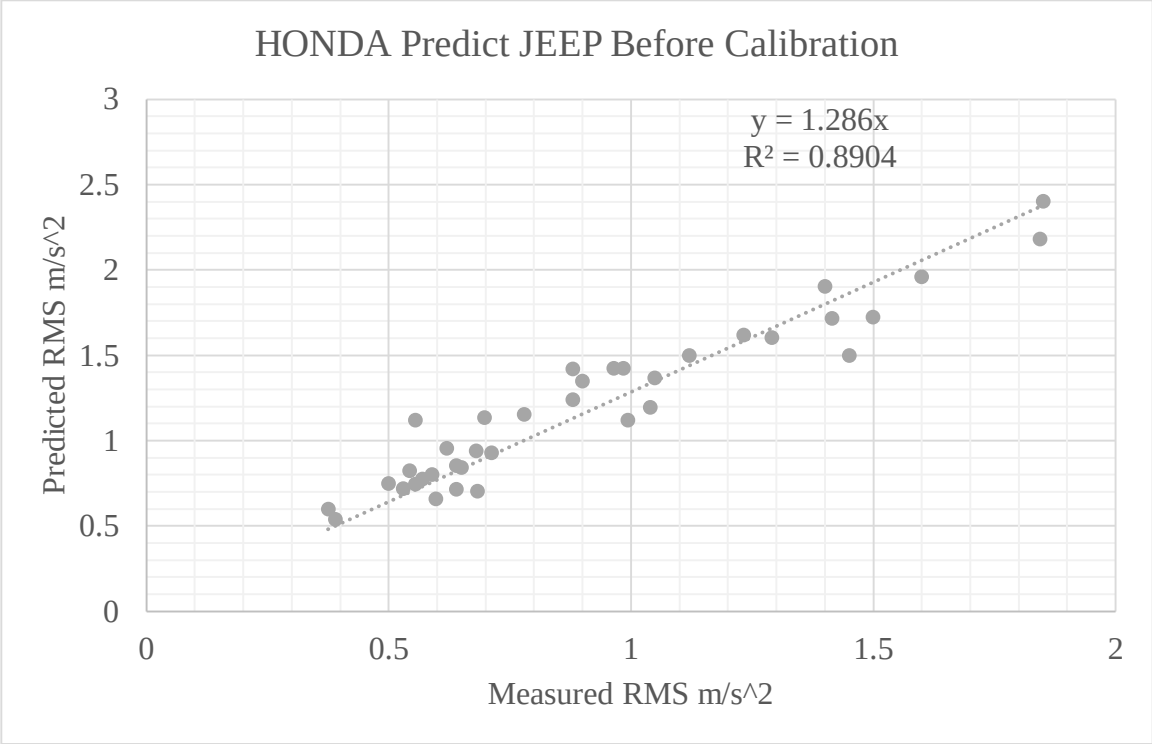
HONDA Predict JEEP Before Calibration
y = 1.286x
R² = 0.8904
Predicted RMS m/s^2
Measured RMS m/s^2
0
0.5
1
1.5
2
2.5
3

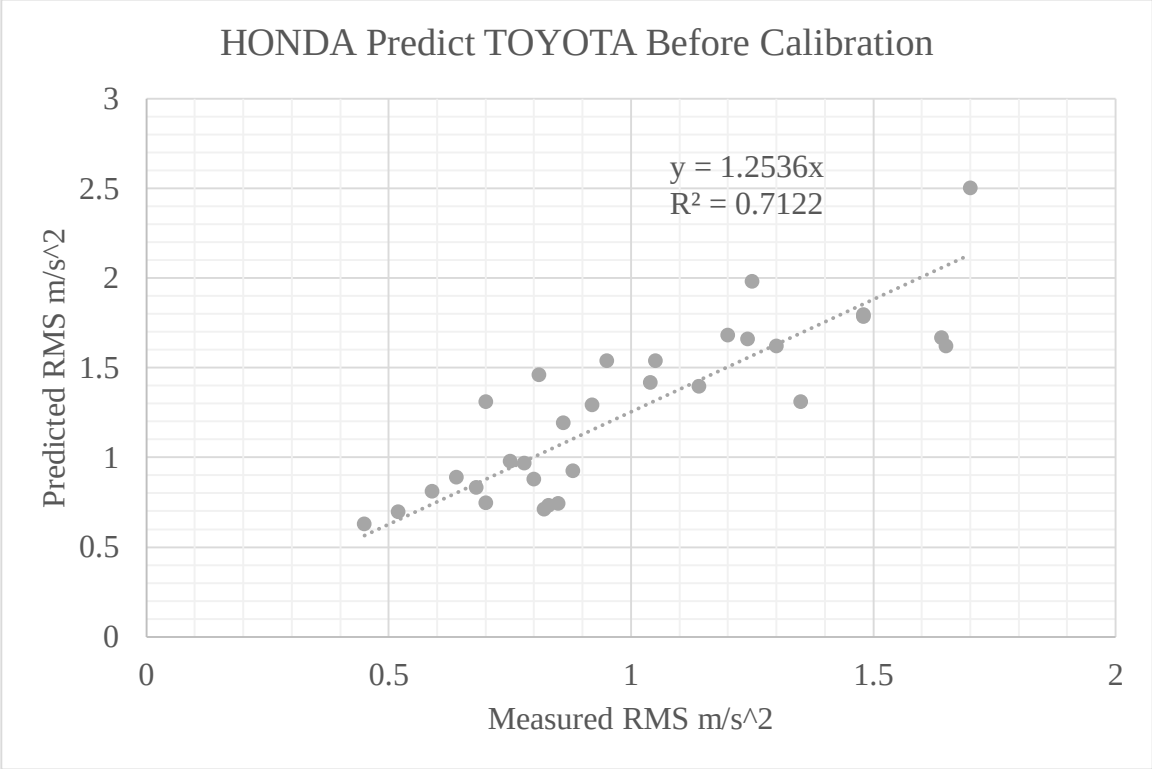
HONDA Predict TOYOTA Before Calibration
y = 1.2536x
R² = 0.7122
Predicted RMS m/s^2
Measured RMS m/s^2
0
0.5
1
1.5
2
2.5
3

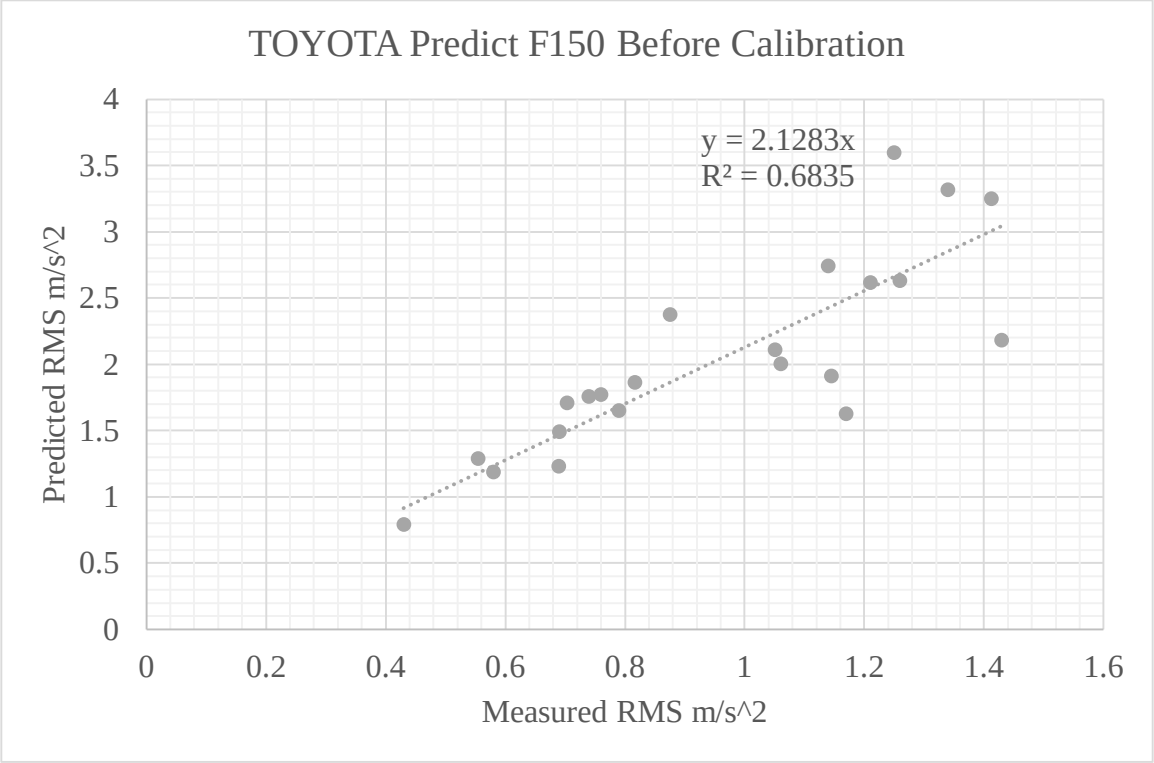
TOYOTA Predict F150 Before Calibration
y = 2.1283x
R² = 0.6835
Predicted RMS m/s^2
Measured RMS m/s^2
0
0.5
1
1.5
2
2.5
3
3.5
4
0
0.2
0.4
0.6
0.8
1
1.2
1.4
1.6

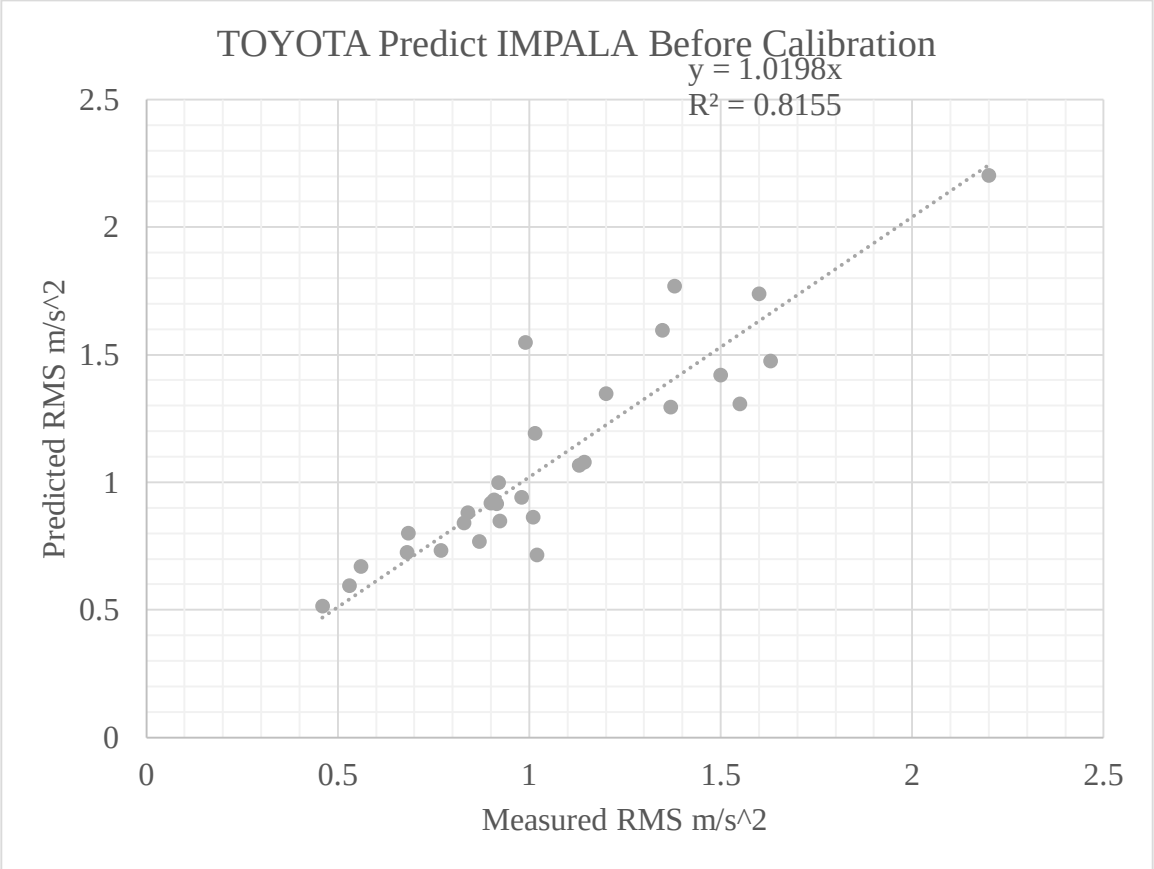
TOYOTA Predict IMPALA Before Calibration
y = 1.0198x
R² = 0.8155
Predicted RMS m/s^2
Measured RMS m/s^2
0
0.5
1
1.5
2
2.5
0
0.5
1
1.5
2
2.5

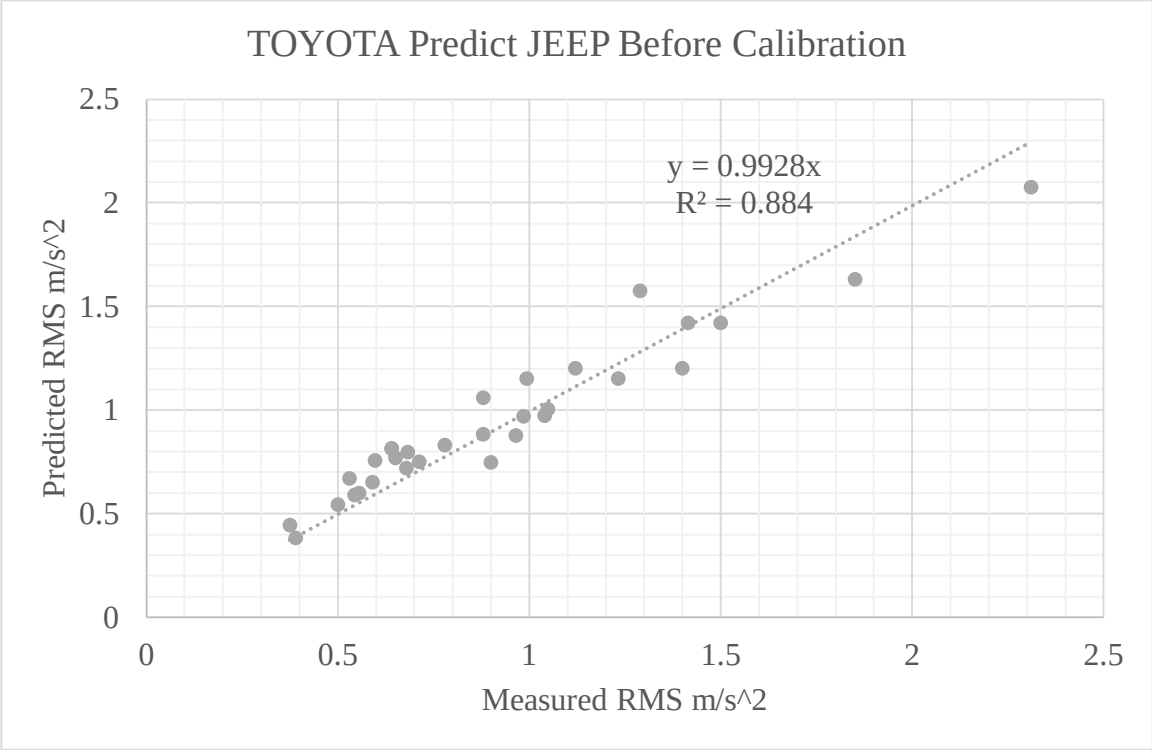
TOYOTA Predict JEEP Before Calibration
y = 0.9928x
R² = 0.884
Predicted RMS m/s^2
Measured RMS m/s^2
0
0.5
1
1.5
2
2.5

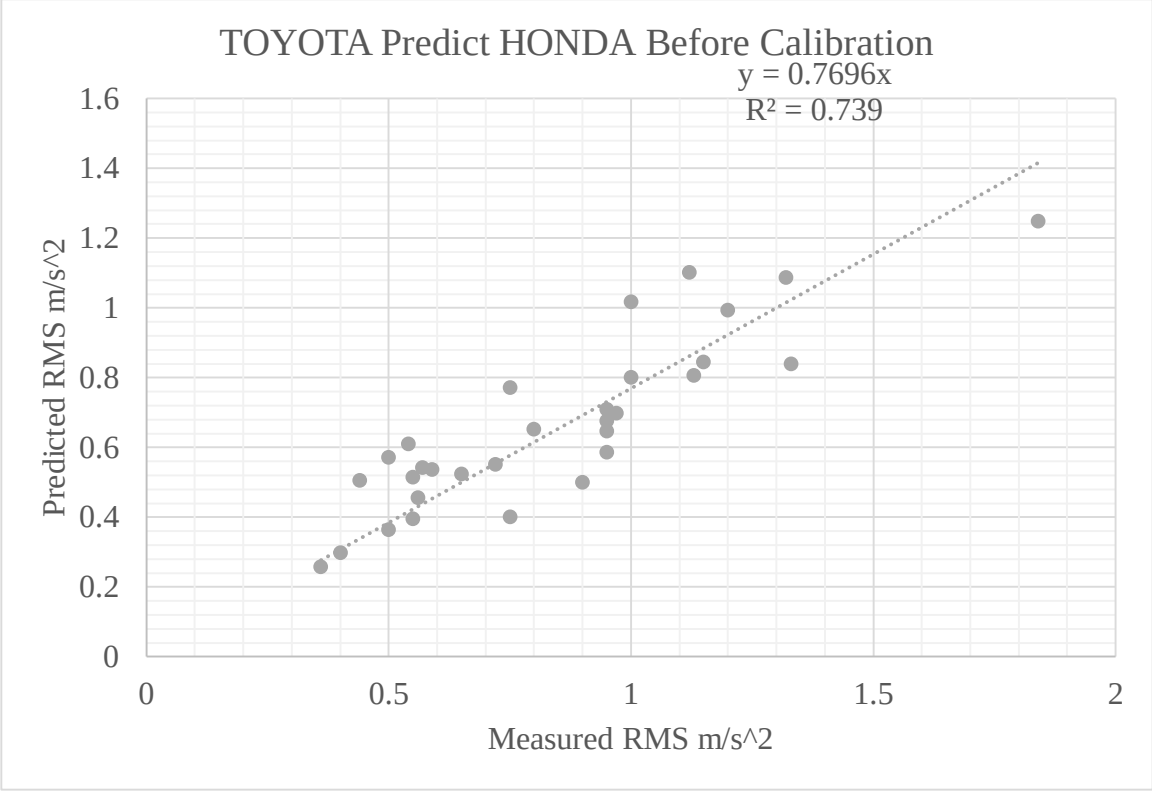
TOYOTA Predict HONDA Before Calibration
y = 0.7696x
R² = 0.739
Predicted RMS m/s^2
Measured RMS m/s^2
0
0.2
0.4
0.6
0.8
1
1.2
1.4
1.6
0.5
1.5
2

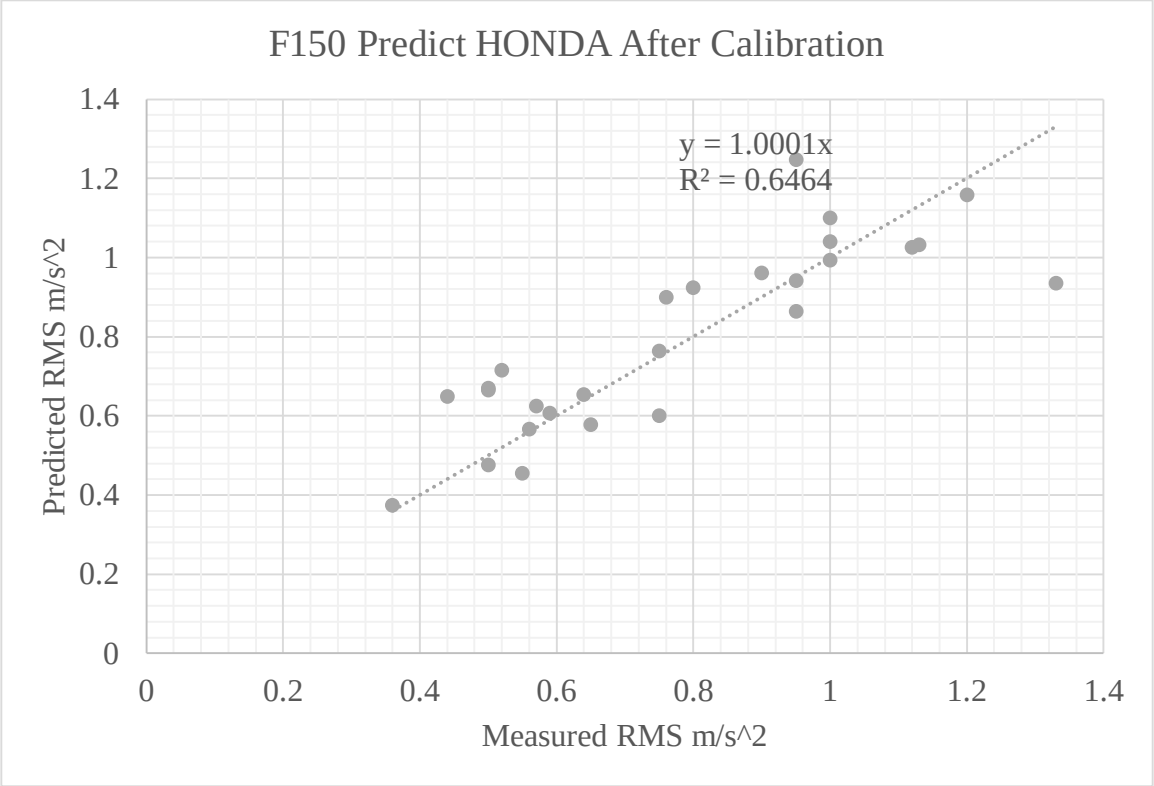
F150 Predict HONDA After Calibration
y = 1.0001x
R² = 0.6464
Predicted RMS m/s^2
Measured RMS m/s^2
0
0.2
0.4
0.6
0.8
1
1.2
1.4

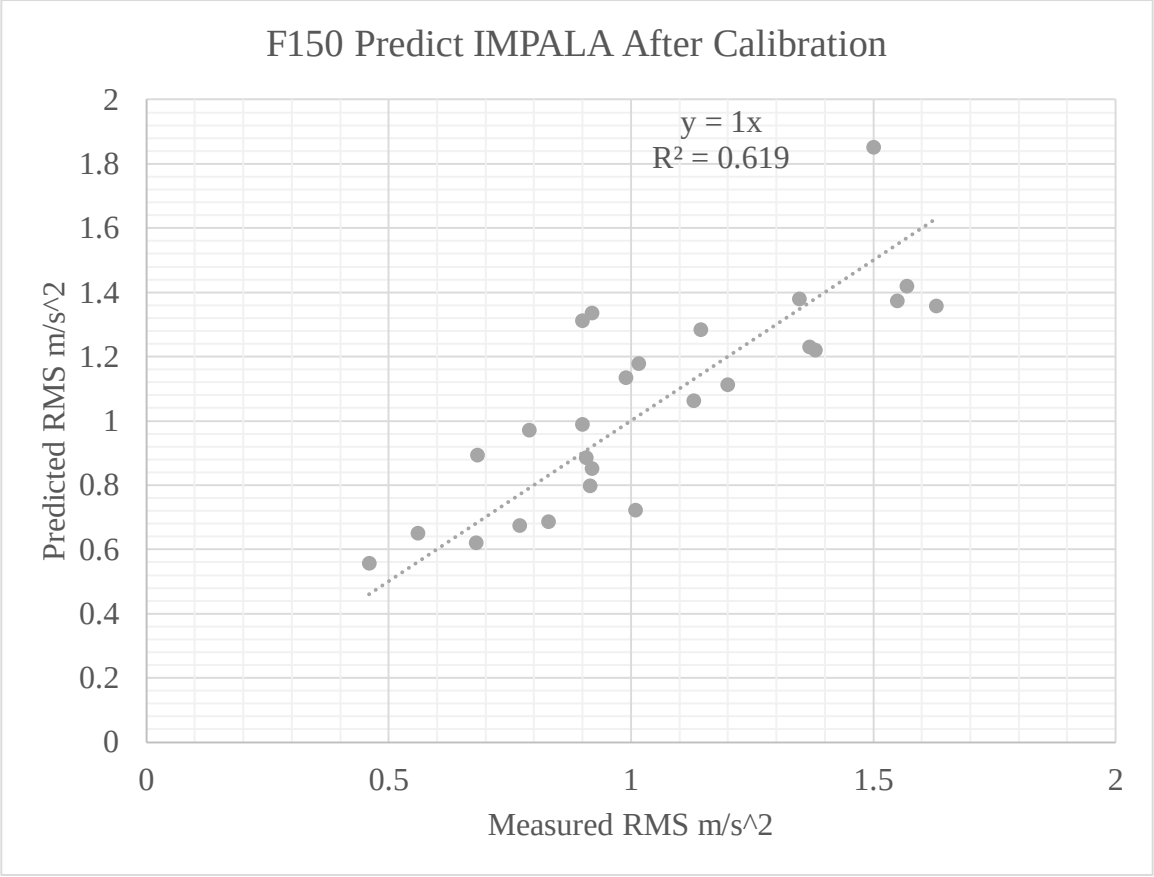
F150 Predict IMPALA After Calibration
y = 1x
R² = 0.619
Predicted RMS m/s^2
Measured RMS m/s^2
0
0.5
1
1.5
2

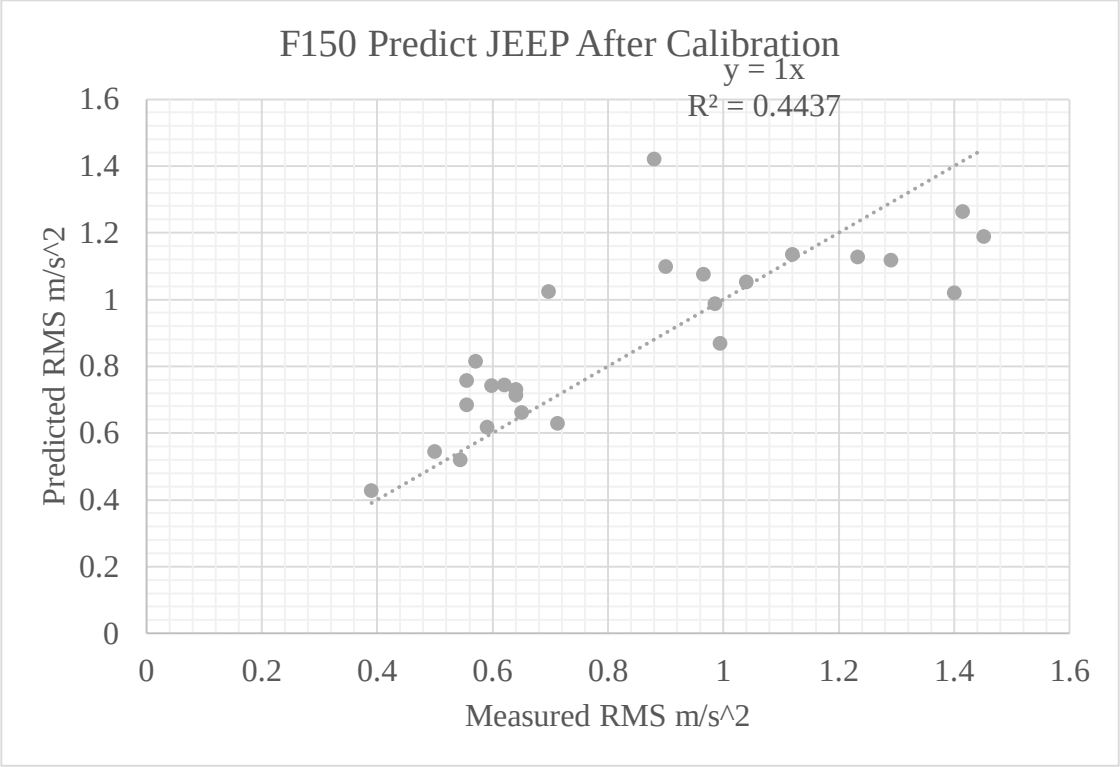
F150 Predict JEEP After Calibration
y = 1x
R² = 0.4437
Predicted RMS m/s^2
Measured RMS m/s^2
0
0.2
0.4
0.6
0.8
1
1.2
1.4
1.6

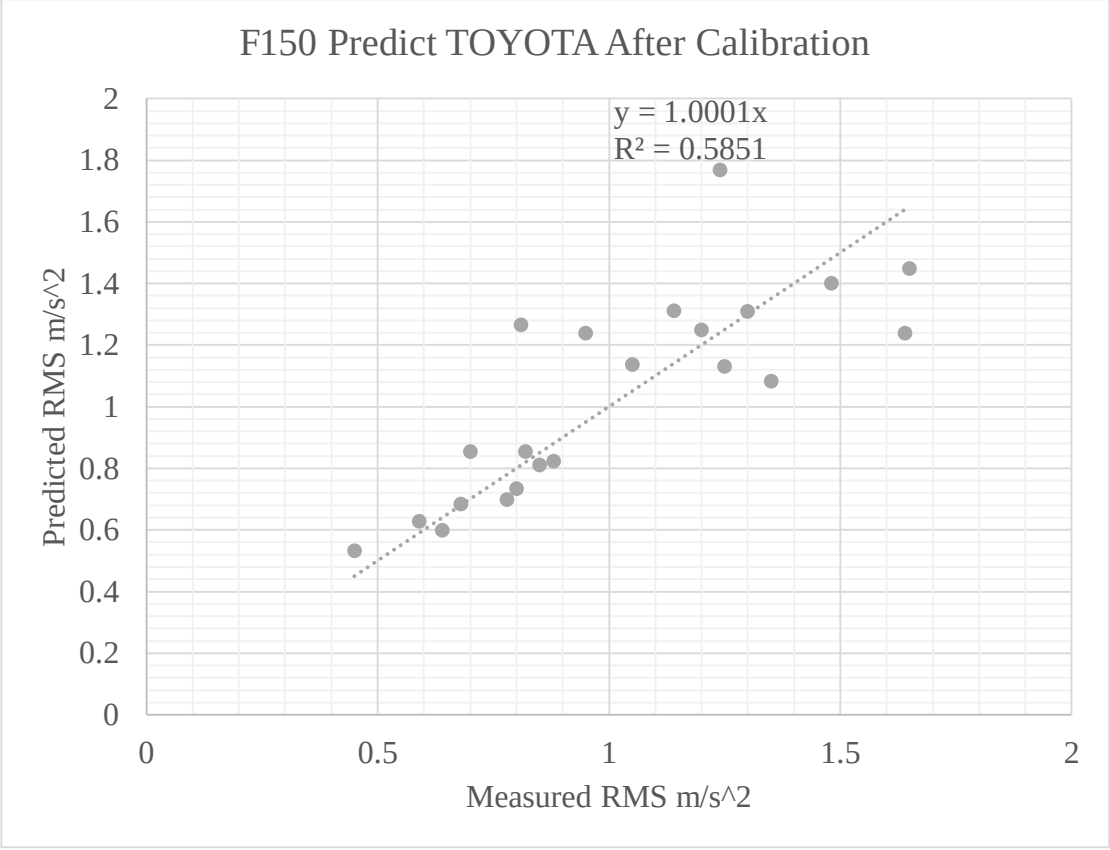
F150 Predict TOYOTA After Calibration
y = 1.0001x
R² = 0.5851
Predicted RMS m/s^2
Measured RMS m/s^2
0
0.5
1
1.5
2

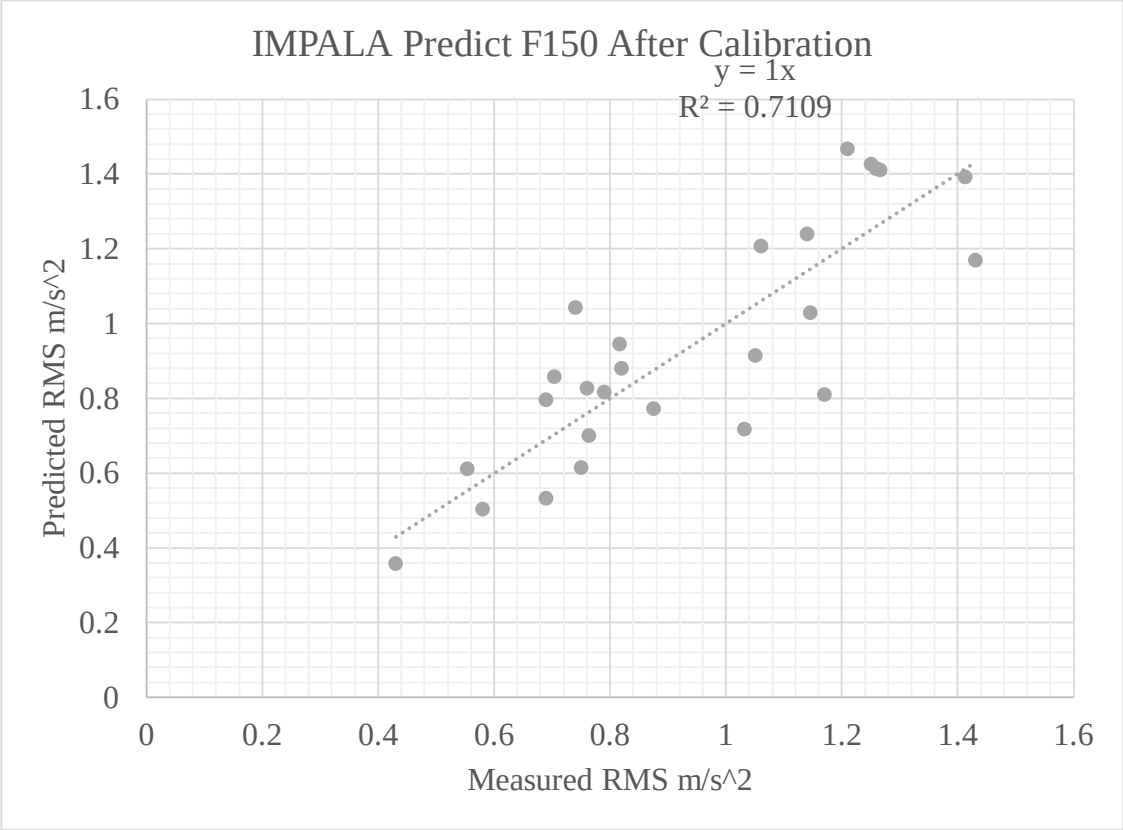
IMPALA Predict F150 After Calibration
y = 1x
R² = 0.7109
Predicted RMS m/s^2
Measured RMS m/s^2
0
0.2
0.4
0.6
0.8
1
1.2
1.4
1.6

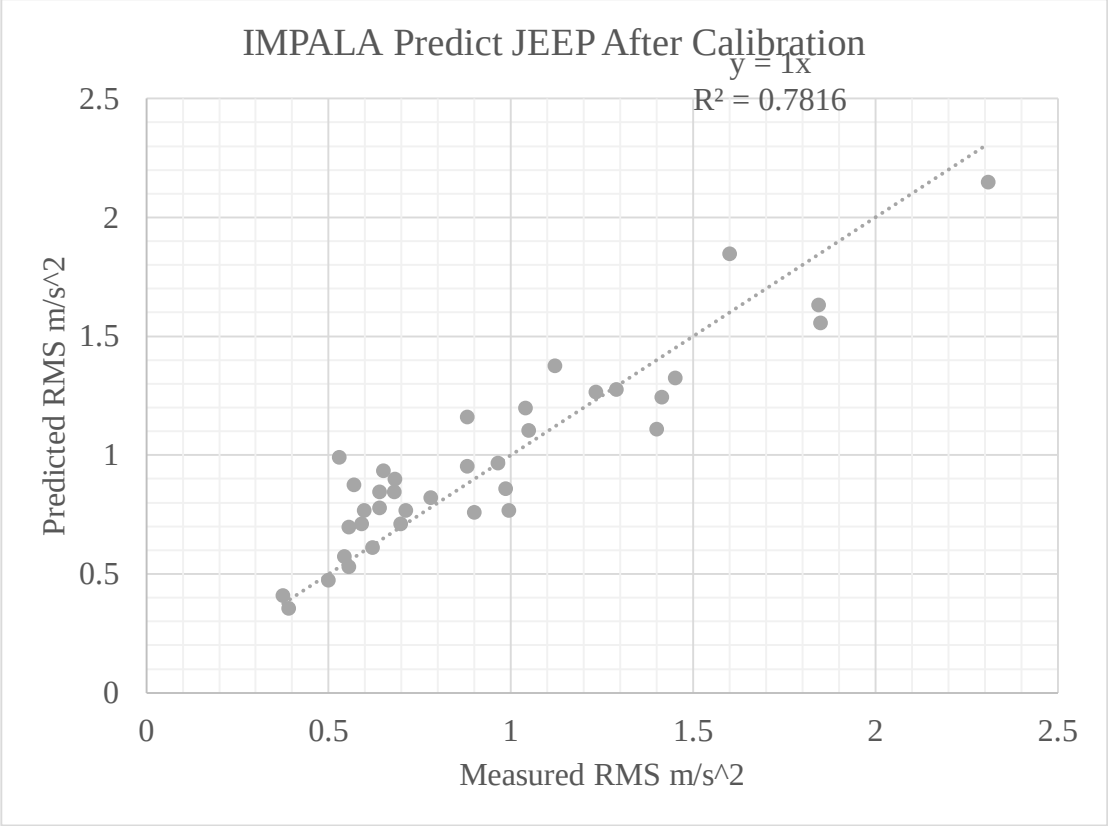
IMPALA Predict JEEP After Calibration
y = 1x
R² = 0.7816
Predicted RMS m/s^2
Measured RMS m/s^2
0
0.5
1
1.5
2
2.5

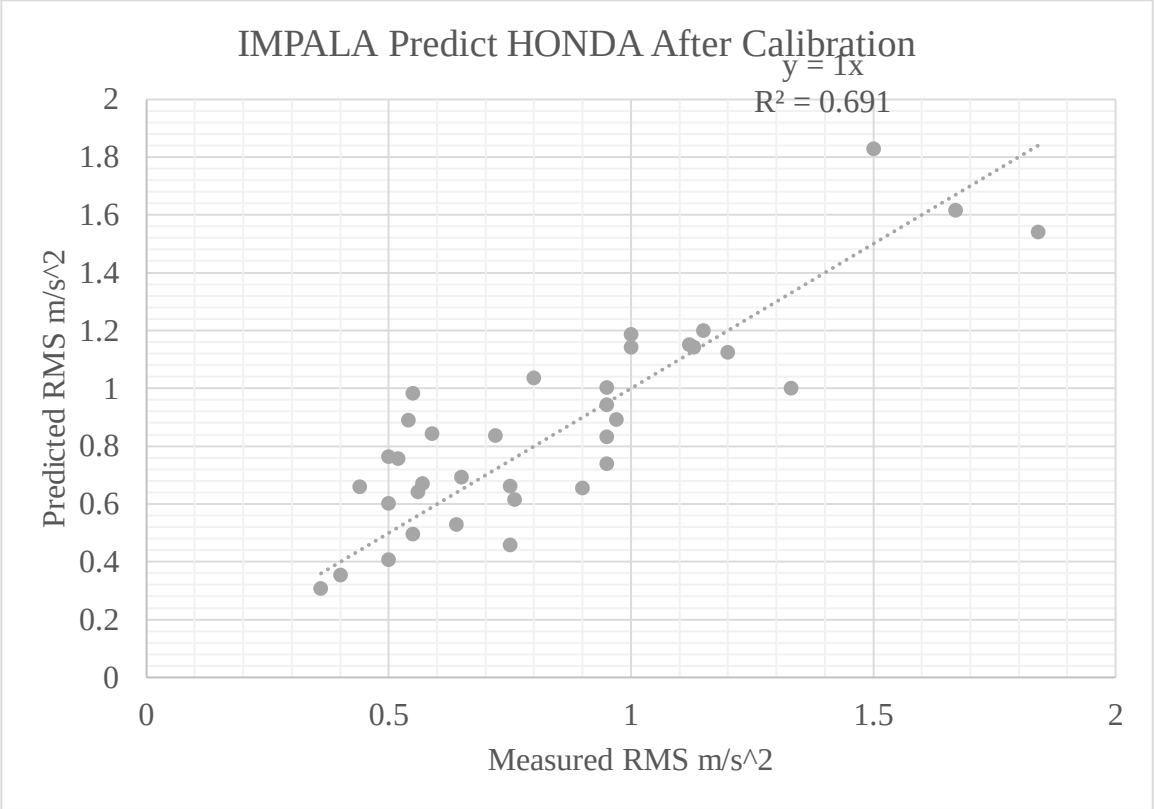
IMPALA Predict HONDA After Calibration
y = 1x
R² = 0.691
Predicted RMS m/s^2
Measured RMS m/s^2
0
0.2
0.4
0.6
0.8
1
1.2
1.4
1.6
1.8
2
0
0.5
1
1.5
2

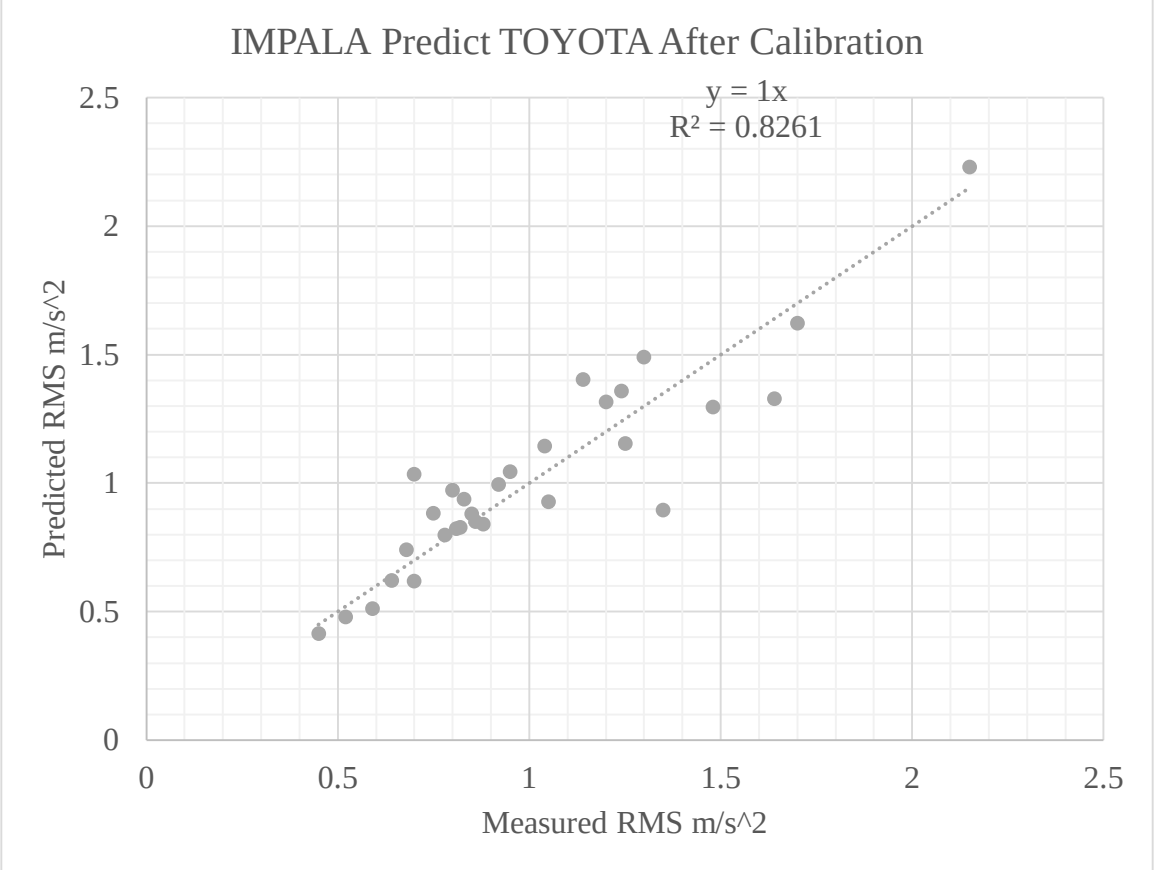
IMPALA Predict TOYOTA After Calibration
y = 1x
R² = 0.8261
Predicted RMS m/s^2
Measured RMS m/s^2
0
0.5
1
1.5
2
2.5
0
0.5
1
1.5
2
2.5

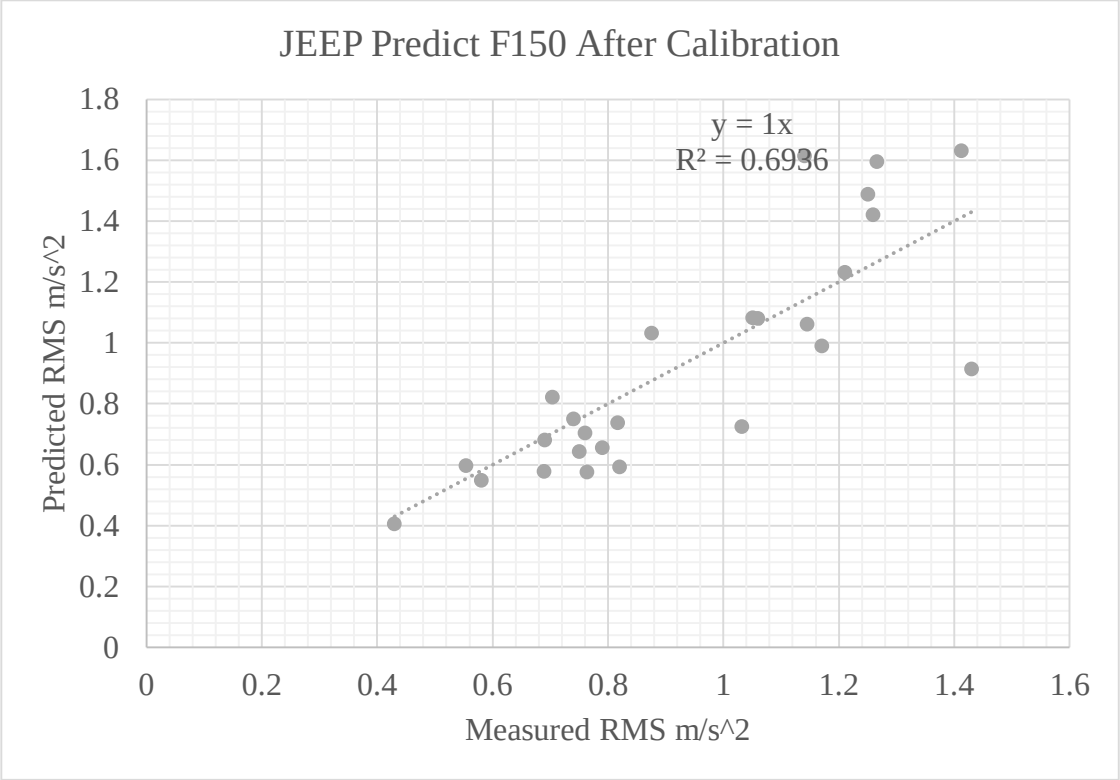
JEEP Predict F150 After Calibration
y = 1x
R² = 0.6936
Predicted RMS m/s^2
Measured RMS m/s^2
0
0.2
0.4
0.6
0.8
1
1.2
1.4
1.6
1.8

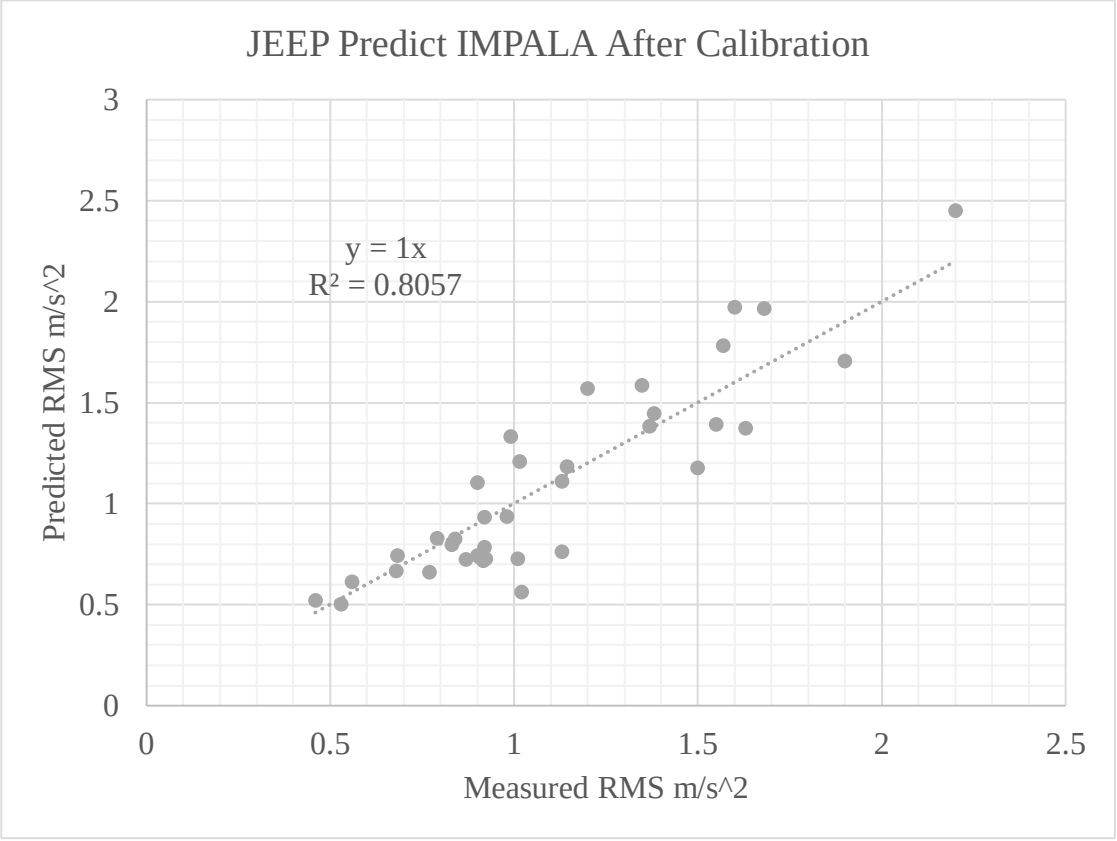
JEEP Predict IMPALA After Calibration
y = 1x
R² = 0.8057
Predicted RMS m/s^2
Measured RMS m/s^2
0
0.5
1
1.5
2
2.5
3

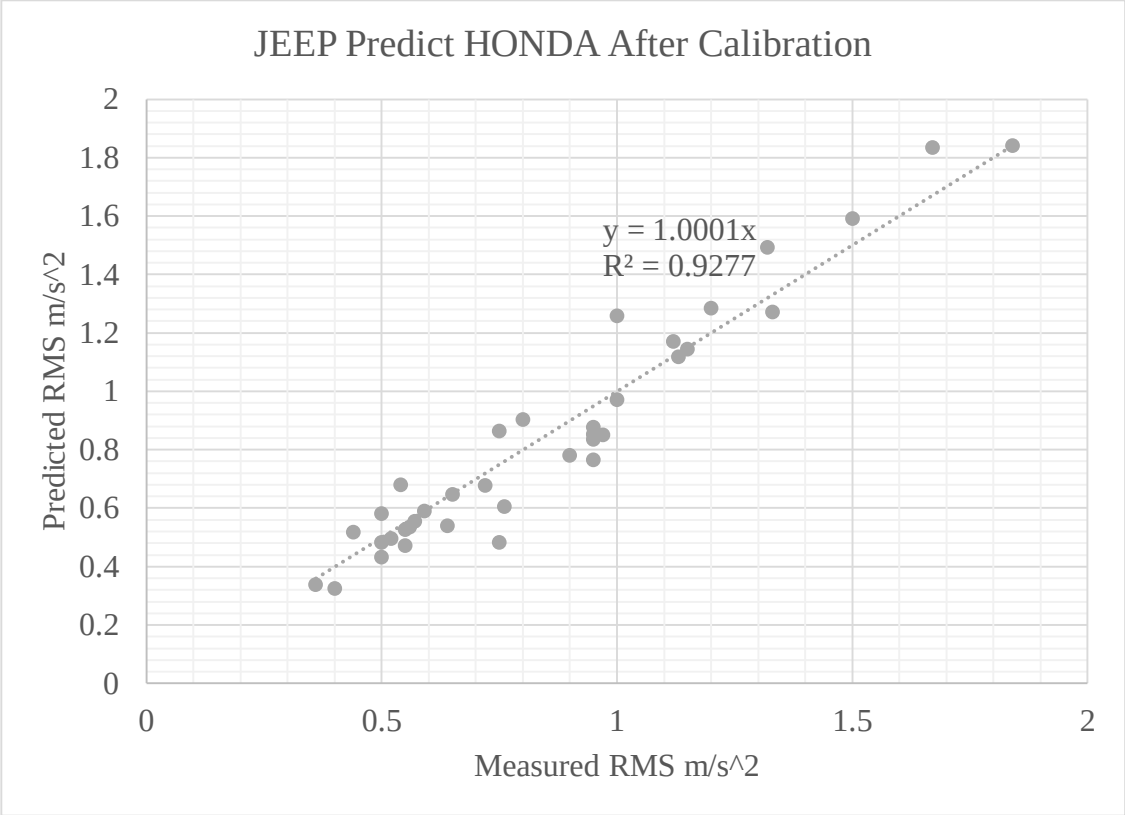
JEEP Predict HONDA After Calibration
y = 1.0001x
R² = 0.9277
Predicted RMS m/s^2
Measured RMS m/s^2
0
0.2
0.4
0.6
0.8
1
1.2
1.4
1.6
1.8
2
0
0.5
1
1.5
2

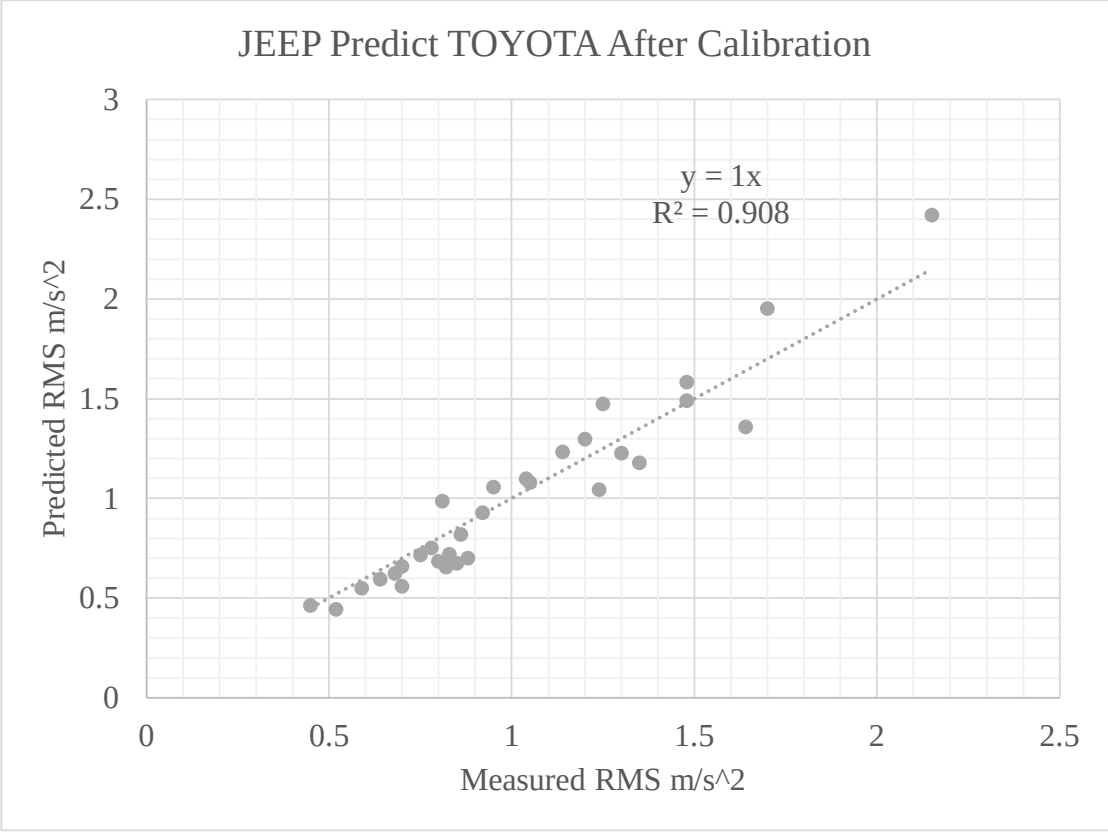
JEEP Predict TOYOTA After Calibration
y = 1x
R² = 0.908
Predicted RMS m/s^2
Measured RMS m/s^2
0
0.5
1
1.5
2
2.5
3
0
0.5
1
1.5
2
2.5

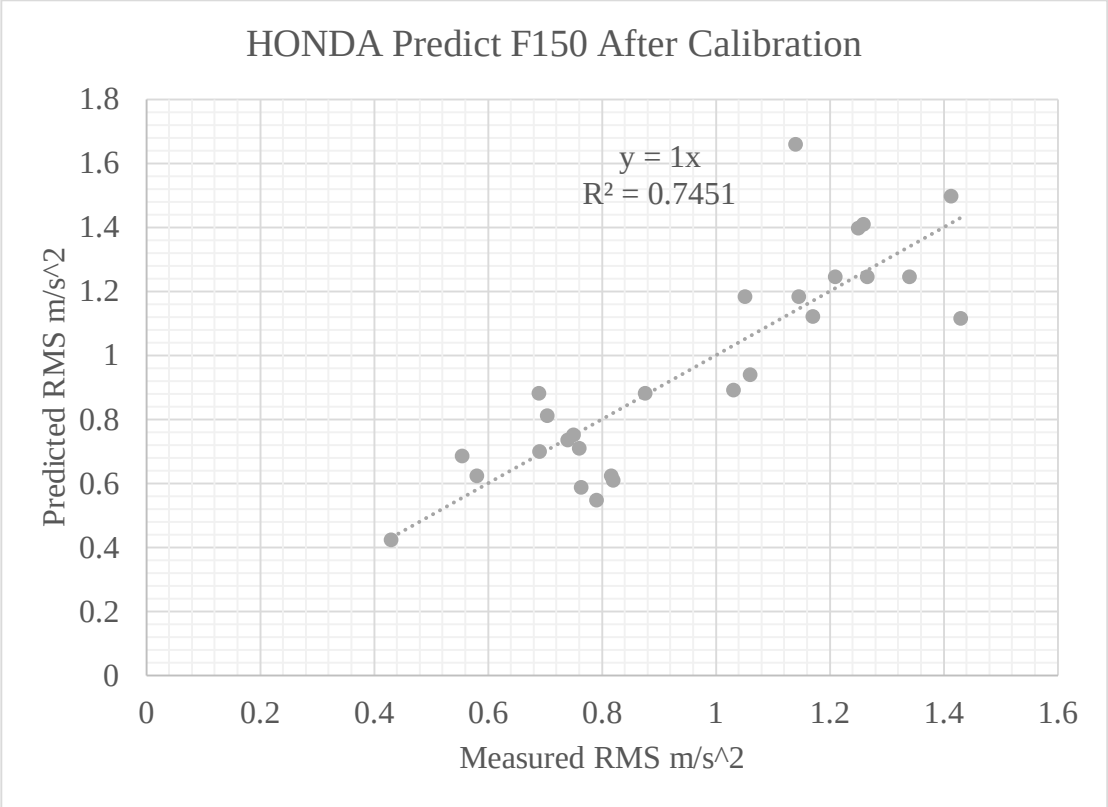
HONDA Predict F150 After Calibration
y = 1x
R² = 0.7451
Predicted RMS m/s^2
Measured RMS m/s^2
0
0.2
0.4
0.6
0.8
1
1.2
1.4
1.6
1.8

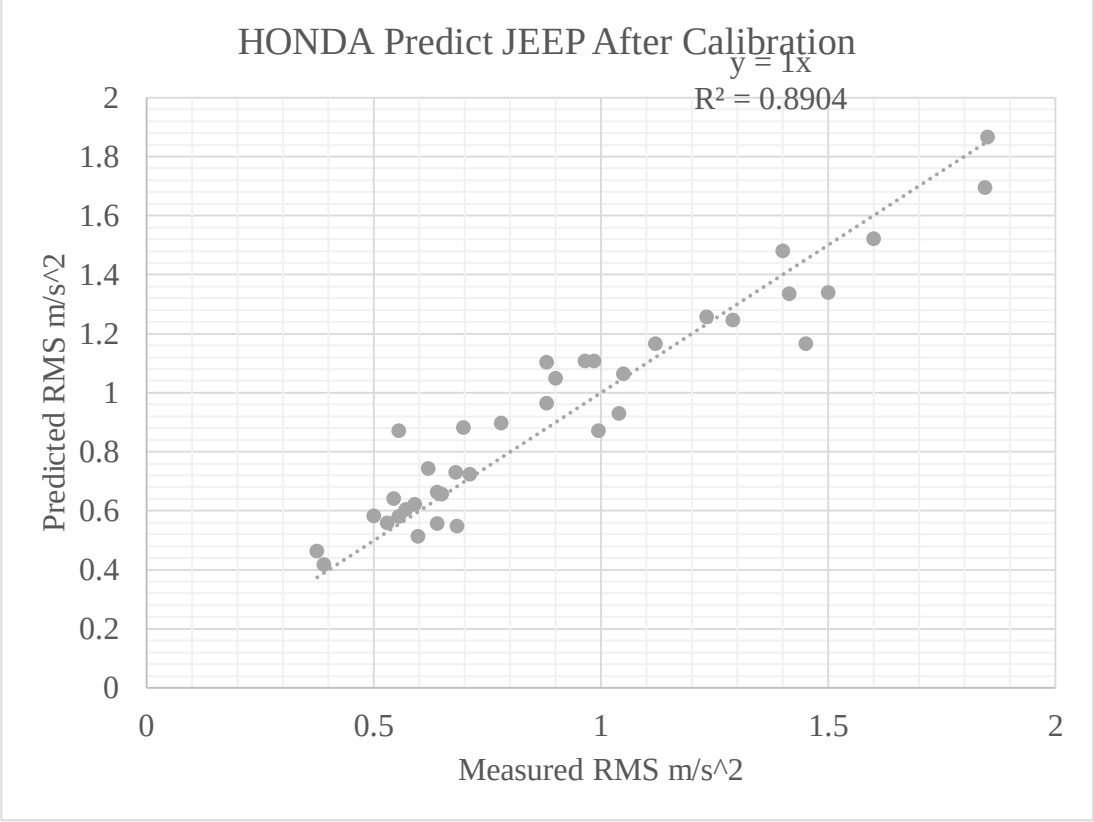
HONDA Predict JEEP After Calibration
y = 1x
R² = 0.8904
Predicted RMS m/s^2
Measured RMS m/s^2
0
0.5
1
1.5
2

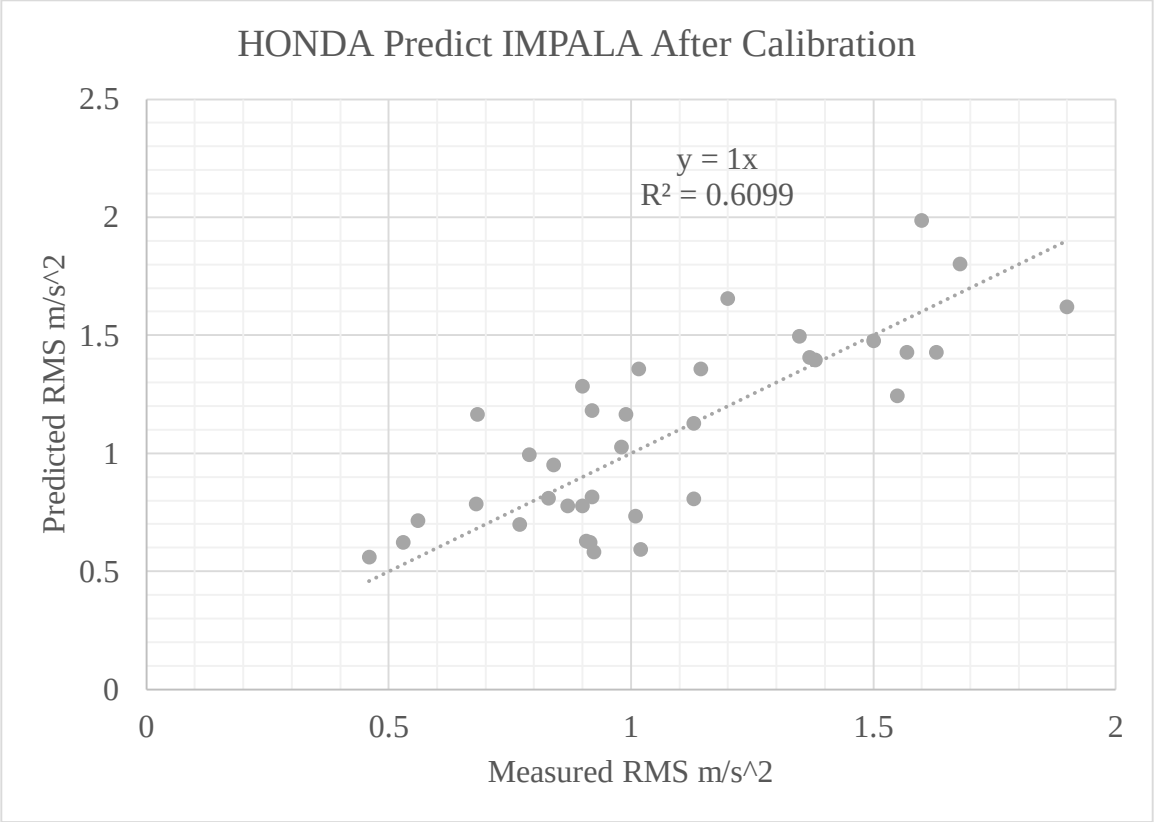
HONDA Predict IMPALA After Calibration
y = 1x
R² = 0.6099
Predicted RMS m/s^2
Measured RMS m/s^2
0
0.5
1
1.5
2
2.5

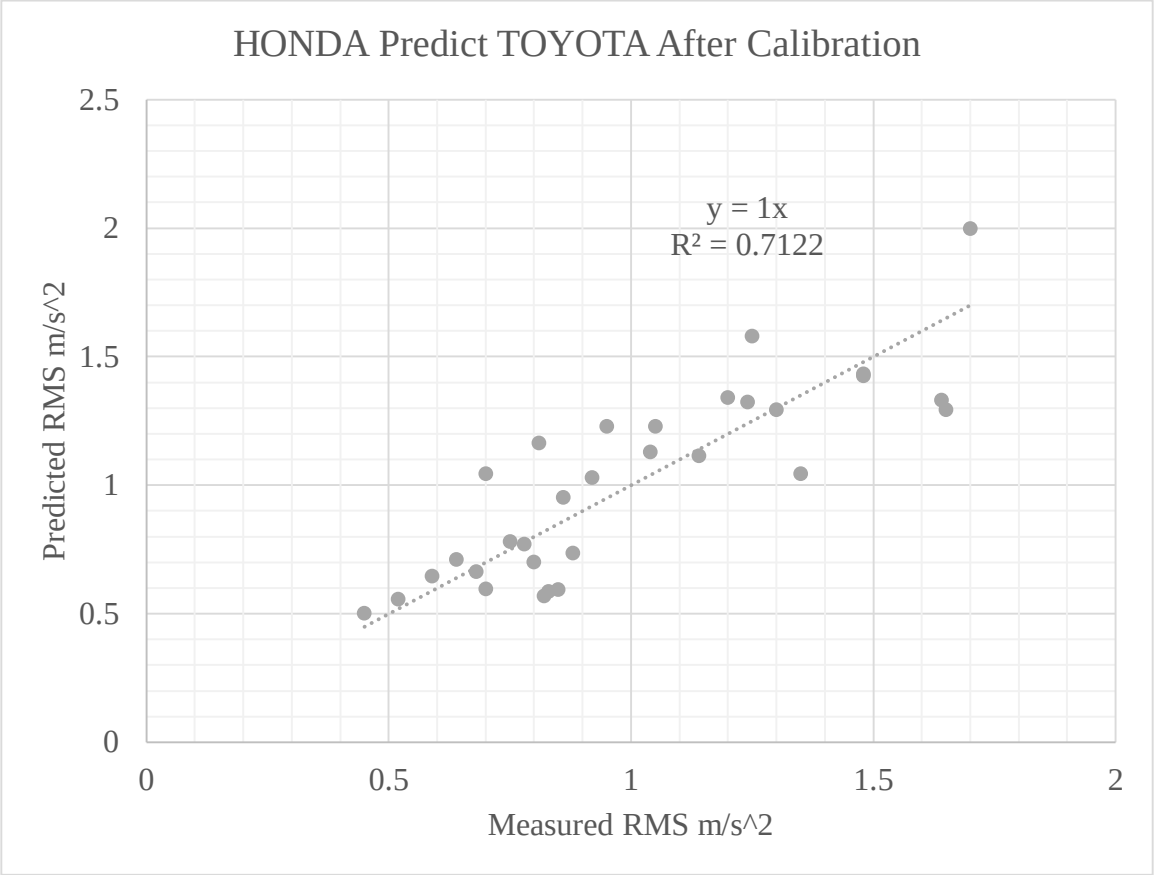
HONDA Predict TOYOTA After Calibration
y = 1x
R² = 0.7122
Predicted RMS m/s^2
Measured RMS m/s^2
0
0.5
1
1.5
2
2.5

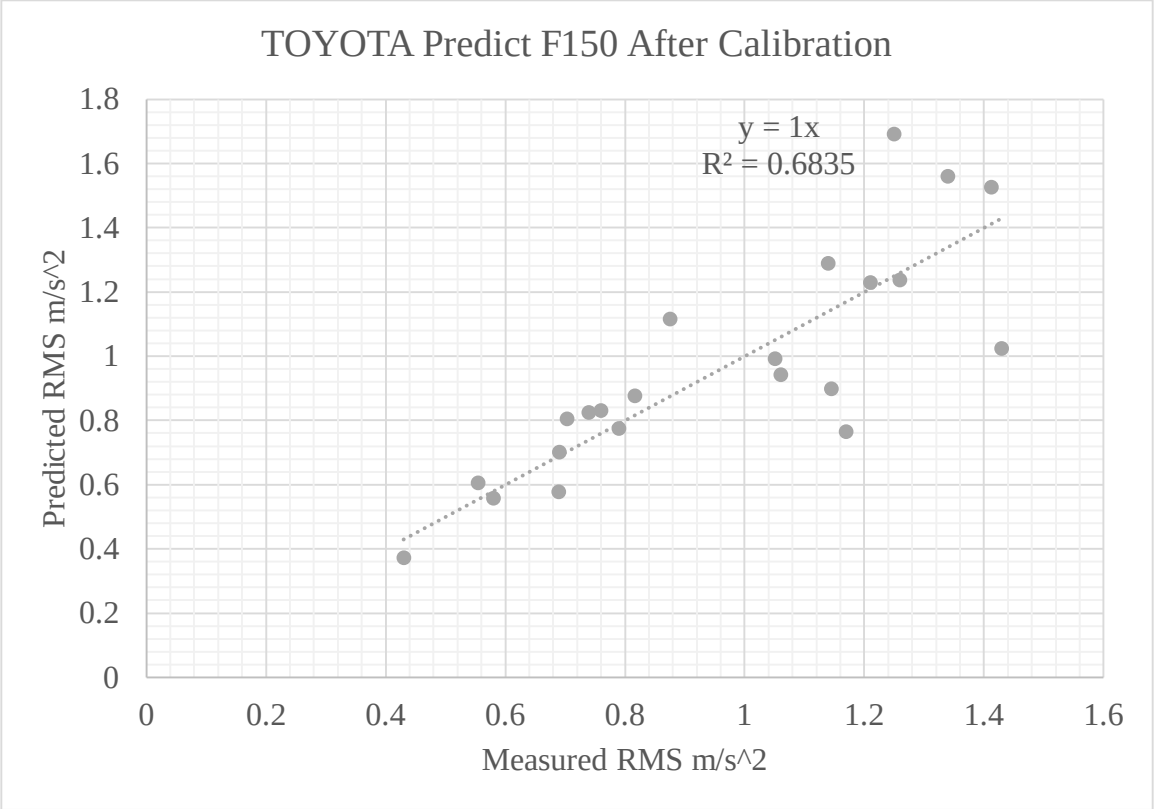
TOYOTA Predict F150 After Calibration
y = 1x
R² = 0.6835
Predicted RMS m/s^2
Measured RMS m/s^2
0
0.2
0.4
0.6
0.8
1
1.2
1.4
1.6
1.8

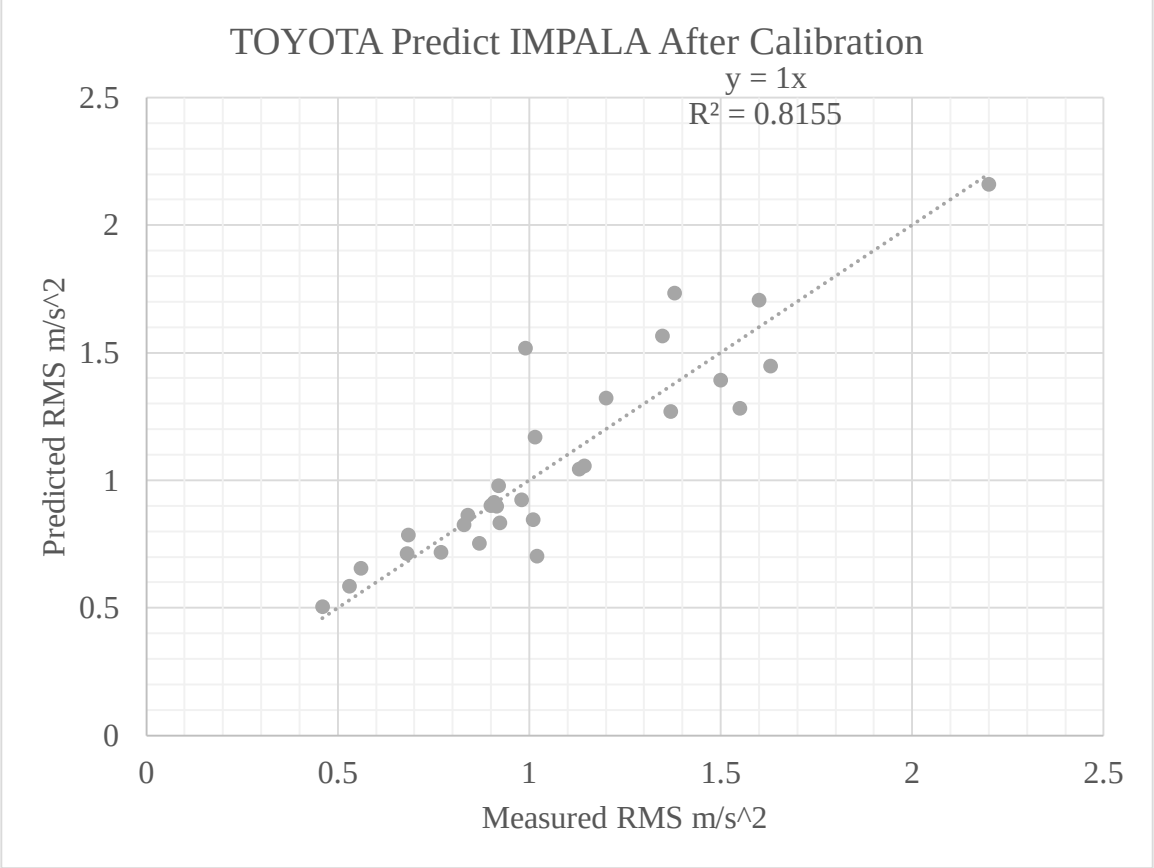
TOYOTA Predict IMPALA After Calibration
y = 1x
R² = 0.8155
Predicted RMS m/s^2
Measured RMS m/s^2
0
0.5
1
1.5
2
2.5

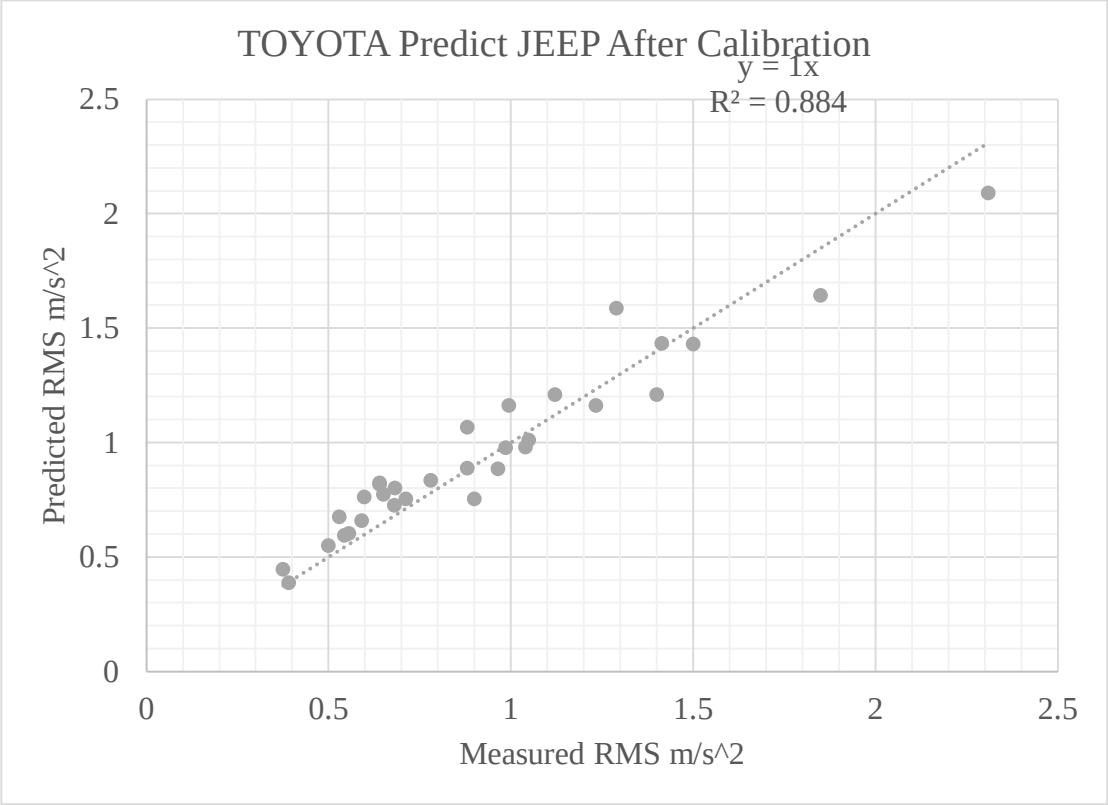
TOYOTA Predict JEEP After Calibration
y = 1x
R² = 0.884
Predicted RMS m/s^2
Measured RMS m/s^2
0
0.5
1
1.5
2
2.5

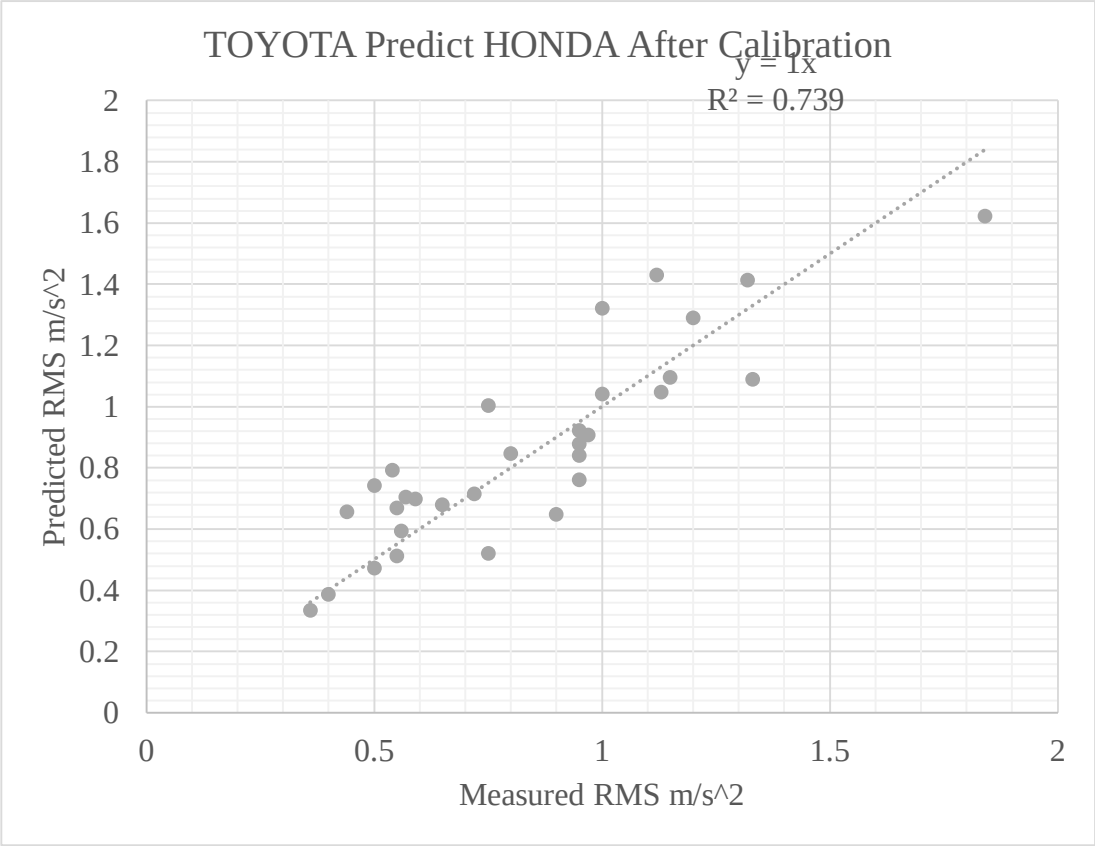
TOYOTA Predict HONDA After Calibration
y = 1x
R² = 0.739
Predicted RMS m/s^2
Measured RMS m/s^2
0
0.2
0.4
0.6
0.8
1
1.2
1.4
1.6
1.8
2

APPENDIX E

Chapter 4 RMS before and after calibration prediction results plots Using Bryan Station Road Crossing

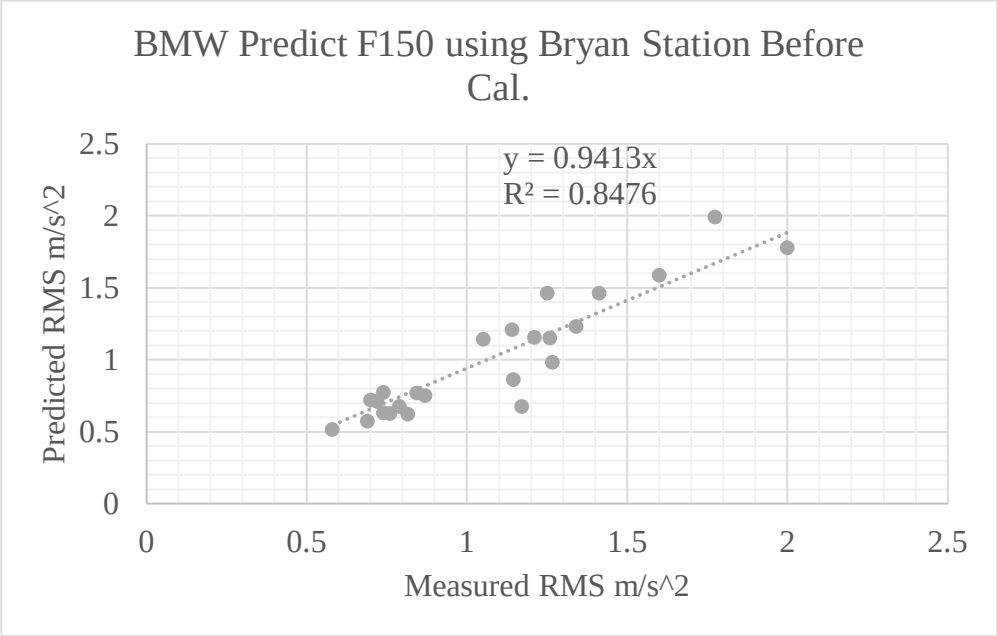

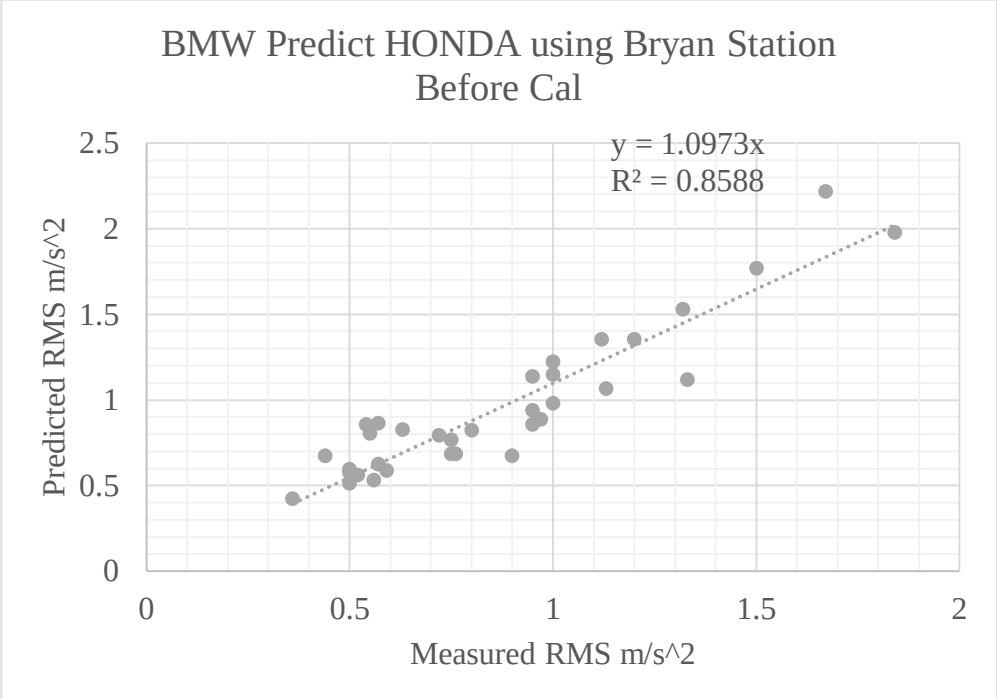

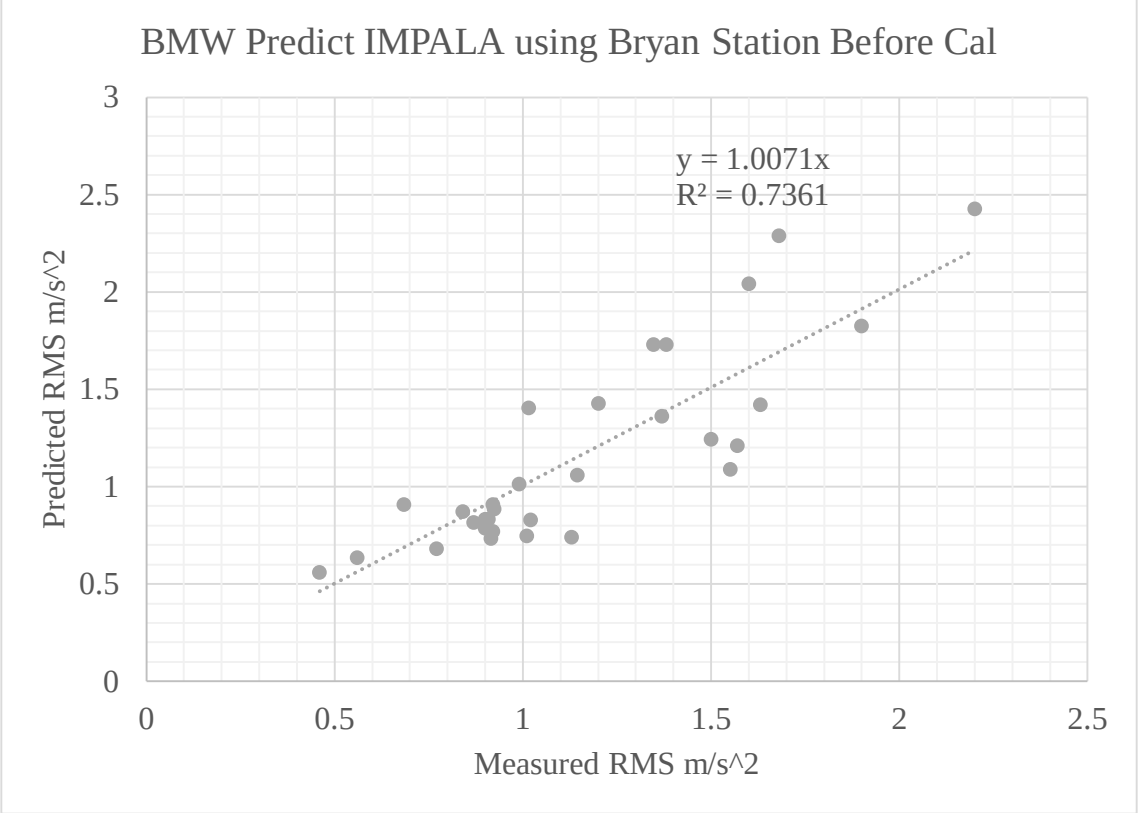
BMW Predict IMPALA using Bryan Station Before Cal
y = 1.0071x
R² = 0.7361
Predicted RMS m/s^2
Measured RMS m/s^2
0
0.5
1
1.5
2
2.5
3

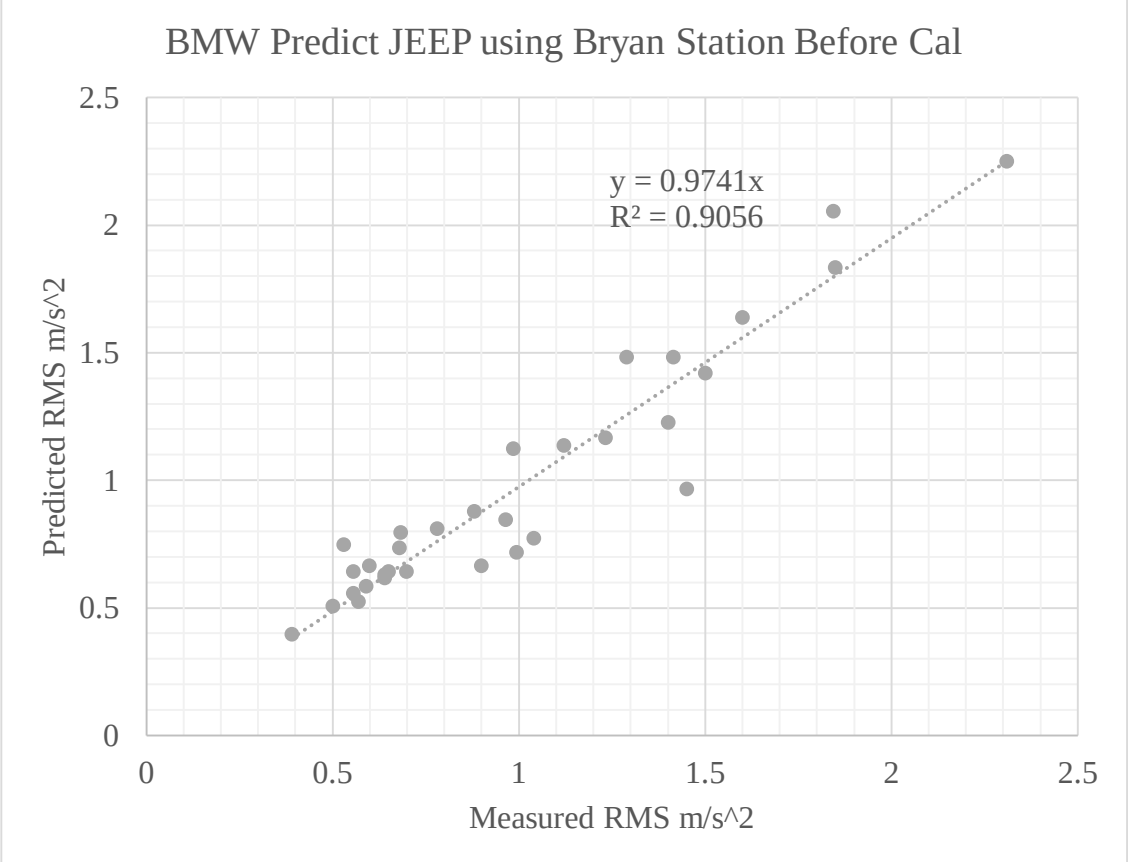
BMW Predict JEEP using Bryan Station Before Cal
y = 0.9741x
R² = 0.9056
Predicted RMS m/s^2
Measured RMS m/s^2
0
0.5
1
1.5
2
2.5

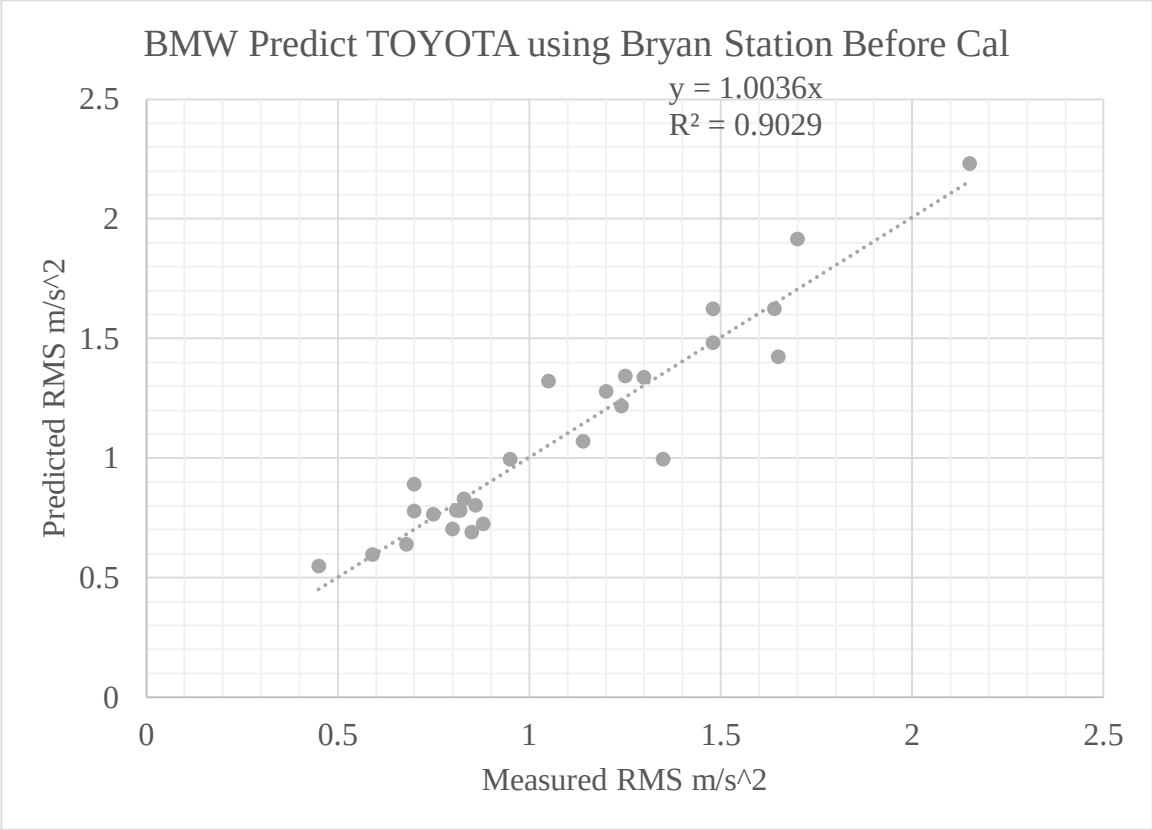
BMW Predict TOYOTA using Bryan Station Before Cal
y = 1.0036x
R² = 0.9029
Predicted RMS m/s^2
Measured RMS m/s^2
0
0.5
1
1.5
2
2.5

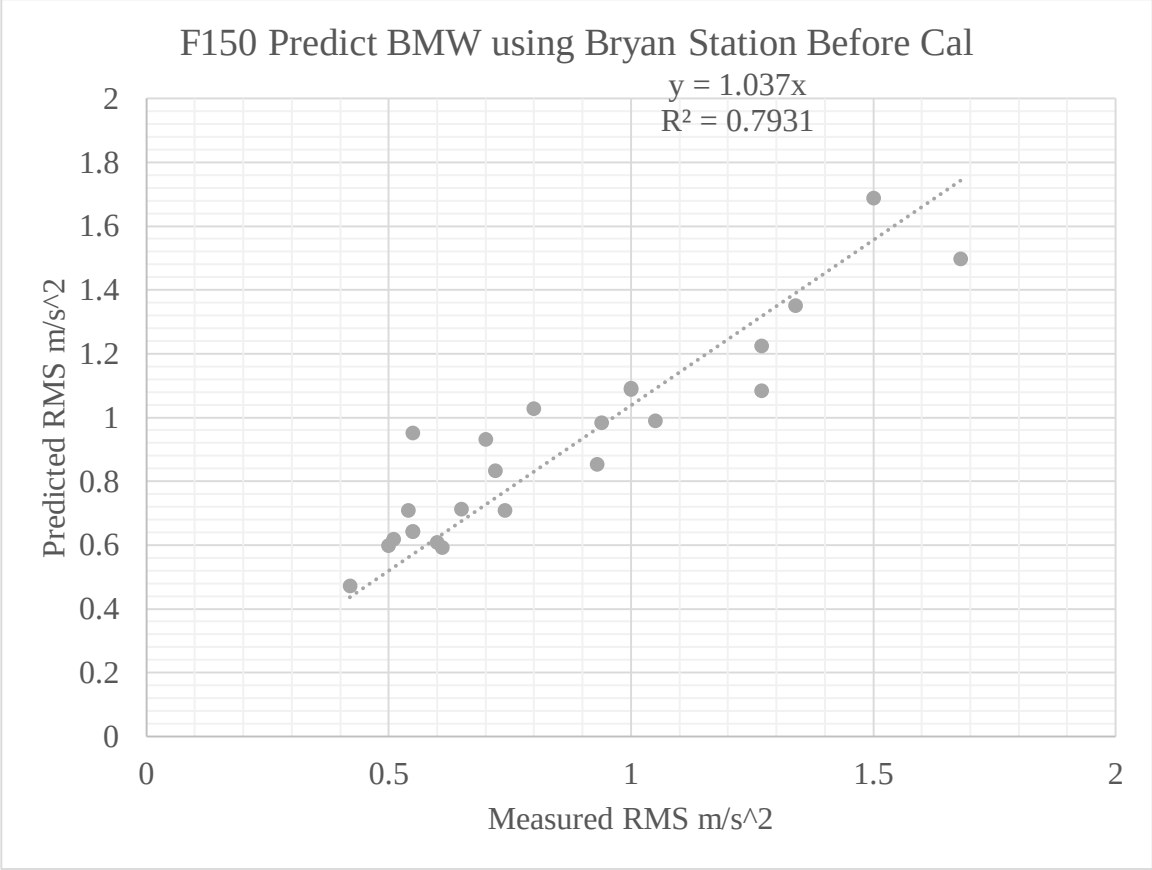
F150 Predict BMW using Bryan Station Before Cal
y = 1.037x
R² = 0.7931
Predicted RMS m/s^2
Measured RMS m/s^2
0
0.2
0.4
0.6
0.8
1
1.2
1.4
1.6
1.8
2

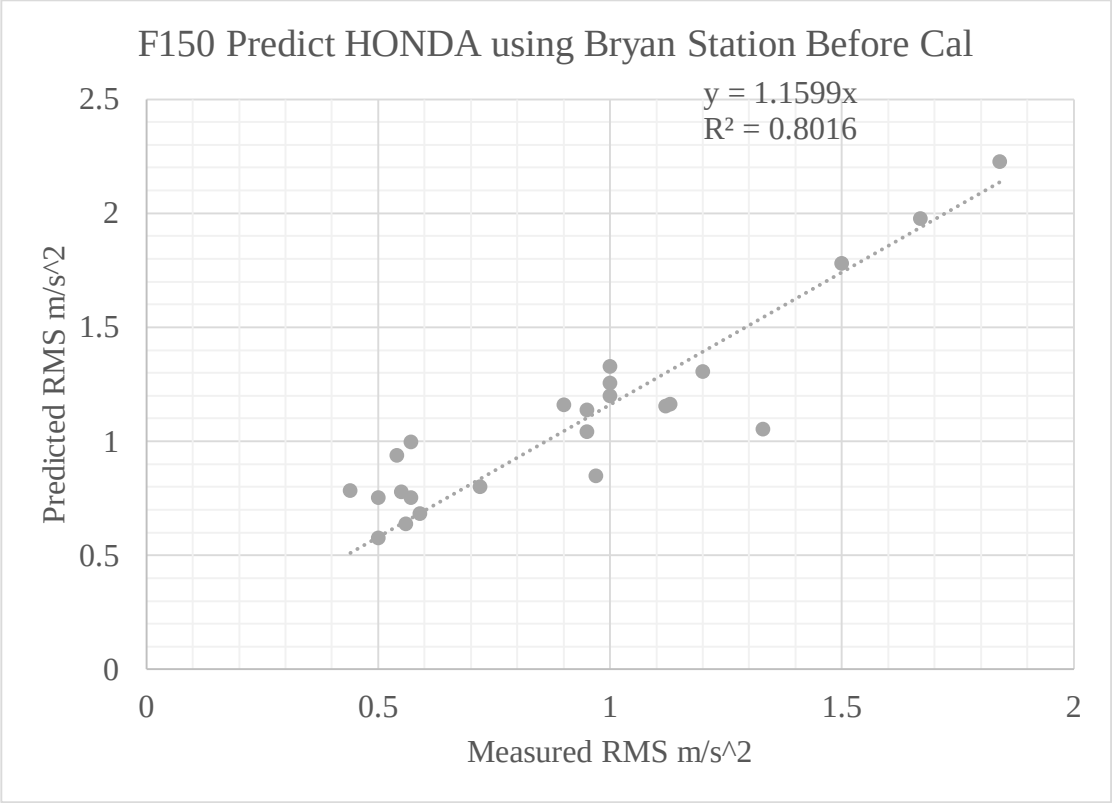
F150 Predict HONDA using Bryan Station Before Cal
y = 1.1599x
R² = 0.8016
Predicted RMS m/s^2
Measured RMS m/s^2
0
0.5
1
1.5
2
2.5

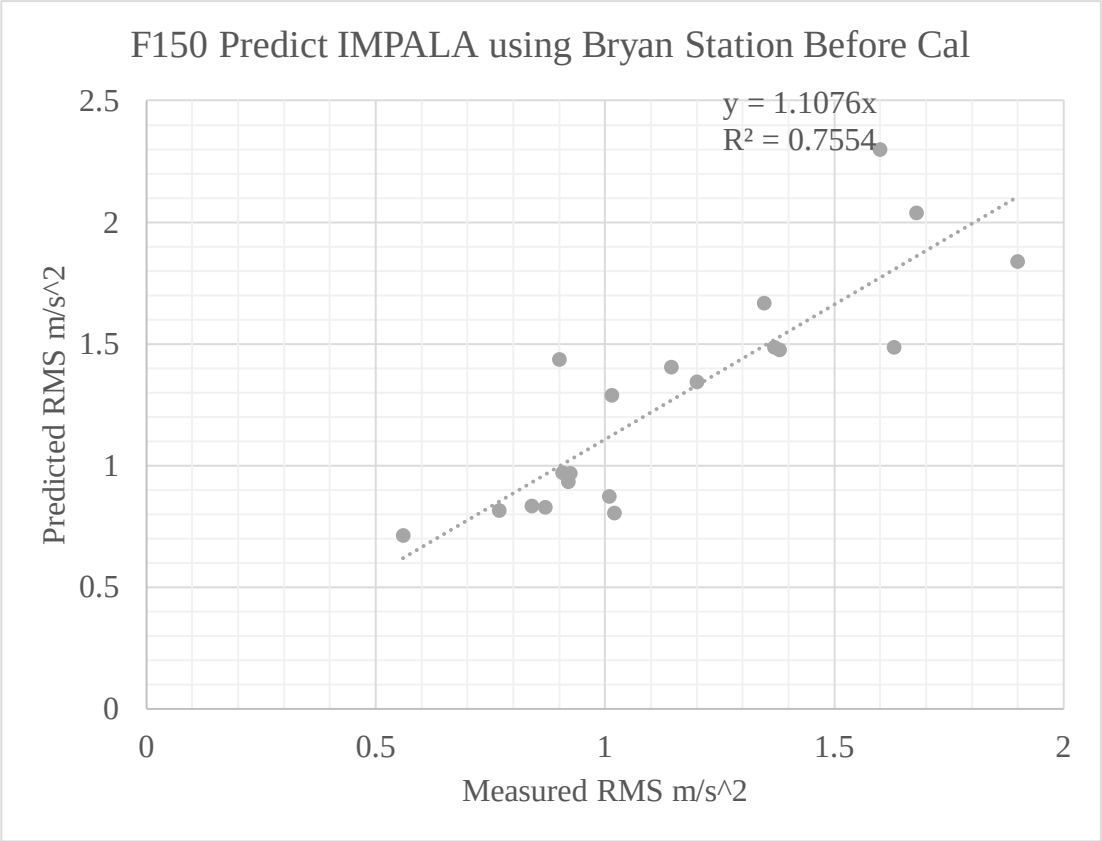
F150 Predict IMPALA using Bryan Station Before Cal
y = 1.1076x
R² = 0.7554
Predicted RMS m/s^2
Measured RMS m/s^2
0
0.5
1
1.5
2
2.5

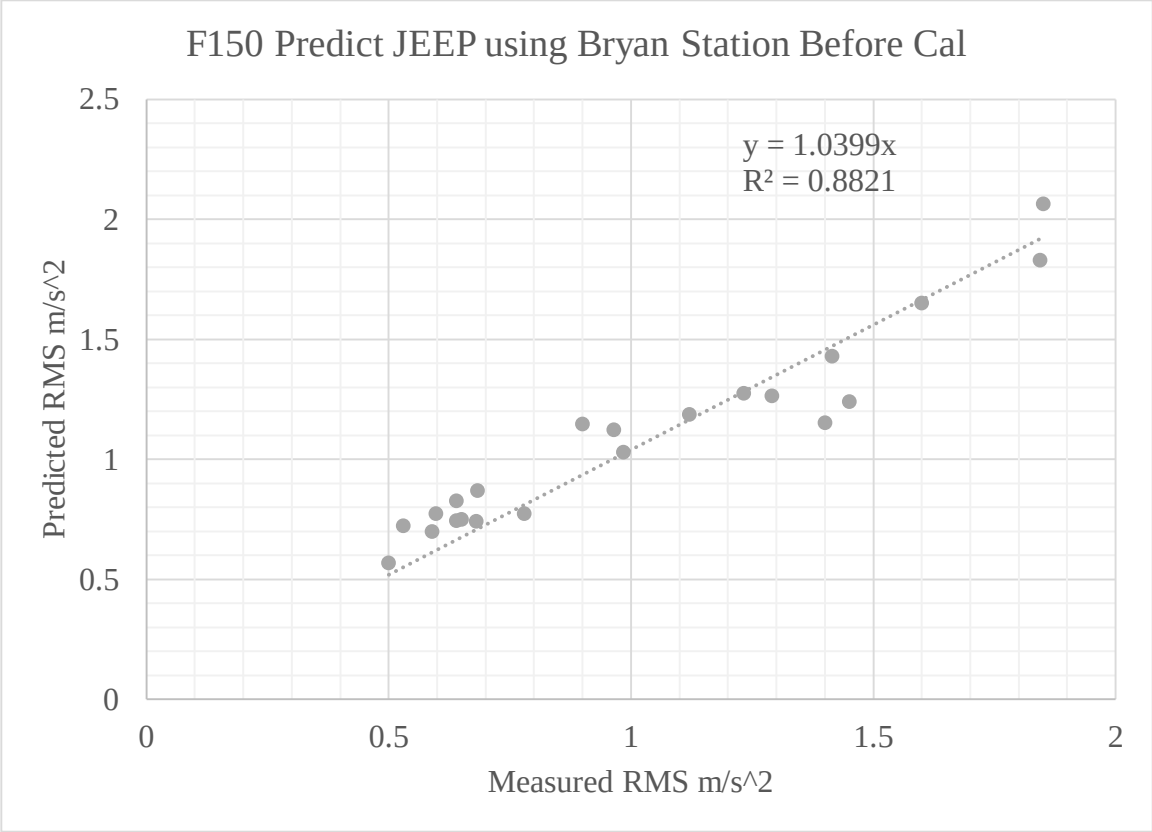
F150 Predict JEEP using Bryan Station Before Cal
y = 1.0399x
R² = 0.8821
Predicted RMS m/s^2
Measured RMS m/s^2
0
0.5
1
1.5
2
2.5

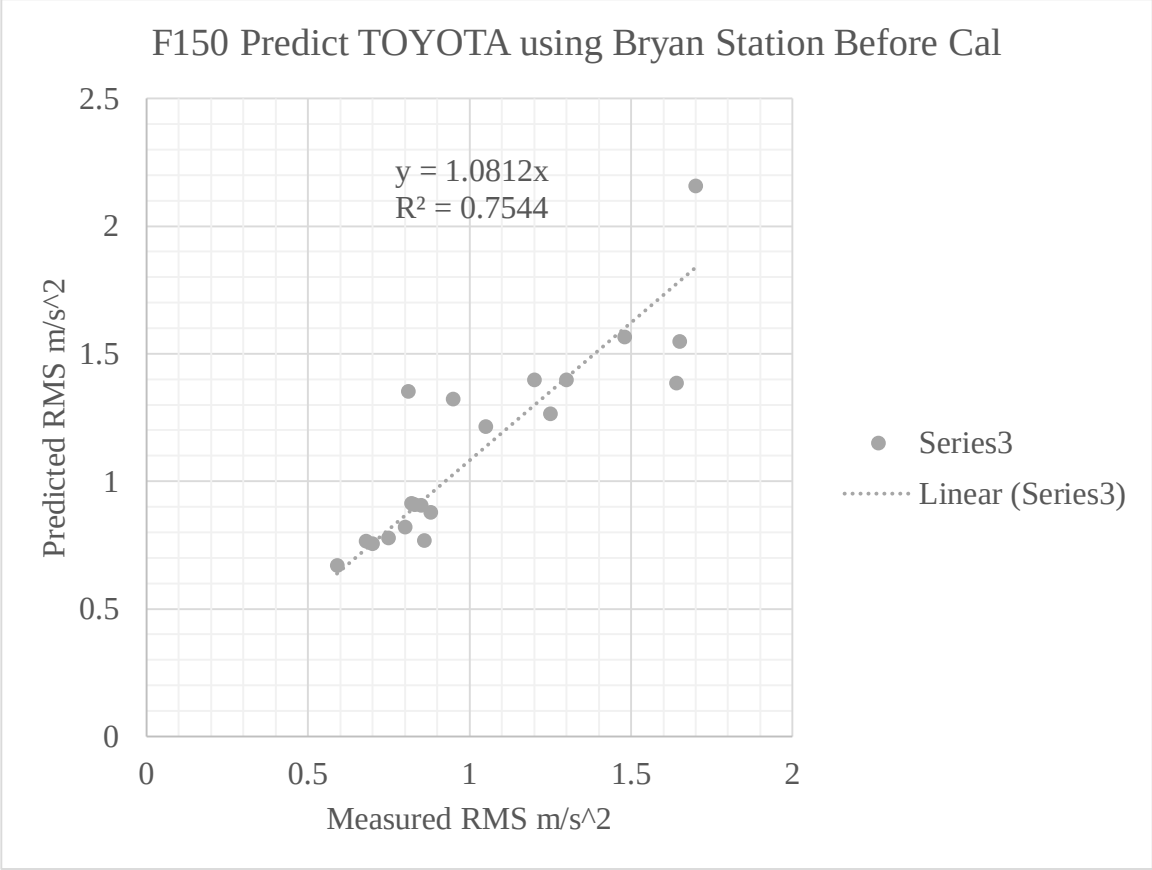
F150 Predict TOYOTA using Bryan Station Before Cal
y = 1.0812x
R² = 0.7544
Predicted RMS m/s^2
Measured RMS m/s^2
Series3
Linear (Series3)
0
0.5
1
1.5
2
2.5

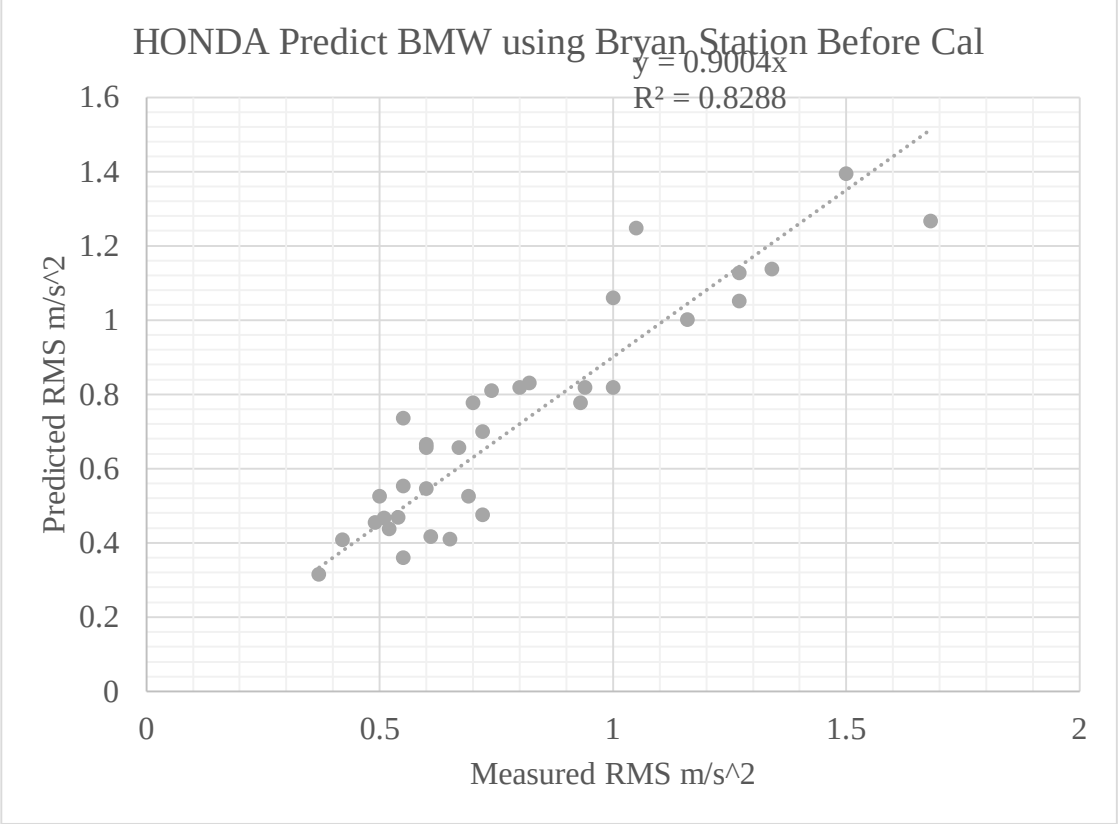
HONDA Predict BMW using Bryan Station Before Cal
y = 0.9004x
R² = 0.8288
Predicted RMS m/s^2
Measured RMS m/s^2
0
0.2
0.4
0.6
0.8
1
1.2
1.4
1.6
0
0.5
1
1.5
2

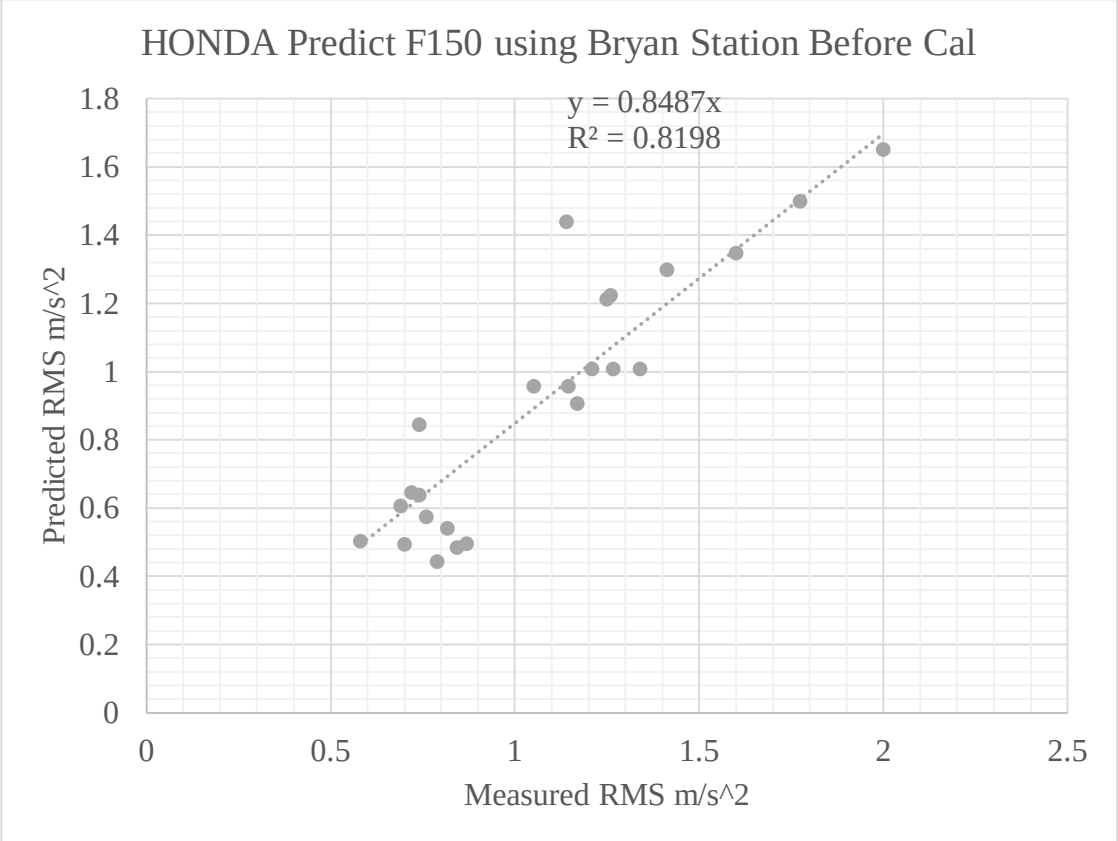
HONDA Predict F150 using Bryan Station Before Cal
y = 0.8487x
R² = 0.8198
Predicted RMS m/s^2
Measured RMS m/s^2
0
0.2
0.4
0.6
0.8
1
1.2
1.4
1.6
1.8
0
0.5
1
1.5
2
2.5

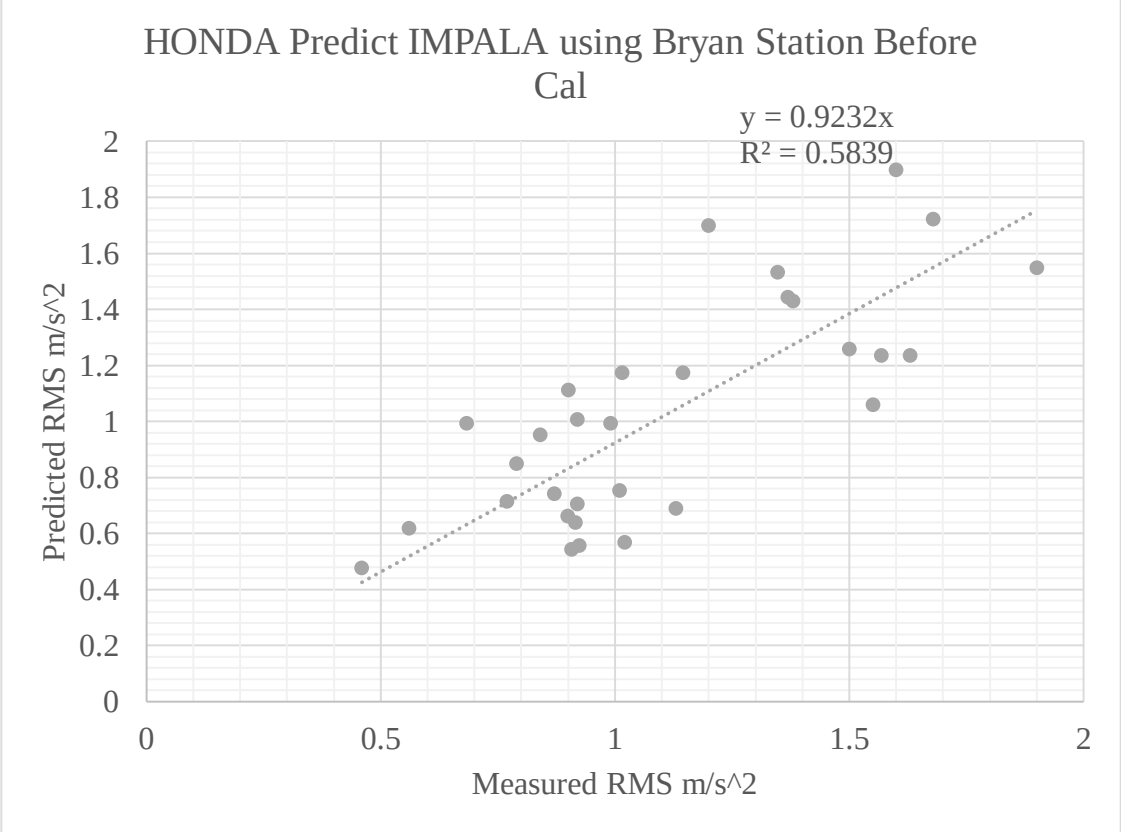
HONDA Predict IMPALA using Bryan Station Before Cal
y = 0.9232x
R² = 0.5839
Predicted RMS m/s^2
Measured RMS m/s^2
0
0.2
0.4
0.6
0.8
1
1.2
1.4
1.6
1.8
2
0
0.5
1
1.5
2

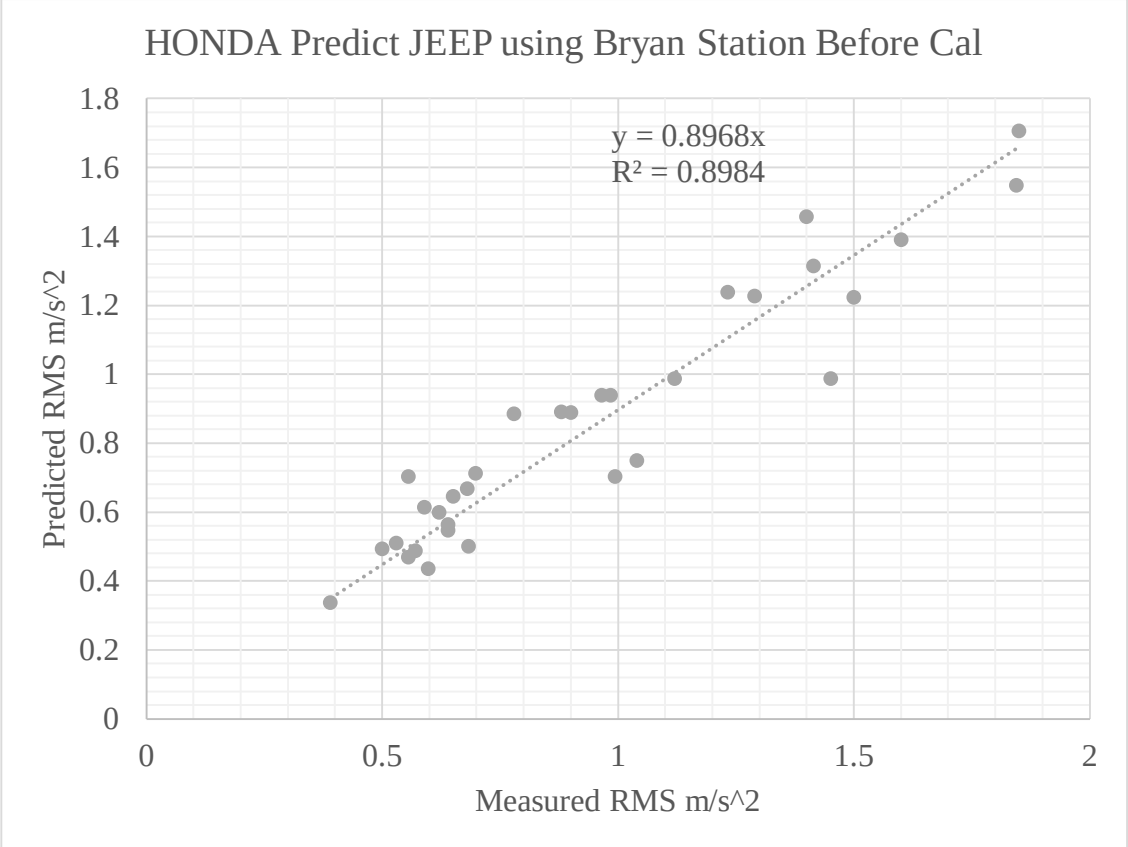
HONDA Predict JEEP using Bryan Station Before Cal
y = 0.8968x
R² = 0.8984
Predicted RMS m/s^2
Measured RMS m/s^2
0
0.2
0.4
0.6
0.8
1
1.2
1.4
1.6
1.8
0
0.5
1
1.5
2

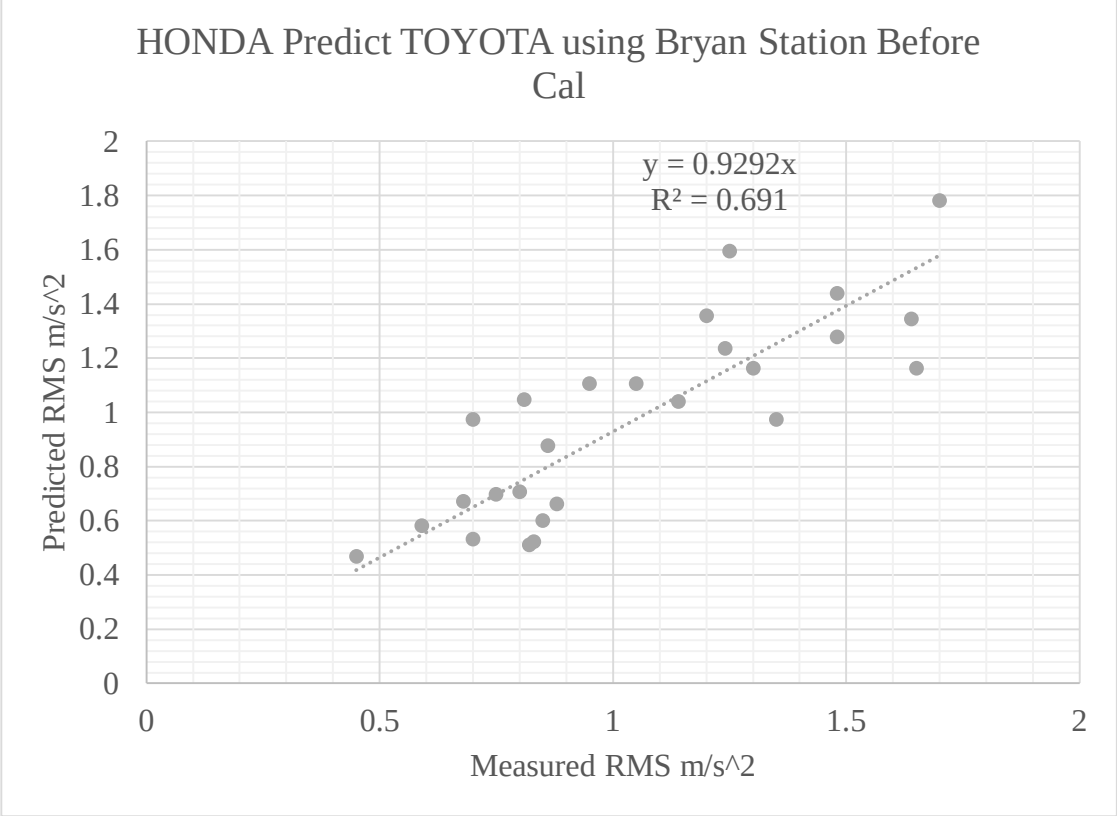
HONDA Predict TOYOTA using Bryan Station Before Cal
y = 0.9292x
R² = 0.691
Predicted RMS m/s^2
Measured RMS m/s^2
0
0.2
0.4
0.6
0.8
1
1.2
1.4
1.6
1.8
2
0
0.5
1
1.5
2

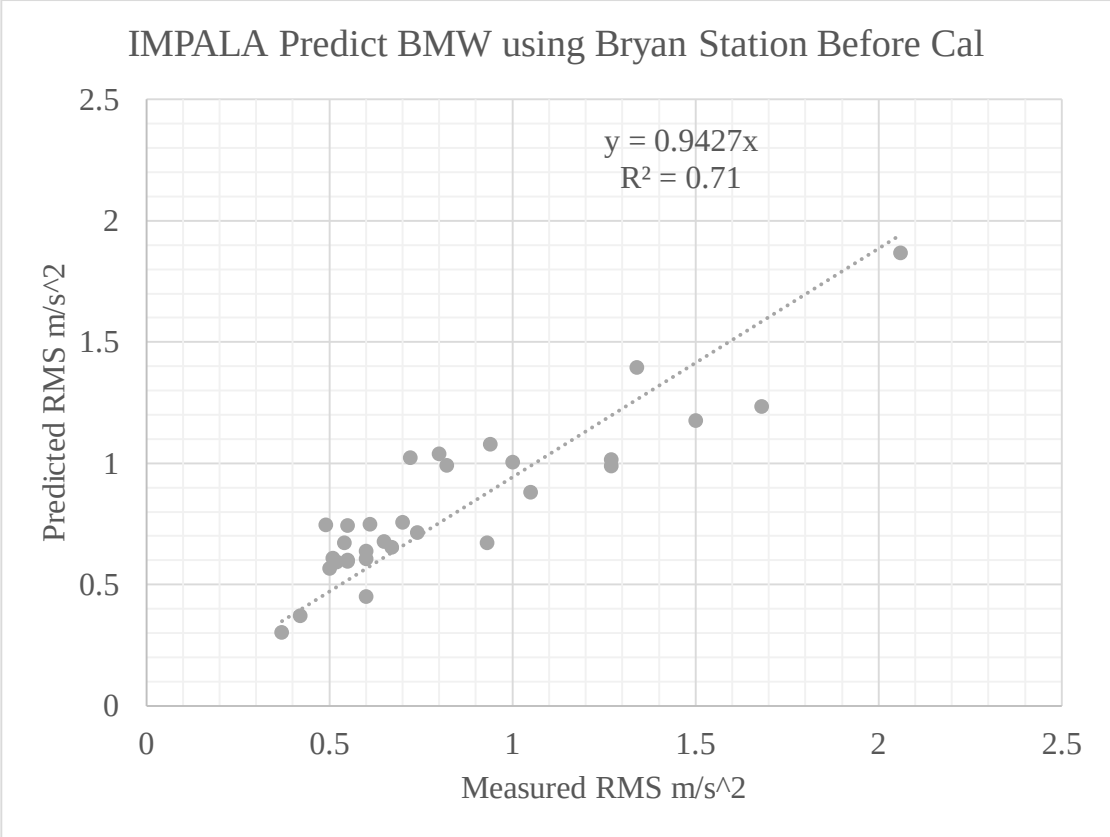
IMPALA Predict BMW using Bryan Station Before Cal
y = 0.9427x
R² = 0.71
Predicted RMS m/s^2
Measured RMS m/s^2
0
0.5
1
1.5
2
2.5
0
0.5
1
1.5
2
2.5

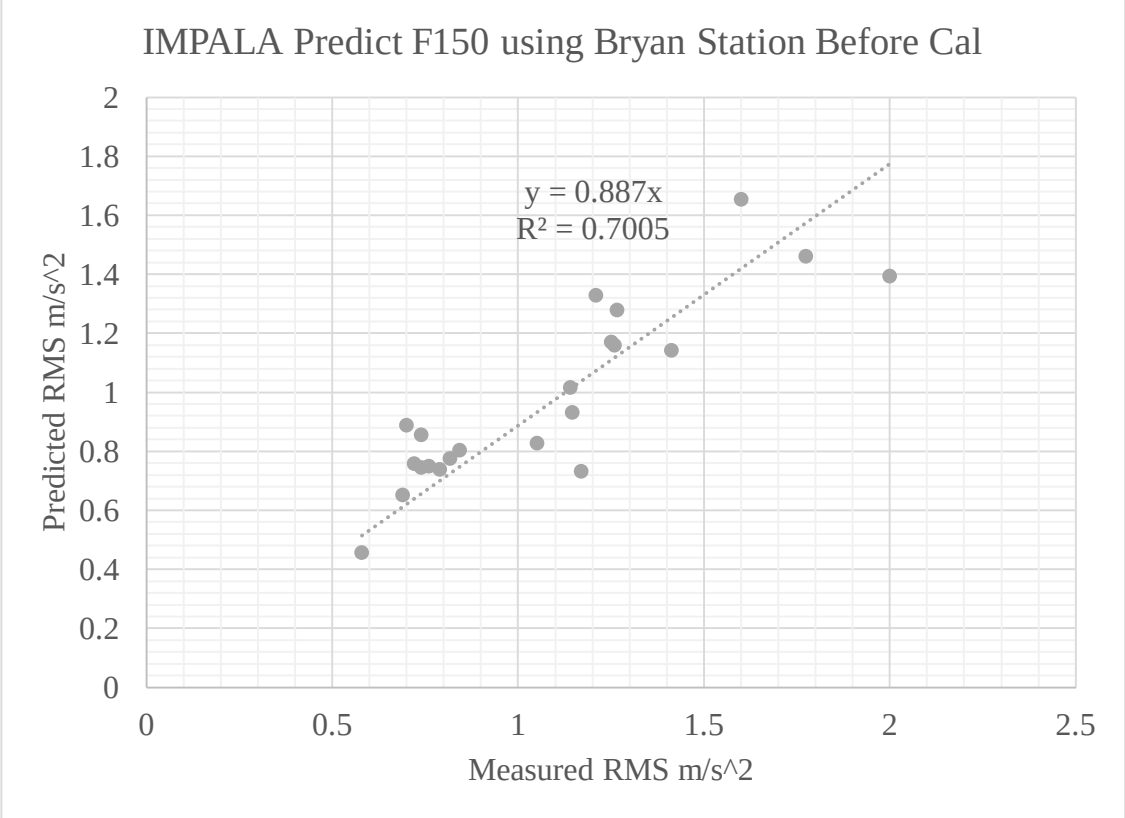
IMPALA Predict F150 using Bryan Station Before Cal
y = 0.887x
R² = 0.7005
Predicted RMS m/s^2
Measured RMS m/s^2
0
0.2
0.4
0.6
0.8
1
1.2
1.4
1.6
1.8
2
0
0.5
1
1.5
2
2.5

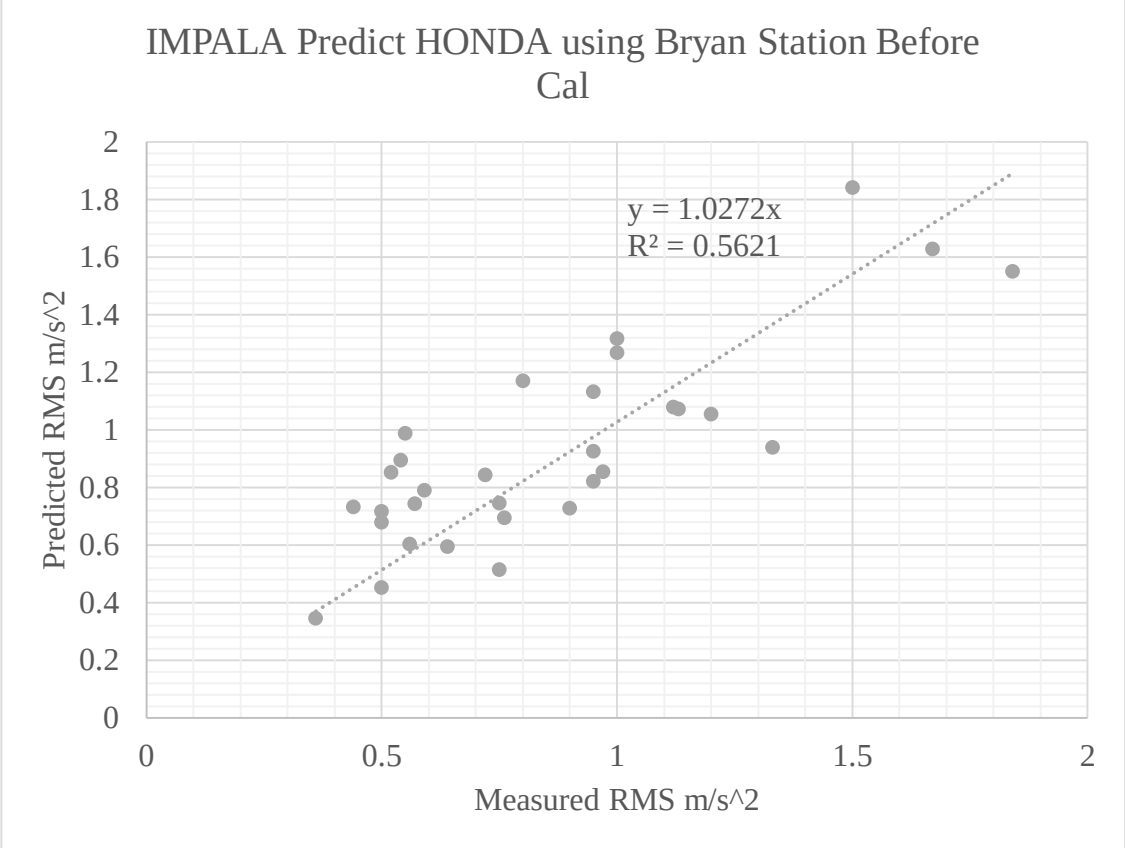
IMPALA Predict HONDA using Bryan Station Before Cal
y = 1.0272x
R² = 0.5621
Predicted RMS m/s^2
Measured RMS m/s^2
0
0.2
0.4
0.6
0.8
1
1.2
1.4
1.6
1.8
2
0
0.5
1
1.5
2

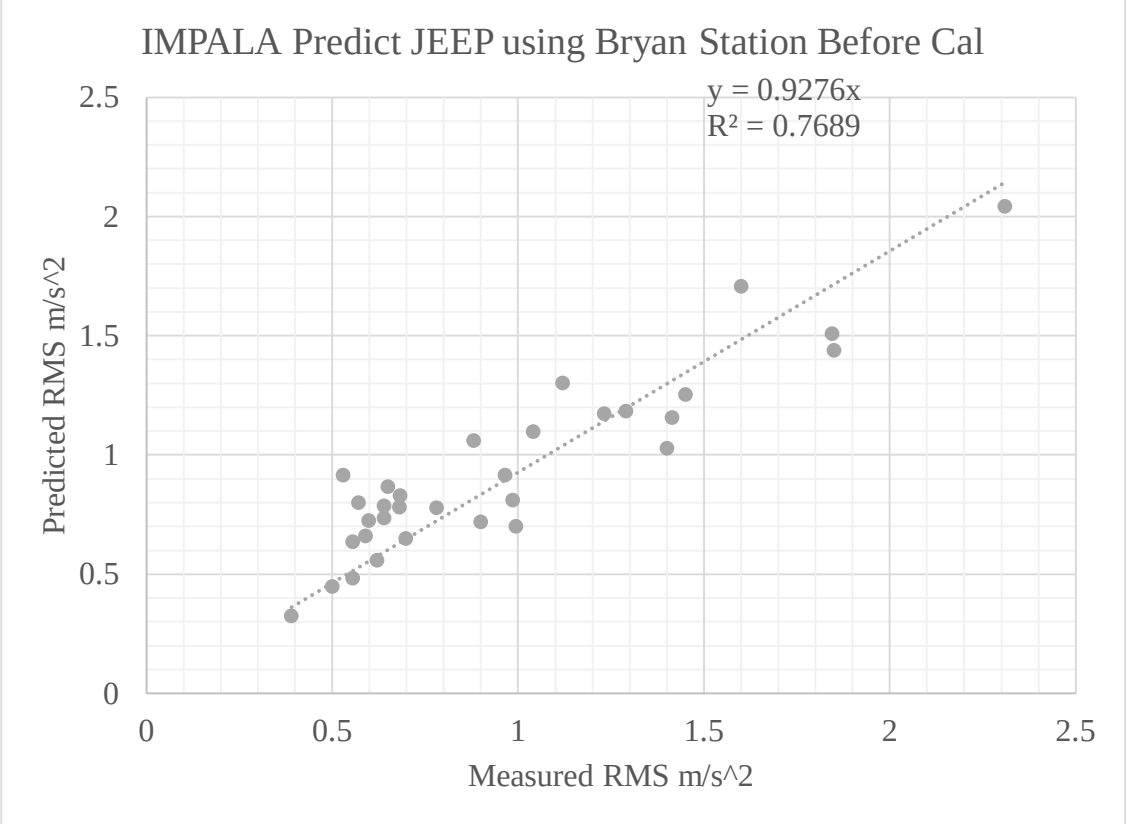
IMPALA Predict JEEP using Bryan Station Before Cal
y = 0.9276x
R² = 0.7689
Predicted RMS m/s^2
Measured RMS m/s^2
0
0.5
1
1.5
2
2.5

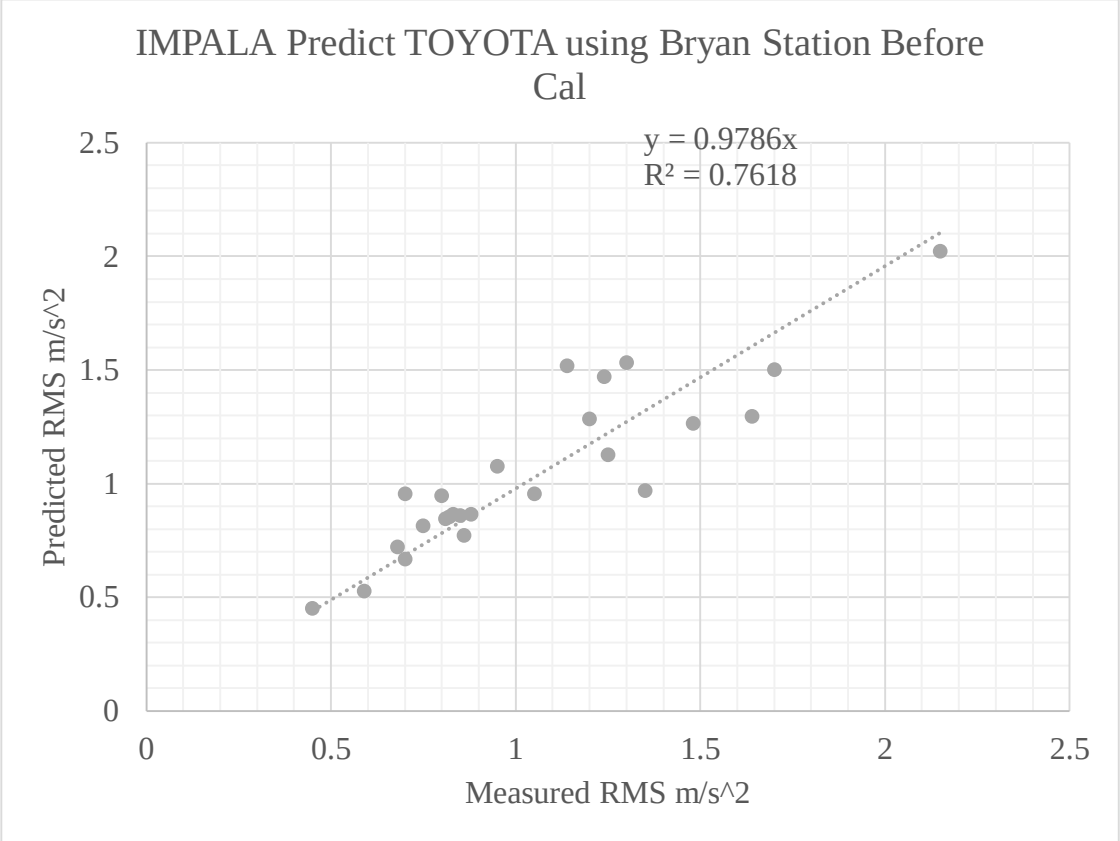
IMPALA Predict TOYOTA using Bryan Station Before Cal
y = 0.9786x
R² = 0.7618
Predicted RMS m/s^2
Measured RMS m/s^2
0
0.5
1
1.5
2
2.5

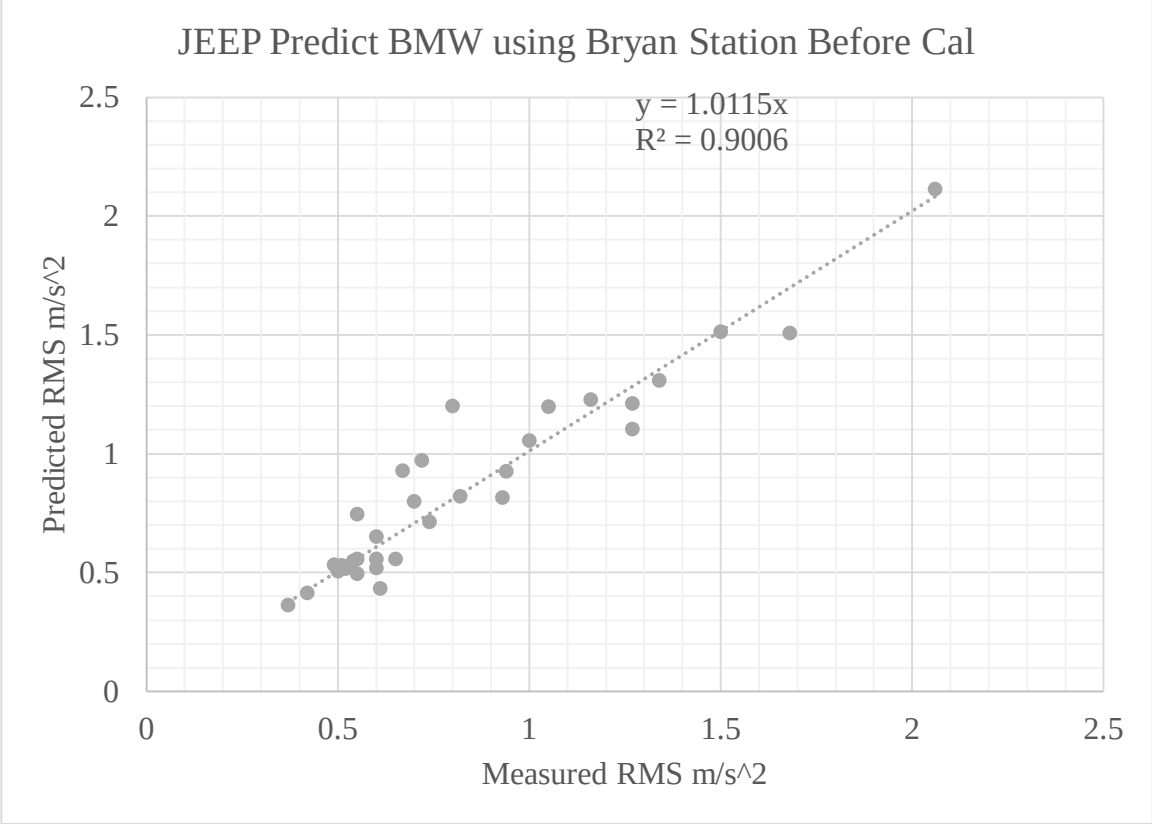
JEEP Predict BMW using Bryan Station Before Cal
y = 1.0115x
R² = 0.9006
Predicted RMS m/s^2
Measured RMS m/s^2
0
0.5
1
1.5
2
2.5

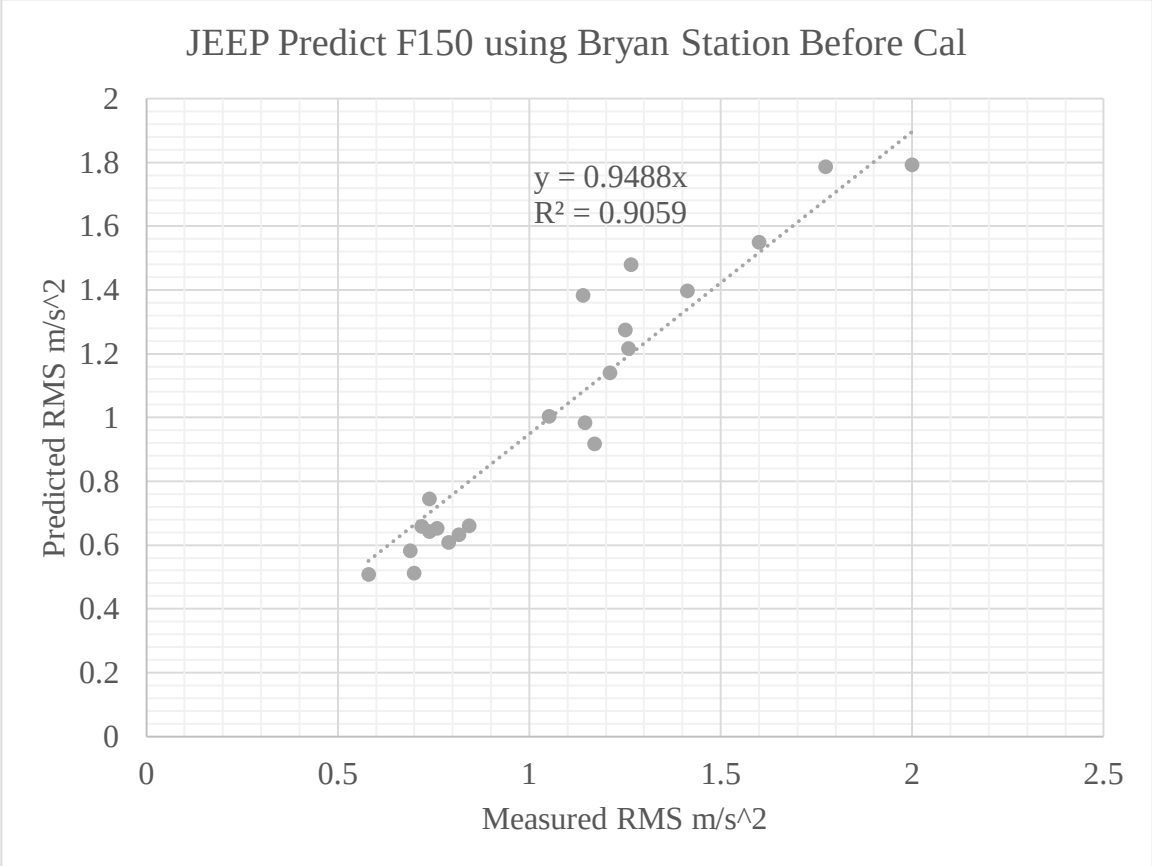
JEEP Predict F150 using Bryan Station Before Cal
y = 0.9488x
R² = 0.9059
Predicted RMS m/s^2
Measured RMS m/s^2
0
0.2
0.4
0.6
0.8
1
1.2
1.4
1.6
1.8
2
2.5

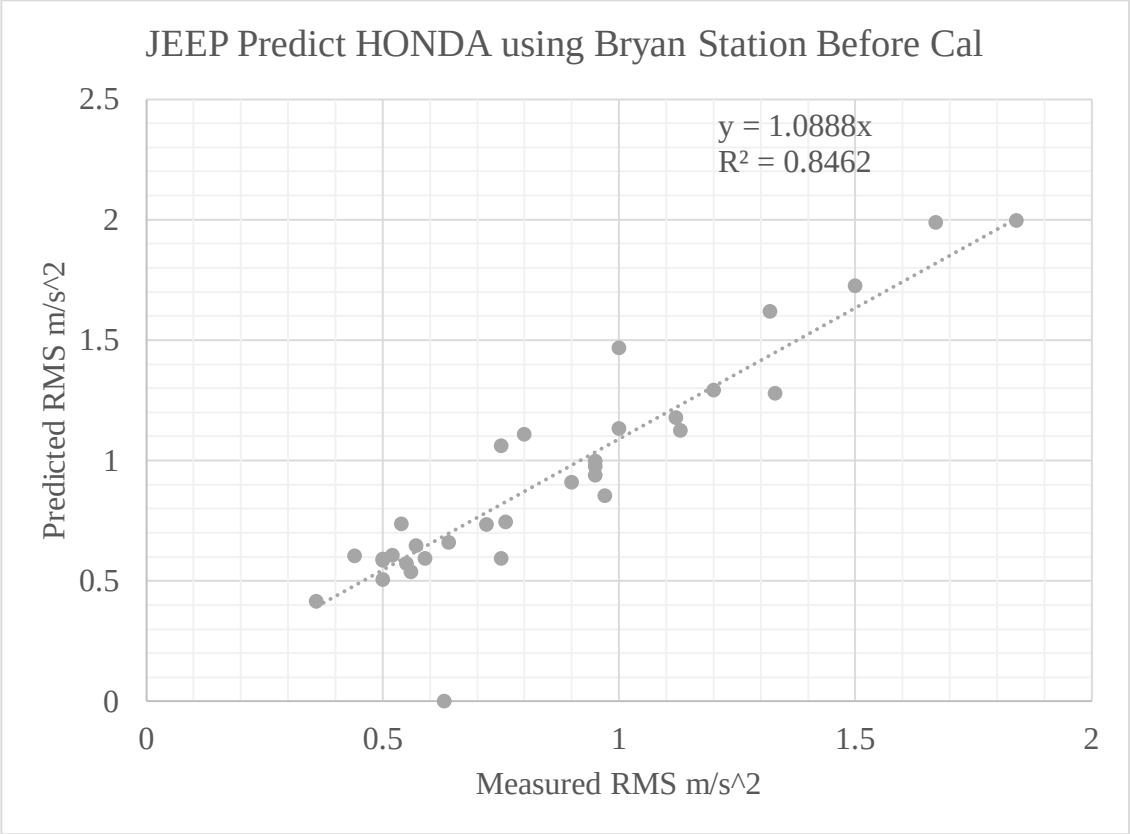
JEEP Predict HONDA using Bryan Station Before Cal
y = 1.0888x
R² = 0.8462
Predicted RMS m/s^2
Measured RMS m/s^2
0
0.5
1
1.5
2
2.5

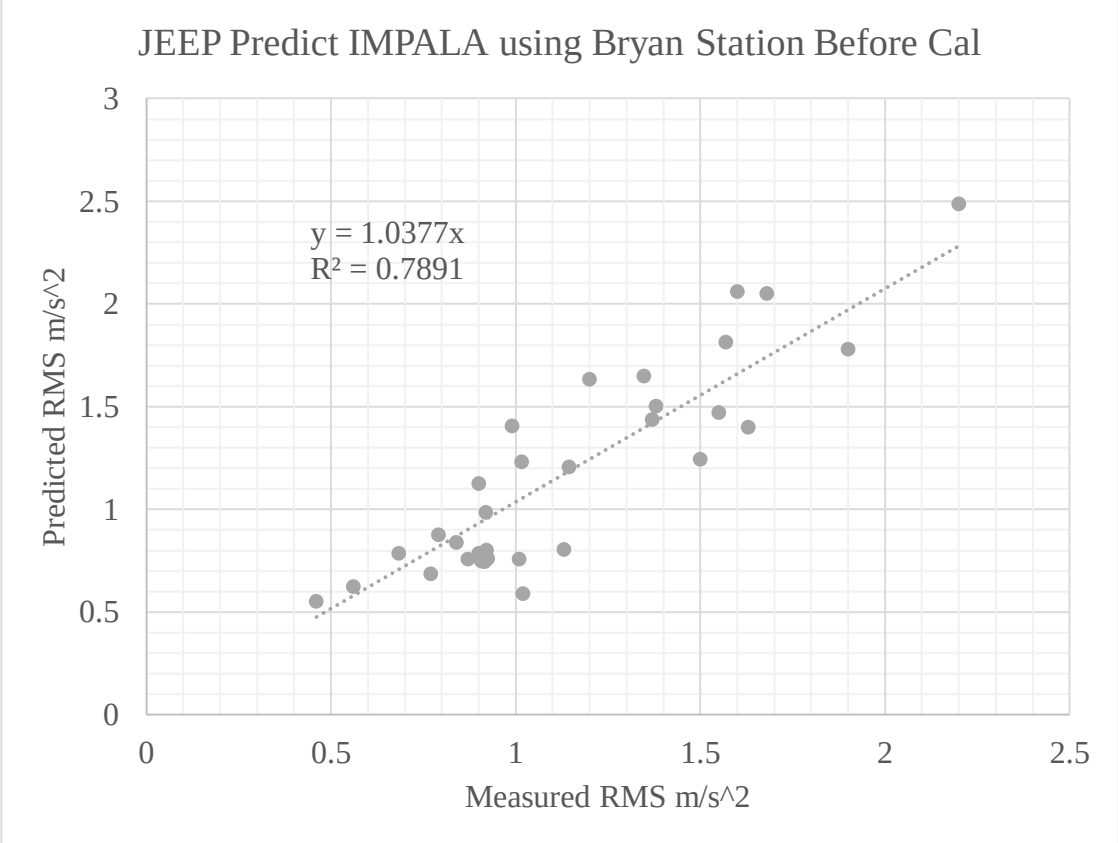
JEEP Predict IMPALA using Bryan Station Before Cal
y = 1.0377x
R² = 0.7891
Predicted RMS m/s^2
Measured RMS m/s^2
0
0.5
1
1.5
2
2.5
3

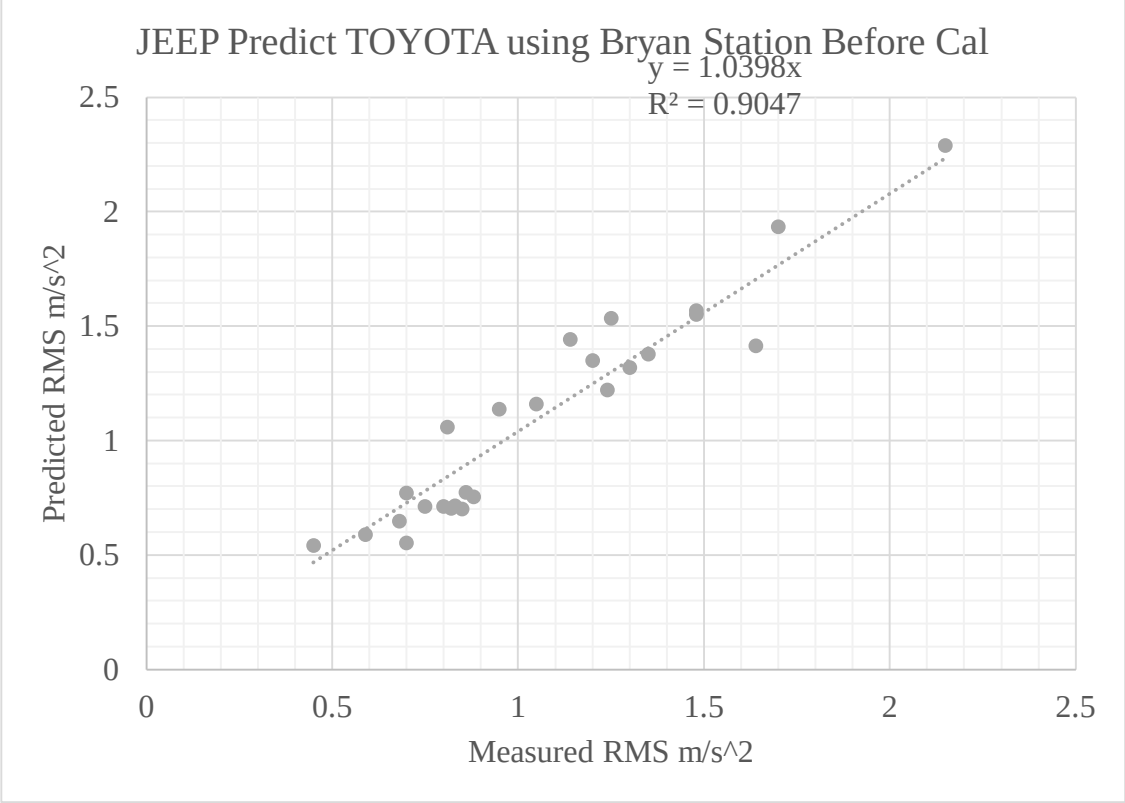
JEEP Predict TOYOTA using Bryan Station Before Cal
y = 1.0398x
R² = 0.9047
Predicted RMS m/s^2
Measured RMS m/s^2
0
0.5
1
1.5
2
2.5

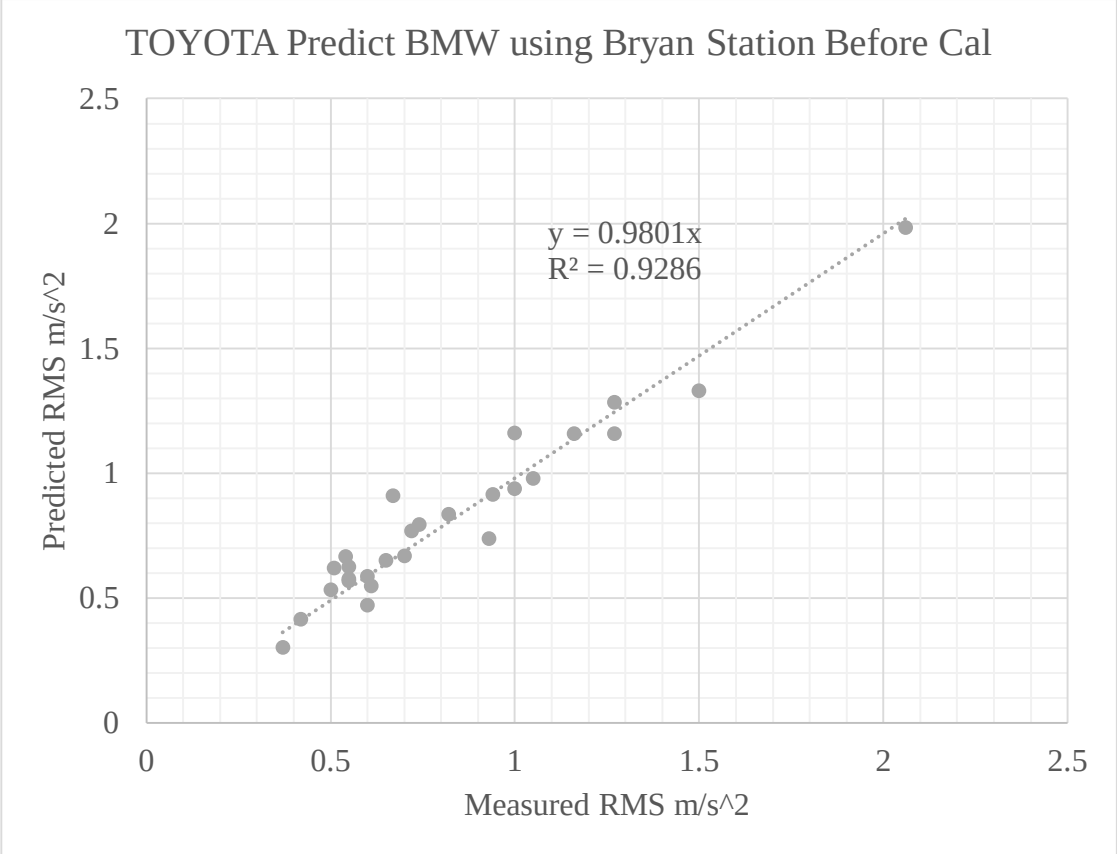
TOYOTA Predict BMW using Bryan Station Before Cal
y = 0.9801x
R² = 0.9286
Predicted RMS m/s^2
Measured RMS m/s^2
0
0.5
1
1.5
2
2.5

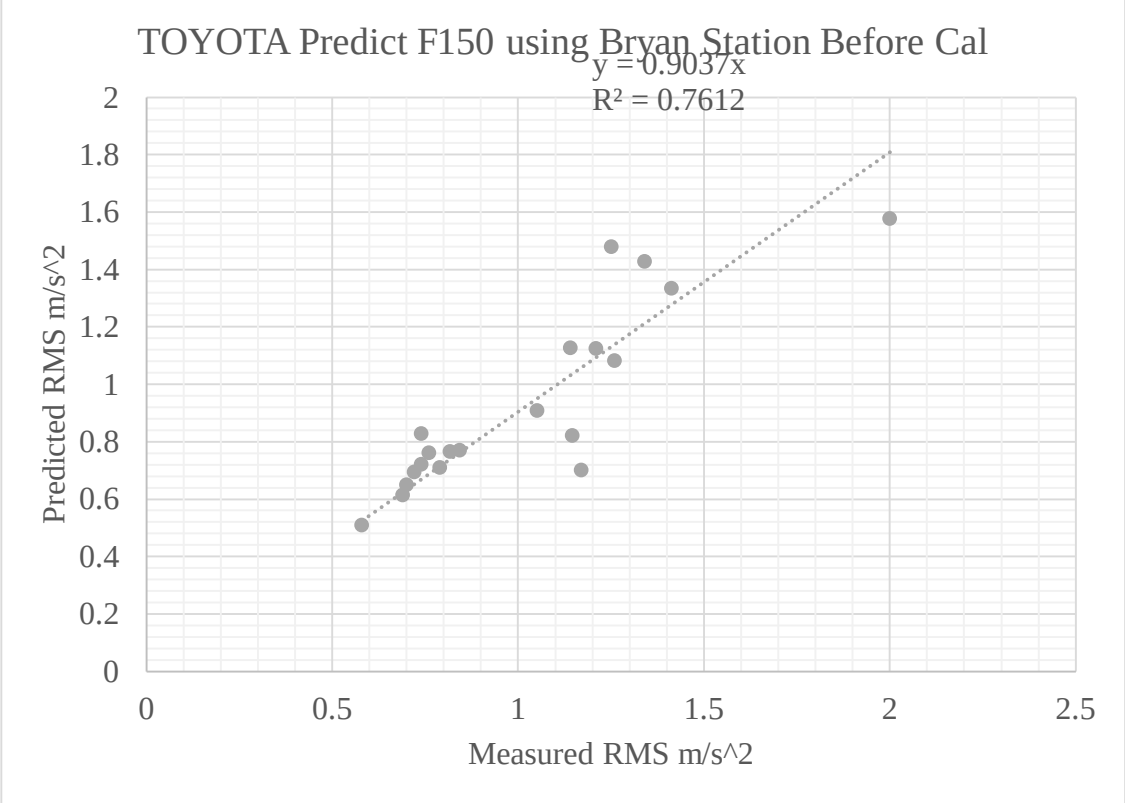
TOYOTA Predict F150 using Bryan Station Before Cal
y = 0.9037x
R² = 0.7612
Predicted RMS m/s^2
Measured RMS m/s^2
0
0.2
0.4
0.6
0.8
1
1.2
1.4
1.6
1.8
2
0
0.5
1
1.5
2
2.5

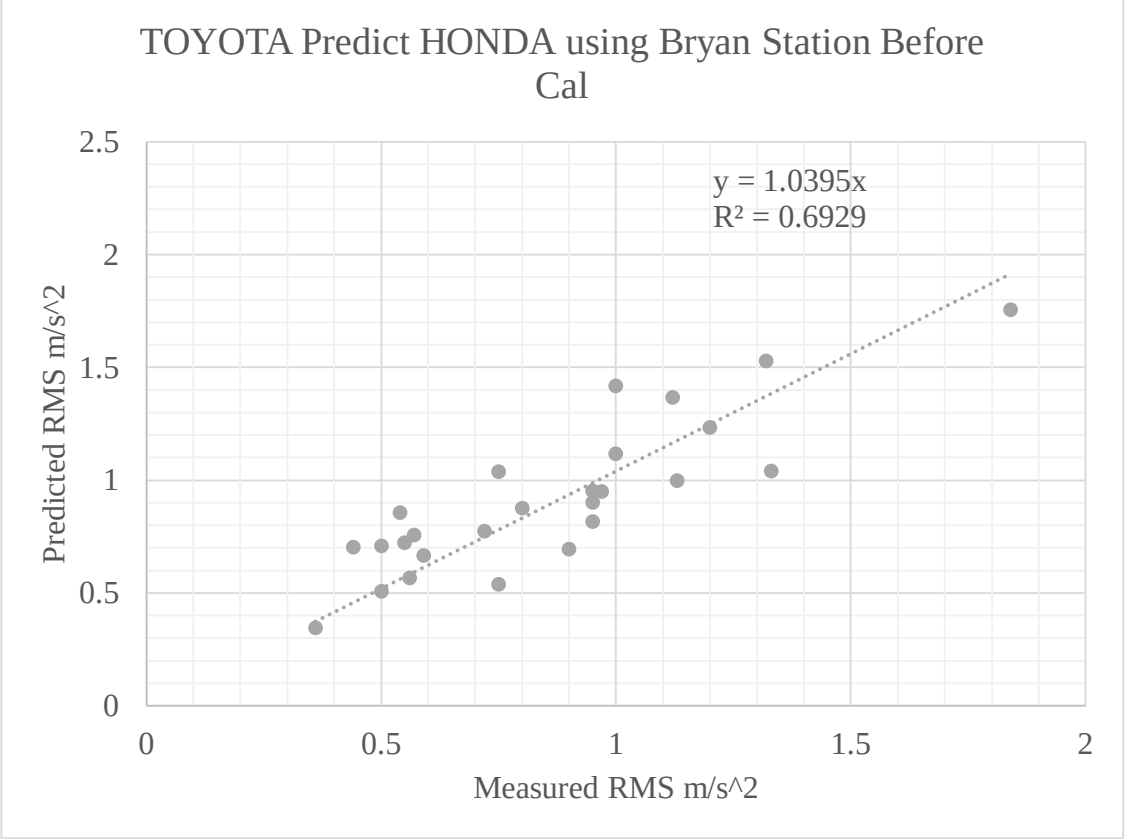
TOYOTA Predict HONDA using Bryan Station Before Cal
y = 1.0395x
R² = 0.6929
Predicted RMS m/s^2
Measured RMS m/s^2
0
0.5
1
1.5
2
2.5
0
0.5
1
1.5
2

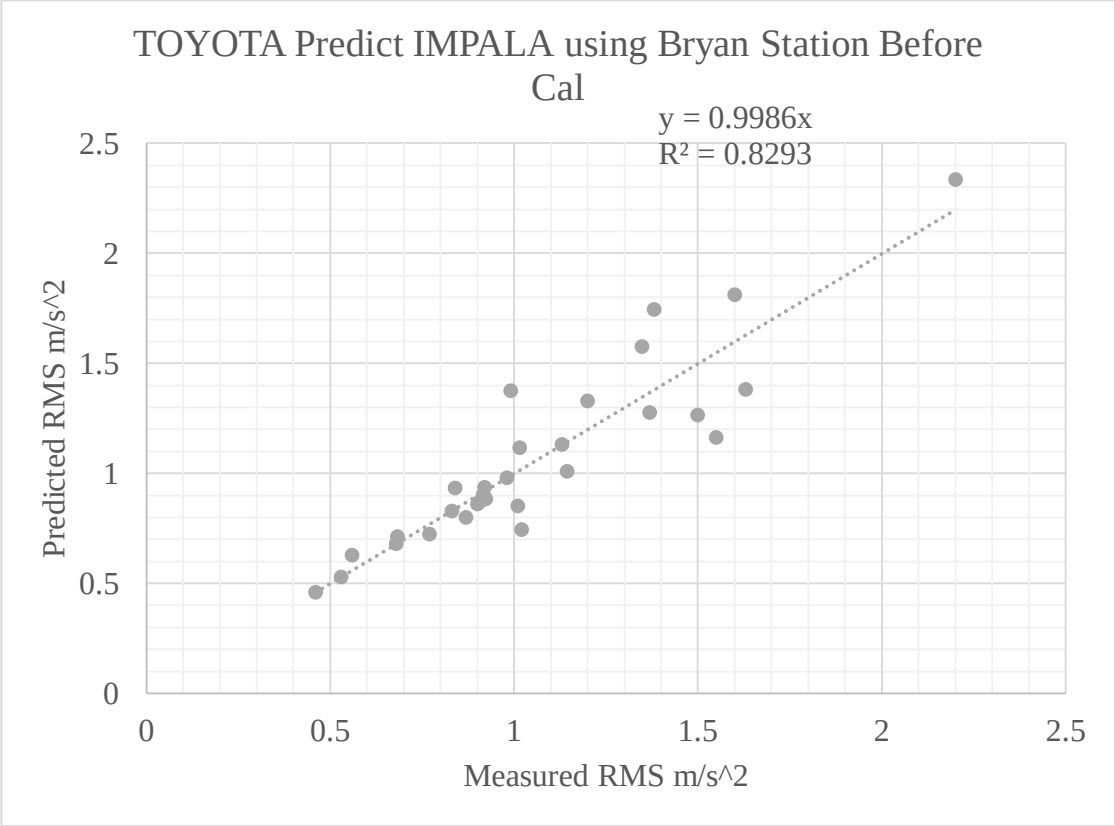
TOYOTA Predict IMPALA using Bryan Station Before Cal
y = 0.9986x
R² = 0.8293
Predicted RMS m/s^2
Measured RMS m/s^2
0
0.5
1
1.5
2
2.5

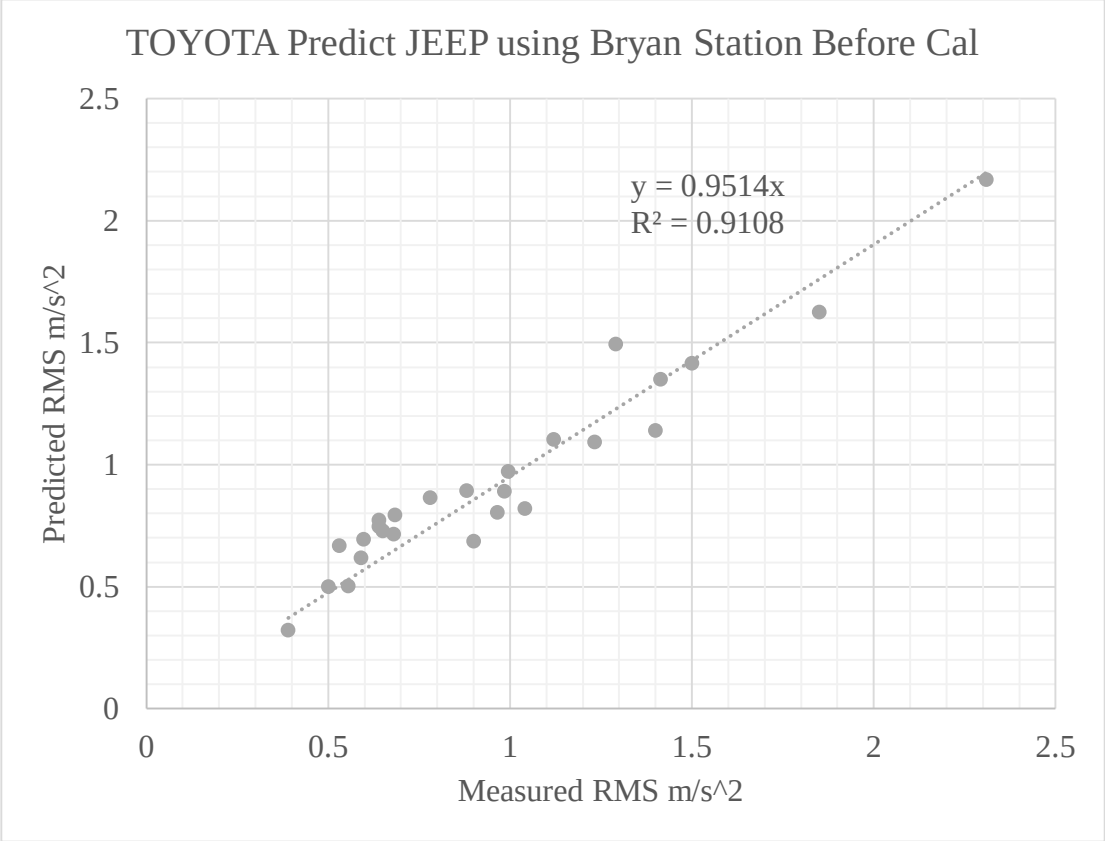
TOYOTA Predict JEEP using Bryan Station Before Cal
y = 0.9514x
R² = 0.9108
Predicted RMS m/s^2
Measured RMS m/s^2
0
0.5
1
1.5
2
2.5

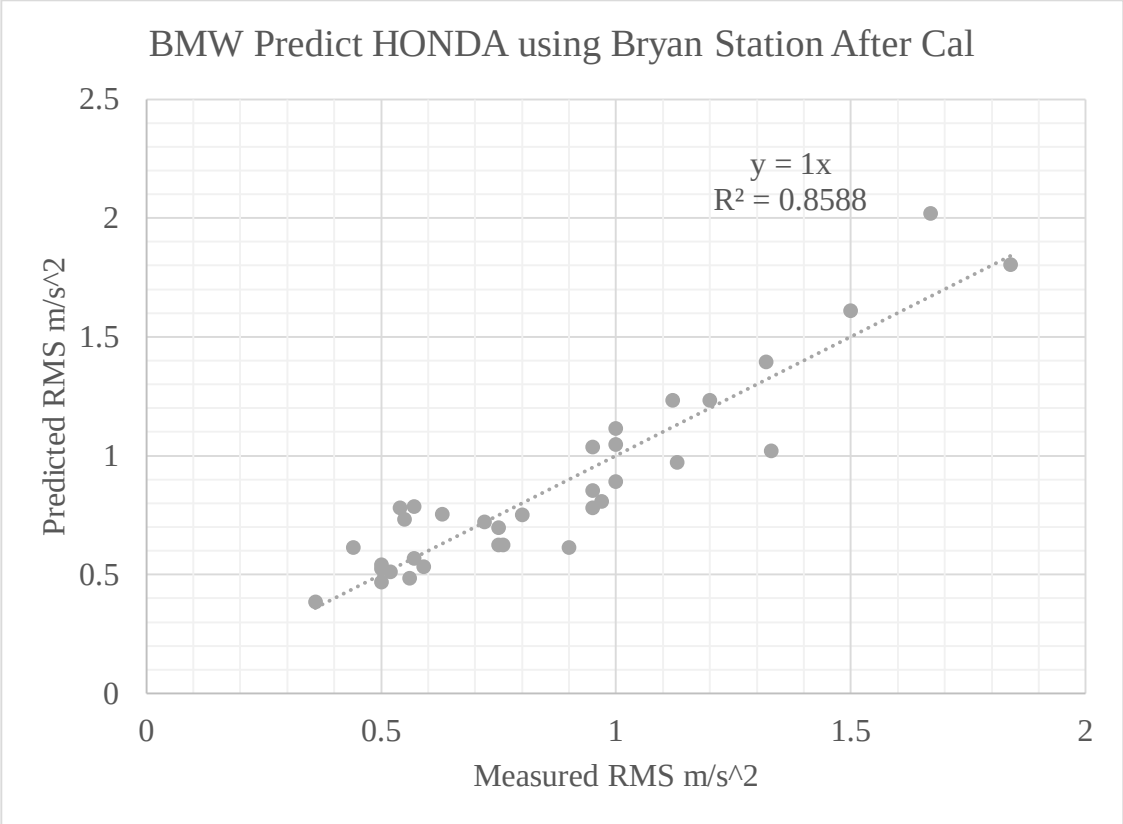
BMW Predict HONDA using Bryan Station After Cal
y = 1x
R² = 0.8588
Predicted RMS m/s^2
Measured RMS m/s^2
0
0.5
1
1.5
2
2.5

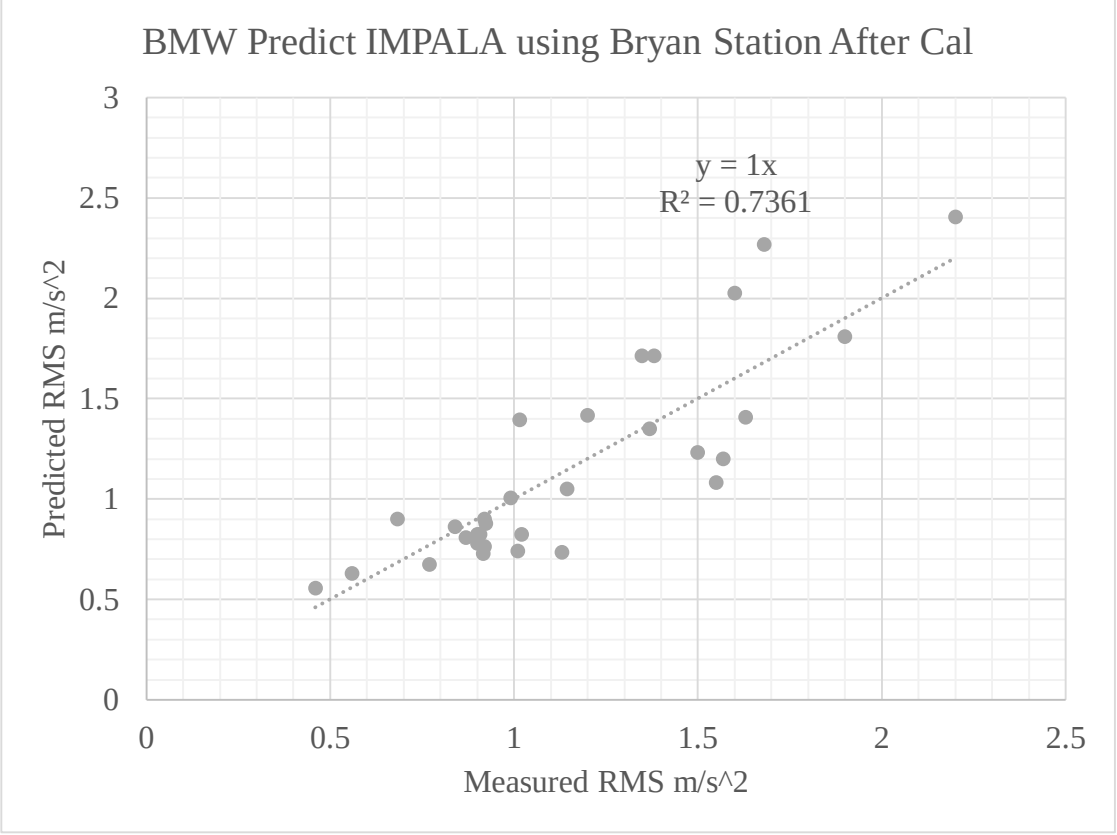
BMW Predict IMPALA using Bryan Station After Cal
y = 1x
R² = 0.7361
Predicted RMS m/s^2
Measured RMS m/s^2
0
0.5
1
1.5
2
2.5
3

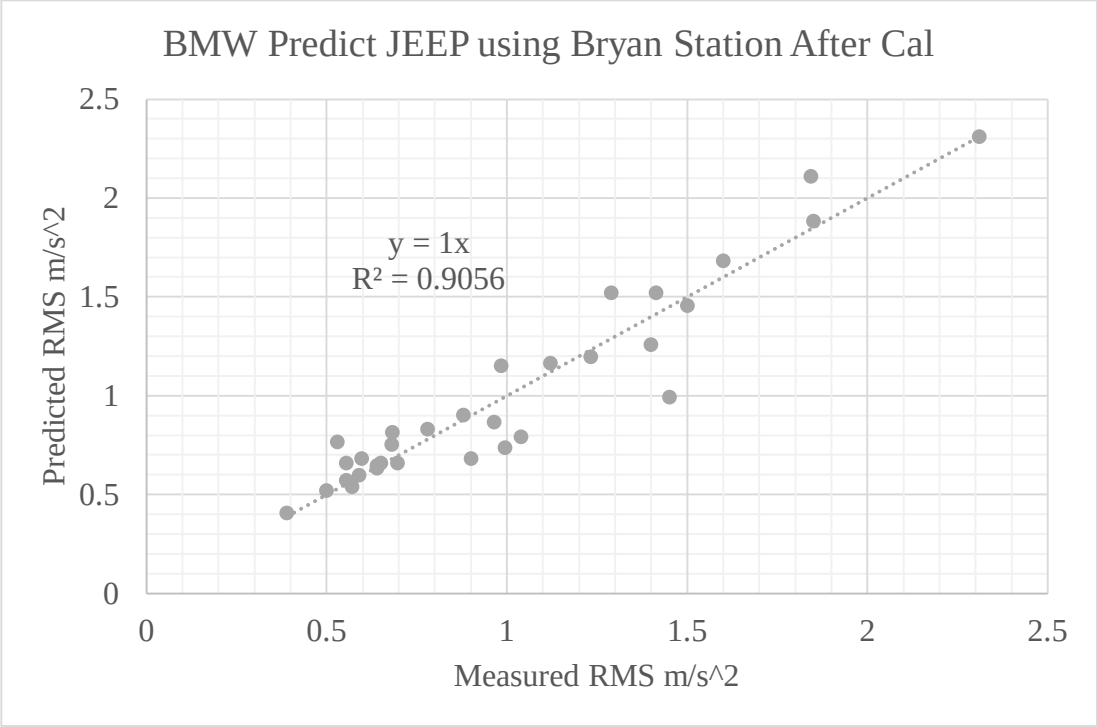
BMW Predict JEEP using Bryan Station After Cal
y = 1x
R² = 0.9056
Predicted RMS m/s^2
Measured RMS m/s^2
0
0.5
1
1.5
2
2.5

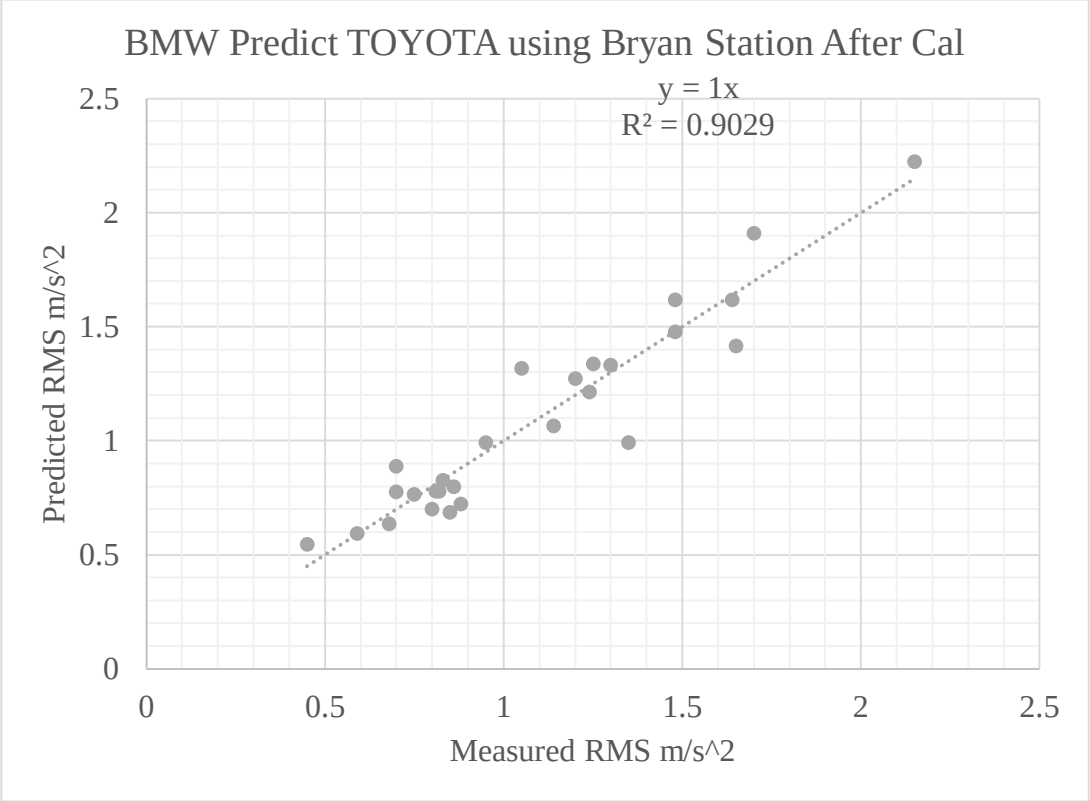
BMW Predict TOYOTA using Bryan Station After Cal
y = 1x
R² = 0.9029
Predicted RMS m/s^2
Measured RMS m/s^2
0
0.5
1
1.5
2
2.5

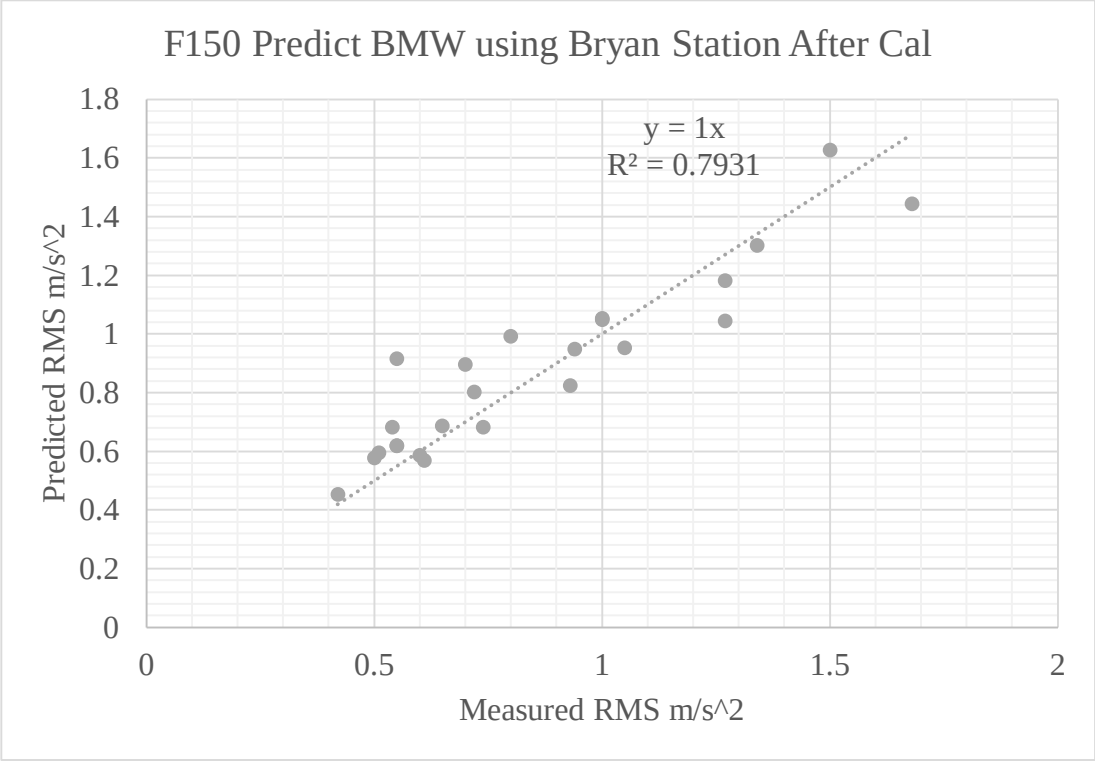
F150 Predict BMW using Bryan Station After Cal
y = 1x
R² = 0.7931
Predicted RMS m/s^2
Measured RMS m/s^2
0
0.2
0.4
0.6
0.8
1
1.2
1.4
1.6
1.8
0
0.5
1
1.5
2

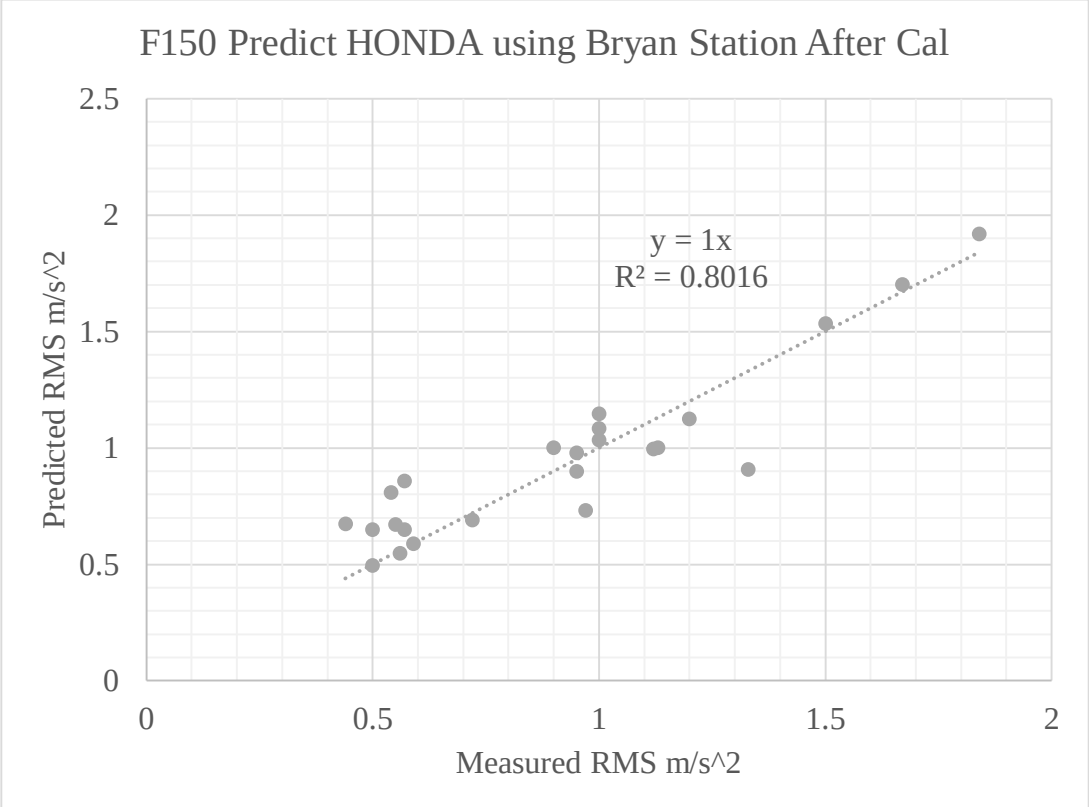
F150 Predict HONDA using Bryan Station After Cal
y = 1x
R² = 0.8016
Predicted RMS m/s^2
Measured RMS m/s^2
0
0.5
1
1.5
2
2.5
0
0.5
1
1.5
2

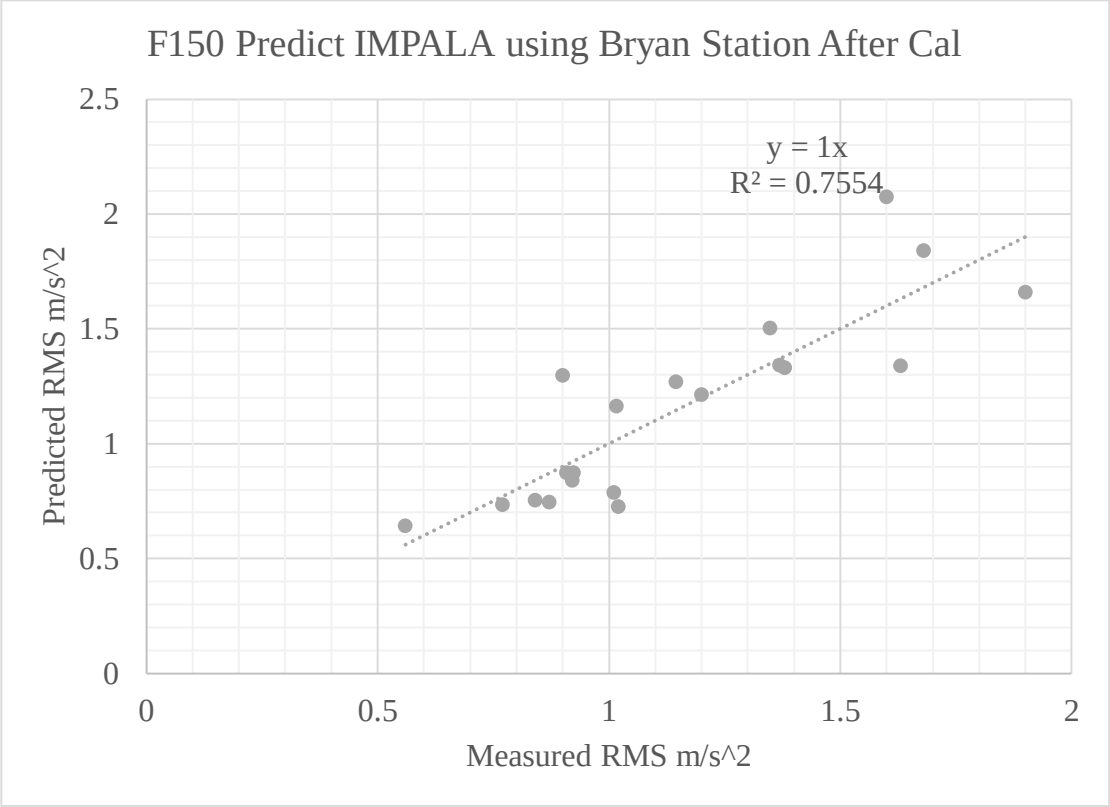
F150 Predict IMPALA using Bryan Station After Cal
y = 1x
R² = 0.7554
Predicted RMS m/s^2
Measured RMS m/s^2
0
0.5
1
1.5
2
2.5

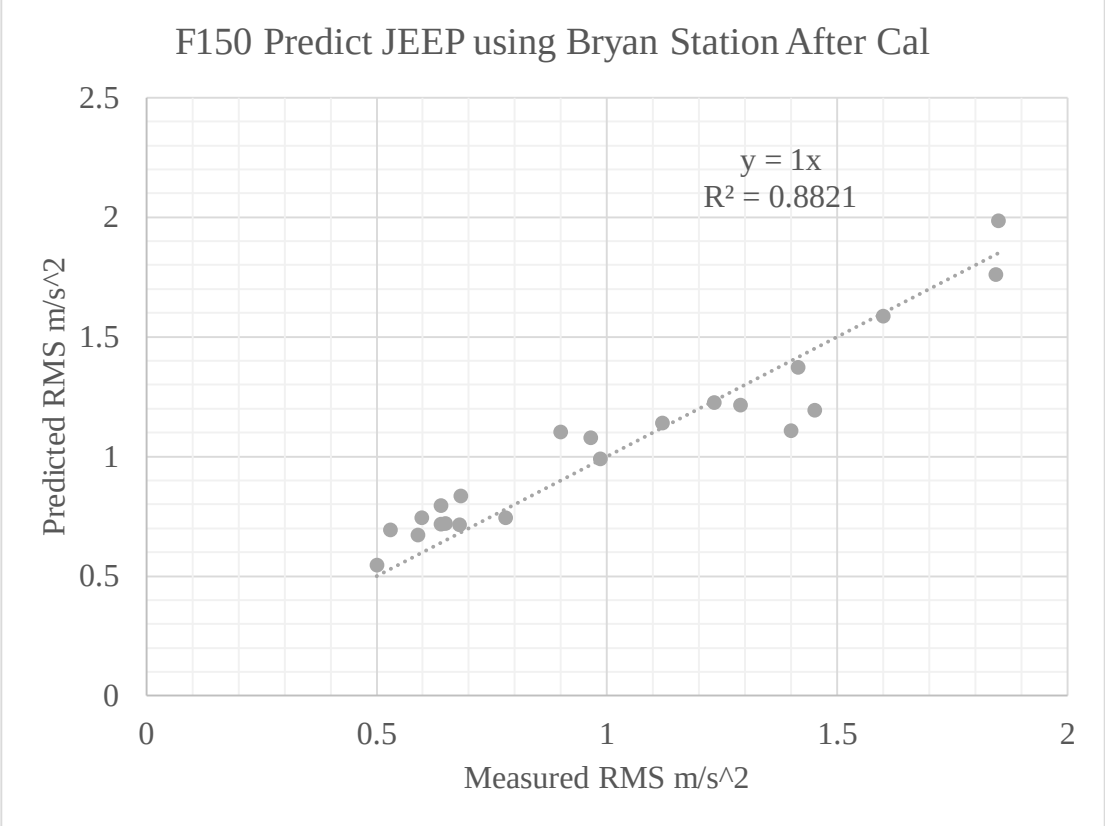
F150 Predict JEEP using Bryan Station After Cal
y = 1x
R² = 0.8821
Predicted RMS m/s^2
Measured RMS m/s^2
0
0.5
1
1.5
2
2.5

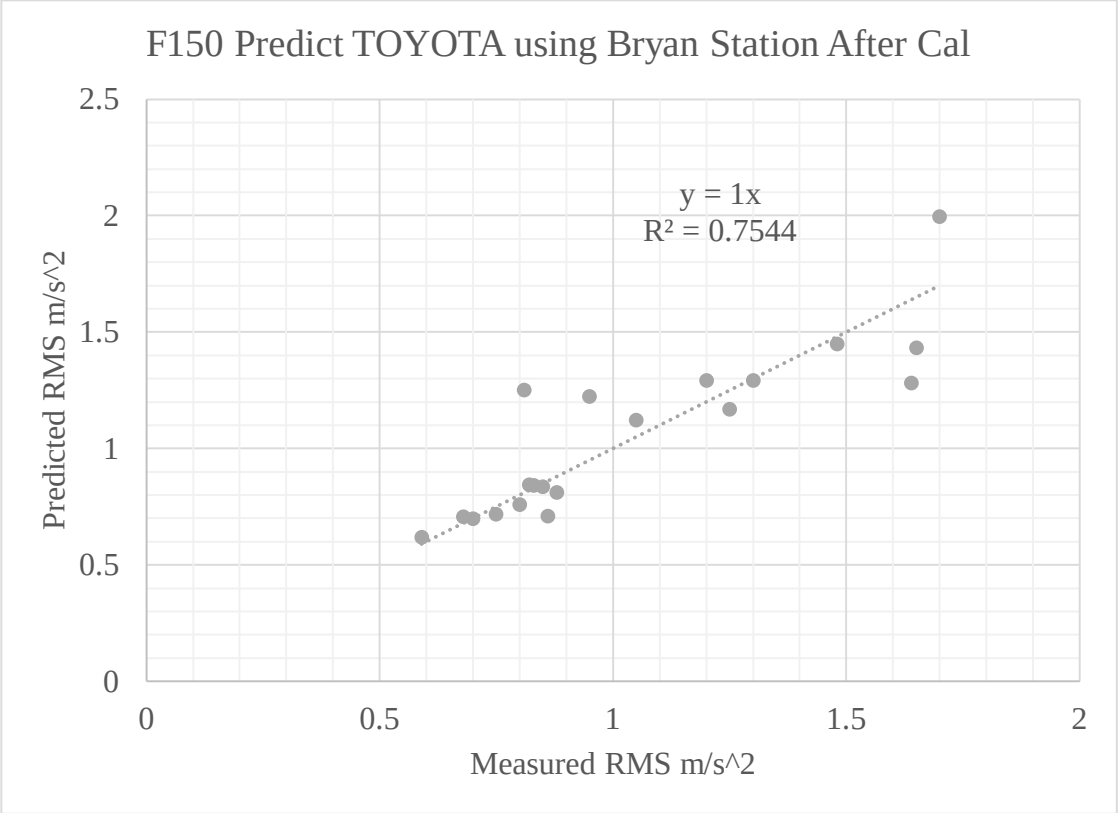
F150 Predict TOYOTA using Bryan Station After Cal
y = 1x
R² = 0.7544
Predicted RMS m/s^2
Measured RMS m/s^2
0
0.5
1
1.5
2
2.5

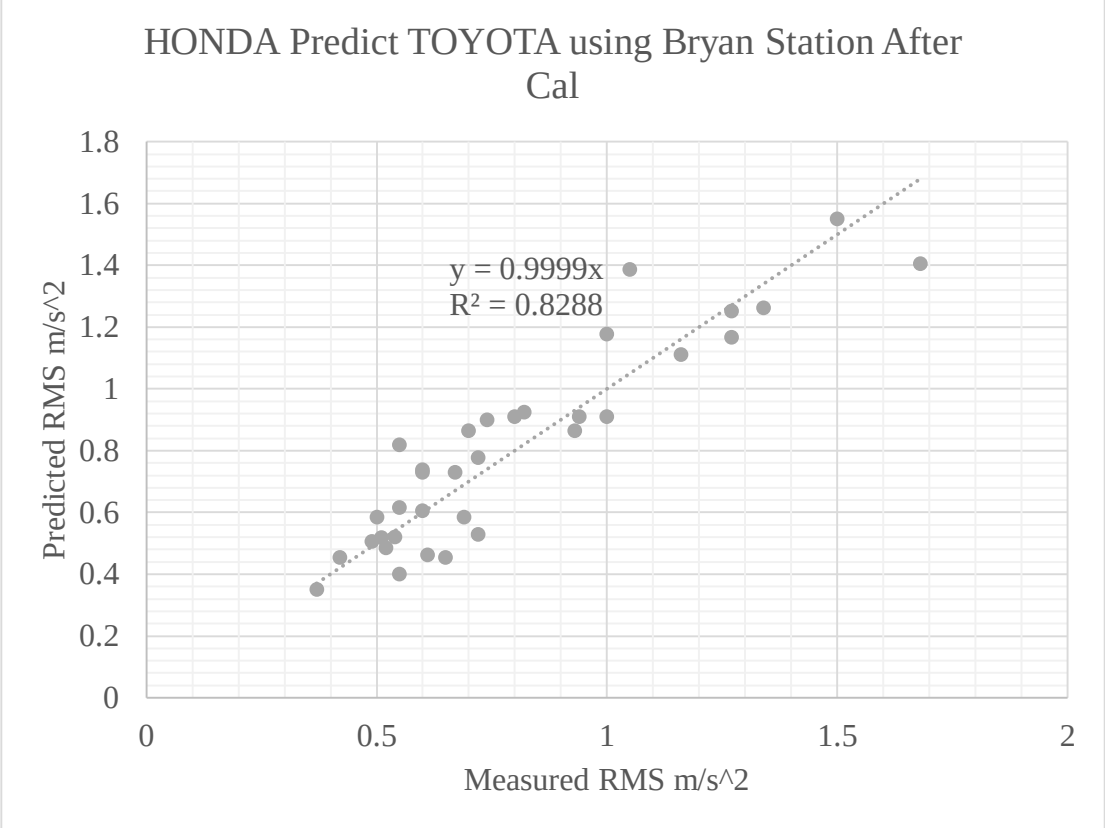
HONDA Predict TOYOTA using Bryan Station After Cal
y = 0.9999x
R² = 0.8288
Predicted RMS m/s^2
Measured RMS m/s^2
0
0.2
0.4
0.6
0.8
1
1.2
1.4
1.6
1.8
2

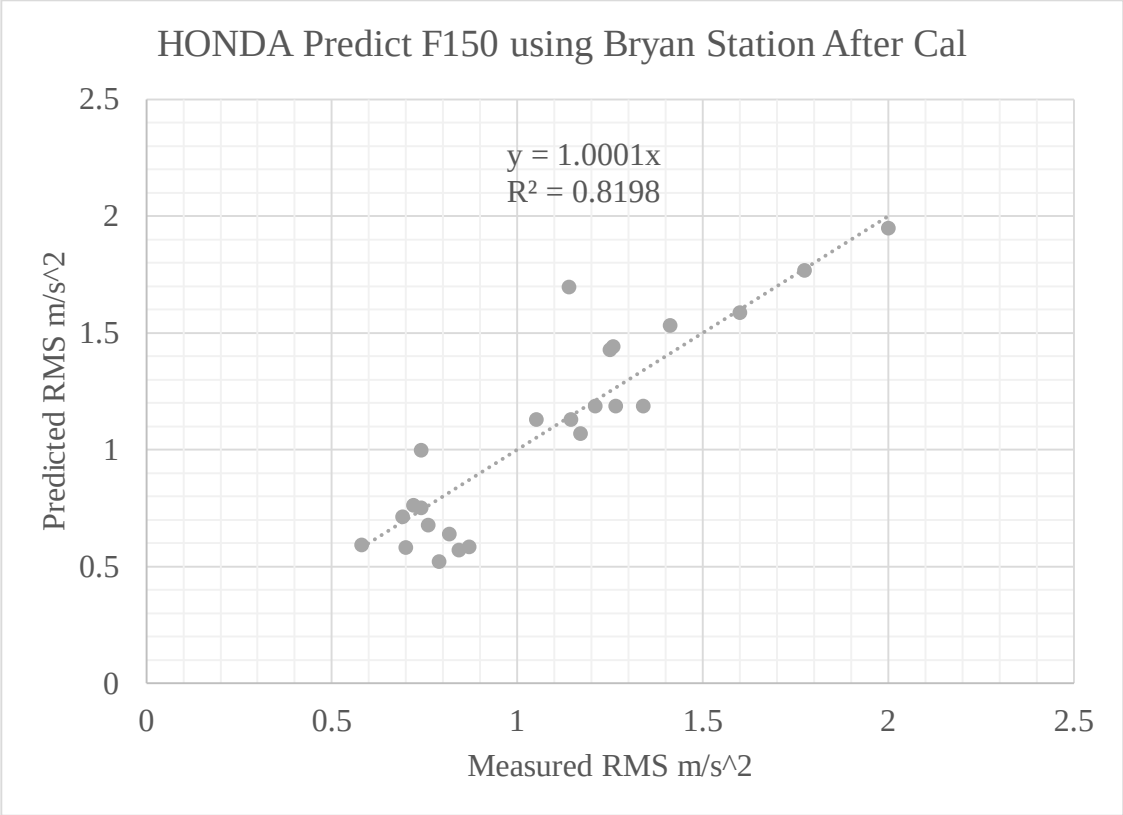
HONDA Predict F150 using Bryan Station After Cal
y = 1.0001x
R² = 0.8198
Predicted RMS m/s^2
Measured RMS m/s^2
0
0.5
1
1.5
2
2.5

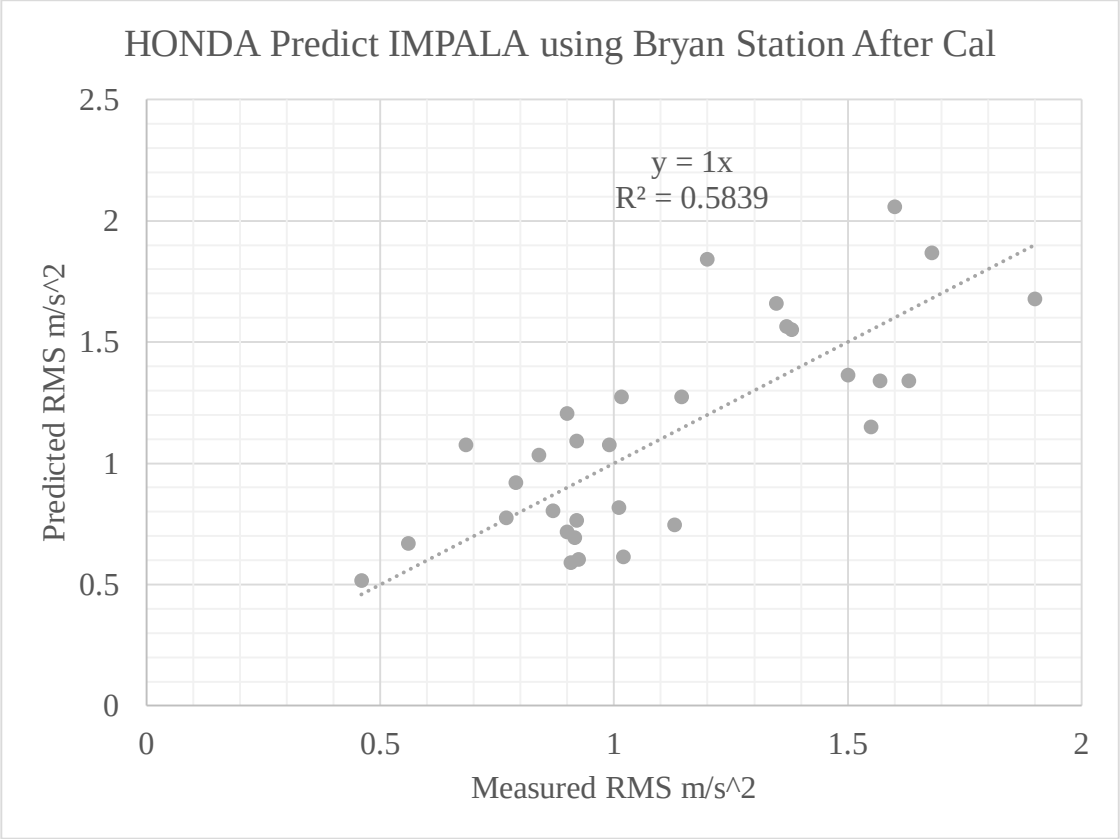
HONDA Predict IMPALA using Bryan Station After Cal
y = 1x
R² = 0.5839
Predicted RMS m/s^2
Measured RMS m/s^2
0
0.5
1
1.5
2
2.5

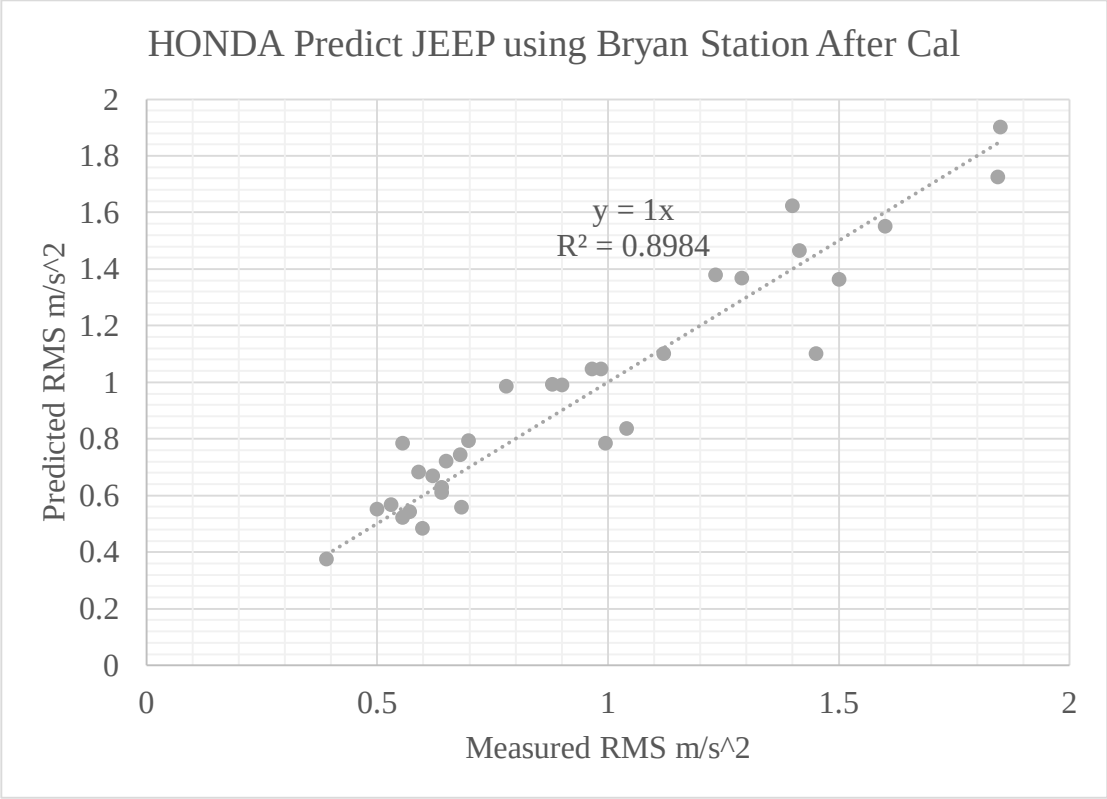
HONDA Predict JEEP using Bryan Station After Cal
y = 1x
R² = 0.8984
Predicted RMS m/s^2
Measured RMS m/s^2
0
0.2
0.4
0.6
0.8
1
1.2
1.4
1.6
1.8
2
0
0.5
1
1.5
2

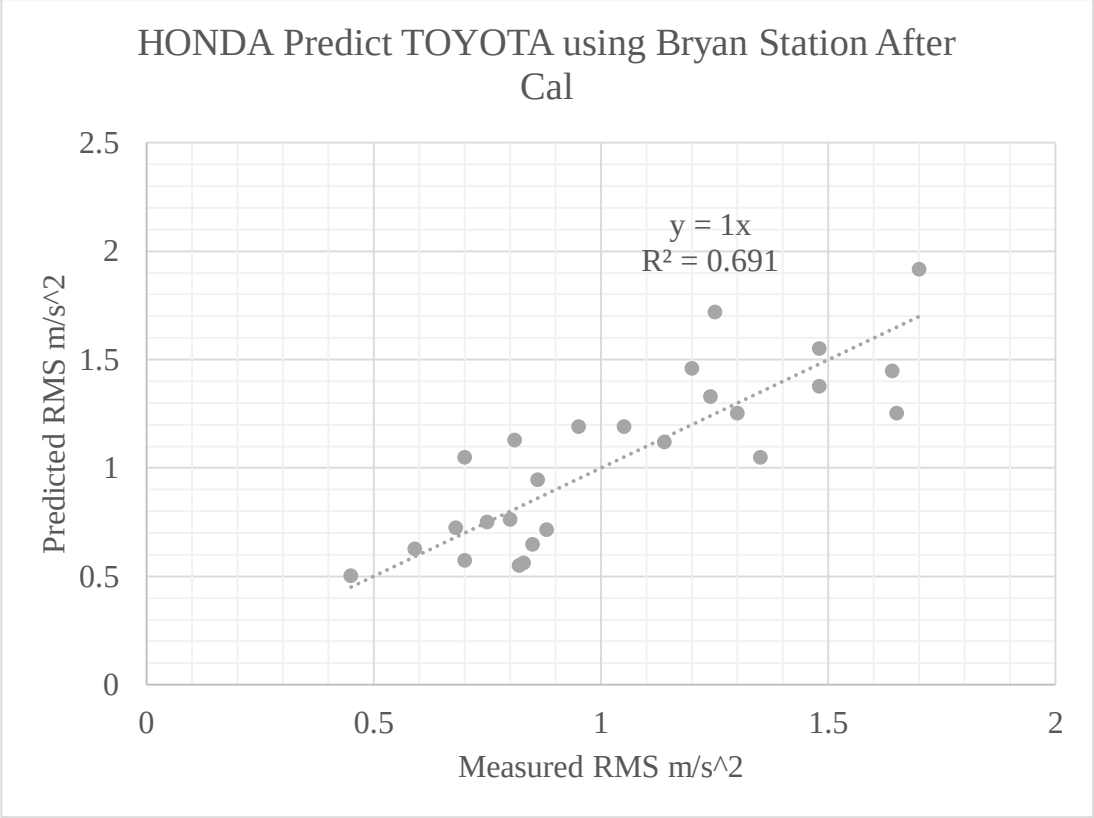
HONDA Predict TOYOTA using Bryan Station After Cal
y = 1x
R² = 0.691
Predicted RMS m/s^2
Measured RMS m/s^2
0
0.5
1
1.5
2
2.5
0
0.5
1
1.5
2

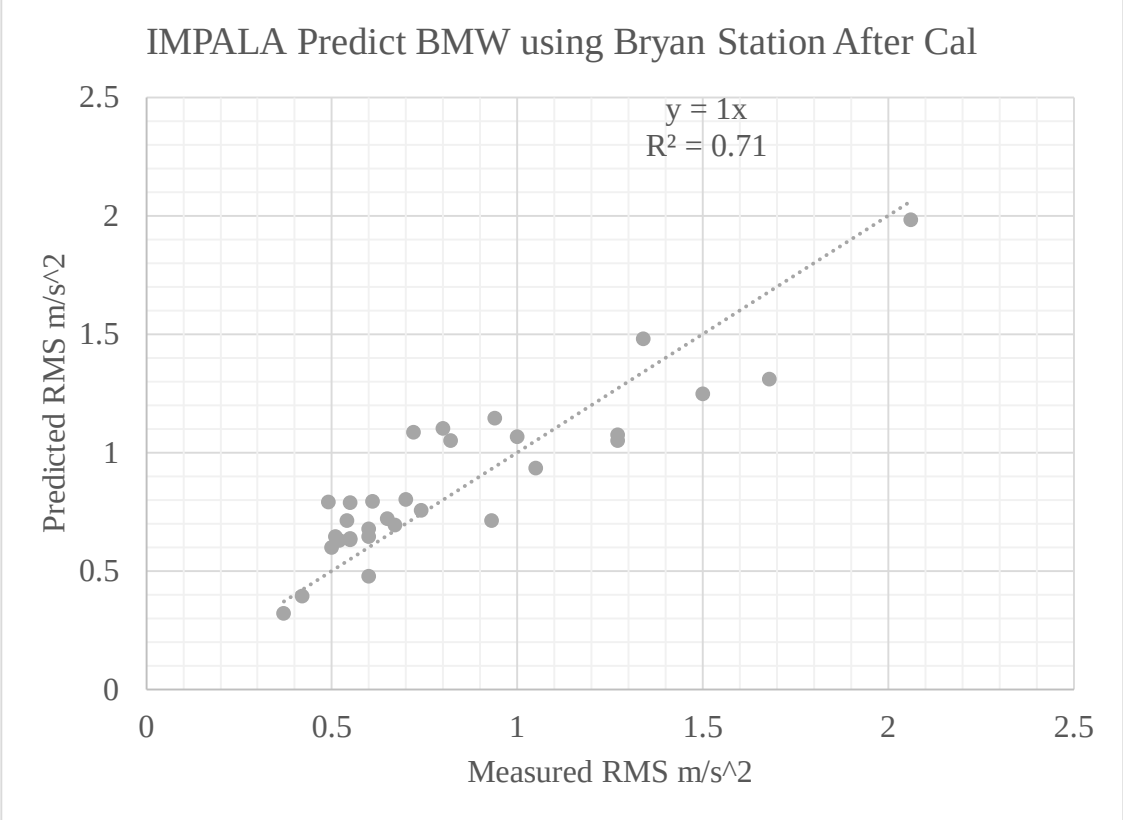
IMPALA Predict BMW using Bryan Station After Cal
y = 1x
R² = 0.71
Predicted RMS m/s^2
Measured RMS m/s^2
0
0.5
1
1.5
2
2.5

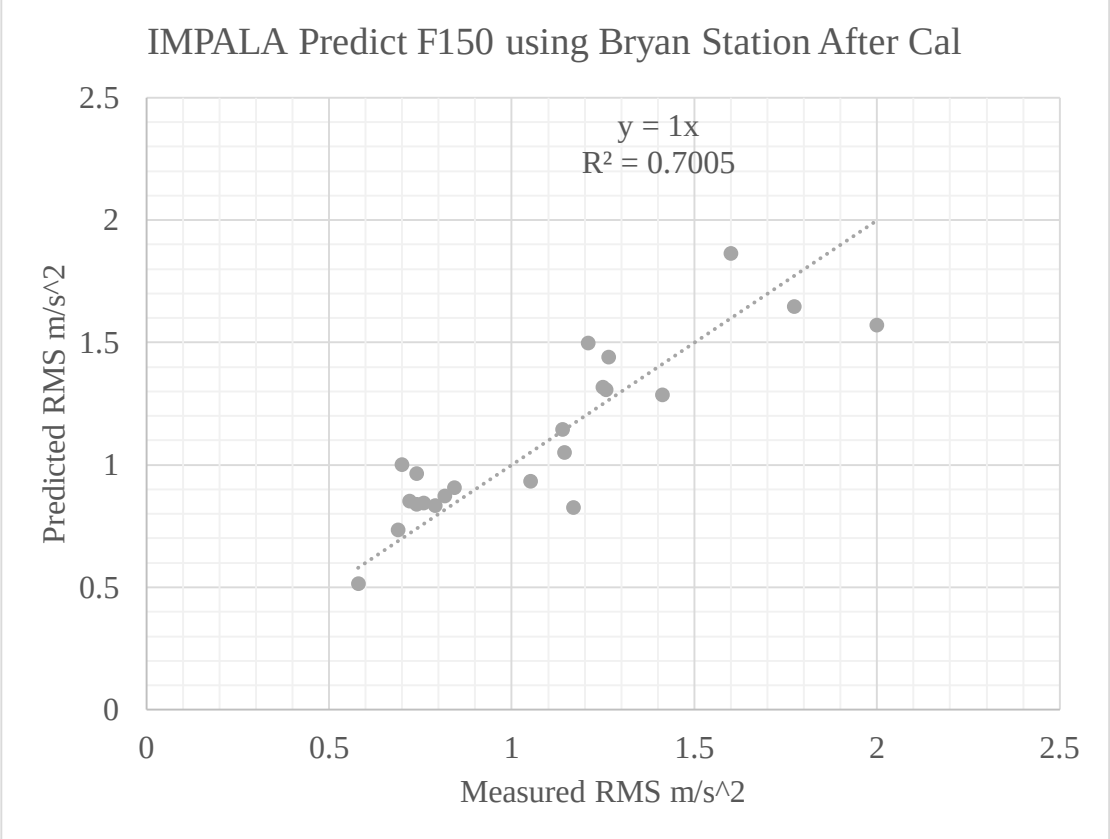
IMPALA Predict F150 using Bryan Station After Cal
y = 1x
R² = 0.7005
Predicted RMS m/s^2
Measured RMS m/s^2
0
0.5
1
1.5
2
2.5

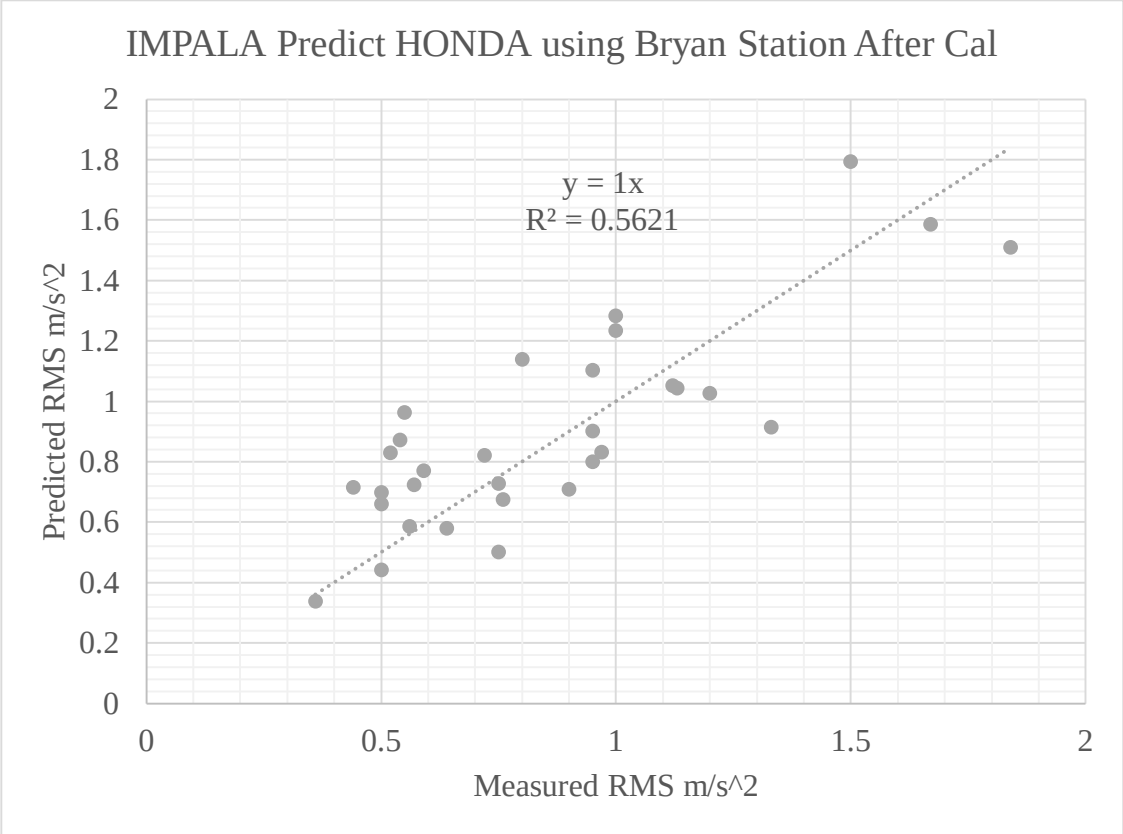
IMPALA Predict HONDA using Bryan Station After Cal
y = 1x
R² = 0.5621
Predicted RMS m/s^2
Measured RMS m/s^2
0
0.2
0.4
0.6
0.8
1
1.2
1.4
1.6
1.8
2
0.5
1.5

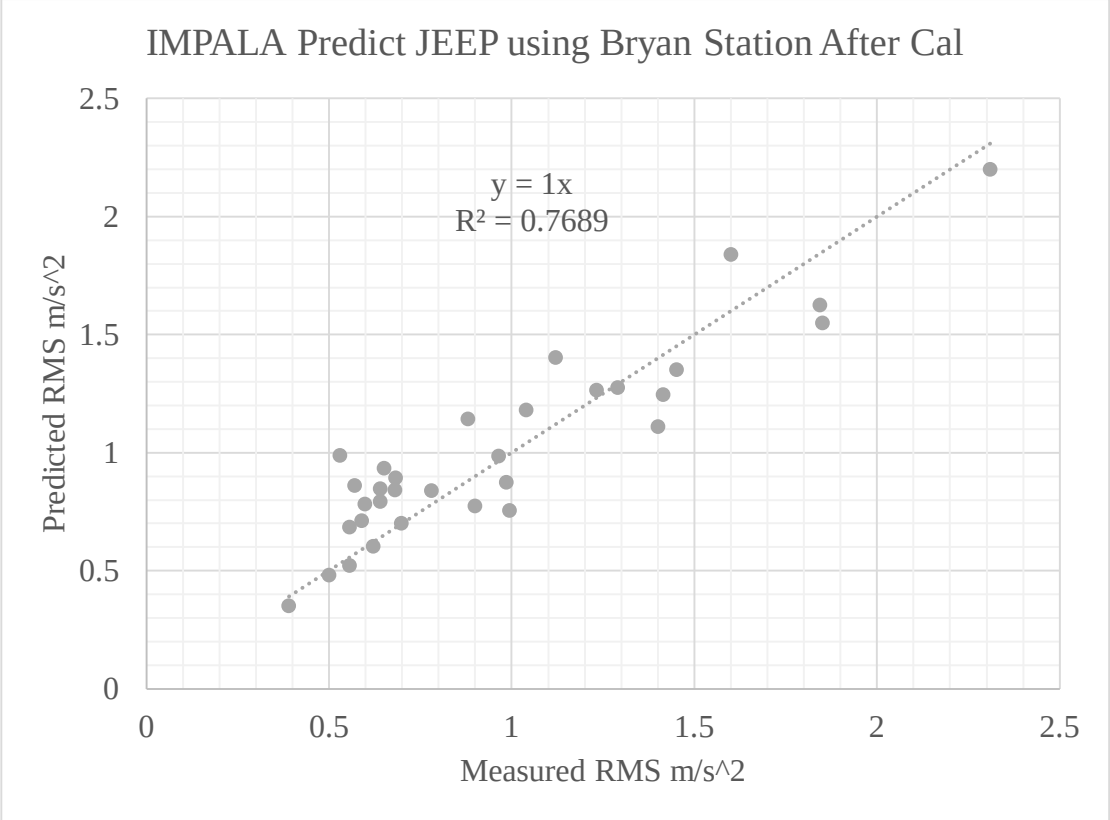
IMPALA Predict JEEP using Bryan Station After Cal
y = 1x
R² = 0.7689
Predicted RMS m/s^2
Measured RMS m/s^2
0
0.5
1
1.5
2
2.5

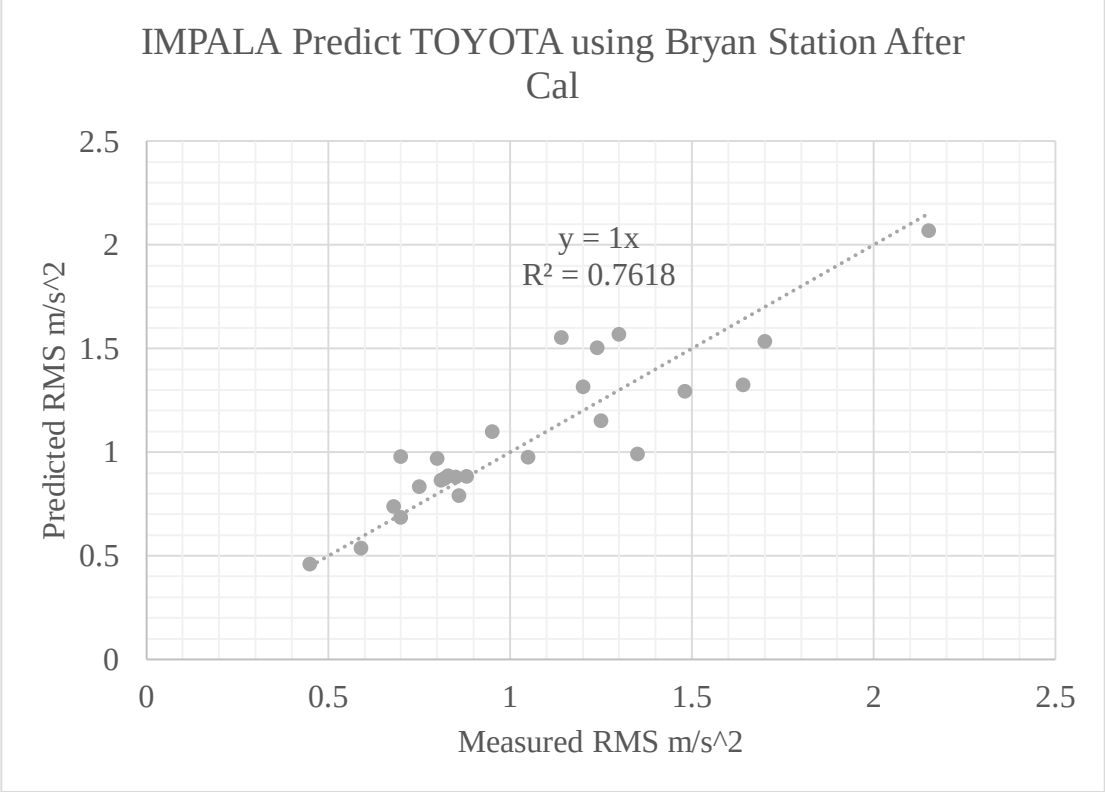
IMPALA Predict TOYOTA using Bryan Station After Cal
y = 1x
R² = 0.7618
Predicted RMS m/s^2
Measured RMS m/s^2
0
0.5
1
1.5
2
2.5

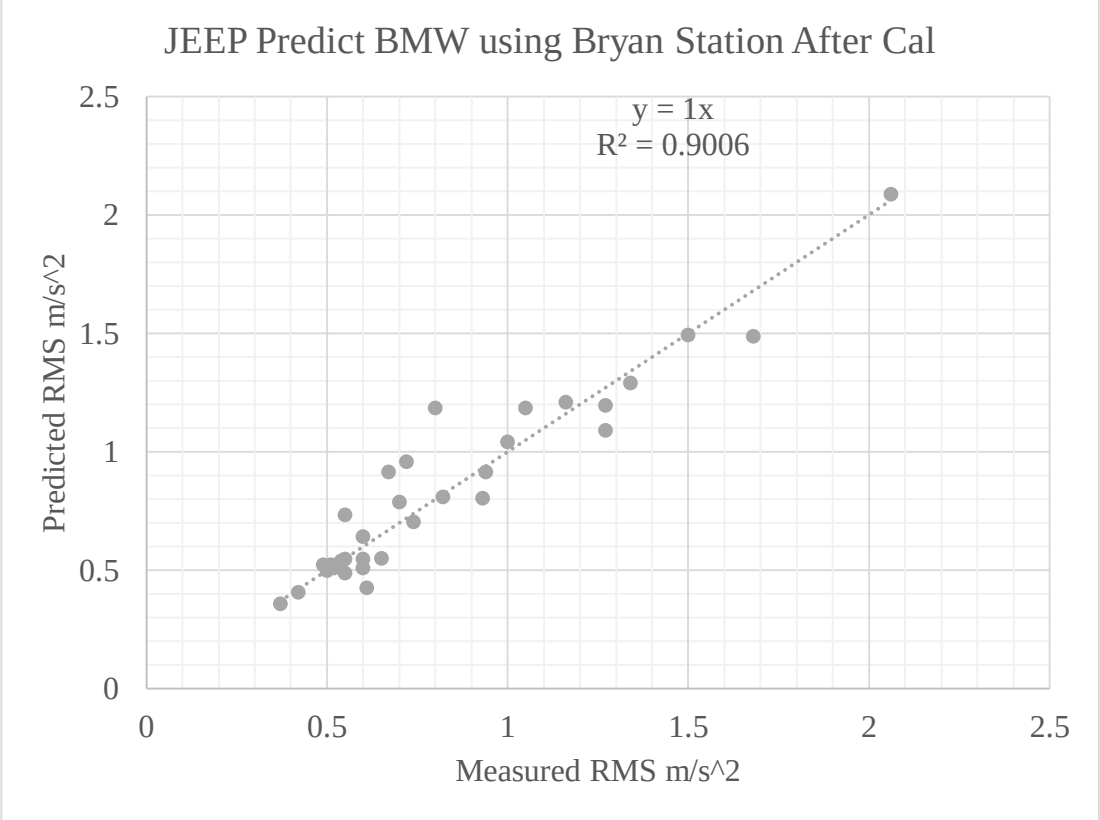
JEEP Predict BMW using Bryan Station After Cal
y = 1x
R² = 0.9006
Predicted RMS m/s^2
Measured RMS m/s^2
0
0.5
1
1.5
2
2.5

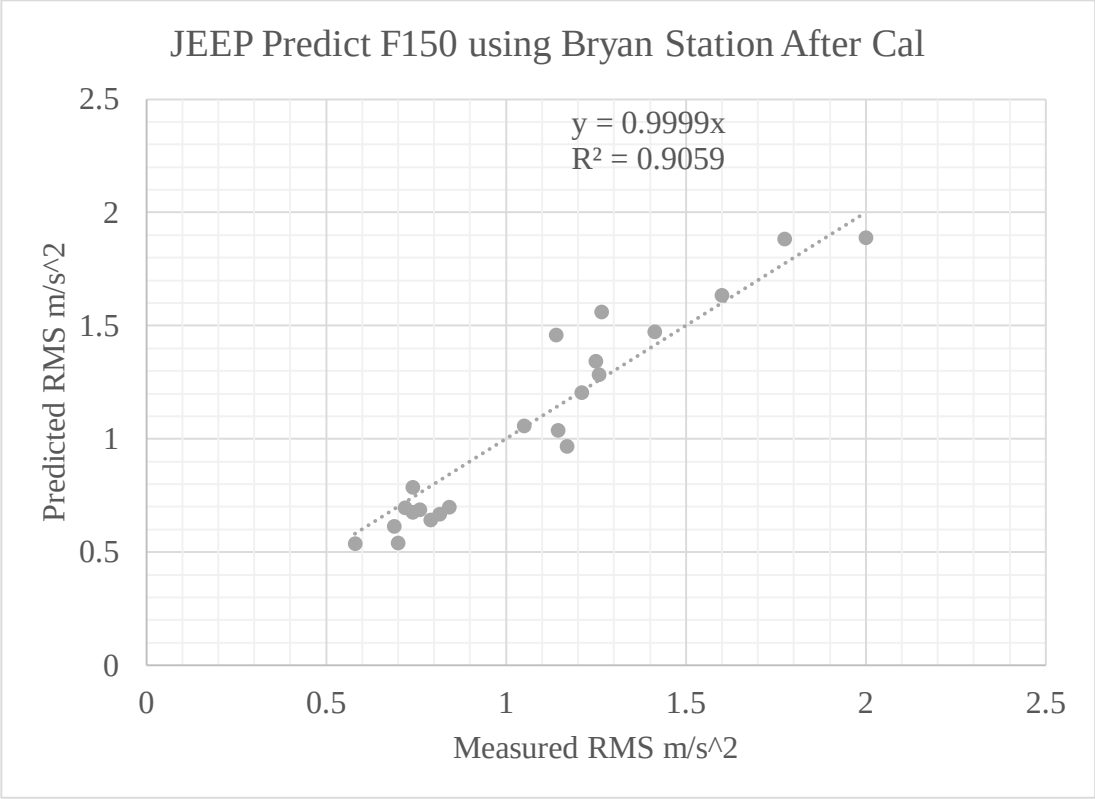
JEEP Predict F150 using Bryan Station After Cal
y = 0.9999x
R² = 0.9059
Predicted RMS m/s^2
Measured RMS m/s^2
0
0.5
1
1.5
2
2.5

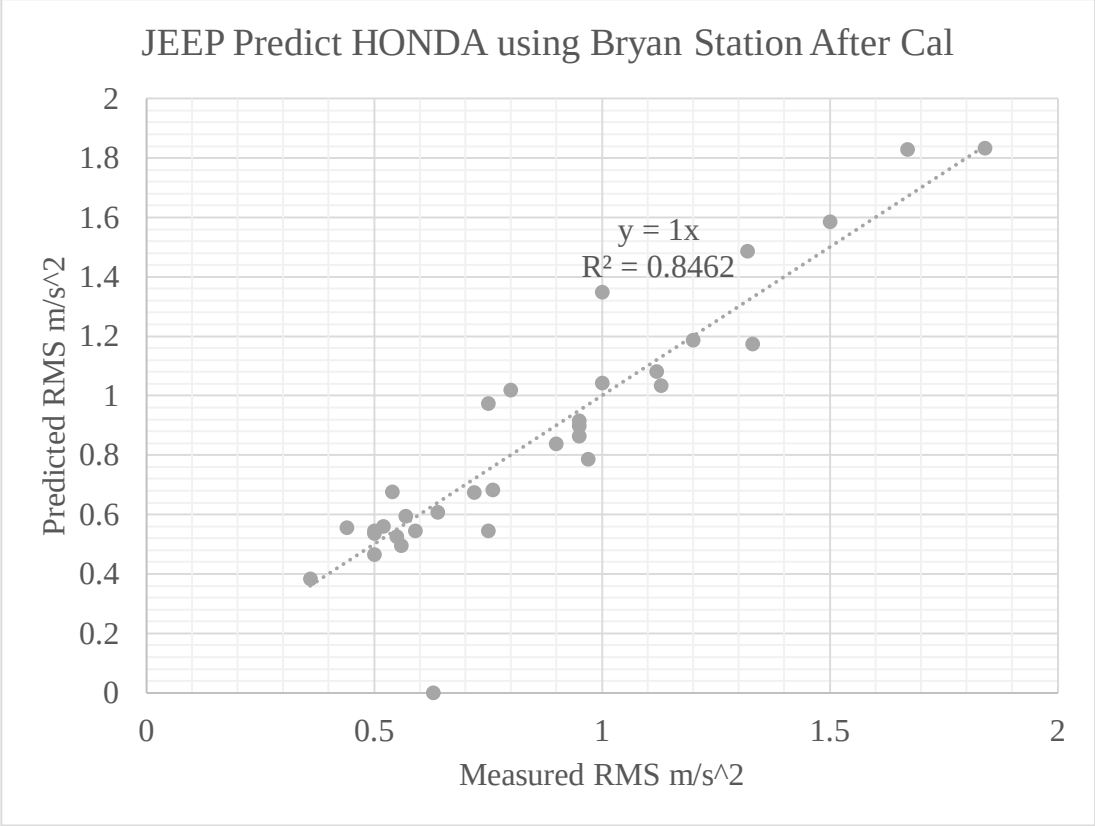
JEEP Predict HONDA using Bryan Station After Cal
y = 1x
R² = 0.8462
Predicted RMS m/s^2
Measured RMS m/s^2
0
0.2
0.4
0.6
0.8
1
1.2
1.4
1.6
1.8
2

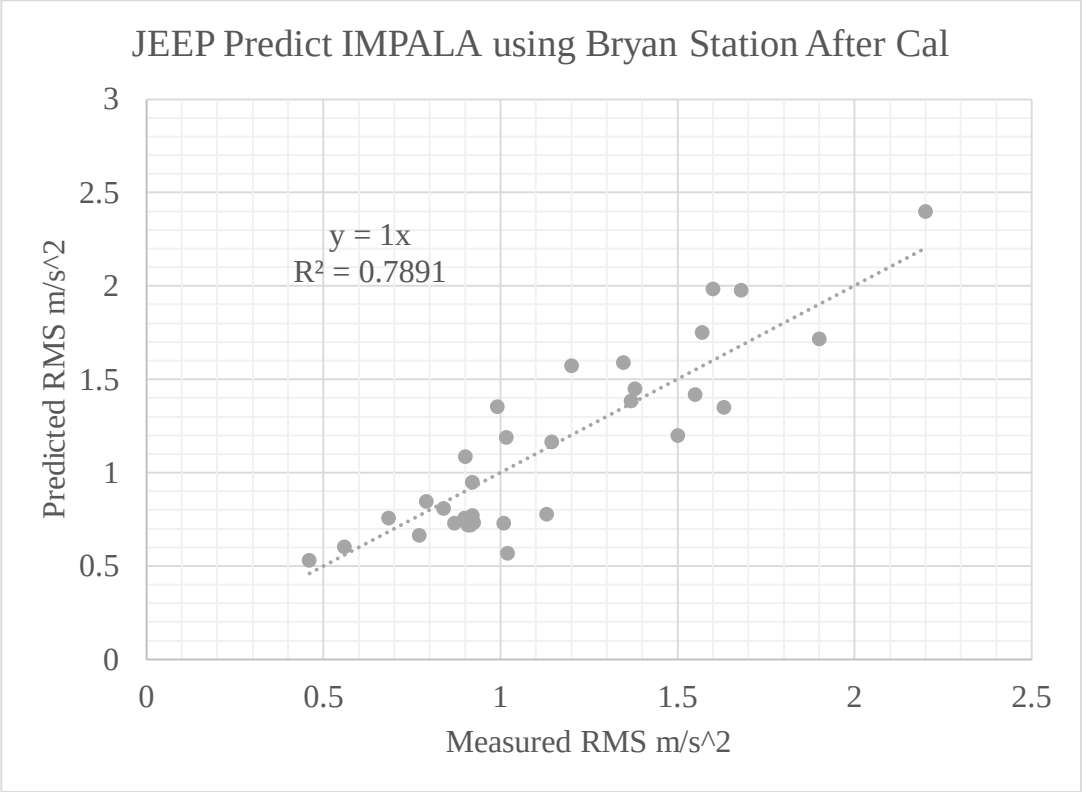
JEEP Predict IMPALA using Bryan Station After Cal
y = 1x
R² = 0.7891
Predicted RMS m/s^2
Measured RMS m/s^2
0
0.5
1
1.5
2
2.5
3

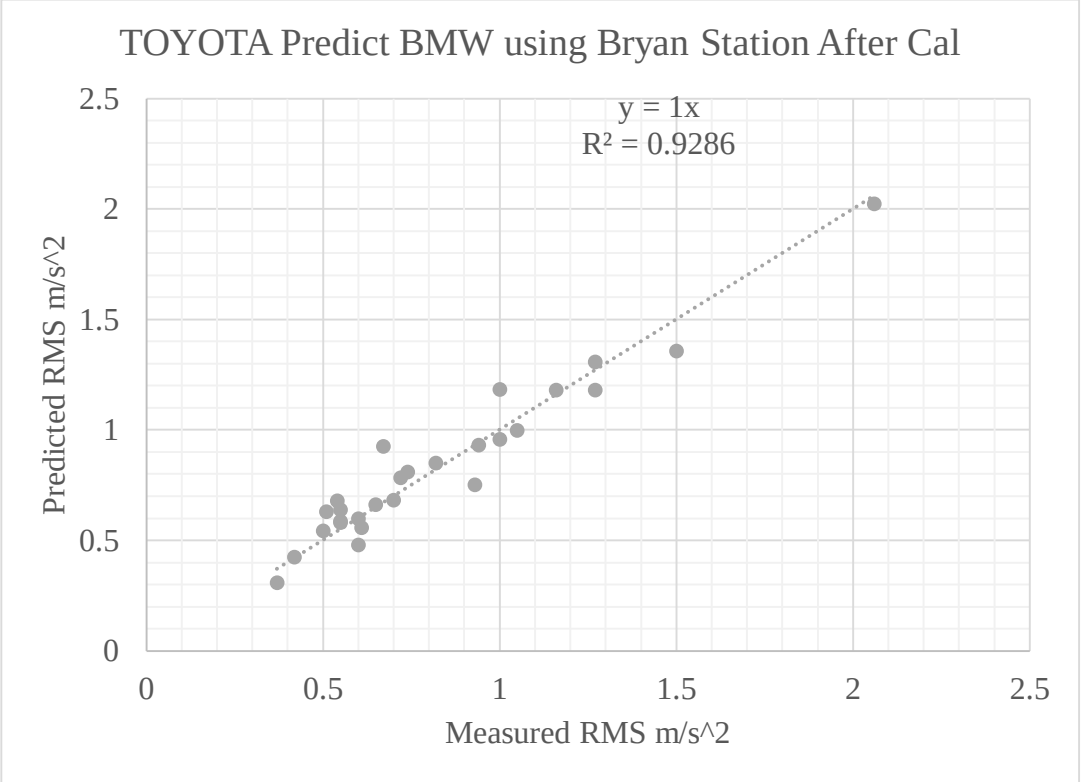
TOYOTA Predict BMW using Bryan Station After Cal
y = 1x
R² = 0.9286
Predicted RMS m/s^2
Measured RMS m/s^2
0
0.5
1
1.5
2
2.5

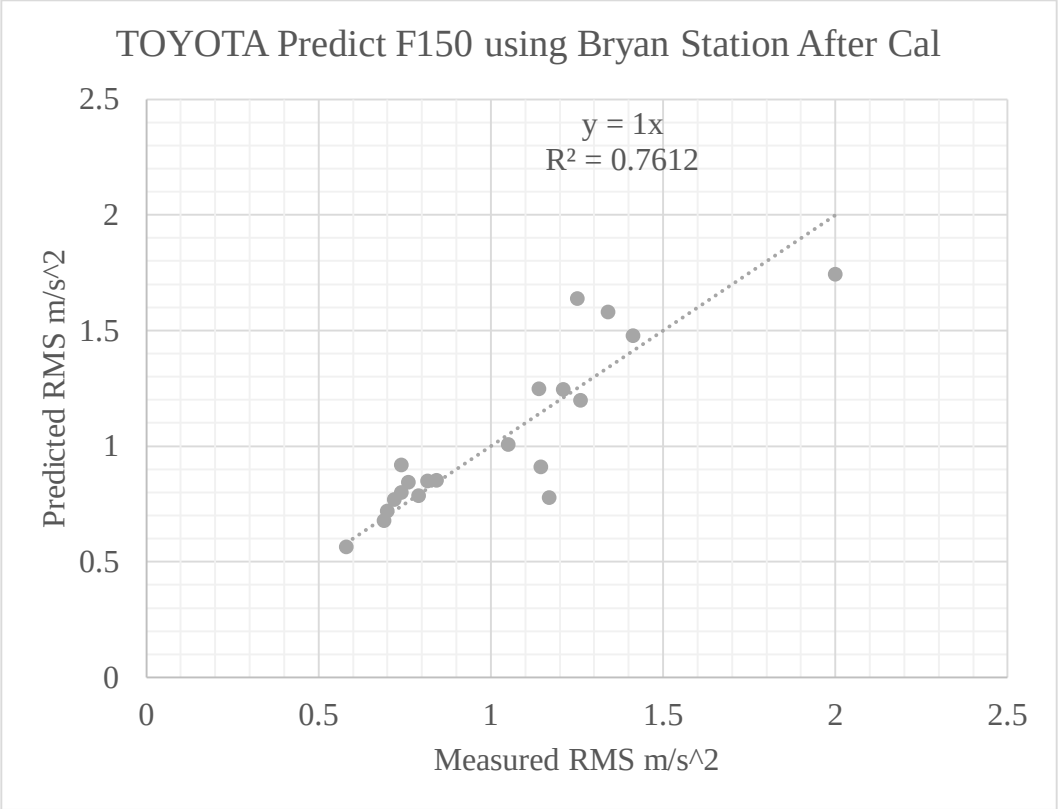
TOYOTA Predict F150 using Bryan Station After Cal
y = 1x
R² = 0.7612
Predicted RMS m/s^2
Measured RMS m/s^2
0
0.5
1
1.5
2
2.5

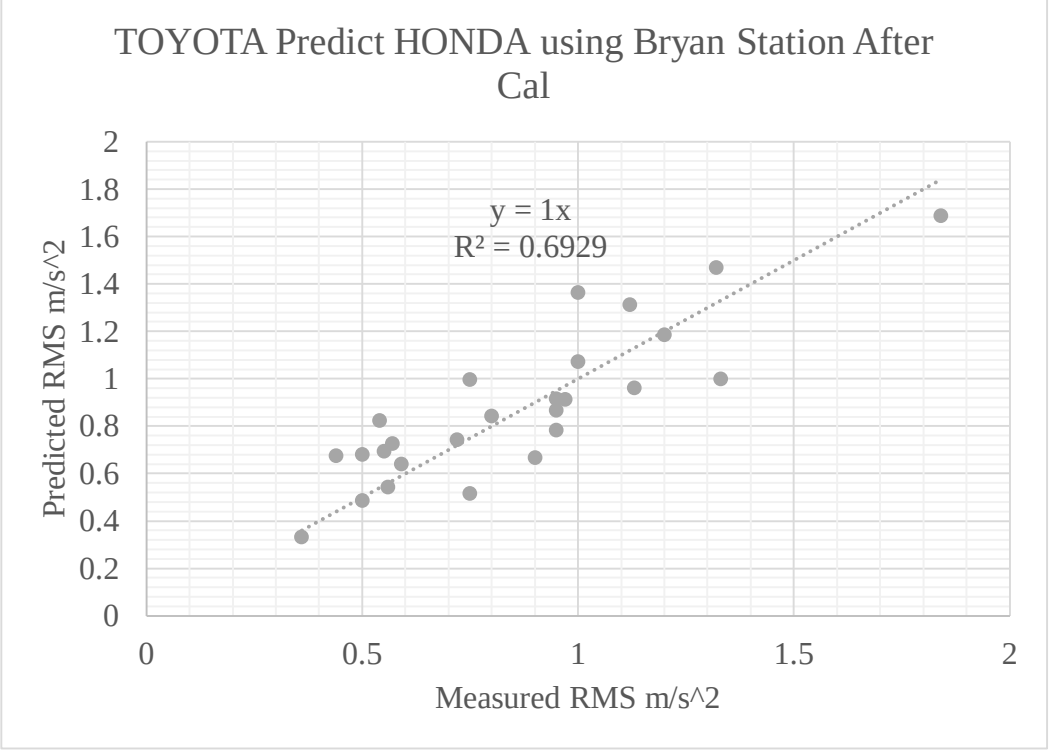
TOYOTA Predict HONDA using Bryan Station After Cal
y = 1x
R² = 0.6929
Predicted RMS m/s^2
Measured RMS m/s^2
0
0.2
0.4
0.6
0.8
1
1.2
1.4
1.6
1.8
2

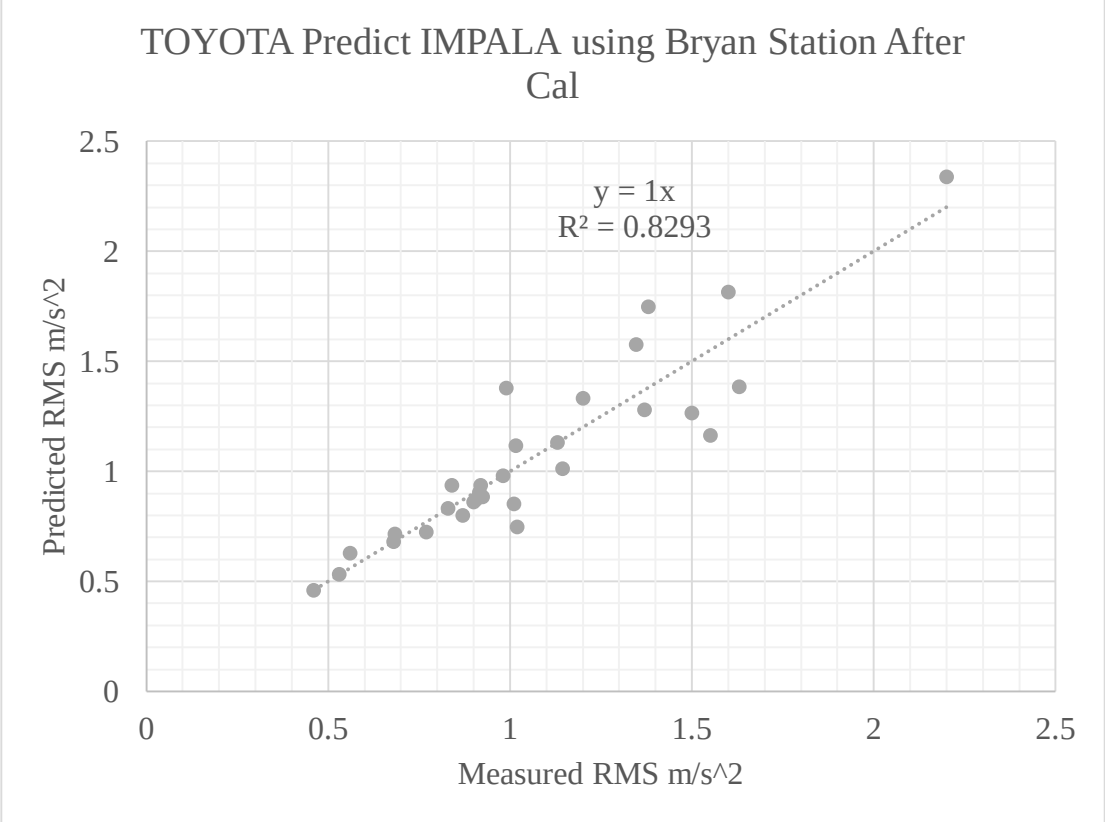
TOYOTA Predict IMPALA using Bryan Station After Cal
y = 1x
R² = 0.8293
Predicted RMS m/s^2
Measured RMS m/s^2
0
0.5
1
1.5
2
2.5

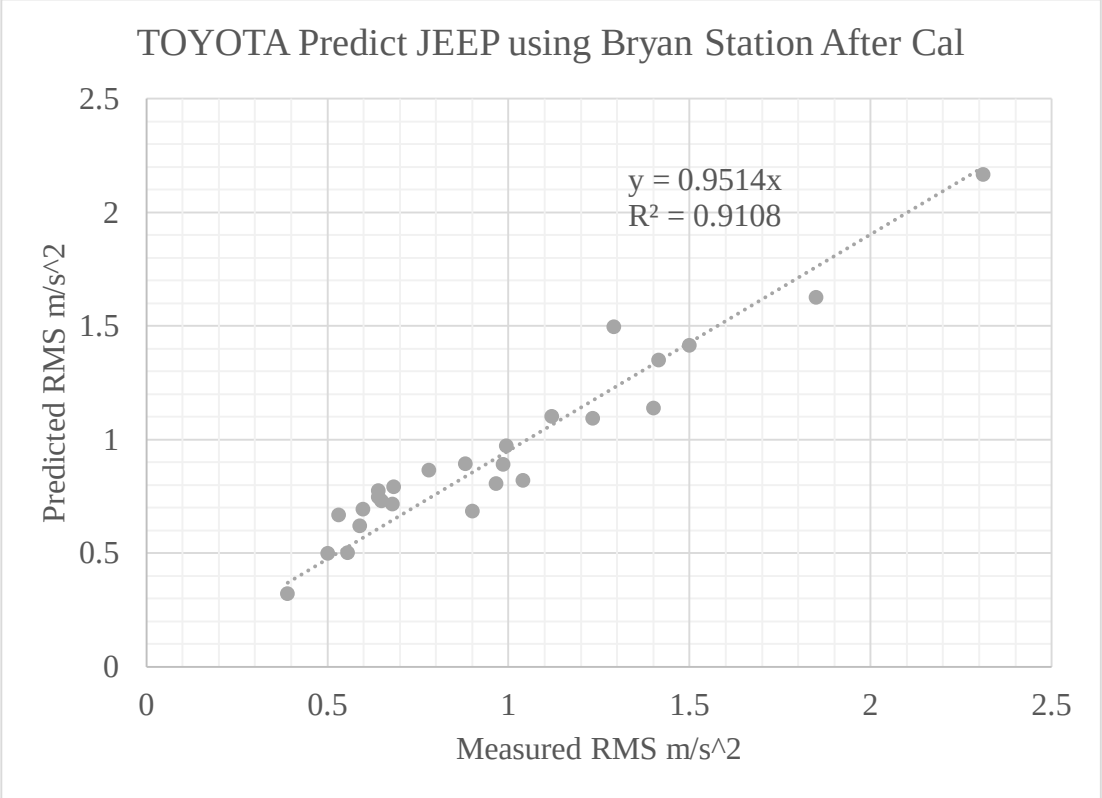
TOYOTA Predict JEEP using Bryan Station After Cal
y = 0.9514x
R² = 0.9108
Predicted RMS m/s^2
Measured RMS m/s^2
0
0.5
1
1.5
2
2.5

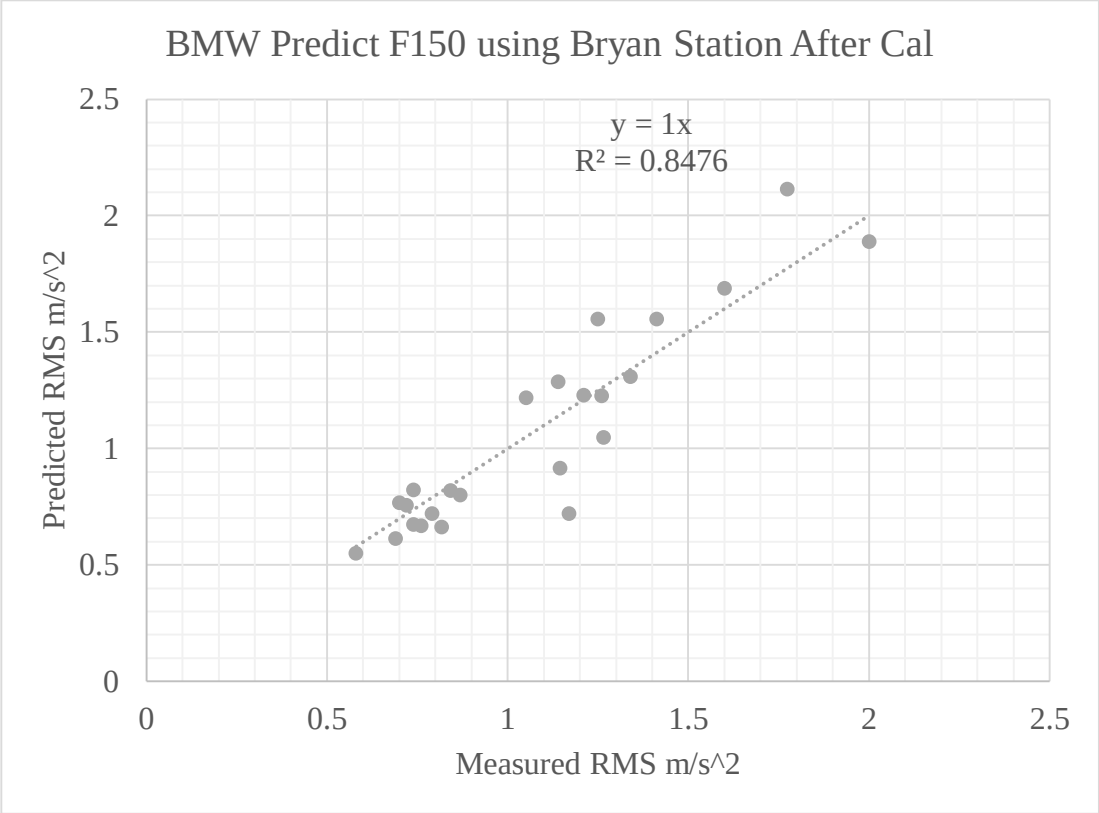
BMW Predict F150 using Bryan Station After Cal
y = 1x
R² = 0.8476
Predicted RMS m/s^2
Measured RMS m/s^2
0
0.5
1
1.5
2
2.5

APPENDIX F

Chapter 6 Profiles fitted to all crossings and calculations

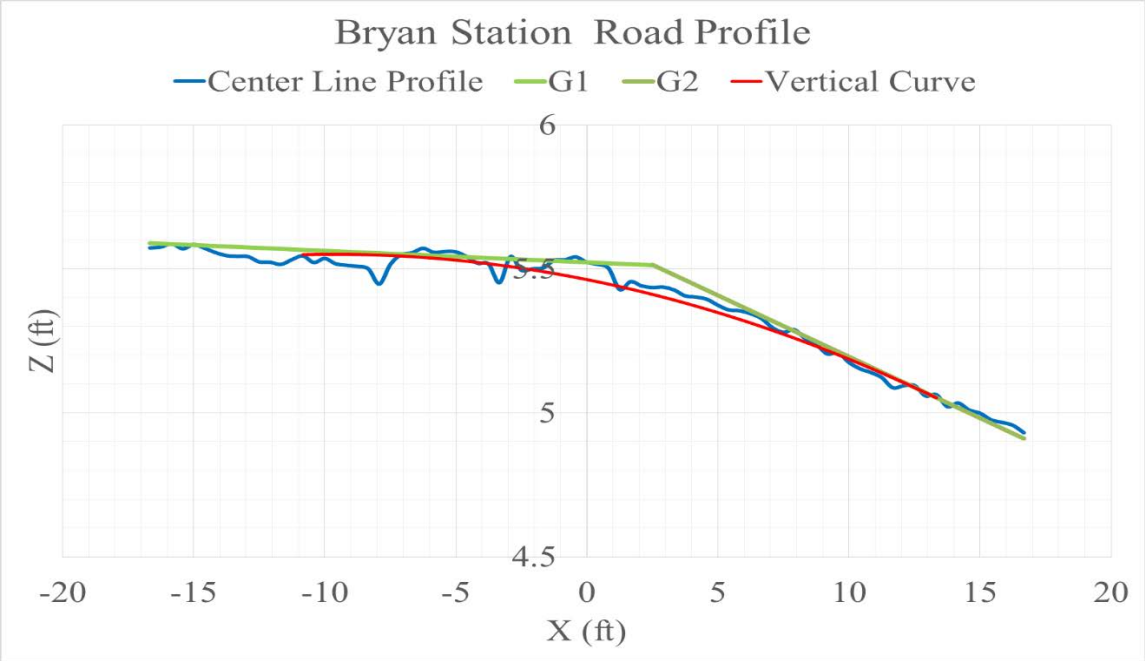

G1 in percentage	0.4
G2 in percentage	-4.3
ABS G2-G1	4.7
Posted Speed Vp	30.0
L feet	25.0
Design Speed	15.8
Acc @ posted speed f/s^2	3.6
Acc @ posted speed m/s^2	1.1
Acc Measured m/s^2	4.0
Delta Acc m/s^2	2.9

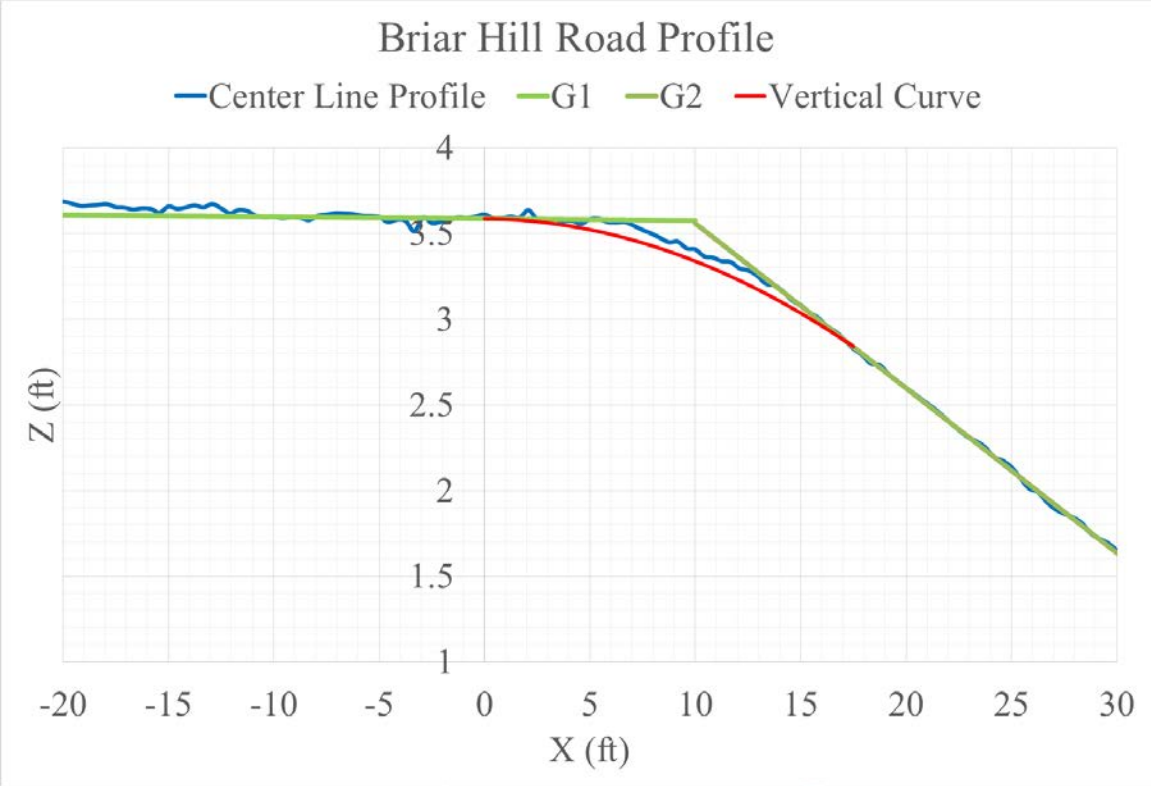

G1 in percentage	-0.1
G2 in percentage	-9.6
ABS G2-G1	9.5
Posted Speed Vp	35.0
L feet	17.5
Design Speed	9.3
Acc @ posted speed f/s^2	14.3
Acc @ posted speed m/s^2	4.4
Acc Measured m/s^2	7.0
Delta Acc m/s^2	2.6

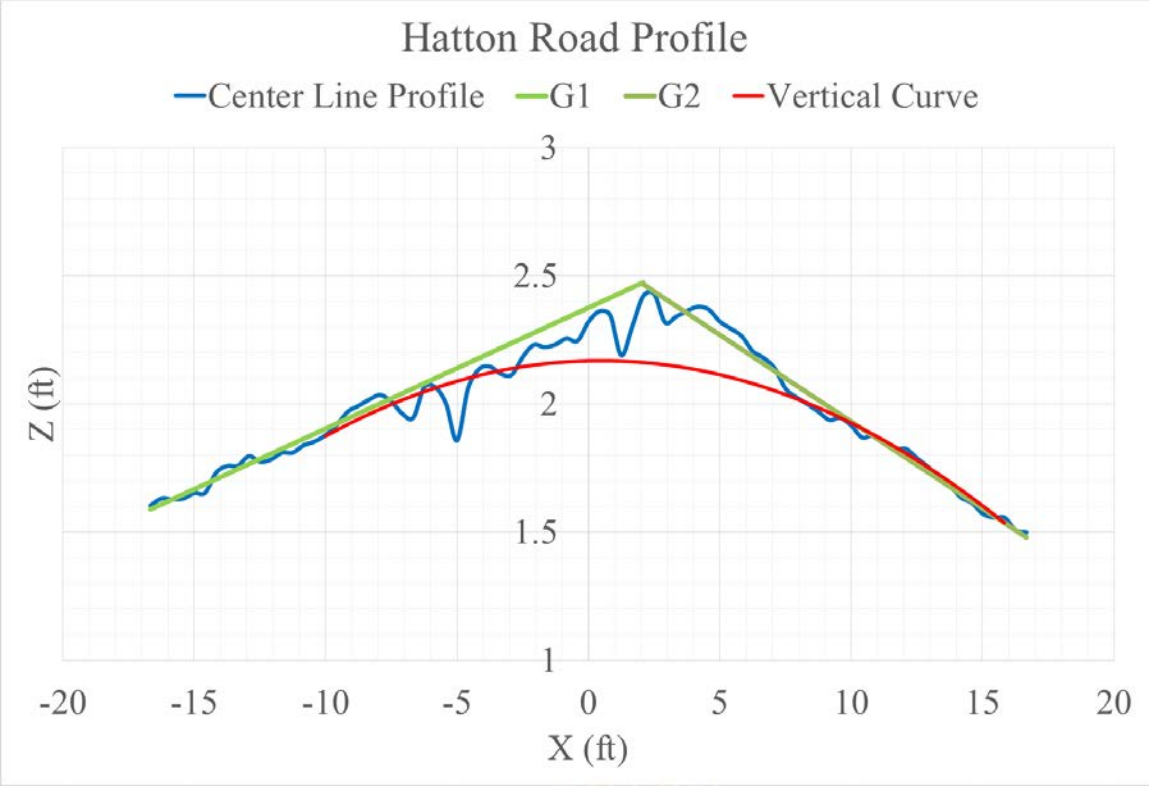

G1 in percentage	7.2
G2 in percentage	-6.8
ABS G2-G1	14.0
Posted Speed Vp	20.0
L feet	26.0
Design Speed	9.3
Acc @ posted speed f/s^2	4.6
Acc @ posted speed m/s^2	1.4
Acc Measured m/s^2	5.0
Delta Acc m/s^2	3.6

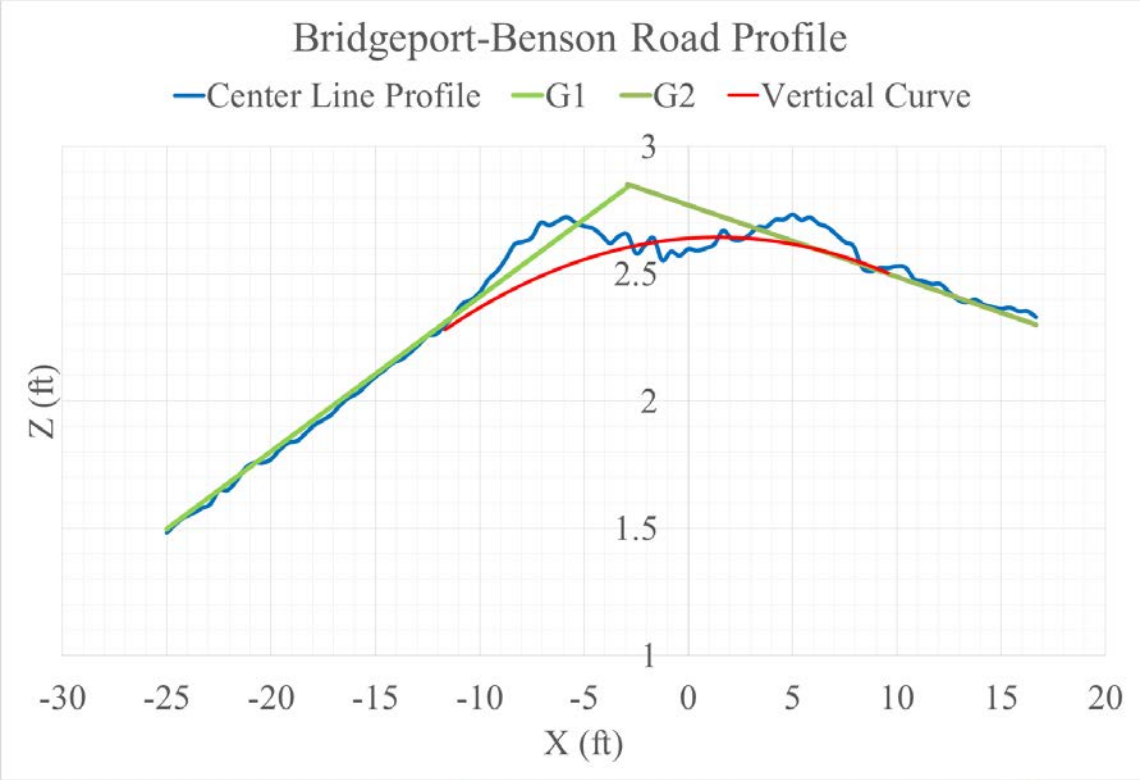

G1 in percentage	6.1
G2 in percentage	-2.8
ABS G2-G1	8.9
Posted Speed Vp	25.0
L feet	21.0
Design Speed	10.5
Acc @ posted speed f/s^2	5.7
Acc @ posted speed m/s^2	1.7
Acc Measured m/s^2	6.0
Delta Acc m/s^2	4.3

REFERENCES

Abouelatta, O. B. (2010). *3D surface roughness measurement using a light sectioning vision system.* Paper presented at the Proceedings of the World Congress on Engineering, London, UK.

American Association of State Highway and Transportation Officials (AASHTO). (2011). *A Policy on geometric design of highways and streets 2011* (6th ed.). Washington DC.

American Railway Engineering Maintenance-of-Way Association (AREMA). (2015). *2015 manual for railway engineering*.

Barsi, Á.-F., István-Lovas, T.-M., Gábor-Takács, B.-T., & Charles-Tóth, Z. (2005). *Mobile pavement measurement system: A concept study*. Paper presented at the Proc. ASPRS Annual Conference, Baltimore, USA, May.

Bauer, L. (1958). Passenger car overhang and underclearance as related to driveway profile design. II. Street and highway design. *Highway Research Board bulletin, 195*, 23-29.

Bemis, S. P., Micklethwaite, S., Turner, D., James, M. R., Akciz, S., Thiele, S. T., & Bangash, H. A. (2014). Ground-based and UAV-based photogrammetry: A multi-scale, high-resolution mapping tool for structural geology and paleoseismology. *Journal of Structural Geology, 69*, 163-178.

Bevilacqua, M., Liguori, C., & Paolillo, A. (2010). *Stereo calibration for a camera - projector pair*. Paper presented at the 2010 IEEE Instrumentation & Measurement Technology Conference Proceedings. http://dx.doi.org/10.1109/imtc.2010.5488055

http://ieeexplore.ieee.org/ielx5/5480448/5487988/05488055.pdf?tp=&arnumber=5488055&isnumber=5487988

Butcher, T. (1973). *Evaluation of Safety Improvements at Highway - Railway Grade Crossings : Interim Report*. Retrieved from http://dx.doi.org/10.5703/1288284313841

http://docs.lib.purdue.edu/cgi/viewcontent.cgi?article=2189&context=jtrp

Casey, C. J. (2011). *Enhancements to the modified composite pattern method of structured light 3D capture.* University of Kentucky Doctoral Dissertations. Retrieved from http://uknowledge.uky.edu/gradschool_diss/226

Clawson, A. L. (2002). *Establishing Design Vehicles for the Hang-up Problem*: West Virginia University Libraries.

Cong, N., Shang, J., Ren, Y., & Guo, Y. (2012). Vehicle Unpaved Road Response Spectrum Acquisition Based on Accelerometer and GPS Data. *Sensors, 12*(12), 9951-9964. doi:10.3390/s120809951

Dynamic Simulation Laboratory (DSL). (2013). Analysis of Train/Track Interaction Forces (ATTIF) Brief. Chicago, IL: University of Illinois at Chicago. Retrieved from https://www.uic.edu/labs/dsl/docs/ATTIF%20Brief_2013.pdf

Eck, R. W., & Kang, S. (1992). Roadway Design Standards to Accommodate Low-Clearance Vehicles *Transportation Research Record*(1356).

Essig, R. (2014, June 4). Community residents discuss proposals for Brannon road at public meeting. *The Jessamine Journal*. Retrieved from http://www.centralkynews.com/jessaminejournal/news/local/community-residents-discuss-proposals-for-brannon-road-at-public-meeting/article_af18eafa-ebfe-11e3-b801-0017a43b2370.html

Faris, W. F., BenLahcene, Z., & Hasbullah, F. (2012). Ride quality of passenger cars: an overview on the research trends. *International Journal of Vehicle Noise and Vibration, 8*(3), 185-199.

Federal Railroad Administration, Office of Safety Analysis. (2016). *Query Accident/Incident Trends. 2.08 Highway-Rail Crossings*. Retrieved from: http://safetydata.fra.dot.gov/OfficeofSafety/publicsite/Query/gxrtally1.aspx

Federal Railroad Administration (FRA). (2016). *Federal Railroad Administration Web Based Accident Prediction Systems (WBAPS)*. Retrieved from: https://www.fra.dot.gov/Page/P0114

Federal Railroad Administration Office of Safety Analysis. (2016). *Highway-Rail Crossing Inventory. 8.05 Crossing Inventory By State*. Retrieved from: http://safetydata.fra.dot.gov/OfficeofSafety/publicsite/Query/invtab.aspx

Fine, R. (1963). Correlation of vertical acceleration and human comfort in a passenger car (0148-7191). Retrieved from

Fitzsimmons, E. J., Souleyrette, R. R., & Nambisan, S. S. (2013). Measuring Horizontal Curve Vehicle Trajectories and Speed Profiles: Pneumatic Road Tube and Video Methods. *Journal of Transportation Engineering, 139*(3), 255-265. doi:10.1061/(asce)te.1943-5436.0000501

Freeman, T. E., & McGhee, K. H. (1995). *Evaluation of a laser road surface tester*. Retrieved from

French, L., Clawson, A., & Eck, R. (2003). Development of design vehicles for hang-up problem. *Transportation Research Record: Journal of the Transportation Research Board*(1847), 11-19.

Garcia-Pozuelo, D., Gauchia, A., Olmeda, E., & Diaz, V. (2014). Bump modeling and vehicle vertical dynamics prediction. *Advances in Mechanical Engineering, 6*, 736576.

Geng, J. (2011). Structured-light 3D surface imaging: a tutorial. *Advances in Optics and Photonics, 3*(2), 128-160. doi:10.1364/AOP.3.000128

Gregg, L., & Foy, W. S. (1955). Triaxial Acceleration Analysis Applied to the Evaluation of Pavement Riding Qualities. *Kentucky Transportation Center Research Report. Paper 1267*.

Horan, T. P. (2013). Evaluating At-Grade Rail Crossing Safety along the Knowledge Corridor in Massachusetts.

Hou, X., Shan, L., & Ma, S. (2007). *Influence of Pavement Roughness on Riding Comfort Based on Whole Vehicle Model*. Paper presented at the International Conference on Transportation Engineering 2007. http://dx.doi.org/10.1061/40932(246)108

Illinois Department of Transportation. (2001). Illinois highway information system : Roadway Information & Procedure Manual. Springfield, IL.

Illinois Department of Transportation. (2014). Illinois highway information system : Roadway Information & Procedure Manual. Springfield, IL.

Jahanshahi, M. R., Jazizadeh, F., Masri, S. F., & Becerik-Gerber, B. (2012). Unsupervised approach for autonomous pavement-defect detection and quantification using an inexpensive depth sensor. *Journal of Computing in Civil Engineering, 27*(6), 743-754.

Jahanshahi, M. R., Karimi, F. J., Masri, S. F., & Becerik-Gerber, B. (2015). U.S. Patent No. 9,196,048.: U. S. P. a. T. Office.

Kang, S., & Eck, R. W. (1991). Low-Clearance Vehicles at Rail-Highway Grade Crossings: An Overview of the Problem and Potential Solutions. *Transportation Research Record*(1327).

Katu, U., Desavale, R., & Kanai, R. (2003). Effect Of Vehicle Vibration On Human Body–RIT Experience. Department of Mechanical Eng., Rajarambapu Institute ofTechnology, Sakharale-415414, htpp://www. Nacomm03. ammindia. org/Articles/Nav001. pdf.

Kertész, I., Lovas, T., & Barsi, A. (2008). Photogrammetric pavement detection system. *ISPRS, Citeseer, 37*.

Khattak, A., Hallmark, S., & Souleyrette, R. (2003). Application of light detection and ranging technology to highway safety. *Transportation Research Record: Journal of the Transportation Research Board*(1836), 7-15.

Lakatos, D. (2010). How to scan objects into 3D using structured light? Retrieved from http://fab.cba.mit.edu/content/processes/structured_light/

Lanman, D., & Taubin, G. (2009). *Build your own 3D scanner: 3D photography for beginners.* Paper presented at the ACM SIGGRAPH 2009 Courses.

Li, Q., Yao, M., Yao, X., & Xu, B. (2009). A real-time 3D scanning system for pavement distortion inspection. *Measurement Science and Technology, 21*(1), 015702. doi:10.1088/0957-0233/21/1/015702

Lonardo, P. M., Trumpold, H., & De Chiffre, L. (1996). Progress in 3D Surface Microtopography Characterization. *CIRP Annals - Manufacturing Technology, 45*(2), 589-598. doi:http://dx.doi.org/10.1016/S0007-8506(07)60513-7

Long, G. (2000). Acceleration characteristics of starting vehicles. *Transportation Research Record: Journal of the Transportation Research Board*(1737), 58-70.

Marzolff, I., & Poesen, J. (2009). The potential of 3D gully monitoring with GIS using high-resolution aerial photography and a digital photogrammetry system. *Geomorphology, 111*(1), 48-60.

Mertz, C. (2011). *Continuous road damage detection using regular service vehicles.* Paper presented at the Proceedings of the ITS World Congress.

Mutabazi, M., & Russell, E. R. (2003). *Identification of Hump Highway/rail Crossings in Kansas*. Retrieved from

Nahvi, H., Fouladi, M. H., & Nor, M. J. M. (2009). Evaluation of whole-body vibration and ride comfort in a passenger car. *International journal of acoustics and vibration, 14*(3), 143-149.

Nickmehr, N. (2011). Ride quality and drivability of a typical passenger car subject to engine/driveline and road non-uniformities excitations. (Master of Science), Link¨oping University

Olsen, M. J. (2013). Guidelines for the use of mobile LIDAR in transportation applications (Vol. 748): Transportation Research Board.

Olympus Corporation. (2016). Roughness (3D) parameter (pp. Height Parameters (amplitude mean in the height direction)).

Operation Lifesaver. (2015). Highway-Rail Grade Crossing Training for Professional Truck Drivers. Retrieved from Stay Alive When You Drive website: http://oli.org/images/page/OLTDGuide15stayalive(1).pdf

Optech Incorporated. (2015). Lynx SG1 Mobile Mapper Summary Specification Sheet. Canada: Optech Incorporated.

Papagiannakis, A. (1995). A roughness model describing heavy vehicle-pavement interaction.

Papagiannakis, A. (1997). *The Need for a New Pavement Roughness Index; RIDE* (0148-7191). Retrieved from

Proctor, C. L., Grimes, W. D., Fournier, D. J., Rigol, J., & Sunseri, M. G. (1995). *Analysis of Acceleration in Passenger Cars and Heavy Trucks* (0148-7191). Retrieved from

Quinn, B. E., & Hildebrand, S. E. (1972). *The effect of pavement roughness on safe vehicle handling characteristics*. Lafayette, Ind.: Purdue Research Foundation.

Ranganathan, P., & Olson, E. (2010, 18-22 Oct. 2010). *Automated safety inspection of grade crossings.* Paper presented at the Intelligent Robots and Systems (IROS), 2010 IEEE/RSJ International Conference on.

Rister, B., McIntosh, L., & Whelan, J. (2013). Utilization of Mobile LiDAR to Verify Bridge Clearance Heights on the Western Kentucky Parkway. Retrieved from

Rose, J. G., Witt, T. W., Renfro, A. F., & Ridgeway, N. E. (2009). Highway-Railway At-Grade Crossings: Rideability Measurements and Assessments.

Rudin-Brown, C., George, M., & Stuart, J. (2014). Human Factors Issues of Accidents at Passively Controlled Rural Level Crossings. *Transportation Research Record: Journal of the Transportation Research Board, 2458*, 96-103. doi:10.3141/2458-12

Sayers, M. W. (1995). On the calculation of international roughness index from longitudinal road profile. *Transportation Research Record*(1501), 1-12.

Sayers, M. W., & Karamihas, S. M. (1998). The little book of profiling. *Transportation Research Institute, University of Michigan*.

Segoe, L. (1931). *Comprehensive plan for Lexington and its Environs*. Cincinnati: Lexington City Planning Zoning Commission.

Shabana, A. A., Aboubakr, A. K., & Ding, L. (2012). Use of the non-inertial coordinates in the analysis of train longitudinal forces. *Journal of Computational and Nonlinear Dynamics, 7*(1), 011001.

Shamayleh, H., & Khattak, A. (2003). *Utilization of LiDAR technology for highway inventory*. Paper presented at the Proceedings of the 2003 Mid-Continent Transportation Research Symposium, Ames, Iowa.

Shanahan, D. F. (2004). Human tolerance and crash survivability. Pathological Aspects and Associated Biodynamics in Aircraft Accident Investigation, RTO-EN-HFM-113, available at: ftp://ftp. rta. nato. int/PubFullText/RTO/EN/RT O-EN-HFM-113/EN-HFM-113-06. pdf accessed on, 28, 10-12.

Shirahatti, A., Prasad, P., Panzade, P., & Kulkarni, M. (2008). Optimal design of passenger car suspension for ride and road holding. *Journal of the Brazilian Society of Mechanical Sciences and Engineering, 30*(1), 66-76.

Smith, C. C., McGehee, D. Y., & Healey, A. J. (1978). The prediction of passenger riding comfort from acceleration data. *Journal of Dynamic Systems, Measurement, and Control, 100*(1), 34-41.

Snare, M. C. (2002). Dynamics model for predicting maximum and typical acceleration rates of passenger vehicles. Virginia Polytechnic Institute and State University.

Sobanjo, J. O. (2006). Design Guidelines for Highway Railroad Grade Crossing Profiles in Florida.

Souleyrette, R., Hallmark, S., Pattnaik, S., O'Brien, M., & Veneziano, D. (2003). *Grade and cross slope estimation from LiDAR-based surface models*. Retrieved from

StudioNoeProductions. (2015). Amazing Limo vs Train Crash Elkhart County [Video file]. Retrieved from https://youtu.be/Ss8RdZLPCvs

United States National Transportation Safety Board. (1996). *Highway accident report highway/rail grade crossing collision near Sycamore, South Carolina, May 2, 1995*. Washington, D.C.: National Transportation Safety Board.

US Department of Transportation, Federal Highway Administration. (2007). *Railroad-Highway Grade Crossing Handbook*.

Van Arman, P., & Al-Nazer, L. (2008). *Automated Technology for Rail-Based Highway-Rail Grade Crossing Surveying*. Paper presented at the IEEE/ASME/ASCE 2008 Joint Rail Conference.

Veneziano, D., Hallmark, S., & Souleyrette, R. R. (2002). Comparison of LIDAR & Conventional Mapping Methods for Highway Corridor Studies.

Ward, C. C., & Iagnemma, K. (2009). Speed-independent vibration-based terrain classification for passenger vehicles. *Vehicle System Dynamics, 47*(9), 1095-1113.

Whelley, P. L., Glaze, L. S., Calder, E. S., & Harding, D. J. (2014). LiDAR-derived surface roughness texture mapping: application to Mount St. Helens pumice plain deposit analysis. *Geoscience and Remote Sensing, IEEE Transactions on, 52*(1), 426-438.

Wiki, O. (2016). Accuracy of GPS data --- OpenStreetMap Wiki. Retrieved from http://wiki.openstreetmap.org/w/index.php?title=Accuracy_of_GPS_data&oldid=957872

Williams, T. A. (2003). Classification of Railroad Crossings in Indiana for Roughness.

Wooldridge, M. D. (2000). Design Guidelines for At-Grade Intersections Near Highway-Railroad Grade Crossings. The Texas A&M University.

VITA

Teng Wang

EDUCATION

Iowa State University Ames. Iowa August 2011
Master of Science in Civil Engineering (Transportation).
Iowa State University, Ames. Iowa May 2009
Bachelor of Science in Civil Engineer.
Lanzhou Jiaotong University, Lanzhou, Gansu, China June 2007
First two years study in Civil Engineering.

SERVICE AND PROFESSIONAL ACTIVITIES

2015	**Passed Principles and Practice of Engineering (PE) exam (Transportation)**, Kentucky, April 2015.
2015 – Present	**Young Professional member**, Transportation Research Board (TRB) Committee on Highway/Rail Grade Crossings (AHB60).
2012 – Present	**Student member**, American Railway Engineering and Maintenance-of-Way Association (AREMA)
2012	**Member**, University of Kentucky ITE Traffic Bowl Team.
2010	**Engineer Intern (EIT)**, Iowa, June 2010.
2010	**Member**, Iowa State University ITE Traffic Bowl Team.
2010 – 2011	**President**. Transportation Student Association (TSA) and Institute of Transportation Engineers (ITE) student chapter at Iowa State University
2009 – Present	**Student member**, Institute of Transportation Engineers.

HONORS AND AWARDS

2013	Transportation Planning and Management Graduate Certificate Program Scholarship ($5,000), sponsored by the Kentucky Transportation Center and College of Engineering, University of Kentucky.
2010	Honorarium from the Transportation Research Board for paper "A Transportation Safety Planning Tool for the City of Ames." at the 12th National Conference on Transportation Planning for Small and Medium-Sized Communities: Tools of the Trade in Williamsburg, Virginia, September 22–24, 2010.
2008	College of Engineering Dean's List, Iowa State University, Spring 2008.

SCHOLARLY PUBLICATION & PRESENTATION

November 2015 Wang, T., Souleyrette, R. R., Aboubakr, A. K., & Lau, D. (2015). A Dynamic Model for Quantifying Rail-Highway Grade Crossing Roughness. *Journal of Transportation Safety & Security*, 00-00. doi:10.1080/19439962.2015.1048016

January 2015 Wang, T., Souleyrette, R. R., Lau, D., Aboubakr, A., & Randerson, E. (2015). *Quantifying Rail-Highway Grade Crossing Roughness: Accelerations and Dynamic Modeling*. Paper presented at the Transportation Research Board 94th Annual Meeting. Washington DC, January, 2015

August 2014 Wang, T., Souleyrette, R. R., Aboubakr, A., & Randerson, E. (2014). *Quantifying Grade Crossing Condition as an Input to Modeling Safety*. Paper presented at the 2014 Global Level Crossing Symposium.

May 2014 Wang, T., Souleyrette, R. R. (2014). *Rail-Highway Grade Crossing Roughness Quantitative Measurement Using 3D Technology* presentation at When Rail Meets Soil, Technical Workshop, Caltrain, San Carlos, CA, May 14, 2014.

April 2014 Wang, T., Souleyrette, R. R., Lau, D., & Xu, P. (2014). *Rail Highway Grade Crossing Roughness Quantitative Measurement Using 3D Technology*. Paper presented at the 2014 Joint Rail Conference

April 2013 Wang, T. (2013). *Rail Crossing Roughness Quantitative Measurement by 3D Technology*. Poster presented at Joint Rail Conference 2013, University of Tennessee, Knoxville, April 16-18, 2013.

January 2013 Wang, T., Souleyrette, R. R., & Gkritza, K. (2013). *Incorporating Safety into Transportation Planning at Smaller Agencies*. Paper presented at the Transportation Research Board 94th Annual Meeting., Washington DC, January, 2013.

August 2011 Master's thesis *Incorporating safety into transportation planning for small and medium-sized communities*, Iowa State University, Ames, Iowa. August 2011.

September 2010 Wang, T. (2010). *A Transportation Safety Planning Tool for the City of Ames*. Paper presented at the 12th National Conference on Transportation Planning for Small and Medium-Sized Communities. Williamsburg, Virginia on Sep 23rd, 2010.

August 2010 Wang, T. (2010). *Incorporating Safety into Transportation Planning for the City of Ames*, presentation at 2010 Mid-Continent Transportation Research Forum in Madison, WI on August 19th. 2010.

November 2009 Wang, T. (2009). *Incorporating Safety into Transportation Planning for Small and Medium-Sized Communities*. Poster presented at 14th Annual Traffic and Safety Engineering Forum, Des Moines, Iowa on Nov 4th, 2009.

October 2009 Wang, T. (2009). *A Transportation Safety Planning Tool for the City of Ames*. TRB 8th National Conference on Transportation Asset Management, Portland, Oregon, October 19-21, 2009.